THE ROLE OF DIXDC1 IN AUTISM SPECTRUM DISORDER

THE ROLE OF DIXDC1 IN AUTISM SPECTRUM DISORDER AND ESTABLISHING A HIGH-CONTENT PHENOTYPING PLATFORM FOR HUMAN ASD MODELS

By

VICKIE KWAN, B.Sc.

A Thesis

Submitted to the School of Graduate Studies in Partial Fulfillment of the

Requirements for the Degree

Doctor of Philosophy

McMaster University

DOCTOR OF PHILOSOPHY (2018) McMASTER UNIVERSITY

Science—Biochemistry Hamilton, ON

TITLE:	The role of DIXDC1 in autism spectrum disorder and establishing a high-content phenotyping platform for human ASD models
AUTHOR:	Vickie Kwan, B.Sc. (McMaster University)
SUPERVISOR:	Dr. Karun K. Singh
NUMBER OF PAGES:	ccxxix, 229

LAY ABSTRACT

Autism spectrum disorder (ASD) describes a group of neurodevelopmental disorders that affects about 1 in 59 children. Children with ASD display deficits in social communication and interaction and repetitive behaviours. Although the cause of ASD remains unknown, ASD is thought to arise from abnormalities in neuronal connectivity (connections between brain cells). Through our collaboration with Dr. Stephen Scherer (Hospital for Sick Children, Toronto), we discovered ASD-associated genetic variants (changes in the genetic code) in a gene named *DIX-domain containing 1* (*DIXDC1)*. We discovered that variants in *DIXDC1* were important for proper development of neuronal connectivity. Next, we were interested in discovering the signalling networks regulating Dixdc1 function in brain development. This data suggests that Dixdc1 is involved in many pathways associated with ASD, and may be implicated in Ehlers-Danlos syndrome (EDS). Finally, we developed a platform for high-content imaging of human-derived neurons to assess synaptic disruptions caused by ASD-associated genes.

ABSTRACT

Autism spectrum disorder (ASD) describes a heterogeneous group of disorders with a worldwide prevalence of 1%. The two core symptoms of ASD are: 1) deficits in social communication and interaction and 2) restrictive and repetitive behaviours. Although the etiology of ASD remains unknown, environmental and genetic factors are believed to contribute to the disorder. Emerging studies suggest that molecules in the Wnt signalling pathway are important for the development of neural connectivity and are associated with ASD. We studied a Wnt signalling molecule named DIX domain containing-1 (DIXDC1) that has previously been linked to psychiatric diseases. We found that DIXDC1 regulates dendrite growth and dendritic spine formation and may function through a novel actin-dependent mechanism to regulate actin dynamics and polymerization. Our collaboration with Dr. Stephen Scherer (Hospital for Sick Children, Toronto) identified rare inherited genetic variants in DIXDC1. These variants caused an impairment of dendritic development. Furthermore, RNA sequencing identified signalling networks that were disrupted in *Dixdc1* KO mouse brains, such as synaptic signalling, wnt signalling, and cell adhesion. These signalling networks are previously been implicated in ASD and we also identified different expressed genes that are strong candidate ASD-susceptibility genes. RNA sequencing also identified a novel genetic disorder that may be associated with Dixdc1 dysregulation, Ehlers-Danlos syndrome.

Lastly, we developed a high-content imaging platform for automated imaging and analysis of human iPS-derived neurons modeling ASD models. We optimized culturing

of human induced-neurons in a 96-well format, and immunostaining of synaptic markers to detect deficits in synapse function. Preliminary data shows that we are able to detect synaptic phenotypes in some ASD-associated iPS cell lines. Further development of the platform should be performed for the detection of a more robust synaptic phenotype and the potential discovery of drug treatments to rescue these phenotypes.

ACKNOWLEDGMENTS

First and foremost, I would like to thank my supervisor, Dr. Karun Singh, for his continuous guidance and support. He has been a great role model for me, and his passion and dedication for his research is truly inspiring. I am grateful for the faith and trust that Dr. Singh has had in me, and for the opportunities he has given me throughout these years.

I would also like to thank my supervisory committee, Drs. Ray Truant and Kristin Hope. Your insightful comments and encouragement have been very helpful over the years. I also thank my fellow lab mates working in the K. Singh lab, who have always been friendly, supportive, and great teammates. Next, I would like to thank my friends for their continuous encouragement and reassurance, especially Elyse Rosa, Dessi Loukov, Claudia Hung, and Maddie Lynch.

I would like to express my gratitude to my family, who have been a constant support for me and have loved me unconditionally, even if they didn't understand what I did. I would like to thank Nick Holzapfel for all of his guidance and support within the lab and outside of the lab. Thank you for believing in me through the good times and the hard times. Last but not least, I would like to thank my best friend, Rex, who has provided me with the emotional support to finish my Ph.D.

TABLE OF CONTENTS

LIST OF FIGURES & TABLES

CHAPTER 1

CHAPTER 2

CHAPTER 4

LIST OF ABBREVIATIONS

ADHD	Attention deficit hyperactivity disorder
ADI-R	Autism diagnostic interview, revised
ADOS	Autism diagnostic observation schedule
ASD	Autism spectrum disorder
ATRX	ATP-dependent helicase
BDNF	Brain-derived neurotrophic factor
CACNA1C	Calcium voltage-gated channel subunit alpha 1 A
CDC	Centers for disease control and prevention
CH	Calponin homology
CHD8	Chromo-domain helicase 8
CNTNAP2	Contactin-associated protein-like 2
CNV	Copy number variant
CTNNB1	Beta-catenin
CUX1	CUT like homeobox 1
DAPI	4',6-diamidino-2-phenylindole
DEG	Differentially expressed genes
DISC1	Disrupted in schizophrenia 1
DIXDC1	DIX domain containing 1
DMEM	Dulbecco's Modified Eagle's Medium
Dox	Doxycycline
DSM-V	Diagnostic and statistical manual of mental disorders - 5

EB	Embryoid body
EDS	Ehlers-Danlos syndrome
EPSC	Excitatory postsynaptic current
ES	Enrichment score
FBS	Fetal bovine serum
FDA	Food and drug administration
FDR	False discovery rate
FMR1/FMRP	Fragile X mental retardation 1/protein
GDNF	Glial cell line-derived neurotrophic factor
GFP	Green fluorescent protein
GO	Gene ontology
GSK3	Glycogen synthase kinase-3
GWAS	Genome-wide association study
HDAC	Histone deacetylase
HDCT	Heritable disorders of connective tissue
HTS	High-throughput screening
ID	Intellectual disability
IGF1	Insulin-like growth factor 1
iN	Induced neuron
iPSC	Induced pluripotent stem cells
KCNQ2	Potassium voltage-gated channel subfamily Q member 2
KO	Knockout

MAP2	Microtubule associated protein 2
MARK1	Microtubule affinity regulating kinase 1
MEA	Microelectrode array
MECP2	Methyl CpG binding protein 2
NDD	Neurodevelopmental disorder
NEAA	Non-essential amino acids
NES	Normalized enrichment score
NeuN	Neuronal nuclei
NGN2	Neurogenin-2
NGS	Next generation sequencing
NPC	Neural progenitor cell
NRXN1	Neurexin-1-alpha
PBS	Phosphate buffered saline
PDD-NOS	Pervasive developmental disorder- not otherwise specified
PFA	Paraformaldehyde
PFC	Prefrontal cortex
PSD95	Postsynaptic density protein 95
PTEN	Phosphate and tensin homolog
RNA	Ribonucleic acid
RNA-Seq	RNA sequencing
ROCK	Rho-associated kinase
rtTA	Reverse tetracycline-control transactivator

SCN2A	Sodium voltage-gated channel alpha subunit 2
SFARI	Simons foundation autism research initiative
SHANK2/3	SH3 and multiple ankyrin repeat domains 2/3
shRNA	Short hairpin RNA
SNV	Single nucleotide variant
SYN2	Synapsin 2
SYX1A	Syntaxin-1A
SZ	Schizophrenia
TCAG	The Centre for Applied Genomics
VGLUT1	Vesicular glutamate transporter 1
WGS	Whole genome sequencing
WES	Whole exome sequencing
WT	Wildtype

CHAPTER 1: INTRODUCTION

1.1 Autism spectrum disorder

1.1.1 Clinical presentation and diagnosis

Autism spectrum disorder (ASD) is a neurodevelopmental disorder (NDD) that describes a heterogeneous group of disorders with varying severity of symptoms with a worldwide prevalence of ~1% (Developmental Disabilities Monitoring Network Surveillance Year Principal et al., 2014). ASD is characterized by two core symptoms: 1) deficits in social communication and interaction, and 2) restrictive, and repetitive behaviours (Diagnostic and Statistical Manual of Mental Disorders-5, DSM-5). ASD may be diagnosed in children around 2-4 years of age, and boys are 4.5 times more likely to be diagnosed with ASD compared to girls (Christensen et al., 2012). The DSM-5 is a tool used by physicians and other professionals to classify development, intellectual and mental health disorders (Developmental Disabilities Monitoring Network Surveillance Year Principal et al., 2014). Previously, the DSM-4 had categorized children with ASD into three distinct categories: Autistic disorder, Asperger's syndrome, and pervasive developmental disorder- not otherwise specified (PDD-NOS) (Miles, 2011). The newly updated DSM-5, published in 2013, now describes children with ASD under the broad spectrum of autism spectrum disorder (Brentani et al., 2013). There are several diagnostic tests used to assess for ASD, the Autism Diagnostic Interview, Revised (ADI-R) (Lord et al., 1994), and Autism Diagnostic Observation Schedule-Generic (ADOS) (Lord et al., 2000).

According to a study performed by the Centre for Disease Control, CDC (2014), the prevalence of ASD is about 1 in 59 children, increased from 1 in 68 children reported in 2012 (Christensen et al., 2012; Developmental Disabilities Monitoring Network Surveillance Year Principal et al., 2014). Many children with ASD develop multiple mental health issues and poor outcomes in education, employment, and relationships (Farley et al., 2009). Consequently, many of the adults with ASD lack autonomy, and require continual emotional and financial support from family members and support services (Farley et al., 2018).

ASD is a very heterogeneous disorder, in terms of clinical presentation (symptoms) and the underlying etiology and pathophysiology. Although the cause of ASD remains unknown, ASD is believed to be caused by environmental and genetic factors, with at least 20% of cases to have a genetic cause (Delorme et al., 2013). Researchers have previously reported that maternal immune activation is a risk factor for ASD and other NDD, such as schizophrenia (Oskvig et al., 2012). Additionally, birth complications, such as hypoxia and trauma, have also been associated with ASD risk (Modabbernia et al., 2017). Much of the current research focuses on the genetic contribution to ASD, however the variability of heritability also assumes the additional effect of environmental factors. ASD includes single-gene disorders, referred to as syndromic autism, that are the more commonly recognized disorders. Many of these "monogenic" disorders are found within approximately 1% of children with ASD (Miles, 2011). For example, Fragile X syndrome, which is caused by mutations in the *fragile x mental retardation 1* (*FMR1*) gene (Comery et al., 1997), Rett syndrome, caused by

mutations in the X-linked *MECP2* gene (Amir et al., 1999), and Timothy syndrome, caused by a mutation in the *CACNA1C* gene encoding for a calcium channel (Splawski et al., 2004); these disorders represent the few disorders with known etiology. Furthermore, included in the genetic risk of ASD, there are many newly discovered susceptibility genes, copy number variations (CNV), and chromosomal abnormalities associated with ASD, described in further detail in later sections (Krumm et al., 2014; Shishido et al., 2014; Yuen et al., 2016).

Due to the lack of knowledge in regards to the etiology and pathophysiology of ASD, there are currently no effective drug treatments to cure ASD. Current treatment involves early behavioural intervention, implemented as soon as ASD is diagnosed in a child (Brentani et al., 2013). Additionally, there are clinical trials using FDA-approved drugs, repurposed to alleviate certain symptoms presented in certain children with ASD (Riikonen, 2016). These drug treatments and current clinical trials will be further discussed in section 1.5 of this chapter.

1.2 The genetics of autism spectrum disorder

Various studies have indicated that ASD and other psychiatric disorders are highly heritable and have estimated the heritability of ASD to be up to 90% (Christensen et al., 2012; Sandin et al., 2014). Twin studies have shown a higher concordance rate between monozygotic twins (60-90%) versus dizygotic twins (0-30%) (Folstein and Rutter, 1977; Hallmayer et al., 2011; Sandin et al., 2014). Studies estimate that 20% of ASD cases is caused by genetics, and the genetic risk vary in both penetrance and strength (Delorme et

al., 2013). The syndromic forms of ASD have been extensively studied, for example Fragile X syndrome (due to mutations in *FMR1)* (Bhakar et al., 2012; Hutsler and Zhang, 2010), Angelman syndrome (*UBE3A*) (Greer et al., 2010), Rett syndrome (*MECP2*) (Amir et al., 1999; Sajan et al., 2016; Xu et al., 2014a), and Williams syndrome (Chailangkarn et al., 2016). These single-gene disorders have been more extensively studied within the field of ASD due to the partial understanding of the etiology of the disorders.

With the emergence of next-generation sequencing and developing technology, sequencing the human genome has become very affordable and accessible to many researchers. Previously, studies employed whole exome sequencing (WES) to sequence the protein encoding portions of the human genome. These studies were crucial in the initial discovery of many of the current strong candidate susceptibility genes and CNVs associated with ASD and other neurodevelopmental disorders (Krumm et al., 2014; Sanders et al., 2012) (Lim et al., 2017). Genome-wide association studies (GWAS) were also used to identify ASD-associated risk genes through studying control and case groups with a high number of samples (Ben-David and Shifman, 2012; Durak et al., 2015). GWA studies utilize chip-based microarray to assay for millions of SNPs that are common in the human population. The frequency of the SNP is expressed as the minor allele frequency (MAF); for example, MAF of 0.40 means that 40% of the population will have the allele of interest (Bush and Moore, 2012). These techniques have been instrumental in identifying many of the important ASD risk-genes still being studied today (Krishnan et al., 2016). However, with the development of new technologies, we are now able to

sequence the entire genome through whole genome sequencing (WGS) (Lim et al., 2017). The laboratory at the Hospital for Sick Children in Toronto has used different WGS platforms to fully sequence the genomes of 5,205 samples, included 2,620 individuals diagnosed with ASD (Yuen et al., 2016; Yuen et al., 2015; Yuen et al., 2017). This data is continuously growing with increasing samples of WGS data, and analysis of these data continues to identify new risk genes for ASD (Yuen et al., 2017).

There are many potential perturbations of the genetic code that may contribute to the development and pathophysiology of ASD, such as insertions, deletions, single nucleotide variants (SNVs), copy number variations (CNVs), chromosomal insertions or deletions (O'Roak et al., 2012b; Pinto et al., 2014; Yuen et al., 2016). The SNVs discovered through WES and WGS may result in *de novo,* rare-inherited mutations, or common variants (Iossifov et al., 2014; Krumm et al., 2014; Krumm et al., 2015; O'Roak et al., 2012b). The contribution of genetics in ASD is widely accepted, however it is largely debated whether *de novo* variants, rare inherited variants, or common gene variations contribute to the strongest risk for developing ASD (Ben-David and Shifman, 2012; Gaugler et al., 2014; Weiner et al., 2017). On one side of the argument, many researchers believe that *de novo* variants contribute more to the development of ASD, because since the variants appears in only the proband the penetrance of the *de novo* variant to cause ASD symptoms must indicate the strength and penetrance of the variant. Alternatively, a previous study estimated that the total risk of autism due to *de novo* mutations was merely 3%, whereas common gene variants comprised of around 50% of the risk for ASD (Gaugler et al., 2014; Robinson et al., 2016). The remaining risk of ASD

is attributed to unknown genetics, environmental factors and interactions between risk factors (i.e. rare and common variants). The large unaccounted risk of ASD reinforces the theory that risk genes may converge on multiple pathways that may be implicated in the disorder, and may attribute to a large portion of the risk for ASD and contribute to the heterogeneity of the disorder. The study of rare-inherited, and common gene variants poses a problem for the study of the etiology of ASD due to the lack of knowledge and understanding of the heterogeneous background.

Next generation sequencing technology has allowed us to develop algorithms to determine which genes are predicted to have stronger effects, or converge on certain signalling pathways known to be associated with ASD (Krishnan et al., 2016). These studies have identified many risk genes (for example, SH3 and multiple ankyrin repeat domains 2 (*SHANK2)* and neurexin-1-alpha *(NRXN1)* genes) and CNV loci (for example, 16p11 deletion and 15q11-13 duplication (Handrigan et al., 2013; Merico et al., 2015; Pagnamenta et al., 2009; Stefansson et al., 2008; Yu et al., 2012)). Multiple studies have investigated the common signalling pathways that have been discovered through WES and WGS, and have generate converging signalling networks that are associated with ASD, and other NDDs as well (McCarthy et al., 2014; Talkowski et al., 2012). For example, some of the signalling pathways associated with ASD, in which ASD-risk genes converge onto, are associated with synaptic signalling pathways (e.g. *SHANK3),* chromatin remodelling pathway *(e.g. CHD8)* and the Wnt signalling pathway (e.g. *Disrupted in schizophrenia-1* (*DISC1), β-catenin, Wnt1, PRICKLE2)*.

Many of the genes discovered through these studies have shown associations with multiple psychiatric disorders, and recent GWAS have shown that some of the SNPs conferring a risk for schizophrenia (SZ) also confer risk for ASD (Talkowski et al., 2012). In addition, studies showed that among monozygotic twins with ASD, the probability of being diagnosed with attention deficit hyperactivity disorder (ADHD) was 44% when compared to 15% for dizygotic twins (Lichtenstein, 2010). This increase in risk was seen with other psychiatric disorders as well, supporting the growing theory that there is cross talk between different psychiatric disorders. Considering the shared comorbidities of ASD with other psychiatric disorders, there is evidence that there are shared genetics between psychiatric disorders, such as bipolar disorder, schizophrenia, and depression (Cross-Disorder Group of the Psychiatric Genomics et al., 2013; Lichtenstein et al., 2010; Robinson et al., 2016). A recent study has also discovered that there are many shared patterns and gene-expression defects across multiple neuropsychiatric disorders, such as autism, schizophrenia, bipolar disorder, depression, and alcoholism (Gandal et al., 2018).

1.2.1 SFARI genes and Autism Speaks MSSNG project

The Simons Foundation Autism Research Initiative (SFARI) is an organization that aims for the better understanding, diagnosis and treatment of ASD. SFARI projects include cohorts of individuals with ASD from the Simons Simplex Collection and Simons Variation in Individuals Project. Due to the increasing number of ASD-risk genes discovered through next-generation sequencing, SFARI has developed a risk gene database, SFARI Gene, to distinguish the risk genes into 7 categories: syndromic,

category 1 (high confidence), category 2 (strong candidate), category 3 (suggestive evidence), category 4 (minimal evidence), category 5 (hypothesized), and category 6 (not supported) (Abrahams et al., 2013). The genes that are curated in this database include 722 scored genes, of which 125 are ASD-linked. An advisory board of geneticists rank genes based on a strict statistic criteria described by the database scores. The syndromic risk genes are genes that are implicated in idiopathic autism, such as *FMR1* in fragile X syndrome, and *UBE3A* in Angelman syndrome. High confidence (category 1) genes require recurrent and convincing mutations that display statistically significant mutation frequency compared to controls with genome-wide significance; these genes are also defined as "likely to be functional". There are currently 24 high confidence genes, which include: *CHD8*, *sodium channel, voltage-gated, type II, alpha subunit* (*SCN2A*), *SH3 and multiple ankyrin repeat domains 3* (*SHANK3*), and *phosphatase and tensin homolog* (*PTEN*). Strong candidate genes (category 2) must also follow similar criteria as high confidence genes, also with convincing and "likely functional" mutations, although rare *de novo* variants in three or more unrelated cases would be accepted for this category. Suggestive evidence genes and minimal evidence genes (category 3 and 4, respectively) include genes that do not meet the criteria for category 1 or 2, but include rare *de novo* variants in two or more cases (suggestive) or putative mutations that are not compared statistically to a control population (minimal) (Abrahams et al., 2013) (pfeliciano@simonsfoundation.org and Consortium, 2018).

Additionally, Dr. Stephen Scherer's laboratory at the Hospital for Sick Children (Toronto, CA) has recently developed a new resource in collaboration with Autism

Speaks (an organization focused on supporting research for better treatment of ASD, understanding ASD, and helping individuals with ASD and their families through advocacy and support) and Google, known as the Autism Speaks MSSNG Project (Yuen et al., 2017). This database contains whole-genome sequencing cohorts of ASD probands, father, mother, and sometimes affected or unaffected siblings (trios or quartets). To date, the whole-genome sequencing data from 2,620 probands, and 5,205 total people have been performed and uploaded onto this database that is available to the research community (Yuen et al., 2016; Yuen et al., 2015; Yuen et al., 2017). With the continual updates on additional fully sequenced data, this group has been able to complete further analysis of newly discovered *de novo* variants and CNVs (Yuen et al., 2017). The ultimate goal of the Autism Speaks MSSNG project is to discover and identify the different subtypes of ASD, which may facilitate more effective treatments of symptoms.

1.3 Pathophysiology of ASD

Although the etiology and pathophysiology of ASD remain largely unknown, ASD has previously been reported to be a critical-period disorder, where a number of ASD-associated risk genes played a role in early inhibition-excitation (E/I) balance (LeBlanc and Fagiolini, 2011). Others ASD risk genes that may affect development of auditory and somatosensory information processing may even cause defects in social interaction and communication, as observed in children with ASD (Delorme et al., 2013). Normal brain development is a very complex process that includes neurogenesis, neuronal migration, followed by the formation of complex synaptic connections

(Molyneaux et al., 2007). These processes take place during prenatal and early postnatal developmental periods, and disruptions at any of these stages of development may cause abnormalities in brain development and function, which can lead to ASD and other NDDs (Figure 1).

Previous studies have reported that an excess of neurogenesis may cause the increase in cerebral size, known as macrocephaly, in certain cases of ASD (Courchesne et al., 2011). Researchers reported an increase in 67% more neurons in the prefrontal cortex (PFC) of children with ASD compared to controls. In addition, children with heterozygous mutations in the high confidence gene *phosphatase and tensin homolog* (*PTEN*) are at risk for macrocephaly, while studies showed that *PTEN* plays an important role in neurogenesis and other later developmental periods as well (Chen et al., 2015b; Lugo et al., 2014; Page et al., 2009; Zhou and Parada, 2012). During neuronal migration, later-born neurons will migrate to the superficial layers of the cortex in what is known as the "inside-out" model of the cortex (Molyneaux et al., 2007). This process is tightly regulated, as neurons migrate along radial glia and change morphology as they reach their final position in the cortex. Disruption in certain genes involved in neuronal migration has also been associated with ASD. For example, *contactin-associated protein-like 2 (CNTNAP2)* gene is a strong candidate gene for ASD that is important for regulation of neuronal migration, and multiple variants in *CNTNAP2* have been discovered in patients with ASD and other NDDs (Gdalyahu et al., 2015; Penagarikano et al., 2011).

Genetic studies have also identified ASD-risk genes that play an important role of synaptic development, leading to the observed pathology of dendritic spine dysfunction seen in post mortem brain tissue and ASD animal models (Bourgeron, 2015; Comery et al., 1997; Ebrahimi-Fakhari and Sahin, 2015; Habela et al., 2016; Hotulainen and Hoogenraad, 2010; Huber et al., 2015; Hutsler and Zhang, 2010; Mullins et al., 2016; Penzes et al., 2011a; Shepherd and Katz, 2011; Volk et al., 2015). This theory was largely based on findings that multiple genes in syndromic forms of ASD; for example, Fragile X syndrome (*FMR1*), Rett Syndrome (*MECP2*), Angelman syndrome (*UBE3A*) and high-confidence risk genes that cause non-syndromic forms of ASDs (ex. the Shank and Neuroligin/Neurexin family of proteins) have important roles during synapse development, maturation, and maintenance (Bourgeron, 2015).

1.3.1 Neuroconnectivity

Many studies have focused on the study of neural connectivity as the underlying cause for ASD. The synapse is composed of several components: the presynaptic axon terminal, the synaptic cleft, and the postsynaptic dendritic spine located on the receiving neuron's dendrite. Briefly, an action potential arrives at the axon terminal, causing the synaptic vesicles filled with neurotransmitters to fuse with the plasma membrane and release its contents into the synaptic cleft. These neurotransmitters then bind to the receptors located on the postsynaptic membrane, clustered in a region known as the postsynaptic density in the dendritic spine, which ultimately leads to the propagation of the signal into the postsynaptic neuron (Bourgeron, 2015). Dendritic spines are actin-rich

protrusions from dendrites, where most excitatory synapses are formed (Hotulainen and Hoogenraad, 2010). During maturation, dendritic spines are highly dynamic and change morphology through the modulation of the actin cytoskeleton. Mushroom-shaped dendritic spines are associated with mature spines that will form a synapse and thin/filopodia and stubby spines are associated with an immature spine (Figure 3). Synapse formation and maturation is important for learning and memory, which has been reported to be disrupted in patients with ASD (Nimchinsky et al., 2002). Futhermore, A study involving proteomic analysis of postmortem ASD brains observed decreased levels of synaptic proteins such as syntaxin-1A (SYX1A) and synapsin-2 (SYN2) in the cerebellum, suggesting that altered synaptic connections may play a role in ASD pathology (Broek et al., 2014).

Early studies using post-mortem ASD brain tissue showed abnormal dendritic spine pathology in pyramidal neurons of the layer 2 cortex (Hutsler and Zhang, 2010). Other synaptic defects in neurons and dendritic spine pathology have been observed in post mortem brain tissue and animal models of ASD (Bourgeron, 2015; Penzes et al., 2011a). Many believe that exaggerated spine formation and/or incomplete pruning cause an increase in dendritic spines, observed in some postmortem ASD brains (Hutsler and Zhang, 2010; Penzes et al., 2011a). In some cases, ASD is hypothesized to result from hyperconnectivity in local circuits and hypoconnectivity between brain regions, attributing the pathology of ASD to the disconnection of brain regions (Geschwind and Levitt, 2007). This contributes to the theory that ASD is a disorder of connections in the brain.

Some of the most studied ASD-risk genes have been shown to play an important role in the regulation of synaptic formation, maturation and plasticity. Synaptic plasticity is the ability of a synapse to strengthen or weaken in response to changes in neuronal activity through synaptic strength and/or number (Bourgeron, 2015). *Neurexin 1 (NRXN1)* is a strong candidate gene that has been implicated in ASD and other disorders, such as intellectual disability (ID), schizophrenia (SZ), and bipolar disorder (BP) with the discovery of many rare variants in individuals with ASD (Ching et al., 2010; Kim et al., 2008). NRXN1 is a neuronal cell-surface receptor, localized to the presynaptic membrane, which regulates the recruitment of synaptic vesicles and bind neuroligins (NLGNs) located on the postsynaptic membrane (Dean et al., 2003). At the postsynaptic membrane, the Shank family of scaffolding proteins is localized at the postsynaptic density (PSD) (Figure 3A). *SH3 and multiple ankyrin repeat domains 3 (SHANK3)* and *SHANK2* are high confidence and strong candidate genes associated with ASD, respectively. Studies have identified *de novo* variants in both the *SHANK3* and *SHANK2* gene in separate individuals with ASD (Berkel et al., 2012; Guilmatre et al., 2014; Yi et al., 2016; Zhou et al., 2016). These proteins are important for protein-protein interactions within the PSD and regulate the growth and maturation of dendritic spines (Berkel et al., 2012; Durand et al., 2012).

1.3.2 Modeling autism spectrum disorder

Modeling ASD in animal models, through gene knockout (KO) or knock-in (KI) mutations, is important to determine the specific brain regions, and behaviours associated

with disruptions of a specific single gene. Additionally, these studies allow us to elucidate the important role that certain ASD risk genes play in synaptic and behavioural phenotypes that are associated with ASD and other NDDs. With the multiple theories attempting to discover the pathophysiology of ASD, there is a need to model the disorder to characterize these defects. Many of the emerging ASD-risk genes discovered through WES and WGS have demonstrated similar defects in phenotypes such as dendrite, dendritic spine morphology, synaptic function, and behaviours in animal models. For example, a mouse with a loss of the *FMR1* gene (known as Fragile X syndrome, an ASD caused by a single gene) showed an increase in dendritic spine density (Comery et al., 1997). Conversely, a mouse model lacking the postsynaptic protein, *SHANK2,* showed a decrease in dendritic spine density (Schmeisser et al., 2012). Although studies show opposing effects of ASD-risk genes, these studies have consistently shown abnormal dendritic spine formation and morphology.

Many studies use the gene KO or knockdown mouse model to demonstrate the importance of a single gene in brain development and the potential associated with ASD with loss of function mutations. Previous studies used RNAi technology to reduce the expression of their gene of interest (de Anda et al., 2012; Durak et al., 2015; Woolfrey et al., 2009); these studies were useful to further expand our understanding of specific genes in the role of neurodevelopment and its potential role in the pathophysiology of ASD. KO mouse models have been critical in establishing the importance of certain high confidence and strong candidate genes (Sowers et al., 2013a). For example, the *Shank2* KO mouse that demonstrated ASD-like behaviours (Schmeisser et al., 2012). Additionally, several

studies generate heterozygous deletion mice to better recapitulate the condition observed in humans. In many cases of ASD where researchers have identified disruptions in a risk gene, the disruption is discovered in only a single allele. This has led many researchers to develop ASD models that are more closely related to the human conditions using a heterozygous approach (Katayama et al., 2016; Uddin et al., 2018). A prominent gene that presents heterozygous mutations in multiple patients is CHD8 (Barnard et al., 2015; Krumm et al., 2015; McCarthy et al., 2014; Merner et al., 2016). Interestingly, these studies showed phenotypes associated with ASD despite the muted gene disruption (Katayama et al., 2016; Wang et al., 2015). These studies demonstrate a potential gene-dosage effect and are better models for future drug discovery. In addition, studies have generated mouse models that mimic the mutations found in human patients with ASD. A recent study compared the synaptic and behavioural effects of highly penetrant mutations in the *SHANK3* gene identified in ASD and SZ patients (Zhou et al., 2016). This study demonstrated the potential differences and similarities that different mutations in the same gene may cause different disorders. Researchers continue to model ASD mutations identified in children with ASD in mouse and human models (discussed in the next section), and show us that the specific mutation discovered in a gene of interest may dictate the severity of phenotypes and the resulting disorder.

An important advantage of mouse models within the field of neurodevelopmental disorder research is the ability to observe behavioural phenotypes. Although these behaviours are not the same as those observed in humans, this information is important for the manifestations of behavioural abnormalities that may be caused by disruptions of a

single or multiple genes, and the possible implications in the human disorder. As previously mentioned, the symptoms observed in children with ASD include deficits in social interactions and communication, and restrictive and repetitive behaviours (Miles, 2011). Children with ASD also tend to display other symptoms and behaviours such as aggressive behaviour, an increase of anxiety, and hypersensitivity to touch (Miles, 2011). These behaviours have been extensively studied in mouse models, and many ASD models demonstrate social deficits and repetitive behaviours, along with other behaviours associated with ASD and related disorders (Clipperton-Allen and Page, 2014; Dong et al., 2016; Kogan et al., 2015; Kwon et al., 2006; Peca et al., 2011; Sowers et al., 2013a; Zhou et al., 2016). For example, *Shank3* mutant mice demonstrated repetitive grooming and deficits in social interaction (Peca et al., 2011).

1.3.3 Modelling ASD in human neurons

Pluripotent human embryonic stem cells have been differentiated into multiple cell types found in the brain (Thomson et al., 1998), which has been beneficial within the field of neurpsychiatric disorders. With the discovery of human induced pluripotent stem cell (iPSC) technology (Takahashi et al., 2007), researchers have been able to generate human neurons derived from patients. These patient-derived neurons give us a lot of information about the disease, and can be potentially used for drug treatment. The caveat with this method is the heterogeneity of many of the diseases studied using iPS cells, patient-specific cell lines provide a lot of information about the single patient, however in diseases where the etiology remain unknown or varied, the information garnered from

these cells remain limited (Brennand et al., 2015). Multiple protocols have been developed to generate human cortical neurons from human embryonic stem (ES) and iPS cells (Shi et al., 2012a; Shi et al., 2012b). There are many different variations of protocols used to differentiate ES and iPS cells into cortical neurons. One of the most common protocols uses defined neural induction media through embryoid body (EB) formation (Shi et al., 2012a). Another method for neural differentiation includes the inhibition of transforming growth factor-β/SMAD signalling pathway (Chambers et al., 2009; Nguyen et al., 2011). A recent study by Zhang et al., demonstrated a new method for the rapid induction of excitatory neurons through the overexpression of a single transcription factor, *Neurogenin-2 (Ngn2)*, in only 2 weeks (Zhang et al., 2013). Since the publication of this work, other labs have adopted this rapid neural induction method to study human-derived neurons (Busskamp et al., 2014; Ho et al., 2016). There are other methods of differentiation to generate other cells found within the brain as well; for example, a differentiation protocol can be found to generate interneurons (Liu et al., 2013), sensory neurons (Boisvert et al., 2015), and motor neurons (Sances et al., 2016). Excitingly, there continues to be new protocols developed to generate different types of neurons (useful for looking at different disorders affecting different areas of the brain).

Early research using human iPS-derived neurons to study ASD utilized iPS cells derived from individuals with ASD. A group at Stanford generated iPS-derived neurons from individuals with Timothy's syndrome, caused by a point mutation in an alternatively spliced exon of *CACNA1C*, that encodes for the voltage-gated channel $Ca_v1.2$(Pasca et al., 2011). This study demonstrated that $Ca_v1.2$ is important for the regulation of cortical

neuron differentiation in humans. Naturally, many researchers set to recapitulate phenotypes observed in ASD mouse models in iPS-derived neurons. These studies have been important to validate the observations seen in mouse models, but have also highlighted the importance of a human-specific phenotype that cannot be seen in any mouse model (Farra et al., 2012; Pasca et al., 2011; Shcheglovitov et al., 2013). Additionally, with the introduction of CRISPR/Cas9 technology, gene editing has become a relatively cheap, fast, and efficient method to introduce SNVs, insertions or deletions (indels), into the genome (Qi et al., 2013; Ran et al., 2013a; Ran et al., 2013b). Researchers have generated control iPS cells (from a parent or sibling control), and induce a KO or a patient-specific mutation through a gene-editing technique. These isogenic cell lines are important because they also carry the disease-relevant background found in the specific patient. Multiple studies have generated heterozygous and full knockout iPS cell lines using CRISPR/Cas9 technology to further elucidate the role of specific ASD risk genes on neuronal morphology, synaptic phenotypes, and altered signalling networks (Hazelbaker et al., 2017; Wang et al., 2015; Yi et al., 2016). In addition to these experiments studying human iPS-derived neurons in a 2D-culture, researchers have developed protocols to generate 3-dimensional neuronal cultures known as cerebral organoid (Fatehullah et al., 2016; Quadrato et al., 2016; Wang et al., 2017).

Although the study of ASD and other neurodevelopmental disorders requires animal models for the observation of behavioural phenotypes, the human brain is vastly difference than smaller mammals. For this reason, it is necessary to measure morphological and functional phenotypes in human neurons that may better recapitulate

what is happening in the human brain. Additionally, human models allows for potential drug screens on human-derived cells, and in combination with mouse model validation is important for the discovery for novel drug treatments.

1.3.4 Wnt signalling-associated ASD models

The Wingless (Wnt) signalling pathway is a highly conserved pathway, crucial for embryonic development in most tissues of the body (Munji et al., 2011; Salinas and Zou, 2008). There is evidence from multiple studies that associate the Wnt signalling pathway with ASD (Oliva et al., 2013). Wnt signalling may be divided into two separate pathways: i) "canonical" signalling, which functions by inhibiting GSK3 phosphorylation of β-catenin, allowing for translocation into the nucleus and initiates transcription of target genes, and ii) "non-canonical" signalling, β-catenin-independent signaling (Salinas and Zou, 2008). Many of the proteins contributing to the Wnt signalling pathway are also found in the synapse and have been shown to play a role in synaptic formation and function (Budnik and Salinas, 2011; Caracci et al., 2016; Okerlund and Cheyette, 2011; Oliva et al., 2013; Purro et al., 2014; Stamatakou and Salinas, 2014). A summary of the Wnt signalling pathway is displayed in Figure 4.

CHD8 is a high confidence gene for ASD, also associated with other NDDs. Next-generation sequencing studies have discovered multiple *de novo*, truncating, or missense mutations in *CHD8,* mainly predicted to be loss of function mutations (Bernier et al., 2014; McCarthy et al., 2014; Neale et al., 2012; O'Roak et al., 2012a; O'Roak et al., 2012b; Sugathan et al., 2014; Talkowski et al., 2012). CHD8 functions as a transcription

repressor through remodelling of the chromatin structure, and as a binding partner of β-catenin (Subtil-Rodriguez et al., 2014). Recently, CHD8 has been shown to be important for proper cortical neural progenitor proliferation and differentiation into mature neurons (Durak et al., 2016). Additionally, *CTNNB*, which encodes for β-catenin, mutations have also been discovered in children with ASD (Krumm et al., 2014; O'Roak et al., 2012a; O'Roak et al., 2012b; Sanders et al., 2012). β-catenin is a core regulator of the canonical Wnt signalling pathway, and mutations in this gene may play an important role in the pathophysiology of ASD.

There are multiple ASD-associated animal models that have implicated Wnt signalling genes in the disorder. For example, *Disheveled 1*, and *3* (*Dvl1* and *Dvl3*) KO mice show ASD-related behaviours (Belinson et al., 2016; Lijam et al., 1997; Long et al., 2004); these genes are involved in the canonical Wnt signalling pathway. The non-canonical Wnt signalling gene, *Prickle2*, KO mouse model has also shown abnormal behaviours and neuronal morphological defects as well (Nagaoka et al., 2015; Sowers et al., 2013a; Sowers et al., 2013b). These studies are among a few of the current research interested in the association of Wnt signalling with ASD, and these studies indicate the importance of Wnt signalling in proper neural development and the potential of disruptions in this pathway to may result in neurodevelopmental disorder.

1.4 DIXDC1 is a regulator of brain development

1.4.1 DIX-domain containing 1

As previously mentioned, an increasing number of ASD-risk genes have been associated with the Wnt signalling pathway. One such gene is *DIX domain containing-1* (*DIXDC1*), a homolog of the Wnt signalling genes *Disheveled* and *Axin* (Wang et al., 2006). DIXDC1 is the human homolog of Ccd1 in zebrafish, which has been shown to be a positive regulator of the Wnt-TCF/LEF signalling pathway (Shiomi et al., 2003; Soma et al., 2006). DIXDC1 is a scaffold protein that has two distinct isoforms, isoform 1 (long isoform) contains three regulatory domains: a calponin homology domain (CH), coiled-coil domain, and a C-terminal disheveled and axin (DIX) domain, and isoform 2 (short isoform), which lacks the CH domain near the N-terminal region (Wang et al., 2006). The CH domain contains an actin-binding domain, and the coiled-coil domain is responsible for certain protein-protein interactions (Figure 5A).

The role of DIXDC1 in the brain remains poorly studied, however it is a known binding partner of Disrupted in schizophrenia 1 (Disc1), encoded by a risk gene associated with schizophrenia. The interaction between Dixdc1 and Disc1 showed that Dixdc1 is an important regulator of embryonic brain development (Namba and Kaibuchi, 2010; Singh et al., 2010). Dixdc1 regulates neural proliferation and neuronal migration via interaction through Wnt-dependent and Wnt-independent pathways, respectively (Singh et al., 2010) (Figure 5B). While Dixdc1 has been shown to regulate early neural development, its function in the postnatal brain remains unknown. During early postnatal development, there is active synapse formation and pruning; disruptions during this stage of development may cause the pathology of ASD. Little else is known of the role of DIXDC1 in the other tissues of the body. Although, the role of DIXDC1 in regulating the

Wnt signalling pathway has been demonstrated in certain cancers, such as non-small cell lung cancer and colon cancer (Goodwin et al., 2014; Wang et al., 2010; Xu et al., 2014b). This study also showed that DIXDC1 localized to focal adhesions (actin-rich regions) (Goodwin et al., 2014).

1.4.2 The Role of Dixdc1 in Wnt signalling

The role of Dixdc1 in neurodevelopmental disorders remains unknown, however the role of Dixdc1 has been studied in prenatal development. Dixdc1 is a known interactor with Disrupted in schizophrenia 1 (DISC1), a well-established schizophrenia risk gene. The interaction of Dixdc1 with Disc1 plays a role neural progenitor proliferation through the Wnt-GSK3b/b- catenin-dependent signalling pathway (Singh et al., 2010). In this pathway, the Dixdc1-Disc1 interaction regulates β-catenin through GSK3 inhibition. β-catenin stabilization through this interaction resulted in an increase in neural progenitor proliferation. In an alternative, Wnt-independent, pathway, this interaction played a role in neuronal migration. Briefly, Cdk5 phosphorylates Dixdc1, regulation the formation of a Disc1/Dixdc1/Ndel1 complex that regulates neuronal migration (Figure 5B).

Previous studies have also hypothesized that activation of DIXDC1 may be through the canonical Wnt/β-catenin signalling pathway in an unknown post-translational mechanism (Wang et al., 2010). A separate study showed that DIXDC1 promotes gastric cancer invasion through activation of the canonical Wnt signalling pathway (Tan et al., 2016). In this study, the overexpression of DIXDC1 led to the accumulation of β-catenin

in the nucleus, thus activating the Wnt signalling pathway. These studies support the role of DIXDC1 as a positive regulator of the Wnt signalling pathway.

1.4.3 Elucidating the Dixdc1 signalling network

As previously described, DIXDC1 is a known as a positive regulator of the canonical Wnt signalling pathway. Its role in the Wnt signalling pathway is demonstrated through evidence in human cancer studies that showed that DIXDC1 is activated by Wnt signalling, and play a role in cell invasion and metastasis (Goodwin et al., 2014; Tan et al., 2016; Wang et al., 2010). As previously mentioned, Dixdc1 is a known binding-partner of the scaffolding protein Disc1. This interaction is important for the regulation of neural proliferation and neuronal migration. These studies describe a Wnt signalling network for DIXDC1 during embryonic development and in tumorigenesis. The signalling networks surrounding DIXDC1 in later periods of development remain unknown and require further investigation. The STRING database is a database of known and predicted protein-protein interactions. These interactions are computed through laboratory experiments, genomic predictions, co-expression datasets, automated text-mining, and previous databases (STRING database). The interactions described include direction physical interactions, and indirect, functional interactions. The main DIXDC1 interactors mainly fall within the Wnt signalling pathway, and actin-associated proteins.

1.4.4 The role of DIXDC1 in ASD

The continual sequencing of whole genomes of children with ASD has led to an

increase in Wnt signalling genes identified with *de novo* and rare-inherited variants. *DIXDC1* has been identified as a gene that may be associated with ASD, with multiple rare-inherited variants discovered in children with ASD (Kwan et al., 2016; Martin et al., 2016). Additionally, a study demonstrated the effects of null expression of *Dixdc1* on behaviour in mice showing that this mutant mouse displayed abnormal behaviours, such as anxiety-like behaviours, abnormal locomotion and startle reactivity, suggesting its role in psychiatric pathophysiology (Kivimae et al., 2011).

Furthermore, our laboratory has published a paper in *Cell Report* demonstrating that DIXDC1 is a regulator of excitatory neuron dendrite development and synapse function. We described a pathway where MARK1 phosphorylates DIXDC1 to regulate dendrite and spine development through the actin polymerization pathway. Finally, through our collaboration with Dr. Stephen Scherer from SickKids hospital in Toronto, we identified rare missense variants in *DIXDC1* that inhibited the phosphorylation of DIXDC1 and also caused an impairment of dendrite and spine growth (Kwan et al., 2016). This publication will be described in Chapter 2 of this thesis. A separate laboratory also published an article showing similar dendritic and synaptic deficits in their *Dixdc1* KO model, and these phenotypes were rescued through lithium and glycogen synthase kinase-3 (GSK3) inhibitor treatment (Martin et al., 2016). They also identified rare inherited single nucleotide variants from autism patients and showed that some of the variants altered the canonical Wnt signaling activity. These two studies suggest DIXDC1 may play an important role in ASD through the regulation of neural connectivity.

1.5 High-throughput screening

1.5.1 History of high-content screening in neurons

High-throughput screening (HTS) is a platform used to discovery and test different drugs and/or small molecules in a common assay (Sharma et al., 2012). HTS is used to identify new drug targets ("hits") with the potential to cluster and identify functional biological pathways. Oe of the largest hurdles for developing high-throughput or high-content platforms is the high-content culturing of cells and high-throughput image acquisition. As previously mentioned, there is a need to discovery drug treatments to alleviate some of the symptoms displayed by children with ASD. The development of high-content platforms to phenotype patient-specific cells and potential rescue the phenotypes observed through drug treatment remains a goal within the field. However, previous attempts at HTS with neurons have had minimal applications and success. A previous study demonstrated a high-throughput screen of primary mouse excitatory neurons (which are generally easier to culture), and analysis was performed using automated microscopy and survival analysis (Sharma et al., 2012). Although survival analysis was successful, the efficiency and consistency of culturing primary mouse neurons remains an obstacle for a high-content screen.

As many of these platforms are developed for potential drug screenings to treat human diseases, many researchers are focused on developing these platforms using human cells. Researchers have used human iPSC-derived neurons, iCell Neurons, which are commercially available human neurons from Cellular Dynamics (Berry et al., 2015).

Multiple studies have used these commercially available neurons, due to the ease of culturing and species relevant phenotypes (Sherman et al., 2016; Sirenko et al., 2014). Despite the ease of culturing, the analyses performed in these studies remain simple. A recent study, although using primary neuronal cultures have developed a high-content platform to screen shRNAs to target specific synaptogenic to perform downstream analysis on excitatory and inhibitory synapses through immunostaining (Sharma et al., 2013). This work is promising, as many neurodevelopmental disorders have been associated with disruptions in neuron morphology and deficits in synapse formation and function (Berkel et al., 2012; Greer et al., 2010; Platt et al., 2017; Sowers et al., 2013a). Additionally, as we've previously described, many studies are now using iPS-derived neurons from patient samples or mimicking patient-specific mutations to study the pathophysiology associated with ASD and other NDDs (Farra et al., 2012; Forsingdal et al., 2016; Pasca et al., 2011; Wang et al., 2015). Therefore, the interest in finding drug treatments that may reverse the phenotypes observed in these different models of ASD remains a major area of research and interest.

1.5.2 Single transcription factor induction of human iPS cells into neurons

The discovery of iPS technology revolutionized research within the neuroscience field, where researchers are unable to obtain live human sample (from the brain), they were now about to convert patient cells into iPS cells, followed by induction into specific neuronal cell types (REF). Within the field of ASD research, researchers have become interested in the conversion of human stem cells derived from ASD patients or introduce

ASD-specific patient mutations into iPS cells through gene editing (Pasca et al., 2011; Shcheglovitov et al., 2013; Wang et al., 2015). In this way, the genetic diversity of ASD found between patients can be taken into account. However, the slow process and variability of cells generated through traditional iPS cell differentiation to neurons presents some problems. For example, in cases where researchers may be interested in a specific cell type, it still remains difficult to produce neurons of a single cell type, and the neurons generate through neuronal induction remain heterogeneous in nature. Studies that attempted to generate a homogenous neuronal population have only been able to produce neuronal purity of 15-80% purity (Hu et al., 2010; Wu et al., 2007)

Zhang et al. recently showed an approach to convert iPS cells into induced neurons (iN) using a single transcription factor, *Neurogenin-2* (*Ngn2*) (Zhang et al., 2013). This method allows for the rapid conversion of iPSCs into iN cells that readily form synapses and have been shown to form functional connections by 2 weeks in cultures, compared to the traditional 6-8 weeks (Ho et al., 2016; Zhang et al., 2013) (Figure 6). The researchers showed that the iN cells generated from this protocol produced relatively homogenous neuronal populations, which may allow for high-throughput imaging of these cells. Additionally, the population of neurons produced was positive for layer II/III cortical neuron markers, such as VGLUT2, and CUX1(Boccitto et al., 2016); neurons of layer II/III have been extensively studied for abnormalities in human and mouse ASD models. A recent study published by the Sudhof lab used the NGN2-induction method to generate human heterozygous *SHANK3* mutants associated with autism (Yi et al., 2016). *SHANK3* is a high confidence ASD risk-gene that has

multiple single-gene mutations associated with the disorder (Durand et al., 2012). This study generated human iPS-derived neurons and performed morphological, synaptic, and functional analysis. Specifically, they measured the changes in dendrite length, total branches, soma size, and synaptic puncta density and size. Researchers observed a decrease in totally neurite length, number of primary processes, totally number or branches, and synaptic puncta density (Yi et al., 2016). Excitingly, these observations were consistent with previous work published using *Shank3* heterozygous mouse models (Peca et al., 2011; Shcheglovitov et al., 2013; Zhou et al., 2016), which suggests that this NGN2-method may recapitulate phenotypes observed in mouse models and in other human iPS-derived neurons through traditional induction methods.

There are caveats to this method of neuron differentiation, for example the homogenous population of neurons does not recapitulate what is observed in human brains, with the network of cell signalling between all types of cells. Thus, the phenotypes observed using this model might not describe the whole picture. Despite this, the use of this method for iPS conversion into mature excitatory neurons has been used in increasingly more studies (Ho et al., 2016; Yi et al., 2016). With the many methods for human iPS conversion into neurons, researchers must decide within their model, which method suits the study best and how best to relate these results back to the human neurological disorder.

1.5.3 Drug treatments for ASD

There is currently no cure for ASD and other NDDs, and treatments to alleviate some of the symptoms of these disorders also remain scarce. There is one drug, Risperidone, which the Food and Drug Administration (FDA) has approved for treating ASD. Risperidone is an antipsychotic mediation that is prescribed to children with ASD to treat for irritability. There are several studies that have shown that Risperidone may reduce symptoms of irritability and lethargy from children with moderate to severe symptoms of ASD (Levine et al., 2016; Williams et al., 2006). Other drugs used to alleviate specific ASD symptoms are "off-label", meaning they were originally FDA-approved to treat other conditions. For example, selective serotonin re-uptake inhibitors (SSRIs), such as fluoxetine, have been prescribed to treat anxiety and depression in some children and adults with ASD (Doyle and McDougle, 2012). Naltrexone is another FDA-approved drug that was originally introduced to prevent alcohol and opiate addiction effects and has been shown, in some cases, to improve hyperactivity and restlessness (Doyle and McDougle, 2012). Many of these drugs do not work for everyone and may be associated with severe side effects. This highlights the need to find treatments that target specific pathways known to be dysregulated in ASD, that are safe to prescribe to children and with less side effects. There are many ongoing clinical trials that are testing the efficacy of different repurposed drugs. For example, Tideglusib is being tested to treat the core and associated symptoms of ASD (ClinicalTrials.gov, Identifier: NCT02586935). As a GSK-3 inhibitor, Tideglusib may suggest the importance and ability to target the Wnt signalling pathway for effective treatment of ASD symptoms. As previously discussed, there is a convergence of common signalling pathways associated with ASD, and this

may provide potential targets for drug treatment (Krishnan et al., 2016; Pinto et al., 2014; Voineagu et al., 2011).

Insulin-like growth factor 1 (IGF1) is a drug that many researchers are interested in for the treatment of children with ASD. IGF1 is a growth factor that regulates the development and cellular functions in neurons, glia, and other cells in the brain (Bianchi et al., 2017). A study looking at neurons derived from patients with the 22q13 deletion, Phelan-McDermid syndrome, showed that IGF1 treatment promoted the excitatory synapse formation, through potentially decreasing SHANK3 protein expression, *SHANK3* is a confidence ASD-risk gene, and increasing PSD95 presence in neurons (Shcheglovitov et al., 2013). In a separate study, treatment of *Mecp2* mutant mice, Rett syndrome model, with recombinant IGF1 improved behavioural phenotypes and excitatory synaptic deficits (Castro et al., 2014). Although IGF1 is not FDA-approved, IGF1 is a drug of interest because it has been heavily studied in other clinical trials, and may suggest the synaptic signalling pathway as a "druggable" pathway for future clinical trials (Delorme et al., 2013).

1.6 Thesis objectives

The overall objective of my PhD thesis was to characterize the role of DIXDC1 on the pathophysiology of ASD and the development of a high-content platform for the characterization of ASD-associated phenotypes. The first goal of my PhD project was to determine the role of DIXDC1 in postnatal brain development, through characterization of neuronal morphology (dendritic growth and dendritic spine growth and maturation).

We determined that phosphorylation of Dixdc1 isoform 1, by MARK1, regulates neuronal morphology through actin and microtubule cytoskeletal dynamics. Additionally, in collaboration with Dr. Stephen Scherer (Hospital for Sick Children, Toronto), we demonstrated that ASD-associated rare-inherited variants in *DIXDC1* impair phosphorylation and dendrite and dendritic spine development. These results were published in *Cell Reports* in the fall of 2016. This majority of the experiments in this study were performed by me, with assistance as stated in the Preface of Chapter 2. We next wanted to further elucidate the mechanism in which DIXDC1 exerts its observed effects during embryonic (Singh et al., 2010), and postnatal development (Kwan et al., 2016; Martin et al., 2016). To do this, we performed RNA sequencing on RNA extracted from embryonic and young adult mouse cortices. We developed an RNA-Seq pipeline to identify differentially expressed genes and perform gene set enrichment analysis (GSEA). We discovered differentially expressed genes in the *Dixdc1* KO brain, and specific pathways that were altered during different times during development. The experiments were performed by me, and I performed analysis on RNA sequencing reads with assistance from Dr. Nicholas Holzapfel.

The last goal of my PhD was to develop a high-content phenotyping platform to image cultured human iPS-derived neurons in a 96-well format. The goal of this project was to culture human neurons, derived from ASD iPS cell lines, in a 96-well format in order to image, identify and analyze synaptic protein markers. The long-term goal of this workflow is to create a system where we are able to quickly culture, phenotype neurons, and potentially rescue effects through drugs or gene re-expression. After extensive

optimization and standardization of this protocol, we are able to observe certain changes in synaptic markers and neurite growth, however further research must be performed to detect robust and subtle changes. This system is important to streamline the study of the ever-emerging ASD risk genes. I optimized the culturing and immunostaining protocol, with assistance on analysis from Dr. Tony Collins, and iPS cell lines generated by Dr. Eric Deneault.

The three aims laid out for my PhD thesis were to (1) determine the role of DIXDC1 in postnatal brain development and in the pathophysiology of ASD, (2) investigate altered and differential gene expression of *Dixdc1* KO mice to further elucidate a signalling network, and (3) to develop a high-content imaging platform to of human iPS-derived neurons to phenotype dendritic and synaptic deficits in ASD models.

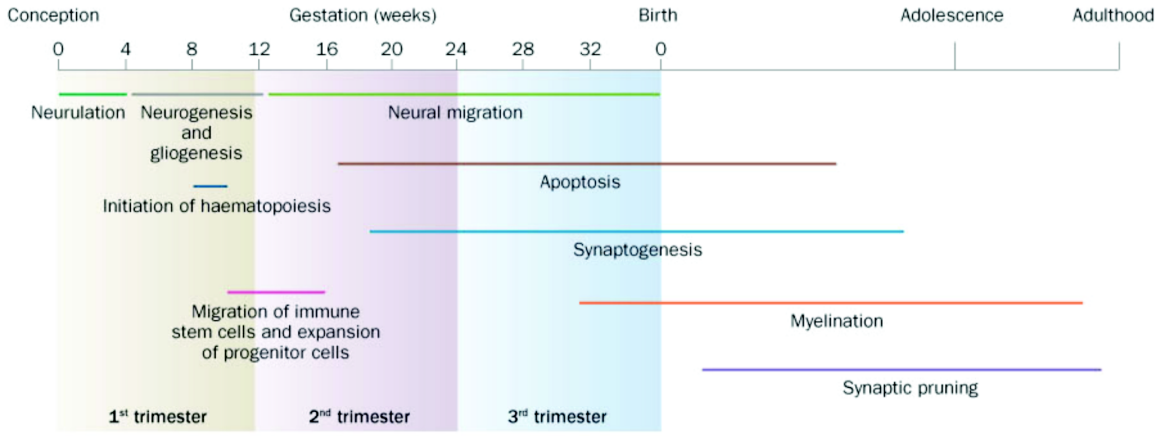

Figure 1: Schematic of human brain development. Periods of neurodevelopment from gestation to adolescence and early adulthood are highly regulated. Neurogenesis and neural migration are completed during gestation, and synaptogenesis and synaptic pruning begin during gestation and end during postnatal development (Figure adapted from Knuesel et al. (2014)).

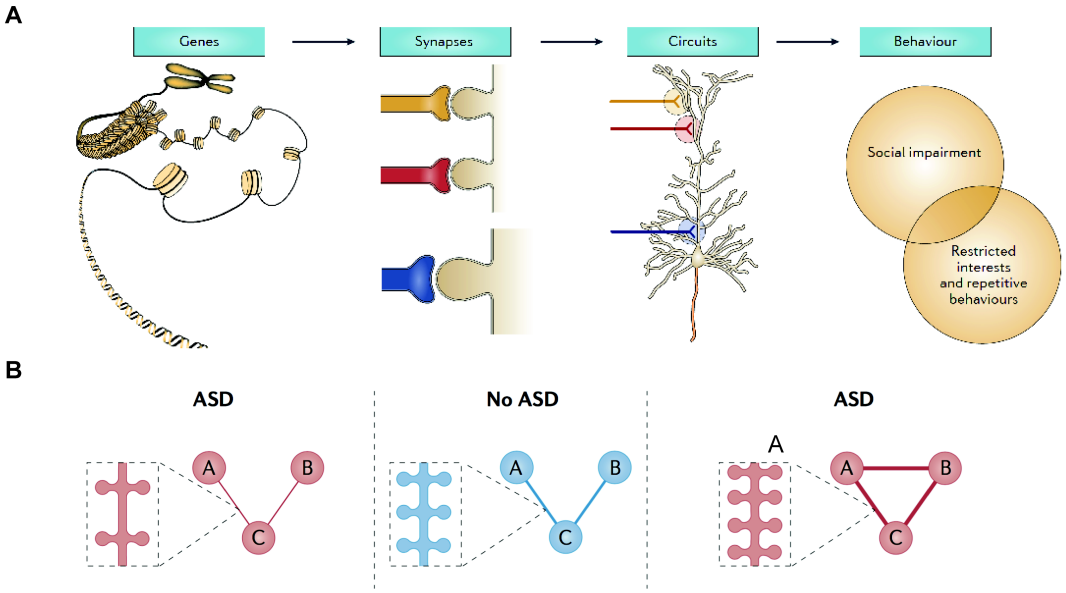

Figure 2: The role of synaptic plasticity in autism spectrum disorder. (**A**) Many genetic mutations that converge on synaptic molecular pathways have been associated with ASD. These mutations may be responsible for deficits in synaptic formation, neuronal circuits, and behavioural phenotypes. Figure adapted from Ghosh et al. (2013). (**B**) Mutations in ASD-associated genes may cause an increase or decrease synaptic strength and connections. Figure adapted from Bourgeron (2015).

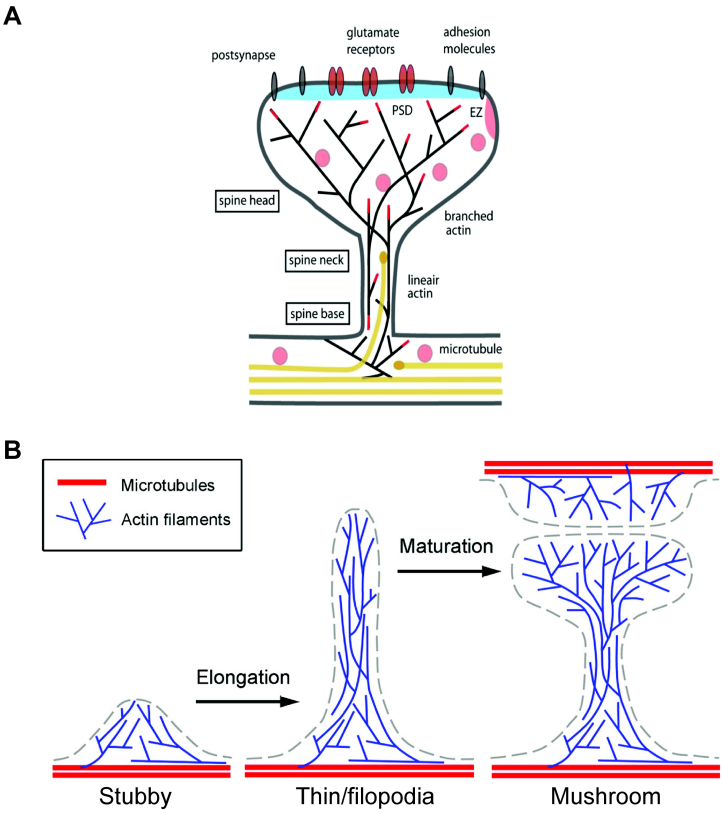

Figure 3: Dendrites and dendritic spines are important for neural connectivity. (**A**) Schematic diagram of a mushroom-shaped dendritic spine with microtubule and actin structures, showing the postsynaptic density (PSD). Figure from Hotulainen and Hoogenraad (2010). (**B**) Dendritic spine morphology is dynamic, and actin form linear and branched filaments to modify the structure of the dendritic spine. Figure from Korobova and Svitkina (2010).

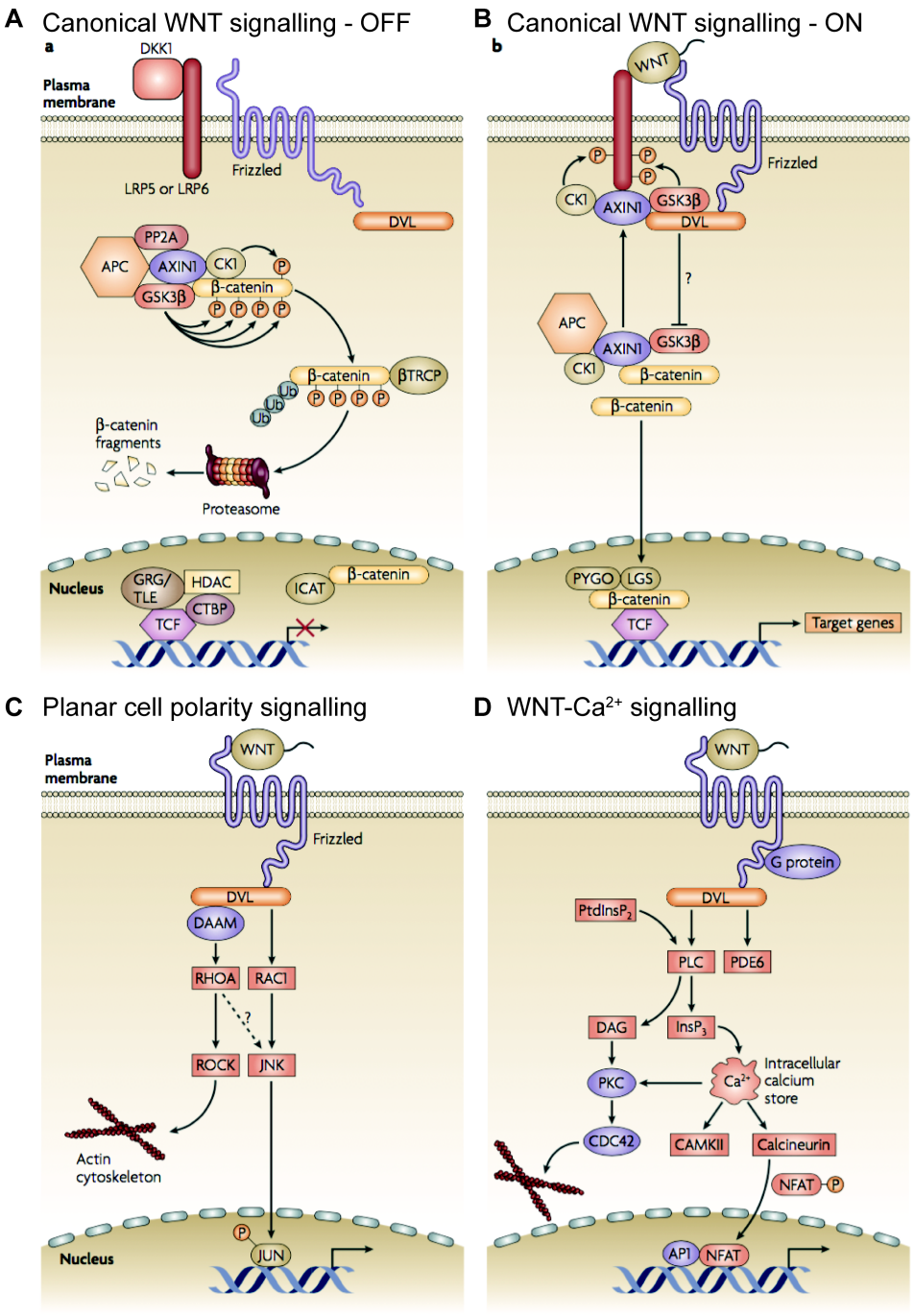
A Canonical WNT signalling - OFF
a
DKK1
Plasma membrane
LRP5 or LRP6
Frizzled
DVL
PP2A
APC
AXIN1
CK1
GSK3β
β-catenin
βTRCP
Ub
β-catenin fragments
Proteasome
Nucleus
GRG/TLE
HDAC
CTBP
TCF
ICAT
B Canonical WNT signalling - ON
b
WNT
Frizzled
CK1
AXIN1
GSK3β
DVL
APC
β-catenin
PYGO
LGS
Target genes
C Planar cell polarity signalling
WNT
Plasma membrane
Frizzled
DVL
DAAM
RHOA
RAC1
ROCK
JNK
Actin cytoskeleton
Nucleus
JUN
D WNT-Ca2+ signalling
WNT
G protein
DVL
PtdInsP2
PLC
PDE6
DAG
InsP3
PKC
Ca2+
Intracellular calcium store
CDC42
CAMKII
Calcineurin
NFAT
AP1
NFAT

Figure 4: Summary of the canonical and non-canonical Wnt signalling pathways. (**A**) For the canonical Wnt signalling pathway, in the absence of a Wnt ligand, β-catenin is phosphorylated in the cytoplasm by casein kinase 1 (CK1) and glycogen synthase kinase 3 (GSK3), leading to the ubiquitylation and degradation by the proteasome. CK1 and GSK3 make up the destruction complex, including axis inhibition protein 1 (AXIN1) and adenomatous polyposis coli (APC). (**B**) Upon Wnt ligand binding to the Frizzled receptor complex, the destruction complex is inactivated and β-catenin accumulates in the cytoplasm and translocates into the nucleus. In the nucleus, β-catenin binds to T-cell factor (TCF) and lymphoid enhancer factor (LEF) transcription factors to recruit co-factors to begin transcription. (**C**) Planar cell polarity (PCP) signalling does not involve β-catenin, and functions through the activation of small GTPases RAS homologue gene-family member A (RHOA), activating Jun N-terminal kinase (JNK) and RHO-associated coiled-coil-containing protein kinase 1 (ROCK), which leads to the regulation and remodeling of the cytoskeleton and changes in cell adhesion. (**D**) The Wnt/Ca^{2+} signalling pathway is regulated by G proteins and phospholipases, and results in an increase in free calcium in the cytoplasm. This increase in calcium activates protein kinase C (PKC), calcium calmodulin mediated kinase II (CAMKII), and calcineurin; this results in the activation of nuclear factor of activated T cells (NFAT). Figure from Staal et al. (2008).

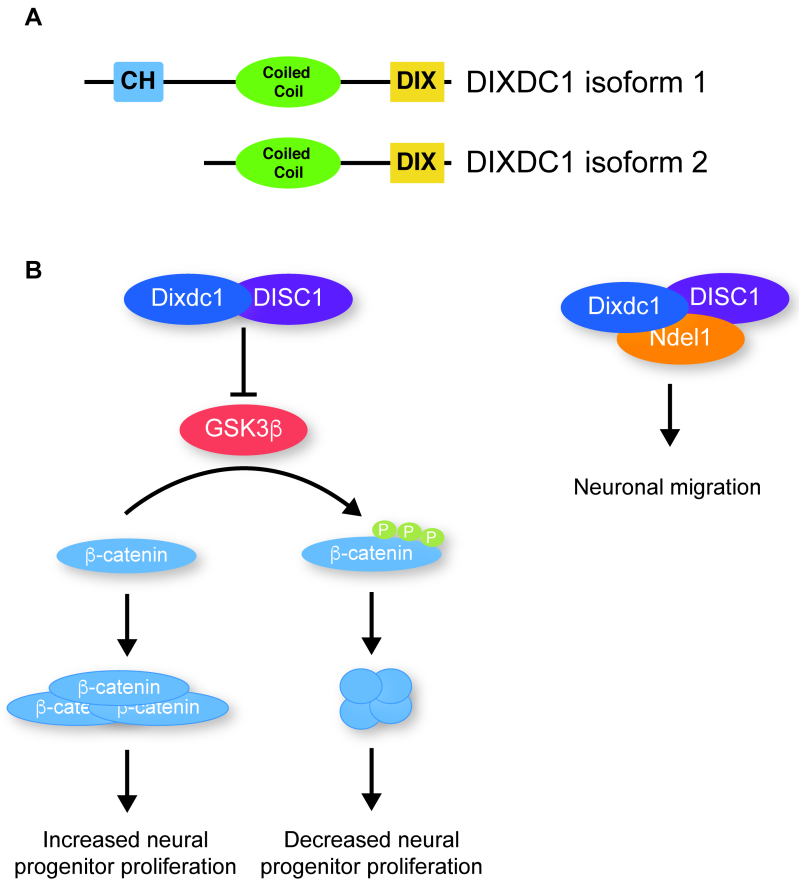

Figure 5: Dixdc1 is a regulator of embryonic development in the mouse brain. (**A**) Schematic of isoform 1 and 2 of the Dixdc1 protein with three functional domains: calponin homology (CH), coiled-coil and DIX. (**B**) Diagram of the role Dixdc1 and DISC1 interaction in neural progenitor proliferation and neuronal migration. Dixdc1 and DISC1 interaction inhibits GSK3b, preventing the degradation of b-catenin, resulting in increased neural progenitor proliferation. The interaction of Dixdc1, DISC1 and Ndel1 is important for proper neuronal migration, in a Wnt-independent pathway. Figure adapted from Singh et al. (2010).

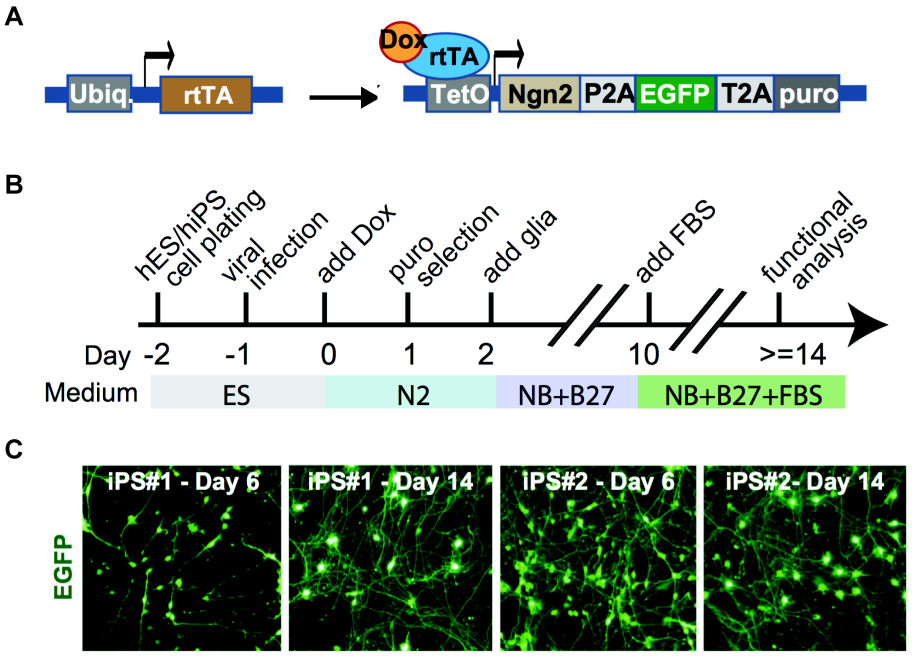

Figure 6: Rapid single-step generation of human iPS-derived induced neurons. (**A**) Design of lentiviral vectors for Ngn2-mediated conversion of ESCs and iPSCs to iN cells. Cells are transduced with (1) a virus expressing rtTA and (2) a virus expressing an NGN2/EGFP/puromycin resistance gene as a fusion protein linked by P2A and T2A sequences. (**B**) Timeline describing induced neuron generation, from viral infection to functional analysis. (**C**) Representative images of induced neurons differentiated from two different human iPS cell lines at day 6 and day 14. Figure adapted from Zhang et al. (2013).

CHAPTER 2: DIXDC1 PHOSPHORYLATION AND CONTROL OF DENDRITIC MORPHOLOGY IS IMPAIRED BY RARE GENETIC VARIANTS

Kwan, V., Meka, D.P., White, S.H., Hung, C.L., Holzapfel, N.T., Walker, S., Murtaza, N., Unda, B.K., Schwanke, B., Yuen, R.K.*, et al.* (2016). DIXDC1 Phosphorylation and Control of Dendritic Morphology Are Impaired by Rare Genetic Variants. Cell reports *17*, 1892-1904.

AUTHORS

Vickie Kwan, Durga Praveen Meka, Sean White, Claudia L. Hung, Nicholas T. Holzapfel, Susan Walker, Nadeem Murtaza, Brianna Unda, Birgit Schwanke, Ryan K.C. Yuen, Kendra Habing, Chloe Milsom, Kristin Hope, Ray Truant, Stephen W. Scherer, Froylan Calderon de Anda, and Karun K. Singh

PREFACE

This manuscript was published in *Cell Reports,* on November 8, 2016. This project was designed by Vickie Kwan and Dr. Karun K. Singh. The majority of the experiments were performed and data collected by Vickie Kwan, with assistance from Nicholas Holzapfel, Nadeem Murtaza, Dr. Chloe Milsom, Kendra Habing, and Brianna Unda. Durga Praveen Meka performed cytoskeleton dynamic experiments. Dr. Sean White performed electrophysiology experiments, and Dr. Susan Walker, and Dr. Ryan Yuen performed genetic sequencing and analysis. All of the data was analyzed, interpreted, and figures were generated by Vickie Kwan. The manuscript was written by Vickie Kwan and Dr. Karun K. Singh.

We would like to thank Dr. Reuben Shaw (Salk Institute for Biological Sciences) for generously providing reagents to test the phosphorylation of DIXDC1. This work was supported by grants to K.K. S. (Natural Sciences and Engineering Research Council, Bickell Medical Foundation, Scottish Rite Charitable Foundation, Krembil Foundation, Brain Canada Platform Support Grant, and the Ontario Brain Institute (OBI)), S.W.S. (OBI, Canadian Institutes of Health Research (CIHR)), K.J.H (CIHR and the Ontario Institute of Cancer Research) and R.T. (CIHR, Krembil and CHDI Foundations).

2.1 ABSTRACT

The development of neural connectivity is essential for brain function, and disruption of this process is associated with Autism spectrum disorders (ASDs). DIX domain containing 1 (*DIXDC1*) has previously been implicated in neurodevelopmental disorders, but its role in postnatal brain function remains unknown. Using a knockout mouse model, we determined that DIXDC1 is a novel regulator of excitatory neuron dendrite development and synapse function in the cortex. We discovered that MARK1, previously linked to ASDs, phosphorylates DIXDC1 to regulate dendrite and spine development through modulation of the cytoskeletal network, in an isoform-specific manner. Finally, rare missense variants in *DIXDC1* were identified in ASD patient cohorts using genetic sequencing. Interestingly, the variants inhibit DIXDC1 isoform 1 phosphorylation causing impairment to dendrite and spine growth. These data reveal that DIXDC1 is a novel regulator of cortical dendrite and synaptic development, and provide mechanistic insight into morphological defects associated with neurodevelopmental disorders.

2.2 INTRODUCTION

Dendritic spines are the primary sites of excitatory synaptic inputs and are necessary for cognitive function (Ebert and Greenberg, 2013; Jeste and Geschwind, 2014; Penzes et al., 2011a). The importance of dendritic spines is revealed by their functional disruption in individuals with Autism Spectrum Disorders (ASDs) (Tang et al., 2014). Human genetic studies of ASDs have uncovered mutations in multiple synaptic genes (Chen et al., 2015a; De Rubeis et al., 2014; Geschwind and State, 2015; Iossifov et al., 2014), and

synaptic deficits are observed in multiple genetic mouse models of ASDs (Bhakar et al., 2012; Sudhof, 2008; Volk et al., 2015). One of the downstream mechanisms causing synaptic dysfunction is disruption to the cytoskeletal network (De Rubeis et al., 2013; Dolan et al., 2013; Duffney et al., 2013; Durand et al., 2012; Han et al., 2013; Hori et al., 2014; Lin et al., 2015), which can be reversed by pharmacologically targeting cytoskeletal signaling in some mouse models of ASDs, suggesting a potential therapeutic option to restore synaptic function (Dolan et al., 2013; Duffney et al., 2015; Huang et al., 2013). The integrity of the cytoskeleton is essential for synapse development and plasticity, as alterations to the dynamic nature of actin and tubulin impairs synapse function including dendritic spine formation and stability (De Rubeis et al., 2013; Gu et al., 2010; Lei et al., 2016; Muhia et al., 2016; Murakoshi et al., 2011; Um et al., 2014; Woolfrey and Srivastava, 2016).

There is emerging evidence that Wingless (Wnt) signaling is also linked to ASDs and psychiatric disorders. This is supported by the identification of mutations in genes that modulate the Wnt pathway (Cao et al., 2012; Kalkman, 2012; Krumm et al., 2014; Martin et al., 2013; Okerlund and Cheyette, 2011; Wilkinson et al., 2011). Corroboration from genetic mouse models or human iPS cell models strengthen the notion that altered Wnt signaling can cause disease phenotypes (Brennand et al., 2011; Fang et al., 2014; Ishizuka et al., 2011; Mohn et al., 2014; Okerlund et al., 2010; Sowers et al., 2013a; Srikanth et al., 2015; Topol et al., 2015). The Wnt and synaptic signaling pathways also intersect, suggesting convergence onto one of many common disease-signaling networks. There are many examples of Wnt signaling molecules that play a dual role at the synapse (Ciani et

al., 2015; Okerlund et al., 2010; Sowers et al., 2013a; Turner et al., 2015); examples include Disheveled-1 or Dact1 that stimulate JNK and Rac signaling to induce dendrite/synaptic growth, and β-catenin can directly stimulate synaptic growth (Okerlund et al., 2010; Yu and Malenka, 2003). Furthermore, Disrupted in Schizophrenia 1 (*DISC1*), Ankyrin G (*ANK3*), and Adenomatous polyposis coli (*APC)* regulate canonical Wnt signaling and also synapse plasticity (Hayashi-Takagi et al., 2014; Hayashi-Takagi et al., 2010; Mao et al., 2009; Srikanth et al., 2015; Wen et al., 2014). These studies indicate that Wnt signaling molecules have important local roles at the synapse during postnatal development, in addition to their role in canonical Wnt/β-catenin-mediated transcriptional activity.

The link between Wnt signaling and ASDs prompted us to study if *DIXDC1* regulates the development of neural connectivity. DIXDC1 regulates embryonic neural progenitor cell proliferation via Wnt/β-catenin signaling, and cerebellar axonal growth through c-jun kinase (JNK) signaling (Ikeuchi et al., 2009; Shiomi et al., 2005; Shiomi et al., 2003; Singh et al., 2010; Soma et al., 2006). However, whether DIXDC1 plays a role in postnatal dendrite and synapse development, and the mechanism by which this occurs, remains unknown. DIXDC1 is linked to psychiatric disorders due to binding to DISC1 (Singh et al., 2010), and preliminary characterization of a *DIXDC1* knockout (KO) mouse model displays behavioral deficits consistent with psychiatric behaviors (Kivimae et al., 2011). Since DIXDC1 expression in newborn postmitotic neurons is associated with the cytoskeleton (Singh et al., 2010; Wu et al., 2009), it may regulate dendrite and synapse development in a local manner. In this regard, DIXDC1 can be phosphorylated and

recruited to actin-rich focal adhesions by MAP/microtubule affinity-regulating kinase 1 (MARK1) in human osteosarcoma cell lines (Goodwin et al., 2014). MARK1 is a polarity protein (also known as Par-1c) that regulates hippocampal synaptic growth and function (Wu et al., 2012). Interestingly, MARK1 was previously characterized as a susceptibility gene for ASDs (Maussion et al., 2008), suggesting it may partner with DIXDC1 to regulate synaptic development in the normal brain and play a role in ASD disease pathology.

Given these observations, we explored whether DIXDC1 regulates postnatal cerebral cortex development. We found that DIXDC1 regulates cortical excitatory dendrite and dendritic spine growth. Specifically, phosphorylation of a key C-terminal residue in both isoforms of DIXDC1 by MARK1 is required for dendrite and spine growth; however, the direct modulation of the cytoskeleton was primarily mediated by DIXDC1 isoform 1, suggesting isoform 2 signals through a different pathway. We also identified inherited, rare missense variants in *DIXDC1* from genetic sequencing of ASD patient cohorts and discovered they reduce phosphorylation of DIXDC1 isoform 1, resulting in impaired actin dynamics and neuronal morphology. Together, our data reveal that a novel MARK1-DIXDC1 signaling network is important for mammalian dendrite and synaptic development. Additionally, these data mechanistically outline how rare genetic variants in *DIXDC1* may contribute to disease susceptibility by disrupting neuronal morphology during brain development.

2.3 MATERIALS AND METHODS

Generation of *DIXDC1* knockout mouse and animal experiments

The *DIXDC1* KO mouse was generated by the Knockout Mouse Phenotyping Consortium (KOMP) at the Jackson Laboratory. Briefly, the ZEN-UB1 Velocigne cassette was inserted into DIXDC1 replacing all the coding exons and intervening sequences. The construct was introduced into C57BL/6N-derived VGB6 embryonic stem (ES) cells, and were injected into B6(Cg)-Tyr^{c-2J}/J blastocysts. The resulting chimeric males were bred to C57BL/6NJ females and then to B6N.Cg-Tg(Sox2-cre)1Amc/J to remove neo cassette. All mice were bred and maintained in the Animal Facility at McMaster University. All procedures received the approval of the Animal Research Ethics Board at McMaster University.

Rat experiments were performed according to the German and European Animal Welfare Act and with the approval of local authorities of the city-state Hamburg (Behörde für Gesundheit und Verbraucherschutz, Fachbereich Veterinärwesen) and the animal care committee of the University Medical Center Hamburg-Eppendorf.

Plasmid constructs and biological materials

Plasmids: pCAGIG-Venus were provided by Dr Zhigang Xie (Boston University, MA). ASD-linked DIXDC1 variants, hDIXDC1-WT (isoform 1), hDIXDC1-V43M and hDIXDC1-T612M, were generated by GeneArt® Gene Synthesis (Life Technologies) and inserted into pcDNA3.3 (Life Technologies). hDIXDC1-S592A (isoform 1) and MARK1-WT and -T215A constructs were provided by Dr. Reuben Shaw (The Salk

Institute, San Diego, CA). The cDNA of hDIXDC1-WT isoform 2 (GE Dharmacon) was PCR amplified and inserted into pcDNA3.3. hDIXDC1-S381A and -T401M (isoform 2) mutations were generated using In-Fusion Cloning Plus Kit (Clontech). C-terminal GFP-tagged DIXDC1 constructs: hDIXDC1-WT, -S592A (isoform 1) or hDIXDC1-WT, -S381A (isoform 2) and eGFP were PCR amplified using PrimeSTAR Max DNA polymerase (Clontech). hDIXDC1 PCR products, eGFP were inserted into pcDNA3.3 using In-Fusion Cloning Plus Kit. The sequences for shRNAs targeting DIXDC1 are as follows: control shRNA: 5'-CGGCTGAAACAAGAGTTGG-3', DIXDC1 shRNA #2: 5'-CTAAGAGCGAATCCATTAT -3', the DIXDC1 #1 (DIXDC1 3'UTR) shRNA was obtained from the Broad Institute RNA interference platform: 5'-GCCTATCTCATCGAGATTGTT -3'. Lifeact-GFP and EB3-mCherry were provided by F. Bradke (DZNE, Bonn, Germany).

Antibodies: goat anti-mouse Ccd1/DIXDC1 (dilution, 1:500; R&D systems, AF5599, RRID: AB_2091196), β-actin (dilution 1:1000; Sigma, clone AC-15), PSD-95 (dilution 1:1000; Antibodies Incorporated, 75-028, RRID: AB_2292909), synaptophysin (1:1000; Sigma, clone SVP-38), α-tubulin (dilution 1:1000, Cell Signalling, 2125S, RRID: AB_823663), acetylated tubulin (dilution 1:1000, Sigma, clone 6-11B-1, RRID: AB_823663), MAP2 (dilution 1:1000; Sigma, clone AP-20), MAP2 (dilution 1:200, Sigma, M3696), phospho-Ser592 DIXDC1 (dilution 1:100; gift from Cell Signaling Technologies), anti-mouse MARK1 (dilution 1:1000; Proteintech Group Inc., 21552-1-AP, RRID: AB_10732726), and anti-human MARK1 (dilution 1:1000, Cell Signaling

Technologies, #3319, RRID: AB_2140604), GFP (dilution 1:1000; Aves lab inc., 1020) were used in western blot and immunostaining assays.

Primary neuronal cultures

High-density cortical neuron cultures were prepared from *DIXDC1* KO mouse, C57BL/6 (Charles River) or CD-1 (Charles River) mouse E16 embryos (as indicated) as described previously (Johe et al., 1996). Briefly, collected cortices were collected in HBSS and pooled, and cells were digested in a papain solution (Worthington biochemical) containing DNAse I (Sigma) for 20 minutes at 37°C. Cells were dissociated through triturating and strained, followed by counting of live cells (Countess). Cells were plated at a density of 5-7.5 x 10^5 cells per well onto coverslips coated with poly-D-lysine (0.11 mg/mL, BD Sciences) and laminin (Sigma) in 12-well plates, in plating media (Neurobasal media, NB (Invitrogen) + 10% FBS (Gibco) + penicillin/streptomycin (Invitrogen), glutamine). After 1.5 h, media was changed to culturing media (NB + B27 (Invitrogen) + Pen/Strep, L-glutamine (Invitrogen)). Cultures were treated with 1μM cytosine arabinose (Ara-C) (Sigma) at DIV3/4.

Rat hippocampal neuronal cultures and transfections

Isolated hippocampi (from E18 embryos) were triturated in 1xHBSS (Invitrogen) after digested by papain and DNase for 10 min at 37°C (Worthington). Transfections were performed using the Amaxa Nucleofector system following the manufacturer's manual. For each transfection, 5 x 10^6 cells and 3 μg of DNA mix were used. For co-transfections,

the concentration of pcDNA3.3 control, DIXDC-1 long form Wt, DIXDC-1 S592A, DIXDC-1 short form Wt or DIXDC-1 S381A expressing plasmids was kept 4-fold higher than that of Lifeact-GFP in the DNA mix. After electroporation, neurons for time-lapse imaging, were plated on poly-L-lysine coated tissue culture chamber (Sarstedt) in Neurobasal/B27 medium (Invitrogen), maintained in culture for 18-24 hours at 37°C with 5% CO_2.

Plasmid transfections

Primary neuronal cultures (DIV7) were transfected with 1 µg of appropriate DNA plasmid for 6 hours in Neurobasal medium in the presence of Lipofectamine LTX according to the manufacturer's protocol (Life Technologies). Medium was changed to conditioned medium after 6-hour incubation period. HEK 293FT cells were grown to 40-60% confluence in Dulbecco's modified Eagle's medium with 10% fetal bovine serum and penicillin/streptomycin. Cells were transfected with appropriate DNA in DMEM without antibiotics using Lipofectamine 2000 according to manufacturer's protocol (Life Technologies). Cells were ~95% confluent at the time of harvesting.

Jasplakinolide treatment

DIV14 primary neuronal cultures were treated with 1µM jasplakinolide, JPK (Millipore, 420107) 2 hours prior to fixation. Briefly, 5µL of 0.1mM JPK was added to 450µL of media (5µL DMSO added to controls). Cells were incubated at 37°C for 2 hours and fixed with 4% formaldehyde for 15 minutes at room temperature.

Trans-synaptic labeling of primary cortical neurons

Primary neuronal cultures (DIV7) were transfected with HTB vector and shRNAs using Lipofectamine LTX. Cultures were infected with modified rabies virus at DIV10 and fixed with 4% formaldehyde at DIV14 for analysis.

Viral construction and packaging

Short hairpin sequences for RFP (5'-GTGGGAGCGCGTGATGAAC -3'), DIXDC1 shRNA #2 (5'-CTAAGAGCGAATCCATTAT-3') and DIXDC1 #1 (3'UTR) (5'-GCCTATCTCATCGAGATTGTT -3') were cloned into the shRNA vector H1GIP (Hope Lab). The Lentiviral shRNA was prepared as described in Ichim *et al.* (2011). Briefly, LV shRNA RFP, DIXDC1 shRNA #1 and DIXDC1 shRNA #2 was generated by Lipofectamine 2000 (ThermoFisher Scientific) transfection of H1 shRNA hairpin vector, psPAX2 (packaging), pMD2.G (envelope) into HEK293FT cell line. At 60h after transfection, supernatants were collected was centrifuged at 25000rpm for 2 hours. Following centrifugation, media was discarded and the viral pellet was resuspended in PBS.

Intracranial injections in to postnatal mice

At postnatal day 3 (P3), CD-1 mice (Charles River) were collected and anaesthetized using isoflurane for 30 seconds. Using a micropipette, 2-3 μL of lentivirus was manually injected (piercing the cranium) approximately half way between the eye and ear and just off the midline. Mice were harvested at P21 and fixed in 4% paraformaldehyde for 48

hours. 50 μm sections were cut using a vibratome (Leica) and collected in PBS. Brain slices were then mounted onto Superfrost Plus adhesion slides (Thermo Scientific) and underwent the staining procedure (as described above).

Golgi staining of mouse brains

DIXDC1 KO mice were generated by the Knockout Mouse Phenotyping Program (KOMP) at The Jackson Laboratory. Golgi staining was performed on P30 DIXDC1 KO and wildtype C56BL/6J mice brains as described (FD Rapid GolgiStain™ Kit, FD NeuroTechnologies, Inc.). Briefly, mice were anaesthetized, decapitated, and brains were removed quickly. Brains were washed in ddH_2O twice and incubated in Solution A for 8 days in the dark at room temperature. Brains were then washed in ddH2O twice and incubated in Solution C for 72 hours in the dark at room temperature. Brains were then washed with ddH2O and incubated in 30% sucrose/PBS in the dark at 4°C overnight. 150 μm sections were cut using a vibratome (Leica) (Speed: 5.5, frequency: 7) and collected in 0.6% sucrose/PBS. Brain slices were then mounted onto Superfrost Plus adhesion slides (Thermo Scientific) and underwent the staining procedure as per the manual. Brain slices on slides were blinded and then imaged using Zeiss Axiocam ICm1 microscope camera. Z-stacks were acquired at 1 μm intervals. NeuronJ software was used to trace the dendrites of the layer II/III somatosensory neurons and sholl analysis was performed using Sholl Analysis plugin on ImageJ software.

Immunoprecipitation

HEK 293FT cell lysates. Transfected cells were washed with PBS and lysed in ice-cold 1X PXL buffer (0.1% SDS, 0.5% deoxycholate, 0.5% NP-40) with protease inhibitors (Roche). 4 μg of DIXDC1 antibody (R&D systems) was incubated with Protein G Dynabeads (Life Technologies) in citrate phosphate buffer (pH 5) for 2 hours at room temperature. The antibody-bead complex was incubated with equal quantity of cleared cell lysates for 6 hours at 4°C. The beads were then washed 4 times with ice-cold NT2 (50mM Tris-HCl, 150mM NaCl, 1mM $MgCl_2$, 0.05% NP-40) buffer before boiling in 2X Laemmli sample buffer. Following SDS-PAGE to separate the proteins, blots were incubated with anti-DIXDC1 or anti-phospho-DIXDC1Ser592. *Brain lysates.* Whole brain or cortices from P30 CD-1 mice were dissected and homogenized in RIPA lysis buffer (10mM Tris-Cl (pH 8.0), 1mM EDTA, 0.1% SDS, 140mM NaCl) containing protease inhibitors, followed by 20 minute centrifugation at 14,000rpm at 4°C. Lysates were processed as cleared HEK lysates.

F- to G-actin ratio

The F- to G-actin ratio was measured with a G-/F-actin ratio in vivo assay kit (Cytoskeleton, BK037) according to the manual. Briefly, P28 WT and KO mice brains were lysed in F-actin stabilization buffer. F-actin was pelleted by centrifugation and the resulting soluble fraction contained the G-actin. Actin quantification was performed by western blot analysis using the provided rabbit anti-actin antibody (Cytoskeleton). Band intensities were quantified using ChemiDoc MP system.

Rac1 pull-down activation assay biochem kit

Active Rac1 (GTP) was measured according to the manufacturer's instructions (Cytoskeleton, BK035-S). Briefly, post-natal day 5 WT and KO brains were lysed and cleared and quickly snap-frozen in liquid nitrogen. After protein quantification, 500 μg of protein was loaded onto PAK-PBD beads. The beads specifically bound Rac-GTP (active Rac1) and were centrifuged to pull down the bead pellet. Active Rac1 levels and total Rac levels were analyzed by western blot.

Rho pull-down activation assay biochem kit

Active Rho (GTP) was measured according to the manfacturer's instructions (Cytoskeleton, BK036-S). Briefly, post-natal day 5 WT and KO brains were lysed and cleared and quickly snap-frozen in liquid nitrogen. After protein quantification, 500 μg of protein was loaded onto Rhoketin-PBD beads. The beads specifically bound Rho-GTP (active Rho) and were centrifuged to pull down the bead pellet. Active Rac1 levels and total Rac levels were analyzed by western blot.

Immunofluorescence

Primary neuronal cultures (DIV14) fixed and immnostained. Briefly, neurons were fixed with with 4% formaldehyde. After blocking and permeabilization solution of 10% normal goat serum/0.06% Triton X-100/PBS, neurons were incubated overnight at 4°C with primary antibody dilutions. Neurons were then washed with PBS and incubated with Alexa-Fluor 488- and Alexa-Fluor 568-conjugated secondary antibodies and mounted onto slides with ProLong Gold Antipode mounting medium.

Western blot analysis

Proteins from cell lysates were separated on 10% SDS-polyacrylamide gels at 100V and transferred to PVDF membrane (Bio Rad). Membranes were blocked in TBS-Tween (50 mM Tris-HCl pH 7.4, 150 mM NaCl, 0.1% Tween-20) with 3% non-fat dry milk for 1 hour at room temperature and then incubated in primary antibody dilution overnight at 4°C. Membranes were washed for 30 minutes with TBS-T and incubated 1.5 hours at room temperature with horseradish-peroxidase-conjugated antibodies (GE) and then washed for 1 hour in TBS-T. Immunoreactivity signals were detected by enhanced chemiluminescence (GE). Protein quantification was performed using ChemiDoc MP imaging, Band Analysis tooks of ImageLab software (Bio Rad). All detected bands were quantified on non-saturated bands as detected by the software.

Electrophysiological recordings

Coronal brain slices (400 μm) were prepared from a vibratome (VT1200 Leica Microsystems, Germany) in ice cold sucrose-based slicing solution containing the following composition adapted from BrainSliceMethods.com (in mM): 160 Sucrose, 2.5 KCl, 10 $MgSO_4$, 1.25 NaH_2PO_2, 25 glucose, 30 $NaHCO_3$, 20 hepes, 5 Na-ascorbate, 3 Na-pyruvate, 2 thiourea, 0.5 $CaCl_2$. Slices recovered for 45 minutes at 30°C, followed by at least 45 min at room temperature. Visually guided whole-cell recordings (BX51WI, Olympus) were performed at 30°C using an Axoclamp 700B amplifier (Molecular Devices, USA) from patch electrodes (pulled from P-97 electrode puller, Sutter Instruments, USA) containing a cesium based intracellular solution (in mM): 100 CsCl,

100 gluconic acid, 10 hepes, 0.5 EGTA, 10 Na-phosphocreatine, 2 MgATP, 0.5 NaGTP, pH 7.3). Brain slices were continuously superfused in artificial cerebrospinal fluid (aCSF), bubbled with mix of 95% O2/5% CO2 at a rate of 1-2 mL/min in a submersion-type chamber. Composition of aCSF (in mM): 120 NaCl, 2.5 KCl, 1 MgSO4, 26 NaHCO3, 10 glucose, 2 $CaCl_2$. 1 μM TTX and 100 μM picrotoxin was added to the bathing medium to block Na-dependent action potentials and GABA currents, respectively. Recordings were performed at -70 mV using Clampex 10.6 (Molecular Devices), corrected for a calculated -10 mV junction potential and analysed using the Template Search function (User created from at least 20 separate events, template match threshold of 2, fit with the product of 2 exponentials) from Clampfit 10.6 (Molecular Devices).

Epi-fluorescence time-lapse imaging

Epi-fluorescence time-lapse imaging was performed on an inverted Nikon microscope (Eclipse, Ti) with a 60x objective (NA 1.4). During time-lapse imaging, cells plated on glass-bottomed culture chamber (Sarstedt) were kept in an acrylic chamber at 37°C in 5% CO_2. Light intensity of each channel was set at 1 or 2, with exposure time of 500-700 milliseconds. Images were captured with CoolSNAP HQ2camera (Roper Scientific) using NIS-Elements AR software (version 4.20.01 from Nikon Corporation). Images were captured every 1-2 seconds (total 151 frames) during the 300 sec (5-minute) interval.

F-actin retrograde flow analysis: Kymographs were obtained from the 5 min time-lapse videos of Lifeact-GFP co-transfected rat hippocampal neurons using Multiple Kymograph

plugin in ImageJ. Lines (with width set to 1) were drawn along the neurite shafts to generate the kymographs. Individual retrograde trajectories of F-actin were then traced on the kymographs and their average slope was measured and represented in μm per min.

Counting neurites with growth cones

Growth cones were distinguished by their round or conical shape with thin finger-like filopodia and flat lamellipodia between them. The number of neurites with such growth cones among all the neurites within each cell was manually counted and represented in percentage. Bar graph depicts the mean percentage values obtained from each group.

EB3 anterograde speed analysis

Kymographs were obtained from the 5 min time-lapse videos of EB3-mCherry co-transfected rat hippocampal neurons using Multiple Kymograph plugin in ImageJ. Lines were drawn along the length of each neurite shaft to generate kymographs (with a line width of 1). From the kymographs, slope of each recognizable EB3 comet was measured. Data were represented as average speed of EB3 comets (μm/min).

Counting cells with EB3 comets

The number of cells with clear and distinguishable EB3 comets were counted manually from the 5 min time-lapse videos of EB3-mCherry co-transfected rat hippocampal neurons and represented in percentage. Bar graph depicts the percentage values obtained from each group.

Analysis of dendrite complexity and dendritic spine density

Quantitative analysis of dendrite complexity (sholl analysis) and spine density in cultured cortical pyramidal neurons and layers 2/3 golgi-stained somatosensory neurons was performed using ImageJ software (Sholl Analysis plugin). Neurons expressing GFP (venus) were imaged using 20x and 63x oil immersion objective confocal microscope (Zeiss confocal microscope, LSM700). Analysis parameters as follows: starting radius, 10μm; ending radius, 100 μm; step size, 10 μm. Statistics were performed using Prism statistical package (GraphPad, San Diego, CA). Z stacks of 4-8 images, averaged 2-4 times, 0.6μm stepsize, with 2048x2048 pixel resolution. Dendritic spine density and morphology was measured from secondary branches, from the branch point, ranging from 15-25 μm in length. Thin and filopodia spine density was measured on the secondary dendrite segment, and spine head width (μm), spine length (μm) and spine neck length (μm) were measured using ImageJ software. Spine head width was measured at the diameter of the spine head perpendicular to the length of the spine. Spine length was measured from the tip of the spine head to the interface with the dendrite branch. Following two-dimensional maximum projection images, spine density was measured in ImageJ software, and subjected to statistical analysis (Student's t-test or one-way ANOVA).

Genetic sequencing

Consent was obstained from all participants, as approved by the Research Ethics Boards at The Hospital for Sick Children, McMaster University and Memorial Hospital. We

genotyped all samples on high-resolution microarray platforms for the detection of copy number variants (CNVs). Whole Exome Sequencing (WES) was performed on Life Technologies SOLiD5500xl sequencing platform with target enrichment using Agilent SureSelect 50Mb human all exon capture kit following the manufacturers' protocols.

Briefly, 3µg of genomic DNA were sheared by sonication to a target size of 150 – 180bp and end repair and ligation of AB specific adapter oligos achieved using SOLiD fragment library construction reagents for 30 minutes and 15 minutes respectively. Target fragments of approximately 200bp were size selected by agarose gel electrophoresis with SOLiD library size selection (2%) gel and the recovered DNA amplified using SureSelect Pre-capture primers and Platinum PCR amplification mix (Invitrogen) with conditions of 72°C for 20 minutes, 95°C for 5 minutes followed by 12 cycles of 95°C for 15 seconds, 54°C for 45 seconds, 70°C for 60 seconds and a subsequent final extension of 70°C for 5 minutes. Hybridisation with biotinylated RNA baits corresponding to target regions was carried out using 500ng of prepared library for 24 hours at 65°C and captured DNA recovered with streptavidin coated magnetic beads. The recovered library was amplified and barcode sequencing tag incorporated by amplification with Platinum PCR amplification mix and AB specific SureSelect barcoding primers under conditions of 95°C for 5 minutes, then 95°C for 15 seconds, 54°C for 45 seconds, 70°C for 60 seconds for 12 cycles and a subsequent final extension of 70°C for 5 minutes. Equimolar quantities of six barcoded exome libraries were pooled for sequencing on a single SOLiD5500xl sequencing slide. Preparation of templated beads by emulsion PCR for sequencing was performed using the Life Technology EZBead system according to

manufacturer's instructions and paired-end sequencing carried out using SOLiD ToP chemistry.

Paired end reads were mapped to the reference human genome (build GRCh37) using BFAST version 0.6.5a. Picard tools version 1.35 (http://broadinstitute.github.io/picard/) was used to remove duplicate paired end reads and local realignment in colorspace carried out with SRMA version 0.1.15. GATK version 1.1.28 was used for calling of SNPs and in/dels. Rare variants were defined as those with frequency less than 1% in population databases (based on The 1000 genomes project, the NHLBI Exome sequencing project and the Exome Aggregation Consortium) and all novel or rare non-synonymous variants were validated using Sanger sequencing. Sanger sequencing was also conducted for all available family members to confirm segregation of the variants. Whole Genome Sequencing (WGS) was performed as previously reported(Yuen et al., 2015). For WES, 101 probands were sequenced as trios (probands plus parents) and 288 cases were sequenced without parents. For WGS, 200 trios were sequenced (probands plus parents) and 85 multiplex quad families (two affected siblings plus parents). The numbers presented in the results section reflect that 18 of the trios that underwent WES also received WGS as trios. Furthermore, 37 of the case only (without parents) WES samples also underwent WGS as trios, and 26 of the case only WES samples underwent WGS as quads. Therefore a total of 308 probands received WES only, 204 received WGS only, and 81 received both WES and WGS. WGS had 96.8% covereage and an average 56X sequence depth read.

Statistical Analysis

Compiled data are expressed as mean ± s.e.m. We used the two-tailed Student's *t* test, one-way ANOVA, two-way ANOVA, with *post hoc* Sidak tests for statistical analyses (as indicated). The *P* values in the Results are from *t* tests unless specified otherwise. $P < 0.05$ was considered statistically significant. Two-way ANOVA statistical analysis to measure dendrite complexity (sholl analysis) described in detail in Supplemental Information.

2.4 RESULTS

2.4.1 Expression of DIXDC1 in Neurons

DIXDC1 is expressed in the embryonic nervous system (Shiomi et al., 2005; Shiomi et al., 2003; Singh et al., 2010), but its postnatal expression has not been well characterized. We analyzed brain lysates using a commercial antibody previously used that identifies DIXDC1 isoforms 1 and 2 (Goodwin et al., 2014) (Figure 1A). We found DIXDC1 isoform 1 (~78 kDa) has high expression embryonically and reduced expression throughout the postnatal period, while isoform 2 (~57 kDa) expression peaks during the early postnatal period and is maintained into adulthood (Figure 1B). We also stained cultured days in vitro 14 (DIV14) cortical neurons and found that DIXDC1 is highly expressed in dendrites and co-localizes with the dendrite marker MAP2 (Figure 1C). To determine whether DIXDC1 is present at synapses, we co-stained with post-synaptic density 95 (PSD95) and determined that a small portion (~30%) of PSD95-positive

puncta co-localized with DIXDC1 (Figure 1D). We also biochemically isolated the postsynaptic density (PSD) from 1-month old brains and found that both DIXDC1 isoforms were present in the PSD fraction, with stronger expression of isoform 2 compared to isoform 1 at this time point (Figure 1E). To determine the pattern of expression for each DIXDC1 isoform, we tagged isoform 1 and 2 with green fluorescence protein (GFP) and expressed them in WT cultured cortical neurons. At DIV14, we found that both isoforms were expressed in neurons within the dendrites and spines (Figure 1F, G). Moreover, both isoforms partially co-localized with PSD95 puncta (~30%) (Figure 1G). Together, these data indicate that DIXDC1 is highly expressed in the postnatal cortex and that both isoforms localize to developing dendrite and spine processes, suggesting that they regulate neuronal morphogenesis.

2.4.2 Dixdc1 KO mice have defects in dendrite and dendritic spine development

To study DIXDC1, we obtained a *Dixdc1* KO mouse (from the Jackson Laboratory) that lacks expression of both isoforms (Figure 3E and Figure S1A). Morphological assessment of the cortical structure using layer-specific markers revealed no gross differences (Figure S1B). We performed Golgi-Cox staining on 4-week old WT and *Dixdc1* KO mice and imaged individual layers 2/3 of somatosensory cortical pyramidal neurons. We determined that neurons in KO mice had significantly reduced dendrite complexity compared to WT mice as revealed by Sholl analysis (Figure 2A). To corroborate these data, we transfected cultured cortical neurons at DIV7 with Venus, a spectral variant of GFP and analyzed neuronal morphology *in vitro* at DIV14. Similar to

the *in vivo* findings, we found a significant reduction in dendrite complexity in cultured KO neurons compared to WT (Figure 4A). As a control, we acutely knocked down *DIXDC1* because the complete loss of DIXDC1 from the onset of embryonic development could impair neurogenesis and migration, and have a secondary effect on dendrite growth. We injected lentivirus-expressing short hairpin RNAs (shRNA) in the postnatal cortex (P2/3) and found that P21 cortical neurons with reduced DIXDC1 expression had a strong reduction in dendrite complexity (Figure S2A and S2B). Furthermore, acute knockdown of DIXDC1 *in vitro* also led to a reduction in dendrite complexity (Figure S2C), which was rescued by overexpression of human DIXDC1 that is not targeted by the shRNA (Figure S2D). Taken together, these studies suggest that DIXDC1 is required for dendrite growth in the cortex in a cell-autonomous fashion.

We discovered both DIXDC1 isoforms are present in the PSD with isoform 2 having stronger expression in this compartment at one month of age (Figure 1D and 1E); therefore, we postulated DIXDC1 plays a role in the formation of dendritic spines and synaptic connectivity. We imaged dendritic spines in P28 layer 2/3 cortical neurons from KO mice and found there was a modest but significant reduction in spine density compared to WT (Figure 2B). Additional morphological analysis of dendrites showed a decrease in spine head width and length in KO mice (see methods for measurement parameters), demonstrating that DIXDC1 is required for spine morphogenesis (Figure 2C). *In vitro* experiments confirmed KO neurons had significantly reduced dendritic spine density compared to WT neurons but no major change in the number of immature (thin) spines (Figure 4B). The reduced spine density effect was greater *in vitro* compared to *in*

vivo, similar to other mouse models of psychiatric genes (Mukai et al., 2008), suggesting the possibility of compensatory mechanisms *in vivo*. We also performed *in vitro* and *in vivo* analysis of dendritic spines in cortical neurons after acute knockdown of DIXDC1. We found a significant decrease in dendritic spine density in shRNA-treated neurons compared to controls, which was rescued by expression of human-DIXDC1 *in vitro* (Figure S2E-G). We also found changes in spine morphology, which likely reflect the rapid and strong knockdown of DIXDC1 isoforms in neurons. We controlled for the possibility that the reduction in dendritic spine density may be due, in part, to an overall reduction in dendrite growth. Therefore, we knocked down DIXDC1 at DIV14 when dendrite growth is largely complete, and analyzed cells at DIV17. We still observed that knockdown of DIXDC1 resulted in a significant decrease in dendritic spine density, indicating that DIXDC1 plays a specific role in dendritic spine structure (Figure S2H).

2.4.3 DIXDC1 regulates the development of synaptic connectivity and function

Considering the significant reduction in both dendritic complexity, reduced spine density and spine size in *Dixdc1* KO mice, we examined whether this phenotype extended to alterations in synapse formation and synaptic activity. Under whole-cell voltage-clamp from layer II/III cortical neurons within the somatosensory cortex of acute brain slices (Figure 2D), we observed a significant reduction in miniature excitatory post-synaptic currents (mEPSCs) in 4-week-old *Dixdc1* KO compared to age matched WT controls (Figure 2E). The reduced excitation parallels both the decrease in spine density found in *DIXDC1* KO neurons and the expected total reduction in spine number (Figure 2B and

4B), stemming from the reduced dendritic arbour as identified by Sholl analysis (Figure 2A and 4A). Despite an overall trend towards a reduction in spine size in *Dixdc1* KO neurons, there were no significant differences in mEPSC amplitude from WT controls (Figure 2E). Given these electrophysiological data, we also examined the morphological development of synapses using immunostaining for the presynaptic protein synaptophysin (Kwon and Chapman, 2011). Quantification of transfected (GFP-positive) dendrite arbors revealed that neurons with reduced DIXDC1 expression had a significant reduction in synaptophysin puncta density on the soma and dendrites of GFP-transfected cells compared to controls (Figure S3A). We also measured neural connectivity using a genetically encoded modified Rabies virus that allows fluorescent visualization of retrograde monosynaptic connections (Garcia et al., 2012). We optimized the technique for *in vitro* use, and transfected equal numbers of cultured cortical neurons with an HTB-GFP vector that allows neurons to be infected by a modified Rabies virus. At DIV10 mCherry-Rabies viral particles were applied, which infected HTB-GFP expressing neurons, causing the production of mCherry-tagged viral particles that retrogradely cross synapses once (monosynapses). At DIV14, clusters of mCherry-positive (not expressing GFP) neurons surrounding individual GFP/mCherry-expressing neurons were observed similar to a previous *in vivo* report (Wickersham et al., 2007). Using this assay, we found that individual neurons lacking DIXDC1 had a significantly reduced number of monosynaptically connected neurons within a defined radius, suggesting DIXDC1 expression is required for synaptic connectivity (Figure S3B).

2.4.4 MARK1 phosphorylates DIXDC1 in the brain

Our data indicate that DIXDC1 regulates dendrite and synapse formation; however, the mechanism(s) by which this occurs is unknown. One possibility is that *DIXDC1* regulates downstream transcriptional Wnt/β-catenin signaling which we previously described (Singh et al., 2010); however, given the expression profile of both DIXDC1 isoforms in the dendritic and PSD compartments, we investigated whether a novel pathway is involved. In this regard, a recent study reported that MARK1 phosphorylates human DIXDC1 isoform 1 (isoform 2 was not investigated) and localizes DIXDC1 to actin-rich focal adhesions (Figure 3A) (Goodwin et al., 2014). Given the actin-rich structure of dendritic spines, this raises the possibility that DIXDC1 is regulated in a post-translational manner during synaptic development. We first tested the expression pattern and localization of MARK1. In the developing brain, MARK1 was expressed strongly in the postnatal period, similar to DIXDC1 (Figure 3B). We also found that MARK1 co-localized with DIXDC1 in the dendrites of cultured cortical neurons (Figure 3C), and MARK1 protein was detected in the PSD fraction, similar to DIXDC1 (Figure 3D). This indicates that MARK1 and DIXDC1 are co-expressed in neurons in the same compartments during brain development, suggesting MARK1-dependent phosphorylation of DIXDC1 could impact the development of neuronal morphology.

We then tested whether MARK1 induces phosphorylation of either DIXDC1 isoform by using previously validated constructs and a phospho-specific antibody (Goodwin et al., 2014). Expression of MARK1-WT together with hDIXDC1-WT isoform 1 in HEK293 cells induced robust phosphorylation as previously described (Figure 3F).

We also tested whether isoform 2 can become phosphorylated by MARK1, and we discovered this also occurs in a robust manner (Figure 3G). Both of these phosphorylation events were inhibited by a substitution of Serine-592 to Alanine (S592A) in isoform 1 or a S381A mutation in isoform 2 (Figure 3F and 3G). Given that these experiments are performed in HEK293 cells, we next tested whether either DIXDC1 isoform was endogenously phosphorylated *in vivo*. We examined mouse brain lysate at one month of age and found that both DIXDC1 isoforms are robustly phosphorylated, which was eliminated in the KO mouse (Figure 3E). Together these data demonstrate that MARK1 induces phosphorylation of both DIXDC1 isoforms in the brain, potentially regulating their function during neurodevelopment.

2.4.5 Phosphorylation of DIXDC1 is required for dendrite and spine growth

Given that MARK1 phosphorylates DIXDC1, we asked whether this pathway regulates dendrite and spine growth. We first examined the ability of each DIXDC1 isoform to induce dendrite and spine growth in WT cortical neurons, hypothesizing that isoform 2 may have a more prominent role in this process given its high expression at the PSD. We co-transfected cultured neurons using GFP and a specific isoform of DIXDC1 using a previously validated ratio to ensure the majority of analyzed cells are co-transfected (Krey et al., 2013). Interestingly, we found that when both WT DIXDC1 isoforms 1 and 2 were overexpressed individually, they both significantly increased dendrite branching, albeit with slightly different growth curves (Figure S4A). Both isoforms also significantly increased the density of dendritic spines to the same extent,

however there was no change in the proportion of thin (immature) spines (Figure S4B). We also tested mouse DIXDC1 (isoform 1) to determine if there are species-specific differences; however, none were detected (Figure S4C and S4D). We next tested the ability of each DIXDC1 isoform to increase (rescue) dendrite and spine defects in the KO cultures. We determined that expression of either isoform significantly increased dendrite growth and spine formation in KO cortical neuron cultures to the same extent (Figure 4C-F). Therefore, despite the higher expression of isoform 2 compared to isoform 1 at the PSD, these data imply that both DIXDC1 isoforms are able to rescue dendrite and spine growth to the same degree, and both isoforms play a prominent role in this process.

To determine the role of MARK1-phosphorylation on the DIXDC1 isoforms in the regulation of dendrite and spine formation, we used phospho-mutant versions of each isoform and expressed them either in the WT or *Dixdc1* KO background. First we introduced GFP alone, GFP plus hDIXDC1-WT (isoform 1 or 2) or the phospho-dead version of either DIXDC1 isoform (hDIXDC1-S592A or -S381A) into cortical neurons cultured from *DIXDC1* KO neurons, and analyzed dendrite complexity and dendritic spine morphology at DIV14. Overexpression of hDIXDC1-S592A (isoform 1) in KO neurons was not able to stimulate dendrite growth and increase dendritic spine density compared to hDIXDC1-WT (isoform 1) (Figure 4C and 4E). Similarly, overexpression of hDIXDC1-S381A (isoform 2) was also unable to increase dendrite branching or dendritic spine density in KO neurons compared to hDIXDC1-WT (isoform 2) (Figure 4D and 4F). We also found that expression of hDIXDC1-WT isoform 1 or 2 in the KO background led to a significant decrease in the proportion of thin (immature) spines compared to the

phosphorylation mutants for either isoform which did not change spine morphology, indicating that overexpression in the KO background impacts spine maturity. These data suggest that phosphorylation of either isoform is required for dendrite outgrowth and spine formation. Next, we examined both phospho-dead isoforms of DIXDC1 in the WT background using cultured cortical neurons to determine if inhibiting phosphorylation caused dominant-negative activity in neurons expressing normal levels of DIXDC1. For isoform 1, we determined that expression of hDIXDC1-S592A in WT cultures did not function in a similar manner to hDIXDC1-WT, and actually decreased dendrite branching compared to controls (GFP), while dendritic spine density was slightly lower than controls but significantly different than WT isoform 1 (Figure S5A and S5C). For isoform 2, the phospho-mutant (S381A) did not increase dendrite growth or spine density compared to WT, and its effect was similar to GFP controls (Figure S5B and S5D). These data suggest phospho-dead isoform 1, but not the isoform 2 mutant, possesses some dominant negative activity. As a control, we found no gross differences in expression of the mutants when tested in HEK293 cells to measure the overall levels (Figure S6A).

We were also interested to see if phosphorylation of DIXDC1 was important for its localization in neurons. Cultured DIV14 cortical neurons showed co-localization of GFP-tagged hDIXDC1-WT (isoform 1 and 2) with PSD95 in the dendritic spines (Figure 4G and 4H). However, the hDIXDC1-S592A and -S381A phospho-mutants both demonstrated a significant decrease in PSD95 co-localization puncta density, indicating a disruption to the localization of DIXDC1 to dendritic spines (Figure 4G and 4H). Moreover, the reduced PSD95 puncta that did co-localize with the DIXDC1

phosphorylation mutants were primarily localized to the dendritic shaft, and this was more prominent for isoform 1 (Figure 4H). Taken together, these results strongly indicate that phosphorylation of both DIXDC1 isoforms is critical for the regulation of cortical dendrite and synapse formation.

2.4.6 Phosphorylation of DIXDC1 regulates the cytoskeletal structural integrity

We next investigated how the MARK1-DIXDC1 pathway regulates dendrite and spine growth. Previous lines of evidence suggest that DIXDC1 may have a direct impact on the cytoskeletal network, which would influence dendrite and spine growth. DIXDC1 has previously been associated with the neuronal actin cytoskeleton due to the observation that MARK1-mediated phosphorylation impacts its localization to actin-rich focal adhesions in non-neuronal cells (Goodwin et al., 2014). Second, previous studies demonstrated that DIXDC1 has an N-terminal calponin-homology domain in isoform 1 (Wang et al., 2006). Third, the DIX domain has the ability to localize proteins to the actin network (Capelluto et al., 2002), and fourth, newborn cultured cortical neurons lacking DIXDC1 have reduced filamentous (F-) actin and altered tubulin distribution (Singh et al., 2010). We first focused on whether DIXDC1 is required for integrity of the actin network by measuring the F-actin to G-actin ratio in WT versus KO mouse brain tissue. Using a commercial kit, we detected a significantly reduced F-/G-actin ratio in KO brains (Figure 5A), suggesting that DIXDC1 modulates the polymerization of F-actin in the brain. We next examined a possible mechanism by which this occurs by analyzing the levels and activity of a number of actin polymerization-related proteins in *DIXDC1* KO

brains compared to WT. We observed a significant decrease in Rac1-GTP activity, but not Rho-GTP levels in *DIXDC1* KO brains (Figure 5B), indicating that Rac1 activity is impaired. To determine if actin-regulating proteins were altered downstream of Rac1 activity, we performed additional western blot analysis and found a significant reduction in the Wiskott-Aldrich syndrome proteins, WAVE-2 and N-WASP (Figure 5C). WASPs have been shown to activate the Arp2/3 complex, responsible for nucleating branched actin filaments, promoting spine head growth (Hotulainen and Hoogenraad, 2010), and interestingly, WAVE2 was recently reported to be in a complex with CYFIP1, which itself is deleted in a genomic region associated with ASDs (Bozdagi et al., 2012; De Rubeis et al., 2013; Oguro-Ando et al., 2015; Pathania et al., 2014; Yoon et al., 2014). We also determined a decrease in Profilin-1, a protein important for actin stabilization in spine morphology, and which plays a pathogenic role in Fragile X Syndrome (FXS) (Michaelsen-Preusse et al., 2016) (Figure 5C). These observations suggest that DIXDC1 regulates actin polymerization in the brain. To investigate whether a defect in actin polymerization causes the dendritic spine phenotype in *DIXDC1* KO neurons, we pharmacologically enhanced actin polymerization and asked if this would improve spine growth, a finding that would strengthen the argument that DIXDC1 regulates the dendritic spine actin network. This approach has previously been used to interrogate a similar question for the Copine-6 gene (Reinhard et al., 2016). To test this we used Jasplakinolide (JPK), which is a natural and cyclic compound that promotes actin-polymerization in neurons (Gu et al., 2010)**,** but has no direct effect on DIXDC1 activity. JPK has been used to restore normal F-actin levels, synaptic plasticity and behavior in

mouse model of neurocognitive deficits where actin polymerization is significantly impaired (Huang et al., 2013). We tested a 2-hour treatment and found that 1 μM JPK significantly increased dendritic spine density in *DIXDC1* KO cultures to levels similar to WT cultures treated with JPK (Figure 5D). Importantly, the increase in spine density by JPK was accompanied by a decrease in the proportion of thin spines, suggesting that JPK treatment increases the number of mature, functional spines.

We next explored which DIXDC1 isoform regulated the effects on the actin cytoskeleton and whether MARK1 phosphorylation was required for this effect. To test this, we monitored actin dynamics in primary DIV2-3 hippocampal neurons. We selected this age due to the dynamic nature of actin and microtubule networks, and is highly reliable for live imaging; whereas this is much more difficult, and hence less reliable, in DIV14 or older cultures. Therefore, these experiments were strictly used as an assay to determine which DIXDC1 isoform has the ability to impact the actin network in primary neurons, and whether MARK1-induced phosphorylation was an important factor in this process. To monitor actin, we used Lifeact-GFP, which is a 17-amino acid peptide that labels F-actin with GFP and does not impact its function (Riedl et al., 2008; Riedl et al., 2010). We tracked Lifeact-GFP over time in the developing neurites of DIV2-3 neurons that were transfected with a plasmid on the day of culturing to express a DIXDC1 isoform as well as Lifeact-GFP (Figure 5F, Figure S6E). Given this experimental paradigm, we found that WT-DIXDC1 isoform 1 was able to significantly alter F-actin retrograde speed in neurons as determined by analysis of kymographs which graphically demonstrate the movement of the actin over time (Figure 5F and 5G). However, isoform 2 had no effect,

identifying isoform-specific differences in the regulation of actin (Figure 5F and 5G). Interestingly, both the hDIXDC1-S592A (isoform 1) and –S381A (isoform 2) mutants that are unable to be phosphorylated by MARK1, showed the same effect, and were significantly different than their WT counterparts (Figure 5F and 5G). This suggests that hDIXDC1-WT isoform 1 and 2 have different mechanisms of action in regards to the regulation of actin, and are both regulated by MARK1. We also measured the number of growth cones using Lifeact-GFP to assess the impact of DIXDC1 isoforms on the actin network, since growth cones are rich with F-actin. We found that while the growth cone area was unaffected (data not shown), the percentage of neurites with an intact growth cone was significantly reduced in neurons expressing hDIXDC1-S592A (isoform 1) or hDIXDC1-S381A (isoform 2) compared to hDIXDC1-WT (isoform 1) or the control, indicating that MARK1 phosphorylation of isoform 1 or 2 is required for actin integrity (Figure 5I). This is consistent with our results from Figure 4, demonstrating that the phospho-mutants of isoform 1 or 2 impair dendritic spine formation, which are also rich in actin. Finally, to functionally determine the impact on actin by the hDIXDC1 isoforms, we tested whether JPK could rescue the decrease in dendritic spine density in neurons expressing phospho-dead versions of DIXDC1 isoforms 1 or 2. We found that JPK treatment significantly increased dendritic spine density in neurons expressing hDIXDC1-S592A isoform 1 or hDIXDC1-S381A isoform 2 to levels comparable to treated WT cortical neurons (Figure S6C and S6D. We also observed that JPK treatment significantly reduced the number of thin spines out of the total number of spines analyzed, suggesting that JPK increases the number of mature spines after expression of the isoform 1 and 2

phospho-dead mutants (Figure S6C and S6D). Together, this demonstrates that enhancing actin polymerization improves the spine deficits due to S592/381A mutations. Although JPK treatment does not directly impact the function of DIXDC1, these experiments support the notion that DIXDC1 isoforms regulates dendritic spine growth upstream of F-actin.

Given the dendrite growth defects in *DIXDC1* KO mice, we also examined whether DIXDC1 isoforms and its phosphorylation by MARK1 regulated the microtubule network, which is a major structural component of dendritic arbors. We performed live imaging of microtubules in the same cells expressing Lifeact-GFP described above (Figure S6E). To do this, red fluorescent protein (RFP) tagged EB3 was expressed in neurons, which has been used to monitor the live microtubule network by imaging EB3-RFP comets from kymographs (Akhmanova and Hoogenraad, 2005; Tanaka, 1991). We found that hDIXDC1-WT (isoform 1) was able to significantly alter EB3 anterograde comet speed and the number of neurons with clear and distinguishable EB3-RFP comets (Figure 5F, 5H and 5J), while isoform 2 had no effect, indicating isoform 1 predominantly has the ability to modulate the microtubule network (Figure 5F, H). Furthermore, the hDIXDC1-S592A (isoform 1) had no effect on EB3 comet movements indicating that MARK1-mediated phosphorylation of isoform 1 regulates microtubules (Figure 5F, 5H and 5J). We also examined whether the microtubule defects were detectable on a global level in the brain by performing western blot analysis in WT and KO mice to measure the levels of tubulin and the different modifications that regulate its ability to nucleate. However, we found no overt differences between the levels of

acetylated or tyrosinated tubulin in WT versus KO brains (Figure 5E), suggesting that the microtubule defects in the *DIXDC1* KO animals are not overt.

Overall these data indicate that DIXDC1 isoform 1 is the predominant isoform that regulate the neuronal actin and microtubule cytoskeleton during neurodevelopment, suggesting that it has a different mechanism of action than isoform 2 in regards to modulating the cytoskeleton during dendrite and spine growth.

2.4.7 Rare missense variants in DIXDC1 impair phosphorylation of isoform 1

We were prompted to investigate whether there was a functional link between *DIXDC1* and ASD given that multiple Wnt/synaptic signaling genes are associated with ASD (Krumm et al., 2014). Emerging studies indicate that rare sequence variants/mutations in some ASD-risk genes can have a profound impact on protein function (Bernier et al., 2014; Deriziotis et al., 2014; Russell et al., 2014; Sowers et al., 2013a), demonstrating that subtle changes to protein sequences can alter neural function. Therefore, we asked whether there are genetic sequence variants in *DIXDC1* within ASD cohorts, and if they impair protein function during neural development. We examined genetic data from a Canadian cohort of 308 individuals (probands) that underwent whole exome sequencing and 285 probands that underwent whole genome sequencing (Yuen et al., 2015) (see methods for further details on parental DNA sequencing). From these cohorts, we discovered rare inherited variants in *DIXDC1* isoform 1 at positions Glycine8Glutamic Acid (G8E), Valine43Methionine (V43M), Isoleucine370Leucine (I370L; I159L in isoform 2) and Threonine612Methionine (T612M; T401M in isoform 2)

(Table 1). The V43M and T612M variants were found in 2 independent probands. Given these variants, we examined the biological significance of the V43M and T401/612M variants because they were identified in more than one individual and landed within a functional domain of DIXDC1 linked to actin signaling (the N-terminal calponin-homology domain and the DIX domain that can regulate actin localization). In addition, the I370L variant (isoleucine to leucine substitution), found in the coiled-coil domain is thought to be a conservative substitution. The tested variants were confirmed using Sanger sequencing (Figure 6A, Figure S7C).

We first tested expression of the variants and found both were grossly expressed at similar levels (Figure S6B). Next, we asked whether the variants impaired DIXDC1 phosphorylation given its importance for the ability of DIXDC1 to regulate neural connectivity. Furthermore, a recent study identified that ASD-linked mutations in an unrelated protein, UBE3A, compromise phosphorylation by PKA, indicating protein phosphorylation is an important regulatory mechanism impaired in neurodevelopmental disorders (Yi et al., 2015). To test this in DIXDC1, we overexpressed each isoform and the variants that occur within that isoform (WT, V43M and T612M for isoform 1; WT and T401M for isoform 2) into HEK293 cells together with MARK1 to induce phosphorylation. To our surprise, we discovered that only the variants in DIXDC1 isoform 1 significantly impaired phosphorylation by MARK1 (Figure 6B and 6C). Since the T401M variant in isoform 2 was not reduced in phosphorylation, this suggests the rare variants specifically impact the ability of MARK1 to phosphorylate isoform 1, further indicating that each DIXDC1 is differentially regulated.

To determine if dendrite and spine formation is affected by the variants, we expressed hDIXDC1-V43M and –T612M variants in *DIXDC1* KO neurons. We found that the hDIXDC1-V43M and –T612M variants were unable to increase (rescue) dendrite branching, suggesting a loss of function (Figure 6D). We also found that both variants were unable to increase dendritic spine density compared to hDIXDC1-WT (Figure 6E). Additionally, we expressed the variants into cultured WT cortical neurons and analyzed neuronal morphology to determine if any of the variants possess dominant negative activity. We found that hDIXDC1-WT increased dendrite complexity as expected; however, the hDIXDC1-V43M variant was unable to increase dendrite complexity and performed similar to controls, suggesting it is a loss of function variant but did not have dominant negative activity (Figure S7A). The C-terminal T612M isoform 1 variant also disrupted dendrite complexity but it significantly reduced dendrite growth compared to GFP controls, suggesting it displays dominant negative activity (Figure S7A). This is similar to the effects of the hDIXDC1-S592A isoform 1 mutant on dendrite complexity (Figure S5A), suggesting that mutations within the DIX domain of isoform 1 may be particularly important for phosphorylation-dependent control of DIXDC1. Dendritic spine analysis revealed that both isoform 1 variants (V43M and T612M) were unable to significantly increase spine density compared to hDIXDC1-WT isoform 1 in WT neuronal cultures, and were no different than controls (Figure S7B). Finally, we asked whether JPK treatment would rescue these defects because of the defects in actin dynamics (Figure 5). We found treatment of the hDIXDC1 isoform 1 V43M and T612M

variants with JPK significantly increased dendritic spine density similar to controls (GFP) with JPK, indicating that the dendritic spine defects are reversible (Figure 6F).

Taken together, these data suggest that rare missense variants in *DIXDC1* isoform 1 impair phosphorylation by MARK1, leading to abnormal development of neuronal morphology through a cytoskeletal-based mechanism. This highlights that even subtle sequence variations can have a significant negative impact on neural connectivity.

2.5 DISCUSSION

The mechanism by which genes associated with neurodevelopmental disorders impact brain development remains poorly characterized. Here we studied *DIXDC1*, a gene that was previously linked to ASDs and psychiatric disorders. We reveal that both *DIXDC1* isoforms regulate cortical excitatory neural connectivity. We demonstrate that MARK1 activates DIXDC1 through phosphorylation at the C-terminus, which modulates the ability of DIXDC1 to regulate the mobility of the cytoskeleton, and impact dendrite and dendritic spine growth. Furthermore, we identify that isoform-specific roles for DIXDC1, identifying that isoform 1 predominantly regulates the actin and microtubule cytoskeleton in neurons. Finally, we discovered rare missense variants found in *DIXDC1* from ASD individuals through genetic sequencing studies and functionally interrogate and validate that the sequence variants impair DIXDC1 isoform 1 phosphorylation, leading to a reduction in dendrite and dendritic spine growth. These data delineate how a novel MARK1-DIXDC1 signaling pathway underlies the development of synaptic

connectivity, and reveal a mechanism whereby rare genetic variants have a negative biological impact.

2.5.1 Phosphorylation-dependent control of DIXDC1 in brain development

There is emerging evidence that DIXDC1 regulates multiple stages of cortical development. DIXDC1 was previously shown to regulate neural progenitor proliferation by modulating β-catenin-mediated transcriptional signaling, likely through its association with DISC1 and inhibition of glycogen synthase kinase 3β (GSK3β) to promote Wnt signaling (Mao et al., 2009). As progenitors produce neurons, cyclin dependent kinase 5 (Cdk5) expression in neurons phosphorylates DIXDC1 at Serine 250 to regulate neuronal migration (Singh et al., 2010). While Cdk5 has many targets, it is plausible that Cdk5 acts as a "switch" during neuronal differentiation and maturation, by activating particular molecules, including DIXDC1, to mediate neuronal migration and axon/dendrite growth (Niethammer et al., 2000; Tanaka et al., 2004; Xie et al., 2003). Given our finding that MARK1 induces phosphorylation of DIXDC1 for dendrite and spine growth postnatally, this suggests that different kinases regulate DIXDC1 at discrete stages of pre- and post-natal cortical development.

2.5.2 DIXDC1 isoform regulation of cortical dendrite formation and spine morphology

We determined that both isoforms of DIXDC1 play a role in dendrite and spine growth; however, our data indicate that there are isoform-specific roles for DIXDC1. First, the pattern of protein expression of each isoform suggests that isoform 2 is strongly

expressed during dendritic and spine growth periods compared to isoform 1, based on our biochemical isolation of the PSD. While we did find that both isoforms are phosphorylated in the postnatal brain at one month of age, we did not test if this changes across different developmental time points. We also found that both isoforms can localize to dendrites and PSD95-positive dendritic spines, and rescue dendrite and spine growth in *DIXDC1* KO cultures, indicating that they are able to exert the same function with respect to synapse formation. Therefore, although both isoforms are able to exert the same function during dendrite and spine growth, their mechanism of action is likely to be different since we detected clear differences with respect to the ability to modulate the cytoskeleton. Overall our live imaging studies of the actin and microtubules indicate that DIXDC1 isoform 1 has predominant activity towards the cytoskeleton compared to isoform 2. We also delineate a signaling pathway downstream of DIXDC1 that accounts for this; a Rac1-WAVE-2/N-WASP signaling that ultimately regulates F-actin polymerization through the Arp2/3 complex. Functional analysis of the C-terminal MARK1-phosphorylation site indicates that both the N- and C-terminal domains of isoform 1 regulates the cytoskeleton, consistent with previous studies demonstrating that the actin-binding domain is present only in isoform 1 (Capelluto et al., 2002; Wang et al., 2006). This could also explain why isoform 2 does not have a strong impact on the actin and microtubules in primary neurons. Furthermore, it is also possible that the mechanism by which isoform 2 regulates the cytoskeleton is indirectly through isoform 1, by homo-dimerization via the DIX domain, and the interaction between the isoforms could be regulated by MARK1 phosphorylation at the C-terminus. However, since the C-terminal

ASD-linked T612M variant decreased DIXDC1 phosphorylation in isoform 1 but the corresponding T401M variant did not alter phosphorylation of isoform 2, this further suggests that both isoforms are not regulated in the exact same manner. One explanation is that an additional kinase regulates isoform 1 activity at Threonine612 and acts as a priming site for Serine 592 phosphorylation by MARK1, which does not occur in isoform 2, or the Threonine401 site in isoform 2 is regulated by a different kinase other than MARK1 under endogenous conditions. Given, the strong role of isoform 2 in Wnt signaling (Shiomi et al., 2003), we speculate that the increased expression of isoform 2 in the brain may reflect its requirement by this pathway during dendrite and synapse growth, whereas isoform 1 preferentially regulates the cytoskeleton pathway. In this regard, another interesting notion that needs to be further investigated is the possibility of cross talk between the MARK1-cytoskeleton pathway and the Wnt signaling pathway. Specifically, it is possible that MARK1-phosphorylation of isoform 2 could be involved in regulating canonical Wnt signaling. In this scenario, the C-terminus of DIXDC1 isoform 1 and 2 would be a signaling hub for MARK1 activation that would result in promoting isoform 1 to regulate the cytoskeleton directly, while isoform 2 would activate the Wnt pathway, both pathways ultimately regulating dendrite and dendritic spine growth. Since we have examined all of these parameters under basal conditions, such complexity may be involved during activity-dependent dendrite and dendritic spine growth, as MARK1 is activity regulated (Bernard and Zhang, 2015).

An alternate possibility is that DIXDC1 isoform 2 stimulates GSK3β downstream, a molecule that has clear effects on the neuronal cytoskeleton (Calabrese and Halpain,

2014; Chikano et al., 2015; Morgan-Smith et al., 2014). Therefore, one hypothesis is that DIXDC1 stimulates a GSK3β-dependent pathway that regulates local dendrite and spine growth through actin-dependent signaling. In this manner, GSK3β inhibitors and lithium, which have effects beyond Wnt/β-catenin signaling, would improve synaptic growth through local synaptic signaling. Moreover, this alternate pathway doesn't exclude the possibility that other synaptic regulators such as DISC1, which are known to interact with DIXDC1 during embryonic time points, may play a role in DIXDC1-dependent synapse function (Hayashi-Takagi et al., 2010; Stamatakou et al., 2013).

2.5.3 DIXDC1 signaling in ASDs and the role of missense variants

In the current study, the biological interrogation of *DIXDC1* variants suggests that its function could be impaired in ASDs and other psychiatric conditions. One unresolved finding is that the V43M and T401/612M variants occur, although at very low frequencies, in the control population. V43M occurs at a frequency of < 0.0001, while T612/401M has a frequency between 0.001-0.0001 (Exac Browser, Broad Institute and rs184718561 in dbSNP). Although the V43M and T612/401M variants have strong effects on DIXDC1 protein function, it is unclear how they contribute to disease risk because the variants were inherited from parents who do not have an ASD. However, it is not uncommon for unaffected family members to carry high-risk ASD mutations (Berkel et al., 2010). One explanation is *DIXDC1* variants on their own are not sufficient to cause disease, but they interact with other variants to increase disease risk (Bourgeron, 2015). For example, sequence variations in DIXDC1 could sensitize dendrite and spine effects

for other ASD risk genes that impair the synaptic actin network (De Rubeis et al., 2013; Duffney et al., 2013; Hori et al., 2014; Kalkman, 2012; Yoon et al., 2014). By contrast, protective factors could also be at play in the unaffected parents that abrogate the effects of the *DIXDC1* variants.

Taken together, the current study reveals for the first time that a MARK1-DIXDC1 signaling pathway is an important mechanism regulating developmental neural connectivity. Furthermore, the human genetic evidence and biological follow-up suggests that *DIXDC1* could play a role in neurodevelopmental and neuropsychiatric pathophysiology, which needs to be further explored in larger patient cohorts. This underscores the need to further study the role of DIXDC1 in normal and abnormal brain developmental paradigms to obtain a more complete understanding of its function.

2.6 SIGNIFICANCE

This work was published within the same year as Martin et al. (2016) from the laboratory of Dr. Benjamin Cheyette at the University of California, San Francisco (UCSF). This group demonstrated similar reduced dendritic spines and synapses in a separate *Dixdc1* KO mouse model, through the canonical Wnt signalling pathway. Additionally, they identified single nucleotide variants (SNVs) in individuals with ASD, bipolar disorder and schizophrenia; of these SNVs, some of them showed altered Wnt signalling activity. The phenotypes observed were consistent with our work, however the mechanisms described were different. This work describes the global regulation of Wnt/β-catenin signal transduction within excitatory neurons. Conversely, our work

describes a mechanism where DIXDC1 regulates dendrite and spine growth locally within the dendritic spine through the regulation of the cytoskeleton. It is quite possible that both of these pathways are regulating dendrite and synapse formation, through both DIXDC1 isoform 1 and 2. Further studies should look into the contribution of both signalling pathways on DIXDC1 regulation of excitatory neurons and the identified ASD-associated variants. It may be interesting to determine if the SNVs identified by Martin et al. that did not show altered Wnt signalling activity may be involved in the mechanism we described.

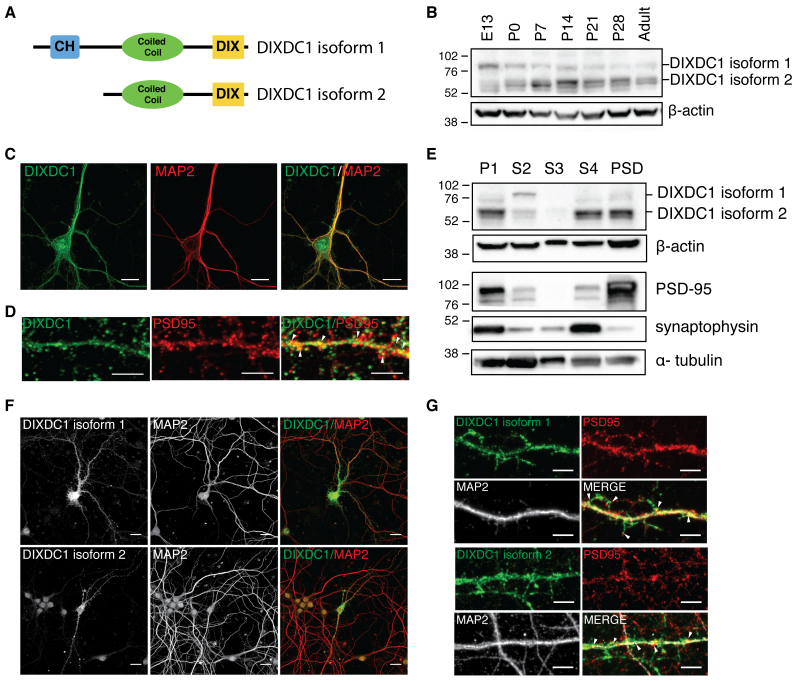

Figure 1: Characterization and localization of DIXDC1. (**A**) Schematic diagram of DIXDC1 protein structure. (**B**) Western blot analysis of mouse brain lysates probed for DIXDC1 (actin-loading control). (**C**) DIV14 cortical neuron cultures show localization of DIXDC1, co-stained for microtubule-associated protein 2 (MAP2). (**D**) DIV14 cortical neurons were immunostained and show co-localization of DIXDC1 with PSD95 (arrows). (**E**) Postsynaptic densities (PSD) fractionated from P28 mouse brains were probed for DIXDC1, actin, PSD95, synaptophysin, and tubulin. P1, nuclear fraction; PSD, post synaptic density; S2, crude cytoplasm; S3, crude synaptic vesicle; S4, crude synaptosomal membrane fraction. (**F** and **G**) Immunostained DIV14 mouse cultures show co-localization of GFP-tagged DIXDC1 isoforms 1 and 2 with PSD95 and MAP2 (arrows). All numerical data are given as mean ± SEM. The scale bars represent 20 mm for (**C**) and (**F**) and 5 mm for (**D**) and (**G**). See also Figure S1.

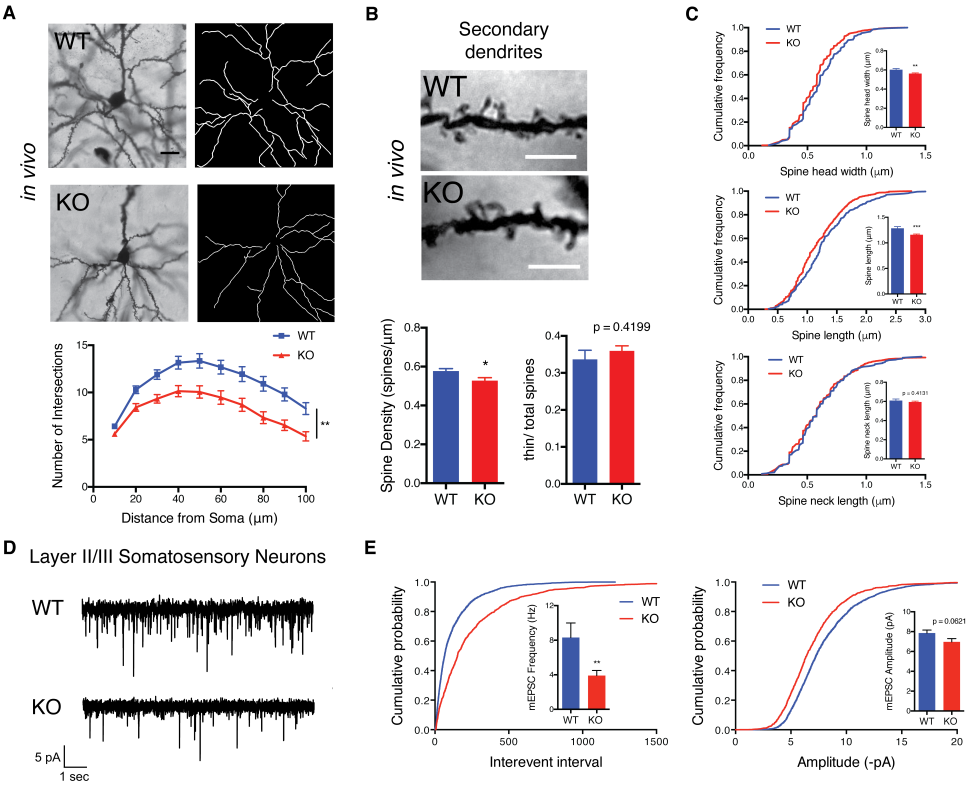
A
in vivo
WT
KO
Number of Intersections
Distance from Soma (μm)
B
Secondary dendrites
in vivo
WT
KO
Spine Density (spines/μm)
thin/ total spines
p = 0.4199
C
Cumulative frequency
Spine head width (μm)
Spine length (μm)
Spine neck length (μm)
D
Layer II/III Somatosensory Neurons
WT
KO
5 pA
1 sec
E
Cumulative probability
Interevent interval
mEPSC Frequency (Hz)
Amplitude (-pA)
mEPSC Amplitude (pA)
p = 0.0621

Figure 2: DIXDC1 is required for dendrite growth and dendritic spine function. (**A**) Golgi-stained layers 2/3 somatosensory neurons from cortex in WT or *Dixdc1* KO mice (P28). Sholl analysis reveals KO mice display a decrease in dendrite complexity (n = 3 mice; two-way ANOVA; post hoc Sidak test: **p < 0.01). See Supplemental Information for detailed statistical methods. (**B**) Morphological analysis of P28 layers 2/3 somatosensory secondary dendrites in *Dixdc1* KO neurons shows decreased spine density and increased thin spines compared to WT neurons (n = 3 mice; t test: *p < 0.05). (**C**) Morphological analysis of spine head width, spine length, and spine neck length (mm) distribution. Spine head width and spine length were decreased in *Dixdc1* KO neurons (n = 3 mice; t test: **p < 0.01; ***p < 0.001; p values for specific distances in Supplemental Information). (**D**) Loss of DIXDC1 reduces excitatory synaptic function. Representative traces of recorded mEPSCs from KO mouse (bottom) and WT control brain slices (top; n > 4 mice). (**E**) KO mice display a significantly reduced mEPSC frequency (two-tailed Mann Whitney U-test: **p < 0.01) with no change in amplitude. Cumulative probability of mEPSC frequency and amplitude shows spine head width and spine length was significantly decreased in KO (n > 4 mice; Kolmogorov-Smirnov t test: ****p < 0.0001). All numerical data are given as mean ± SEM. The scale bars represent 20 mm for (A) and 5 mm for (B). See also Figures S2–S4.

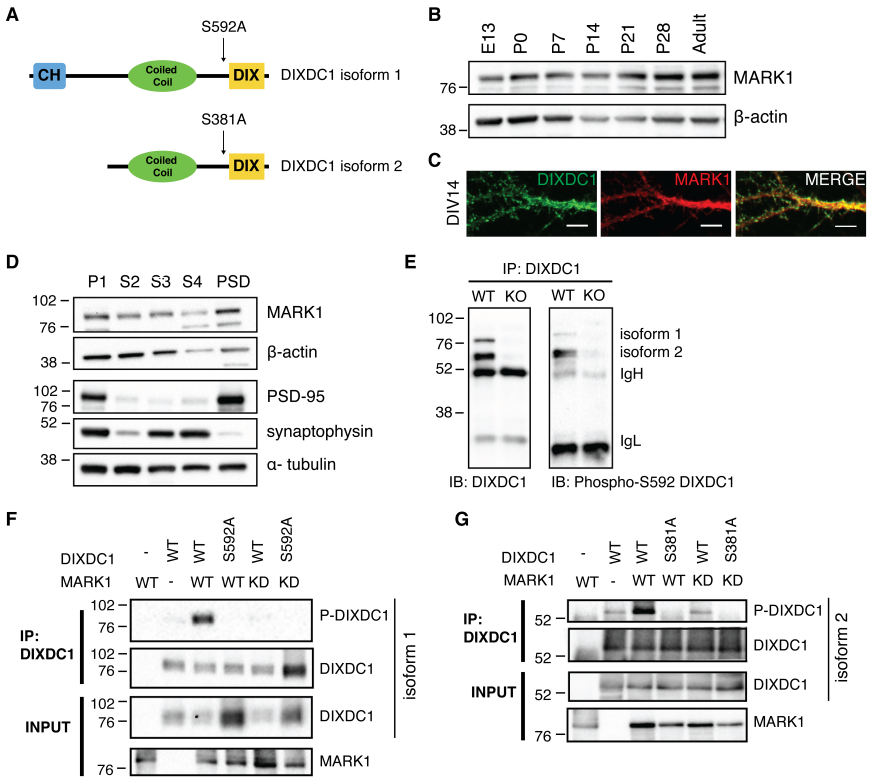
A
S592A
CH
Coiled Coil
DIX
DIXDC1 isoform 1
S381A
Coiled Coil
DIX
DIXDC1 isoform 2
B
E13
P0
P7
P14
P21
P28
Adult
76
MARK1
38
β-actin
C
DIV14
DIXDC1
MARK1
MERGE
D
P1 S2 S3 S4 PSD
102
76
MARK1
38
β-actin
102
76
52
PSD-95
synaptophysin
38
α- tubulin
E
IP: DIXDC1
WT KO WT KO
102
76
52
38
isoform 1
isoform 2
IgH
IgL
IB: DIXDC1
IB: Phospho-S592 DIXDC1
F
DIXDC1 - WT WT S592A WT S592A
MARK1 WT - WT WT KD KD
IP: DIXDC1
102
76
P-DIXDC1
102
76
DIXDC1
INPUT
102
76
DIXDC1
76
MARK1
isoform 1
G
DIXDC1 - WT WT S381A WT S381A
MARK1 WT - WT WT KD KD
IP: DIXDC1
52
P-DIXDC1
52
DIXDC1
INPUT
52
DIXDC1
76
MARK1
isoform 2

Figure 3: MARK1 phosphorylates DIXDC1 at Serine 592/381 in the brain. (**A**) Schematic diagram of MARK1 phosphorylation site at serine 592 of hDIXDC1 isoform 1 and at serine 381 of hDIXDC1 isoform 2. (**B**) Western blot analysis of a time course of CD-1 mouse brain lysates, probed for MARK1 (actin-loading control). (**C**) DIV14 cultured WT cortical neurons were immunostained for DIXDC1 and MARK1 and show co-localization in dendrites. (**D**) Postsynaptic densities (PSDs) fractionated from 1-month-old CD-1 mouse brains probed for MARK1, actin, PSD95, synaptophysin, and tubulin. P1, nuclear fraction; S2, crude cytoplasm; S3, crude synaptic vesicle; S4, crude synaptosomal membrane fraction; PSD, post synaptic density. (**E**) Immunoprecipitation of 1-month-old WT and *Dixdc1* KO mouse brain with anti-DIXDC1 antibody and then probed for DIXDC1 (left) and phospho-Ser592 DIXDC1 (right). (**F**) HEK293FT cells transfected with MARK-WT or T215A (kinase dead [KD]) and hDIXDC1-WT (isoform 1) or hDIXDC1-S592A (phosho-dead; SA). DIXDC1 was immunoprecipitated and probed for p-DIXDC1 S592 and DIXDC1. (**G**) HEK293FT cells transfected with MARK-WT or -KD and hDIXDC1-WT or -S381A (isoform 2). DIXDC1 was immunoprecipitated and probed for p-DIXDC1 S592/S381 and DIXDC1. The scale bar represents 5 mm for (**C**).

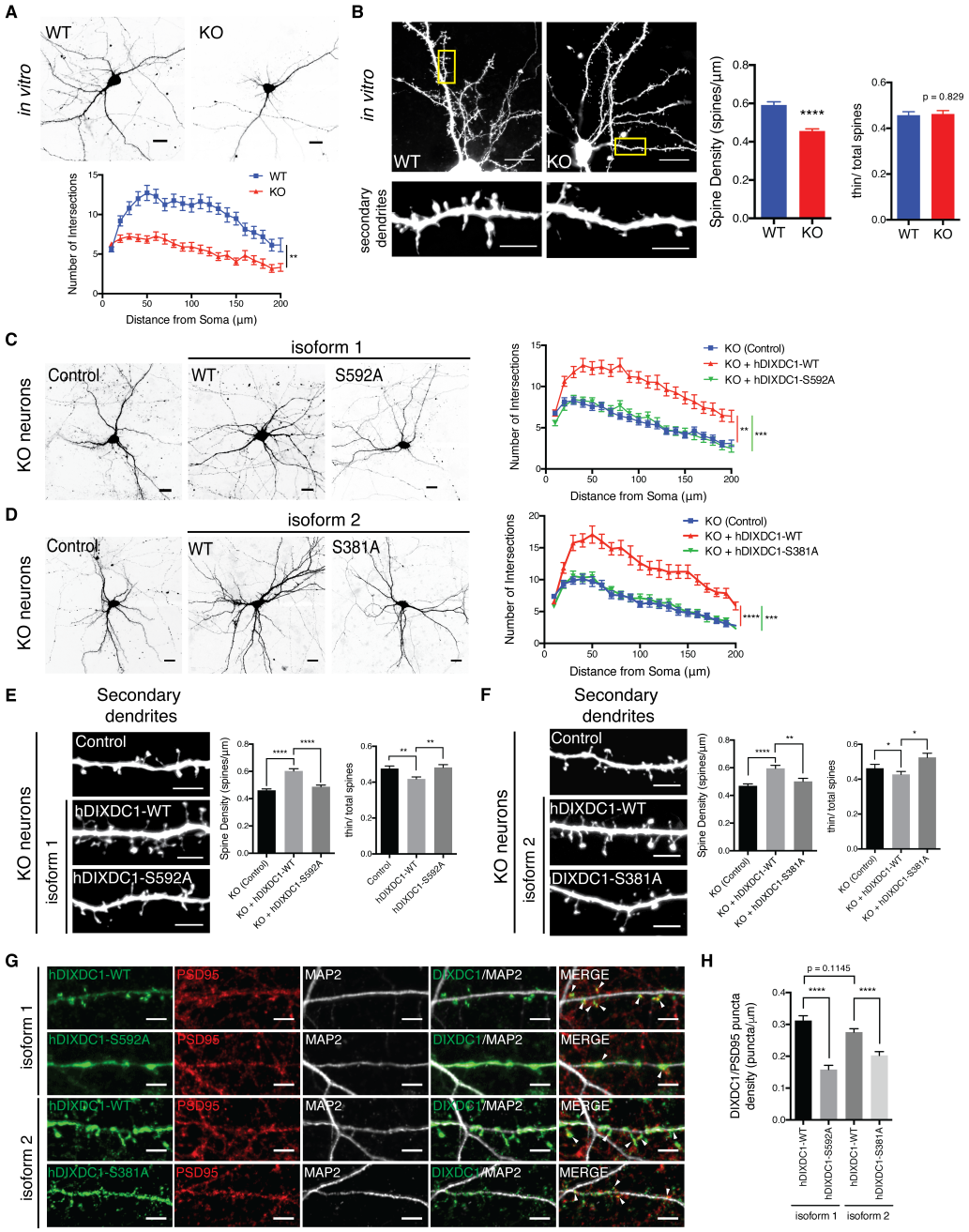

Figure 4: Phosphorylation of DIXDC1 isoforms by MARK1 regulates neuronal morphology. (**A**) Sholl analysis of cultured DIV14 WT and *Dixdc1* KO neurons shows a decrease in dendrite complexity in *Dixdc1* KO neurons (n = 4 cultures; two-way ANOVA

test: **p < 0.01). (**B**) Spine morphological analysis of cultured WT and *Dixdc1* KO neurons showed a decrease in spine density in *Dixdc1* KO neurons at DIV14 (n = 3 cultures; t test: ****p < 0.0001). (**C**) Sholl analysis of overexpression of hDIXDC1-S592A (isoform 1) in *Dixdc1* KO cultures demonstrates no rescue in dendrite growth defects (n = 4 cultures; two-way ANOVA; post hoc Sidak test: **p < 0.01; ***p < 0.001). (**D**) Sholl analysis of overexpressed hDIXDC1-S381A (isoform 2) in *Dixdc1* KO cultures was unable to rescue dendrite growth defects (n = 3 cultures; two-way ANOVA; post hoc Sidak test: ***p < 0.001; ****p < 0.0001). (**E**) Spine analysis reveals that overexpression of hDIXDC1-S592A (isoform 1) in *Dixdc1* KO cultures does not increase dendritic spine density (n = 3 cultures; one- way ANOVA; post hoc Sidak test: **p < 0.01; ****p < 0.0001). (**F**) Spine analysis of overexpressed hDIXDC1-S381A (isoform 2) in *Dixdc1* KO cultures does not increase dendritic spine density (n = 3 cultures; one-way ANOVA; post hoc Sidak test: *p < 0.05; **p < 0.01; ****p < 0.0001). (**G**) Cortical neurons transfected with GFP-tagged hDIXDC1-WT, -S592A (isoform 1), hDIXDC1-WT, or -S381A (isoform 2) and were immunostained with antibodies against GFP, PSD95, and MAP2. Arrows show co-localization of DIXDC1 isoforms 1 and 2 with PSD95. (H) Quantification of DIXDC1 and PSD95 co-localization puncta density on MAP2-positive secondary dendrites (n = 3 cultures; one-way ANOVA; post hoc Sidak test: ****p < 0.0001). All numerical data are given as mean ± SEM. The scale bars represent 20 mm for (**A**), (**C**), and (**D**) and 5 mm for (**B**), (**E**), (**F**), and (**G**). See also Figure S5.

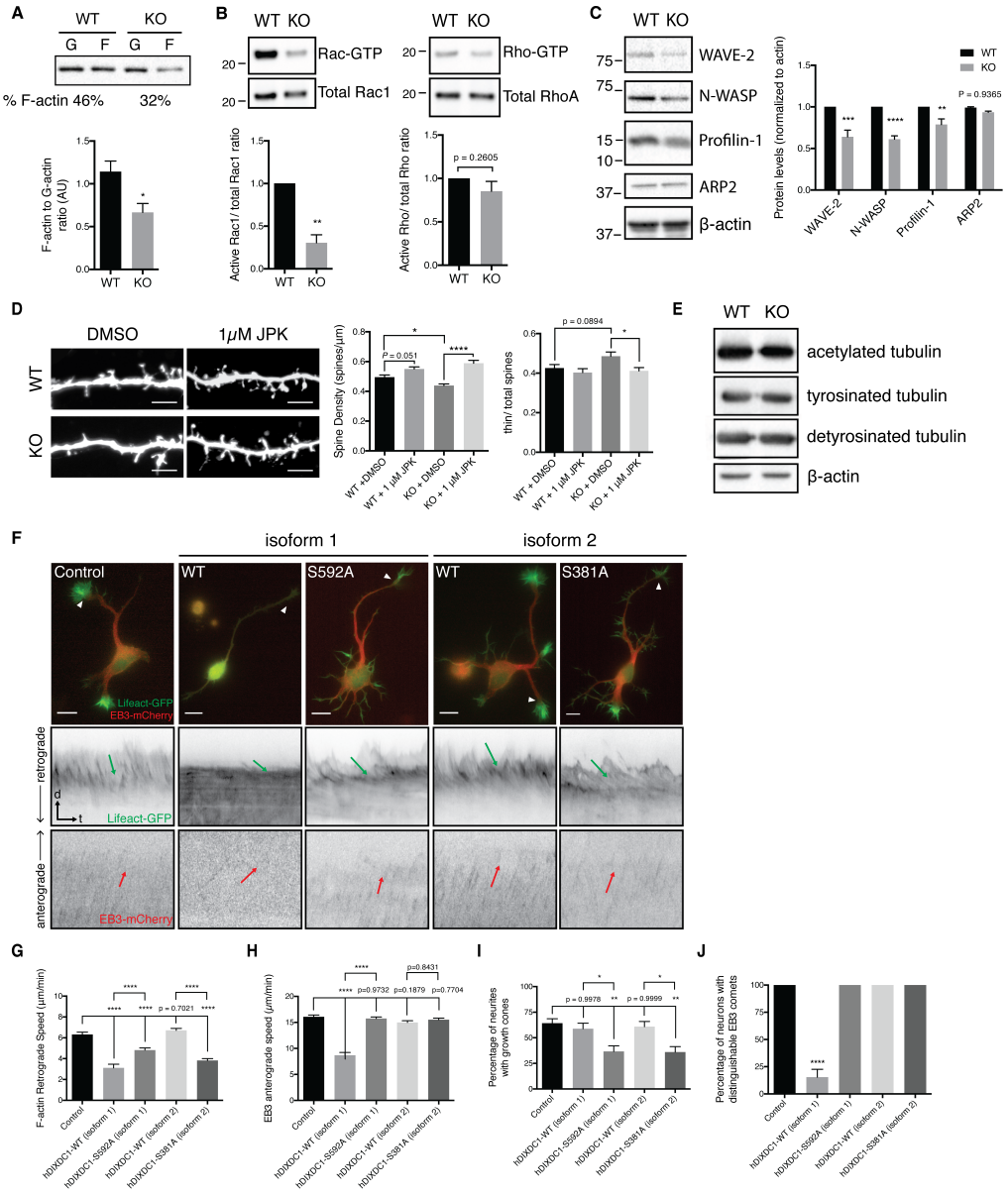

Figure 5: Phosphorylation of DIXDC1 regulates cytoskeleton dynamics and spine growth. (**A**) F- to G-actin ratio was biochemically assayed in P30 WT and *Dixdc1* KO mice. KO brains have a decreased level of F-/G-actin compared to WT mice (n = 3 mice; t test: *p < 0.05). (**B**) Active Rac1 and active RhoA levels were measured in WT and KO brains, and KO brains have decreased level of Rac1-GTP/total Rac1 (n = 3 mice; t test: *p

< 0.05). (**C**) WT and KO whole-brain lysates (P28) were probed for WAVE-2, N-WASP, and profilin-1 levels and show a decrease in all three proteins (n = 3 mice; Wilcoxon signed-rank test: **p < 0.01; ***p < 0.001; ****p < 0.0001). (**D**) DIV14 cultured WT and *Dixdc1* KO cortical neurons treated with 1 mM JPK and assessed morphologically. JPK increased dendritic spine density in KO cultures, similar to treated WT cultures (n = 3 cultures; one-way ANOVA; post hoc Sidak test: *p < 0.05; ****p < 0.0001). (**E**) WT and KO whole-brain lysates (P30) were probed for acetylated tubulin, tyrosinated tubulin, and detyrosinated tubulin. (**F**) Cultured rat hippocampal neurons (DIV2) transfected with Lifeact-GFP and EB3-mCherry, and hDIXDC1-WT, or -S592A (isoform 1), or hDIXDC1- WT, -S381A (isoform 2). Kymographs were generated from time-lapse videos. White arrows show the representative neurite. Green arrows show the speed of F-actin comets, and red arrows show the speed of EB3 comets. (**G**) hDIXDC1-WT isoform 1 alters F-actin retrograde speed. Both hDIXDC1-S592A and -S381A showed similar changes in F-actin speeds (n = 3 cultures; one-way ANOVA; post hoc Sidak test: ****p < 0.0001). (H) hDIXDC1-WT isoform 1 EB3 anterograde speeds were decreased compared to control neurons (n = 3 cultures; one-way ANOVA; post hoc Sidak test: ****p < 0.0001). (**I**) Quantification of the percentage of neurites with growth cones in the indicated conditions (n = 3 cultures; one-way ANOVA; post hoc Sidak test: *p < 0.05; **p < 0.01). (**J**) Quantification of the percentage of neurons with EB3 comets (n = 3 cultures; one-way ANOVA; post hoc Sidak test: ****p < 0.0001). All numerical data are given as mean ± SEM. The scale bars represent 10 mm for (**F**) and 5 mm for (**E**). See also Figure S6.

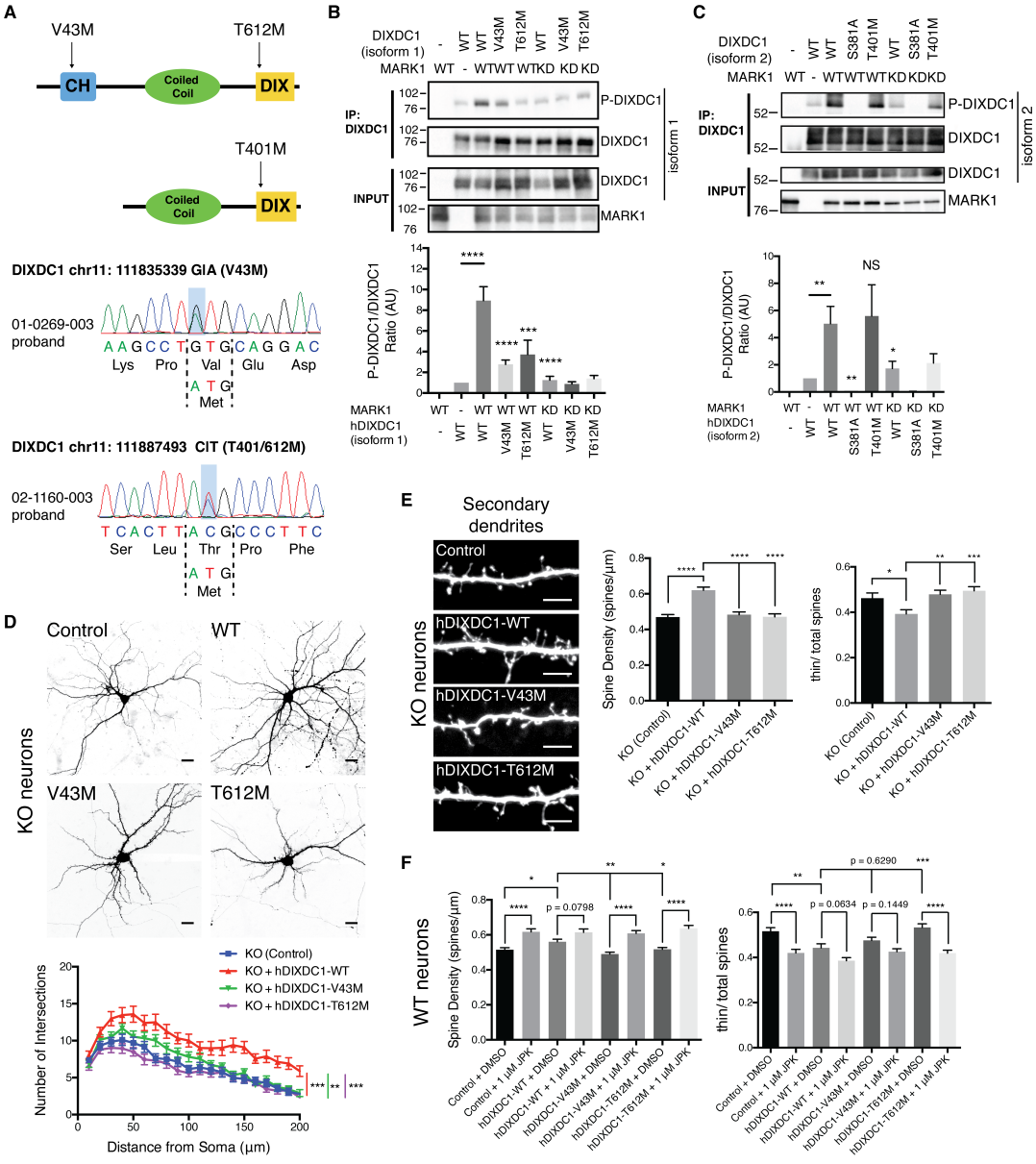
A
V43M
T612M
CH
Coiled Coil
DIX
T401M
DIXDC1 chr11: 111835339 GIA (V43M)
01-0269-003 proband
Lys Pro Val Glu Asp
Met
DIXDC1 chr11: 111887493 CIT (T401/612M)
02-1160-003 proband
Ser Leu Thr Pro Phe
Met
B
DIXDC1 (isoform 1)
MARK1
IP: DIXDC1
INPUT
P-DIXDC1
DIXDC1
MARK1
isoform 1
P-DIXDC1/DIXDC1 Ratio (AU)
hDIXDC1 (isoform 1)
C
DIXDC1 (isoform 2)
isoform 2
NS
hDIXDC1 (isoform 2)
D
Control
WT
V43M
T612M
KO neurons
Number of Intersections
Distance from Soma (μm)
KO (Control)
KO + hDIXDC1-WT
KO + hDIXDC1-V43M
KO + hDIXDC1-T612M
E
Secondary dendrites
hDIXDC1-WT
hDIXDC1-V43M
hDIXDC1-T612M
Spine Density (spines/μm)
thin/ total spines
F
WT neurons
p = 0.0798
p = 0.6290
p = 0.0634
p = 0.1449
Control + DMSO
Control + 1 μM JPK
hDIXDC1-WT + DMSO
hDIXDC1-WT + 1 μM JPK
hDIXDC1-V43M + DMSO
hDIXDC1-V43M + 1 μM JPK
hDIXDC1-T612M + DMSO
hDIXDC1-T612M + 1 μM JPK

Figure 6. ASD-linked genetic variants in *DIXDC1* isoform 1 impair dendrite and spine development in KO neurons. (**A**) Schematic diagram of DIXDC1 (isoform 1) shows the location of the V43M and T612M variants and confirmation by sequencing (family ID: 01-0269 [V43M] and 2-1160 [T612M]). (**B**) Expression of hDIXDC1-V43M and -T612M in HEK293 cells results in a decrease in phosphorylation at DIXDC1 serine592 in the presence of MARK1 (n = 4; one-way ANOVA; post hoc Sidak test: ***p < 0.001; ****p < 0.0001). (**C**) Expression of hDIXDC1 T401M in HEK293 cells does not affect phosphorylation at DIXDC1 serine381 (n = 3; one-way ANOVA; post hoc Sidak test: *p < 0.05; **p < 0.01). (**D**) Sholl analysis of neurons expressing hDIXDC1-V43M and -T612M variants in KO neurons did not reveal an increase in dendritic tree complexity (KO; n = 3 cultures; two-way ANOVA; post hoc Sidak test: **p < 0.01; ***p < 0.001). (**E**) Morphological analysis of neurons overexpressing hDIXDC1-V43M and -T612M in KO neurons did not show an increase in spine density compared to KO (control; n = 3 cultures; one-way ANOVA; post hoc Sidak test: *p < 0.05; **p < 0.01; ***p < 0.001; ****p < 0.0001). (**F**) Morphological analysis of WT neurons expressing hDIXDC1-WT, -V43M, or -T612M and treated with JPK shows a rescue in defects in spine density (n = 3 cultures; one-way ANOVA; post hoc Sidak test: *p < 0.05; **p < 0.01; ***p < 0.001; ****p < 0.0001). All numerical data are given as mean ± SEM. The scale bars represent 20 mm for (**E**) and 5 mm for (**F**). See also Figure S7.

2.7 SUPPLEMENTARY FIGURES

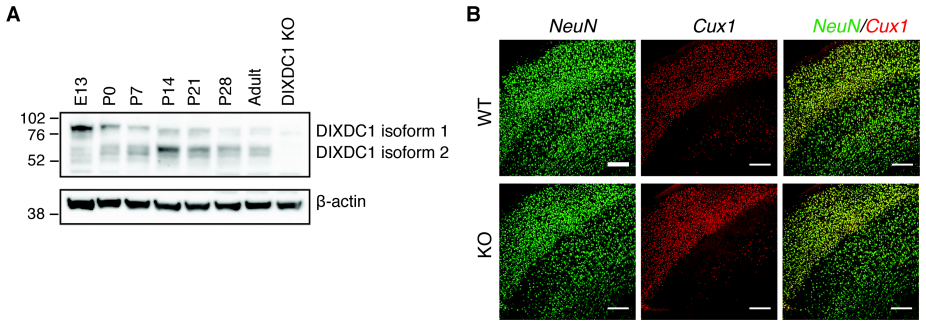

Figure S1, Related to Figure 1. Expression of DIXDC1 and MARK1 in the developing brain.
(A) Western blot analysis of time course CD-1 mouse brains and P28 *DIXDC1* KO brain, probed for DIXDC1 (actin loading control). **(B)** P28 WT and *DIXDC1* KO coronal brain sections showing neurons immunostained with NeuN and Cux1. Scale bar, 200 μm.

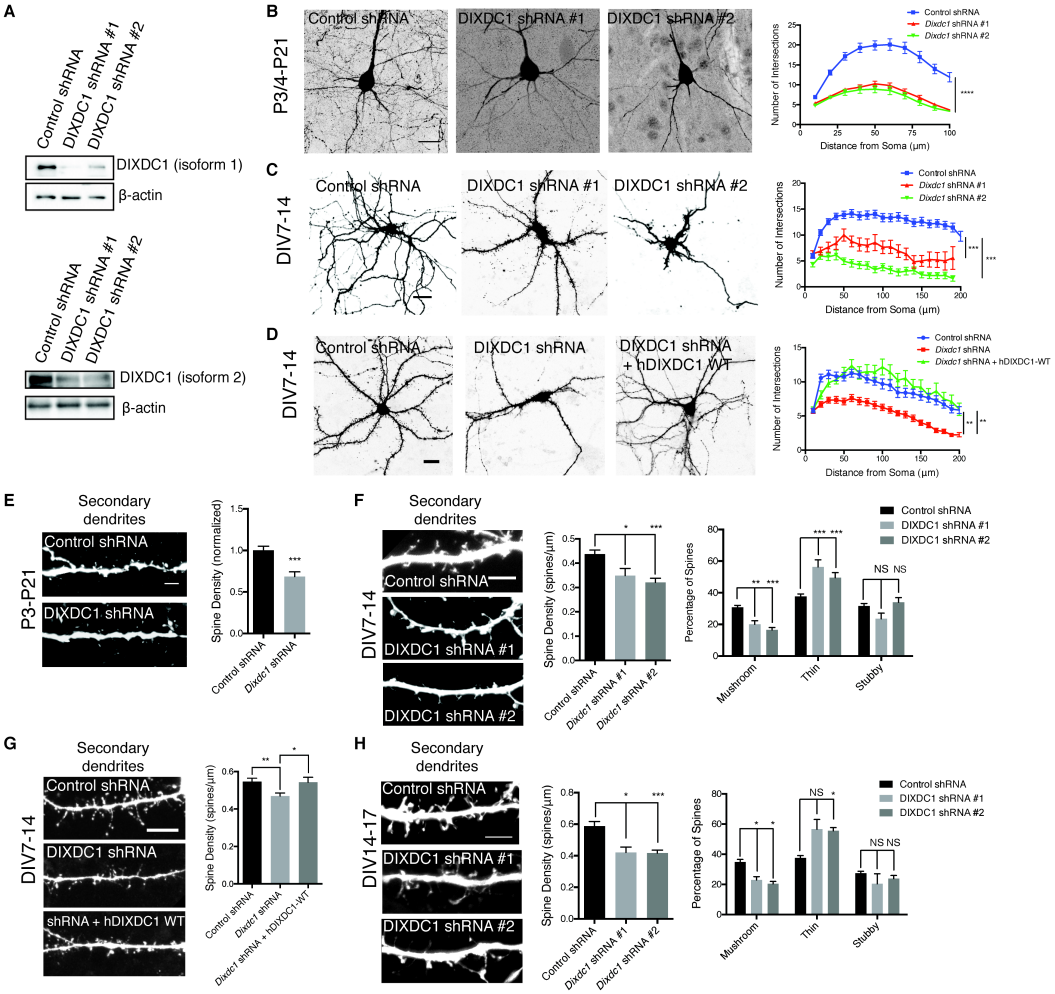

Figure S2, Related to Figre 2. Acute knockdown of DIXDC1 impairs dendrite outgrowth and dendritic spine formation.
(A) Knockdown of mDIXDC1 isoform 1 and 2 with Control shRNA, DIXDC1 shRNA #1 and #2 (actin loading control). **(B)** P3/4 CD-1 WT mice injected with RFP shRNA, DIXDC1 shRNA #1 or #2 lentivirus (H1GIP backbone) and harvested at P21. Sholl analysis showed a decrease in dendrite complexity with reduced DIXDC1 expression (RFP shRNA, n = 37 neurons; DIXDC1 shRNA #1, n = 30 neurons; DIXDC1 shRNA #2, n = 28 neurons; 3 mice; one-way ANOVA, post hoc Sidak test: ****p < 0.0001). **(C)** Reduction of DIXDC1 expression at DIV7 decreased dendritic complexity at DIV14 (Control shRNA, n = 61 neurons; DIXDC1 shRNA #1, n = 12 neurons; DIXDC1 shRNA #2, n = 24 neurons; 3 cultures; one-way ANOVA, post hoc Sidak test: ***p < 0.001). **(D)** Overexpression of hDIXDC1-WT (isoform 1) was able to rescue dendritic complexity defects of DIXDC1 shRNA (Control shRNA, n= 40 neurons; DIXDC1 shRNA #1, n = 31 neurons; DIXDC1 shRNA #1 + hDIXDC1 WT, n = 22 neurons; 3 cultures; one-way ANOVA, post hoc Sidak test: *p < 0.05, **p < 0.01). **(E)** Reduction of DIXDC1 decreased dendritic spine density in P21 layer 2/3 neurons (RFP shRNA, n = 30 neurons, 65 dendrites; DIXDC1 shRNA, n = 20 neurons, 25 dendrites; DIXDC1 shRNA #2, n = 27 neurons, 33 dendrites; 3 mice; one-way ANOVA, post hoc Sidak test: **p < 0.01). **(F)** Dendritic spine analysis at DIV14 showed that reduced DIXDC1 expression results in a decrease in dendritic spine density (Control shRNA, n = 17 neurons, 51 dendrites; DIXDC1 shRNA #1, n = 14 neurons, 26 dendrites; DIXDC1 shRNA #2, n = 19 neurons, 30 dendrites, 3 cultures; one-way ANOVA, post hoc Sidak test: ***p < 0.001). **(G)** Spine analysis at DIV14 showed that hDIXDC1-WT was able to rescue the decrease in dendritic spine density caused by DIXDC1 shRNA (Control shRNA, n = 10 neurons, 20 dendrites; DIXDC1 shRNA #1, n = 10 neurons, 20 dendrites; DIXDC1 shRNA #1 + hDIXDC1-WT, n = 10 neurons, 20 dendrites, 3 cultures; one-way ANOVA, post hoc Sidak test: *p < 0.05). **(H)** Dendritic spine density decreased with a reduction of DIXDC1 expression at DIV17 (Control shRNA, n = 9 neurons, 28 dendrites; DIXDC1 shRNA #1, n = 10 neurons, 20 dendrites; DIXDC1 shRNA #2, n = 10 neurons, 35 dendrites, 3 cultures; one-way ANOVA, post hoc Sidak test: *p < 0.05, ***P<0.001). All numerical data are given as mean ± SEM. Scale bars, 20 μm for **B, C, D** and 5 μm for **E, F, G, H**.

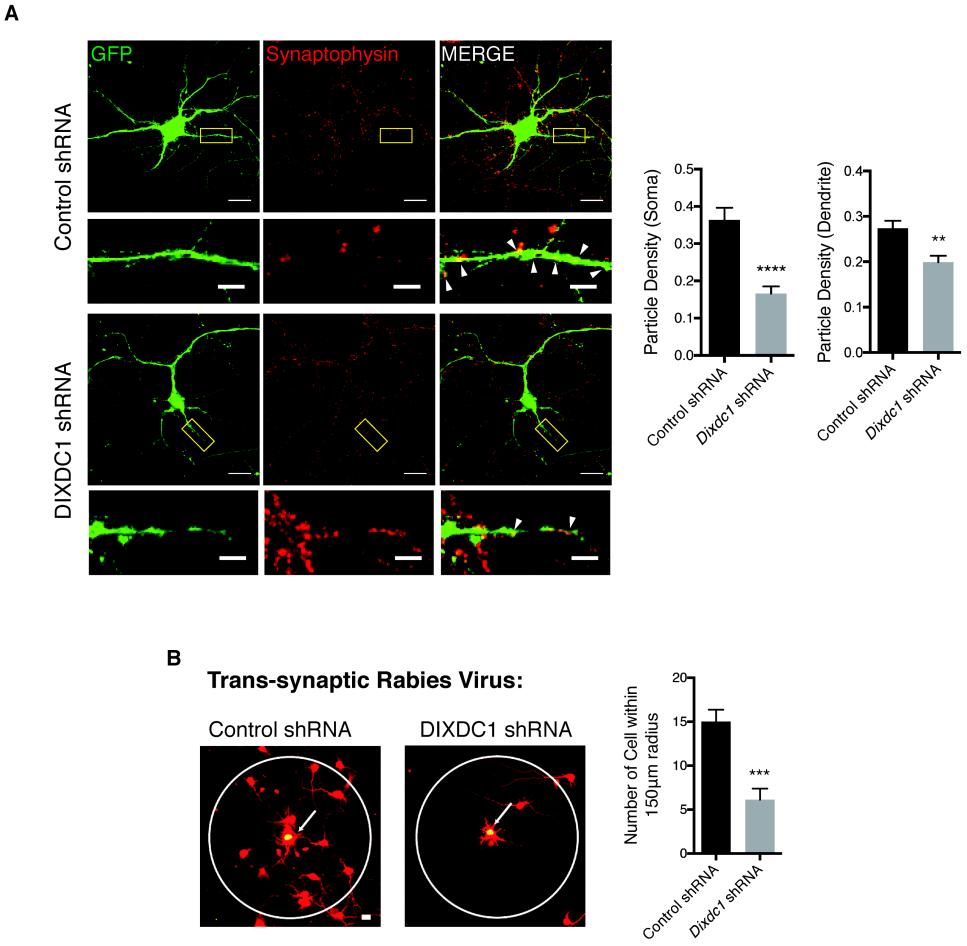

Figure S3, Related to Figure 2. Knockdown of DIXDC1 results in synaptic and neuronal connectivity deficits.
(A) Cultures immunostained using anti-synaptophysin (Sigma) and synaptophysin particle density was reduced on the cell soma and dendrites in neurons with reduced DIXDC1 expression. Arrows indicate synaptophysin puncta (Control shRNA, n = 23 neurons, 61 dendrites; DIXDC1 shRNA, n = 14 neurons, 32 dendrites, 3 cultures; t test: **p < 0.01, ****p < 0.0001). **(B)** Cultured neurons with reduced DIXDC1 expression had reduced number of neurons formed retrograde synapses (Control shRNA, n = 75 neurons; DIXDC1 shRNA, n = 25 neurons, 3 cultures; t test: ***p < 0.001, mean ± SEM). All numerical data are given as mean ± SEM. Scale bars, 20 µm for **A** (top) and **B,** 5 µm for **A** (bottom).

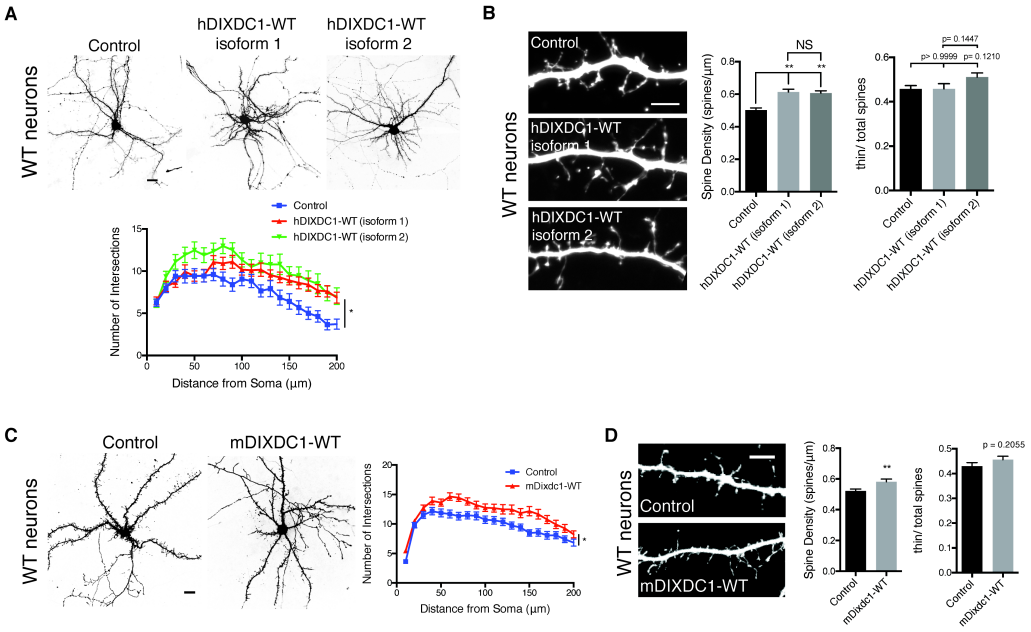

Figure S4, Related to Figure 2. Overexpression of mouse DIXDC1 stimulates dendritic branching and dendritic spine formation.

(A) Sholl analysis of DIV14 cultures showed that isoform 1 and 2 have similar increases of dendritic complexity compared to control (Control, n = 35 neurons; hDIXDC1-WT isoform 1, n = 36 neurons; hDIXDC1-WT isoform 2, n = 36 neurons, 3 cultures; one-way ANOVA, post hoc Sidak test: *p < 0.05). **(B)** Dendritic spine density of cortical neurons showed an increase in dendritic spine density with hDIXDC1-WT isoform 1 and 2 overexpression compared to control, and no difference in dendritic spine density between hDIXDC1-WT isoform 1 and isoform 2. No changes in thin spines detected (Control, n = 29 neurons, 58 dendrites; hDIXDC1-WT isoform 1, n = 27 neurons, 54 dendrites; hDIXDC1-WT isoform 2, n = 30 neurons, dendrites 59, 3 cultures; one-way ANOVA, post hoc Sidak test: **p < 0.01). **(C)** Overexpression of wildtype mouse DIXDC1 (isoform 1) increases dendrite complexity compared to control (Control, n = 79 neurons; mDIXDC1, n = 84 neurons, 3 cultures; t test: *p < 0.05). **(D)** Dendritic spine density increased with overexpression of mDIXDC1-WT. No changes in thin type spines were observed (Control, n = 26 neurons, 62 dendrites; mDIXDC1, n = 20 neurons, 43 dendrites, 3 cultures; t test: **p < 0.01). All numerical data are given as mean ± SEM. Scale bars, 20 µm for **A, C** and 5 µm for **B, D**.

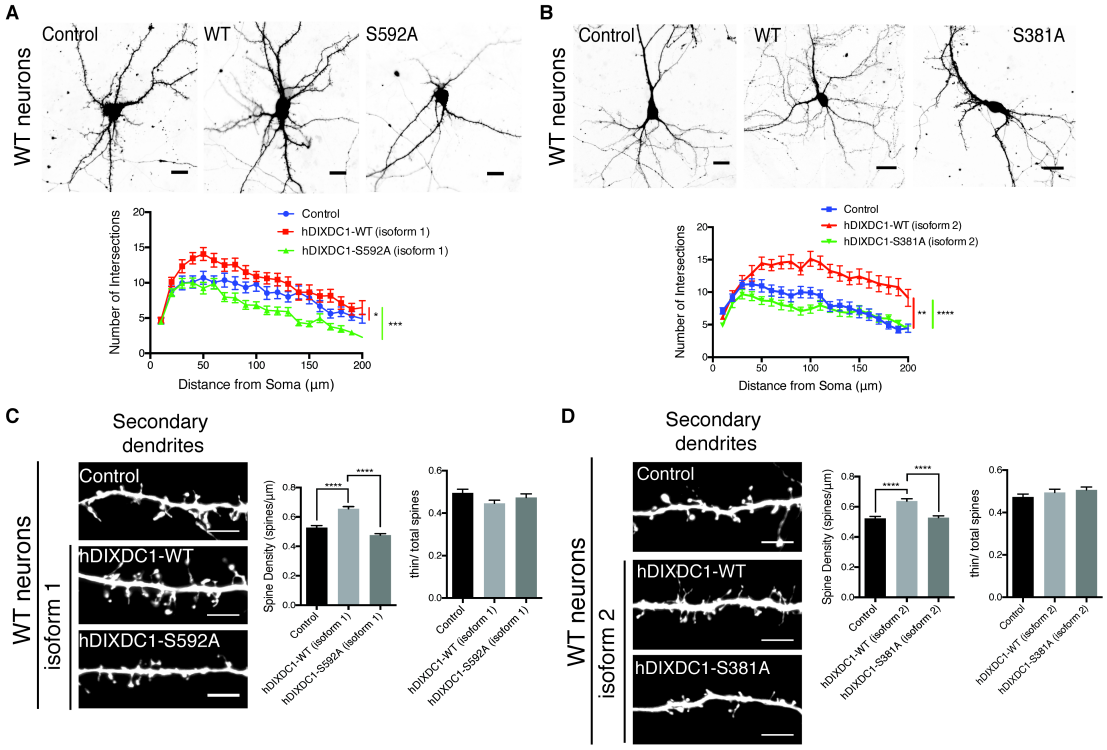

Figure S5, Related to Figure 4. Phosphorylation of DIXDC1 isoforms 1 and 2 by MARK1 regulates neuronal morphology in WT neurons (*in vitro*).
(A) hDIXDC1-WT (isoform 1) overexpression increases dendrite complexity, whereas overexpression of hDIXDC1-S592A decreases dendrite branching compared to controls (Control (GFP), n = 35 neurons; hDIXDC1-WT, n = 38 neurons; hDIXDC1-S592A, n = 41 neurons, 3 cultures; one-way ANOVA, post hoc Sidak test: *p < 0.05, ***p < 0.001). **(B)** hDIXDC1-WT isoform 2 overexpression increases dendrite complexity, and hDIXDC1-S381A overexpression decreased dendritic complexity compared to WT (Control (GFP), n = 32 neurons; hDIXDC1-WT isoform 2, n = 31 neurons; hDIXDC1-S381A, n = 31 neurons, 3 cultures; one-way ANOVA, post hoc Sidak test: **p < 0.01, ****p < 0.0001). **(C)** hDIXDC1-S592A (isoform 1) decreased dendritic spine density compared to WT (Control (GFP), n = 29 neurons, 52 dendrites; hDIXDC1 WT, n = 36 neurons, 77 dendrites; hDIXDC1 S592A, n = 35 neurons, 64 dendrites, 3 cultures; one-way ANOVA, post hoc Sidak test: ****p < 0.0001). **(D)** hDIXDC1-WT (isoform 2) showed an increase in dendritic spine density, whereas hDIXDC1-S381A overexpression decreased dendritic spine density compared to WT overexpression (Control (GFP), n = 31 neurons, 62 dendrites; hDIXDC1-WT, n = 30 neurons, 60 dendrites; hDIXDC1-S381A, n = 30 neurons, 60 dendrites, 3 cultures; one-way ANOVA, post hoc Sidak test: ****p < 0.0001). All numerical data are given as mean ± SEM. Scale bars, 20 µm for **A, B** and 5 µm for **C, D**.

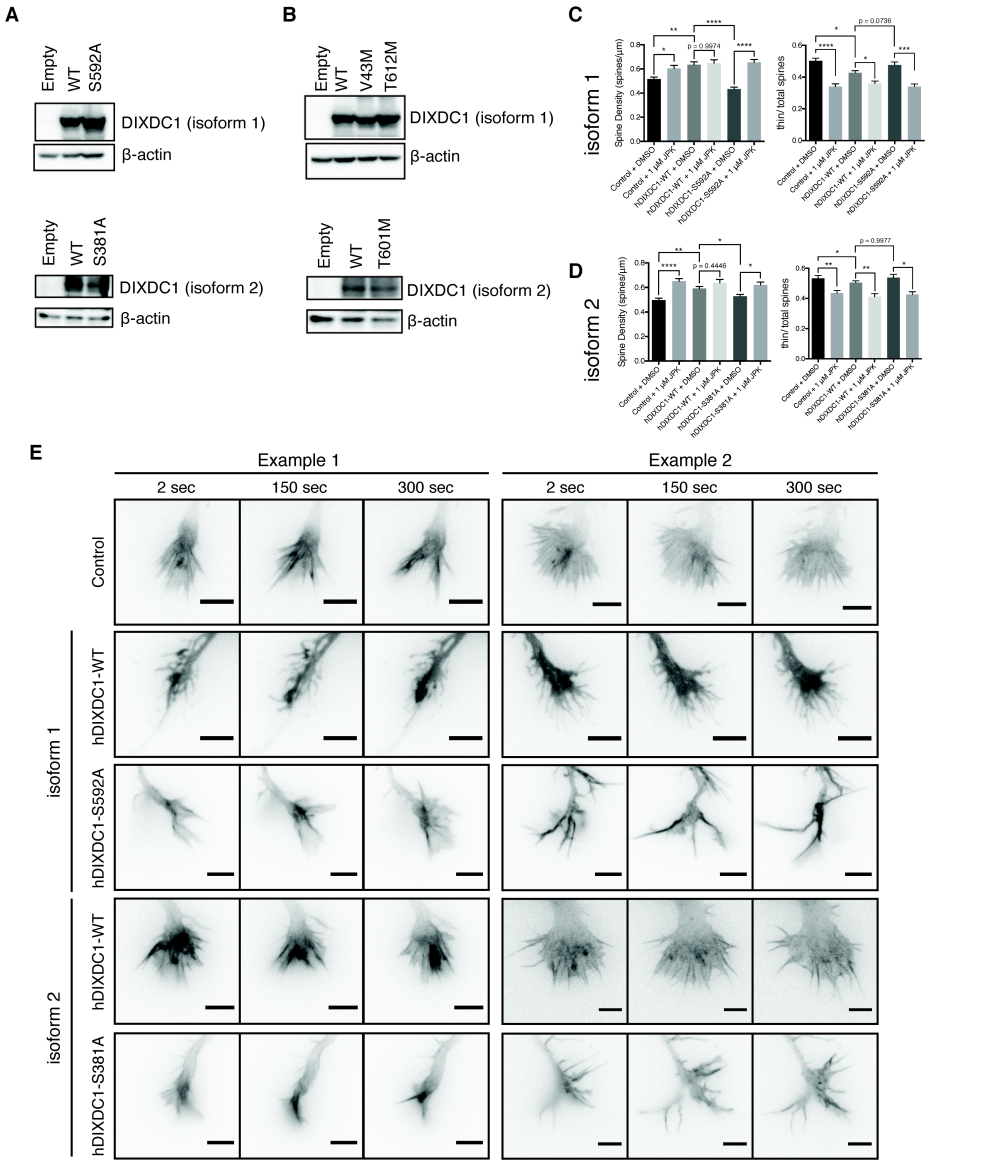

Figure S6, Related to Figure 6. Loss of DIXDC1 function impairs actin motility.

(A) Western blot of HEK293 cells expressing, hDIXDC1-WT, -S592A (isoform 1) and hDIXDC1-WT, -S381A (isoform 2), probed with DIXDC1 antibody (actin loading control). **(B)** Western blot of HEK293 cells expressing hDIXDC1-WT, -V43M, -T612M (isoform 1) and hDIXDC-WT, -T401M (isoform 2) probed with DIXDC1 antibody (actin loading control). **(C)** Cultured cortical neurons transfected with hDIXDC1-WT or -S592A and treated with 1µM JPK at DIV14 showed that JPK could rescue the defect in dendritic spine density (Control (GFP) + DMSO, n = 14 neurons, 27 dendrites; Control (GFP) + 1µM JPK, n = 14 neurons, 28 dendrites; hDIXDC1-WT + DMSO, n = 14 neurons, 26 dendrites; hDIXDC1-WT + 1µM JPK, n = 14 neurons, 28 dendrites; hDIXDC1-S592A + DMSO, n = 15 neurons, 30 dendrites; hDIXDC1-S592A + 1µM JPK, n = 13 neurons, 24 dendrites, 2 cultures; one-way ANOVA, post hoc Sidak test: *p < 0.05, **p < 0.01, ***p < 0.001, ****p < 0.0001). **(D)** JPK treatment of DIV14 neuronal cultures expressing hDIXDC1-S381A was able to rescue dendritic spine density defects (Control (GFP) + DMSO, n = 16 neurons, 32 dendrites; Control (GFP) + 1µM JPK, n = 16 neurons, 32 dendrites; hDIXDC1-WT + DMSO, n = 16 neurons, 32 dendrites; hDIXDC1-WT + 1µM JPK, n = 12 neurons, 24 dendrites; hDIXDC1-S381A + DMSO, n = 13 neurons, 26 dendrites; hDIXDC1-S381A + 1µM JPK, n = 11 neurons, 22 dendrites, 3 cultures; one-way ANOVA, post hoc Sidak test: *p < 0.05, **p < 0.01, ****p < 0.0001). **(E)** Representative images of 2 separate experiments showing Lifeact-GFP (growth cone) at 2sec, 150sec and 300sec time points. All numerical data are given as mean ± SEM. Scale bars, 20 µm for **E.**

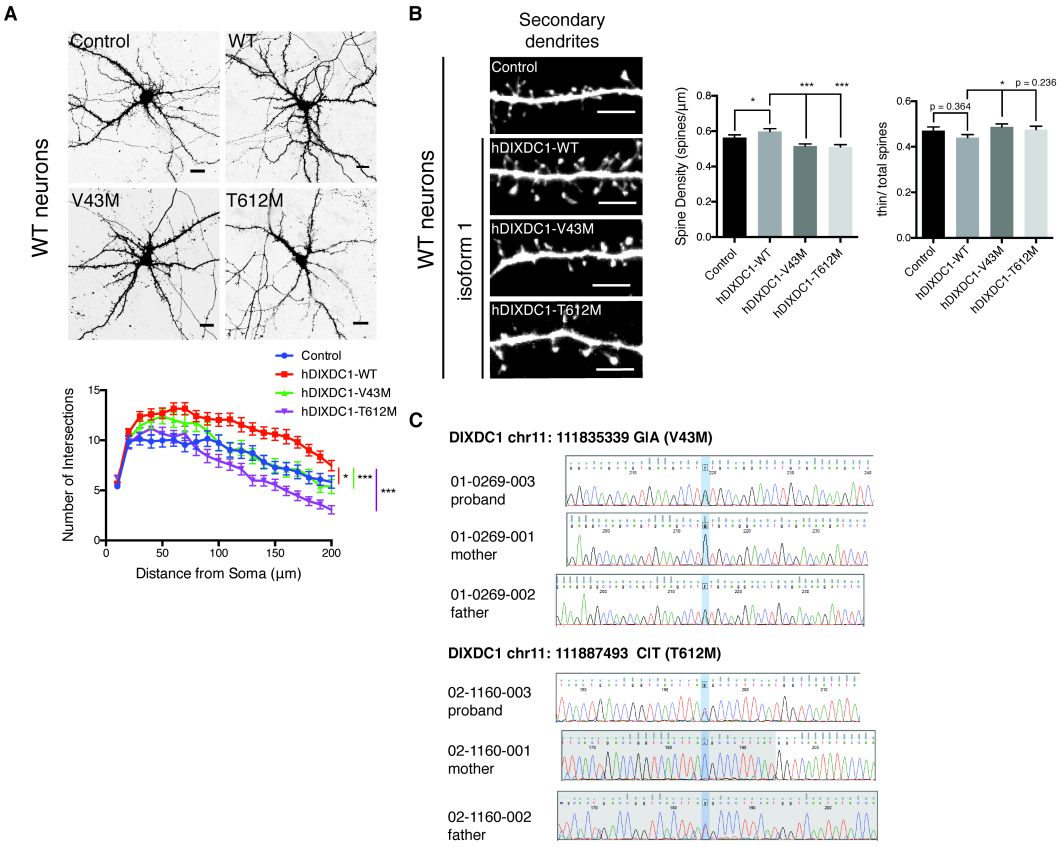

Figure S7, Related to Figure 7. ASD-linked genetic variants in DIXDC1 isoform 1 impair dendrite and spine development in WT neurons.

(A) hDIXDC1-V43M and -T612M variants both decreased dendrite complexity compared to WT (Control (GFP), n = 70 neurons; hDIXDC1-WT, n = 93 neurons; hDIXDC1-V43M, n = 62 neurons; hDIXDC1-T612M, n = 65 neurons, 3 cultures; one-way ANOVA, post hoc Sidak test: *p < 0.05, ***p < 0.001). **(B)** hDIXDC1-V43M and -T612M decreased dendritic spine density compared to WT (Control (GFP), n = 20 neurons, 51 dendrites; hDIXDC1-WT, n = 27 neurons, 71 dendrites; hDIXDC1-V43M, n = 26 neurons, 66 dendrites; hDIXDC1-T612M, n = 25 neurons, 55 dendrites, 3 cultures; one-way ANOVA, post hoc Sidak test: *p < 0.05, ***p < 0.001). **(C)** The genomic region of DIXDC1 from ASD proband, mother, and father was amplified and sequenced from genomic DNA using Sanger sequencing (Family ID: 01-0269 (V43M), and 2-1160 (T612M)). This was used as a confirmation of exome sequencing data that initially identified these variants. All numerical data are given as mean ± SEM. Scale bars, 20 µm for **A** and 5 µm for **B**.

Chromosome	Position (begin)	Reference allele	Child genotype	Amino acid change	Inheritance	1000g_all	NHLBI_all	dbSNP	Polyphen score	Number of cases
chr11	111808246	G	G/A	G8E	paternal	NA	NA	NA	0.998	1
chr11	111835339	G	G/A	V43M	paternal	NA	NA	NA	0.999	2
chr11	111859774	A	A/T	I370L	materna	NA	0.000254	rs373126732	0.946	1
chr11	111887493	C	C/T	T612M	paternal	0.0014	0.000659	rs184718561	1.0	2

Table 1: Rare missense variants in *DIXDC1* discovered through exome and whole genome sequencing of Canadian ASD cohorts. Summary of rare missense variants in *DIXDC1* from Canadian simplex families

REFERENCES

Akhmanova, A., and Hoogenraad, C.C. (2005). Microtubule plus-end-tracking proteins: mechanisms and functions. Current opinion in cell biology *17*, 47-54.

Berkel, S., Marshall, C.R., Weiss, B., Howe, J., Roeth, R., Moog, U., Endris, V., Roberts, W., Szatmari, P., Pinto, D.*, et al.* (2010). Mutations in the SHANK2 synaptic scaffolding gene in autism spectrum disorder and mental retardation. Nature genetics *42*, 489-491.

Bernard, L.P., and Zhang, H. (2015). MARK/Par1 Kinase Is Activated Downstream of NMDA Receptors through a PKA-Dependent Mechanism. PloS one *10*, e0124816.

Bernier, R., Golzio, C., Xiong, B., Stessman, H.A., Coe, B.P., Penn, O., Witherspoon, K., Gerdts, J., Baker, C., Vulto-van Silfhout, A.T.*, et al.* (2014). Disruptive CHD8 mutations define a subtype of autism early in development. Cell *158*, 263-276.

Bhakar, A.L., Dolen, G., and Bear, M.F. (2012). The pathophysiology of fragile X (and what it teaches us about synapses). Annual review of neuroscience *35*, 417-443.

Bourgeron, T. (2015). From the genetic architecture to synaptic plasticity in autism spectrum disorder. Nature reviews Neuroscience *16*, 551-563.

Bozdagi, O., Sakurai, T., Dorr, N., Pilorge, M., Takahashi, N., and Buxbaum, J.D. (2012). Haploinsufficiency of Cyfip1 produces fragile X-like phenotypes in mice. PloS one *7*, e42422.

Brennand, K.J., Simone, A., Jou, J., Gelboin-Burkhart, C., Tran, N., Sangar, S., Li, Y., Mu, Y., Chen, G., Yu, D.*, et al.* (2011). Modelling schizophrenia using human induced pluripotent stem cells. Nature *473*, 221-225.

Calabrese, B., and Halpain, S. (2014). Lithium prevents aberrant NMDA-induced F-actin reorganization in neurons. Neuroreport *25*, 1331-1337.

Cao, F., Yin, A., Wen, G., Sheikh, A.M., Tauqeer, Z., Malik, M., Nagori, A., Schirripa, M., Schirripa, F., Merz, G.*, et al.* (2012). Alteration of astrocytes and Wnt/beta-catenin signaling in the frontal cortex of autistic subjects. Journal of neuroinflammation *9*, 223.

Capelluto, D.G., Kutateladze, T.G., Habas, R., Finkielstein, C.V., He, X., and Overduin, M. (2002). The DIX domain targets dishevelled to actin stress fibres and vesicular membranes. Nature *419*, 726-729.

Chen, J.A., Penagarikano, O., Belgard, T.G., Swarup, V., and Geschwind, D.H. (2015). The emerging picture of autism spectrum disorder: genetics and pathology. Annual review of pathology *10*, 111-144.

Chikano, Y., Domoto, T., Furuta, T., Sabit, H., Kitano-Tamura, A., Pyko, I.V., Takino, T., Sai, Y., Hayashi, Y., Sato, H.*, et al.* (2015). Glycogen synthase kinase 3beta sustains invasion of glioblastoma via the focal adhesion kinase, Rac1, and c-Jun N-terminal kinase-mediated pathway. Molecular cancer therapeutics *14*, 564-574.

Ciani, L., Marzo, A., Boyle, K., Stamatakou, E., Lopes, D.M., Anane, D., McLeod, F., Rosso, S.B., Gibb, A., and Salinas, P.C. (2015). Wnt signalling tunes neurotransmitter release by directly targeting Synaptotagmin-1. Nature communications *6*, 8302.

De Rubeis, S., He, X., Goldberg, A.P., Poultney, C.S., Samocha, K., Cicek, A.E., Kou, Y., Liu, L., Fromer, M., Walker, S.*, et al.* (2014). Synaptic, transcriptional and chromatin genes disrupted in autism. Nature *515*, 209-215.

De Rubeis, S., Pasciuto, E., Li, K.W., Fernandez, E., Di Marino, D., Buzzi, A., Ostroff, L.E., Klann, E., Zwartkruis, F.J., Komiyama, N.H.*, et al.* (2013). CYFIP1 coordinates mRNA translation and cytoskeleton remodeling to ensure proper dendritic spine formation. Neuron *79*, 1169-1182.

Deriziotis, P., O'Roak, B.J., Graham, S.A., Estruch, S.B., Dimitropoulou, D., Bernier, R.A., Gerdts, J., Shendure, J., Eichler, E.E., and Fisher, S.E. (2014). De novo TBR1 mutations in sporadic autism disrupt protein functions. Nature communications *5*, 4954.

Dolan, B.M., Duron, S.G., Campbell, D.A., Vollrath, B., Shankaranarayana Rao, B.S., Ko, H.Y., Lin, G.G., Govindarajan, A., Choi, S.Y., and Tonegawa, S. (2013). Rescue of fragile X syndrome phenotypes in Fmr1 KO mice by the small-molecule PAK inhibitor FRAX486. Proceedings of the National Academy of Sciences of the United States of America *110*, 5671-5676.

Duffney, L.J., Wei, J., Cheng, J., Liu, W., Smith, K.R., Kittler, J.T., and Yan, Z. (2013). Shank3 deficiency induces NMDA receptor hypofunction via an actin-dependent

mechanism. The Journal of neuroscience : the official journal of the Society for Neuroscience *33*, 15767-15778.

Duffney, L.J., Zhong, P., Wei, J., Matas, E., Cheng, J., Qin, L., Ma, K., Dietz, D.M., Kajiwara, Y., Buxbaum, J.D.*, et al.* (2015). Autism-like Deficits in Shank3-Deficient Mice Are Rescued by Targeting Actin Regulators. Cell reports *11*, 1400-1413.

Durand, C.M., Perroy, J., Loll, F., Perrais, D., Fagni, L., Bourgeron, T., Montcouquiol, M., and Sans, N. (2012). SHANK3 mutations identified in autism lead to modification of dendritic spine morphology via an actin-dependent mechanism. Molecular psychiatry *17*, 71-84.

Ebert, D.H., and Greenberg, M.E. (2013). Activity-dependent neuronal signalling and autism spectrum disorder. Nature *493*, 327-337.

Fang, W.Q., Chen, W.W., Jiang, L., Liu, K., Yung, W.H., Fu, A.K., and Ip, N.Y. (2014). Overproduction of upper-layer neurons in the neocortex leads to autism-like features in mice. Cell reports *9*, 1635-1643.

Garcia, I., Huang, L., Ung, K., and Arenkiel, B.R. (2012). Tracing synaptic connectivity onto embryonic stem cell-derived neurons. Stem cells *30*, 2140-2151.

Geschwind, D.H., and State, M.W. (2015). Gene hunting in autism spectrum disorder: on the path to precision medicine. The Lancet Neurology *14*, 1109-1120.

Goodwin, J.M., Svensson, R.U., Lou, H.J., Winslow, M.M., Turk, B.E., and Shaw, R.J. (2014). An AMPK-independent signaling pathway downstream of the LKB1 tumor suppressor controls Snail1 and metastatic potential. Molecular cell *55*, 436-450.

Gu, J., Lee, C.W., Fan, Y., Komlos, D., Tang, X., Sun, C., Yu, K., Hartzell, H.C., Chen, G., Bamburg, J.R.*, et al.* (2010). ADF/cofilin-mediated actin dynamics regulate AMPA receptor trafficking during synaptic plasticity. Nat Neurosci *13*, 1208-1215.

Han, K., Holder, J.L., Jr., Schaaf, C.P., Lu, H., Chen, H., Kang, H., Tang, J., Wu, Z., Hao, S., Cheung, S.W.*, et al.* (2013). SHANK3 overexpression causes manic-like behaviour with unique pharmacogenetic properties. Nature *503*, 72-77.

Hayashi-Takagi, A., Araki, Y., Nakamura, M., Vollrath, B., Duron, S.G., Yan, Z., Kasai, H., Huganir, R.L., Campbell, D.A., and Sawa, A. (2014). PAKs inhibitors ameliorate schizophrenia-associated dendritic spine deterioration in vitro and in vivo during late adolescence. Proceedings of the National Academy of Sciences of the United States of America *111*, 6461-6466.

Hayashi-Takagi, A., Takaki, M., Graziane, N., Seshadri, S., Murdoch, H., Dunlop, A.J., Makino, Y., Seshadri, A.J., Ishizuka, K., Srivastava, D.P.*, et al.* (2010). Disrupted-in-Schizophrenia 1 (DISC1) regulates spines of the glutamate synapse via Rac1. Nature neuroscience *13*, 327-332.

Hori, K., Nagai, T., Shan, W., Sakamoto, A., Taya, S., Hashimoto, R., Hayashi, T., Abe, M., Yamazaki, M., Nakao, K.*, et al.* (2014). Cytoskeletal regulation by AUTS2 in neuronal migration and neuritogenesis. Cell reports *9*, 2166-2179.

Hotulainen, P., and Hoogenraad, C.C. (2010). Actin in dendritic spines: connecting dynamics to function. The Journal of cell biology *189*, 619-629.

Huang, W., Zhu, P.J., Zhang, S., Zhou, H., Stoica, L., Galiano, M., Krnjevic, K., Roman, G., and Costa-Mattioli, M. (2013). mTORC2 controls actin polymerization required for consolidation of long-term memory. Nature neuroscience *16*, 441-448.

Ikeuchi, Y., Stegmuller, J., Netherton, S., Huynh, M.A., Masu, M., Frank, D., Bonni, S., and Bonni, A. (2009). A SnoN-Ccd1 pathway promotes axonal morphogenesis in the mammalian brain. The Journal of neuroscience : the official journal of the Society for Neuroscience *29*, 4312-4321.

Iossifov, I., O'Roak, B.J., Sanders, S.J., Ronemus, M., Krumm, N., Levy, D., Stessman, H.A., Witherspoon, K.T., Vives, L., Patterson, K.E.*, et al.* (2014). The contribution of de novo coding mutations to autism spectrum disorder. Nature *515*, 216-221.

Ishizuka, K., Kamiya, A., Oh, E.C., Kanki, H., Seshadri, S., Robinson, J.F., Murdoch, H., Dunlop, A.J., Kubo, K., Furukori, K.*, et al.* (2011). DISC1-dependent switch from progenitor proliferation to migration in the developing cortex. Nature *473*, 92-96.

Jeste, S.S., and Geschwind, D.H. (2014). Disentangling the heterogeneity of autism spectrum disorder through genetic findings. Nature reviews Neurology *10*, 74-81.

Johe, K.K., Hazel, T.G., Muller, T., Dugich-Djordjevic, M.M., and McKay, R.D. (1996). Single factors direct the differentiation of stem cells from the fetal and adult central nervous system. Genes & development *10*, 3129-3140.

Kalkman, H.O. (2012). A review of the evidence for the canonical Wnt pathway in autism spectrum disorders. Molecular autism *3*, 10.

Kivimae, S., Martin, P.M., Kapfhamer, D., Ruan, Y., Heberlein, U., Rubenstein, J.L., and Cheyette, B.N. (2011). Abnormal behavior in mice mutant for the Disc1 binding partner, Dixdc1. Translational psychiatry *1*, e43.

Krey, J.F., Pasca, S.P., Shcheglovitov, A., Yazawa, M., Schwemberger, R., Rasmusson, R., and Dolmetsch, R.E. (2013). Timothy syndrome is associated with activity-dependent dendritic retraction in rodent and human neurons. Nature neuroscience *16*, 201-209.

Krumm, N., O'Roak, B.J., Shendure, J., and Eichler, E.E. (2014). A de novo convergence of autism genetics and molecular neuroscience. Trends in neurosciences *37*, 95-105.

Kwon, S.E., and Chapman, E.R. (2011). Synaptophysin regulates the kinetics of synaptic vesicle endocytosis in central neurons. Neuron *70*, 847-854.

Lei, W., Omotade, O.F., Myers, K.R., and Zheng, J.Q. (2016). Actin cytoskeleton in dendritic spine development and plasticity. Current opinion in neurobiology *39*, 86-92.

Lin, G.N., Corominas, R., Lemmens, I., Yang, X., Tavernier, J., Hill, D.E., Vidal, M., Sebat, J., and Iakoucheva, L.M. (2015). Spatiotemporal 16p11.2 protein network

implicates cortical late mid-fetal brain development and KCTD13-Cul3-RhoA pathway in psychiatric diseases. Neuron *85*, 742-754.

Mao, Y., Ge, X., Frank, C.L., Madison, J.M., Koehler, A.N., Doud, M.K., Tassa, C., Berry, E.M., Soda, T., Singh, K.K.*, et al.* (2009). Disrupted in schizophrenia 1 regulates neuronal progenitor proliferation via modulation of GSK3beta/beta-catenin signaling. Cell *136*, 1017-1031.

Martin, P.M., Stanley, R.E., Ross, A.P., Freitas, A.E., Moyer, C.E., Brumback, A.C., Iafrati, J., Stapornwongkul, K.S., Dominguez, S., Kivimae, S.*, et al.* (2016). DIXDC1 contributes to psychiatric susceptibility by regulating dendritic spine and glutamatergic synapse density via GSK3 and Wnt/beta-catenin signaling. Molecular psychiatry.

Martin, P.M., Yang, X., Robin, N., Lam, E., Rabinowitz, J.S., Erdman, C.A., Quinn, J., Weiss, L.A., Hamilton, S.P., Kwok, P.Y.*, et al.* (2013). A rare WNT1 missense variant overrepresented in ASD leads to increased Wnt signal pathway activation. Translational psychiatry *3*, e301.

Maussion, G., Carayol, J., Lepagnol-Bestel, A.M., Tores, F., Loe-Mie, Y., Milbreta, U., Rousseau, F., Fontaine, K., Renaud, J., Moalic, J.M.*, et al.* (2008). Convergent evidence identifying MAP/microtubule affinity-regulating kinase 1 (MARK1) as a susceptibility gene for autism. Human molecular genetics *17*, 2541-2551.

Michaelsen-Preusse, K., Zessin, S., Grigoryan, G., Scharkowski, F., Feuge, J., Remus, A., and Korte, M. (2016). Neuronal profilins in health and disease: Relevance for spine

plasticity and Fragile X syndrome. Proceedings of the National Academy of Sciences of the United States of America *113*, 3365-3370.

Mohn, J.L., Alexander, J., Pirone, A., Palka, C.D., Lee, S.Y., Mebane, L., Haydon, P.G., and Jacob, M.H. (2014). Adenomatous polyposis coli protein deletion leads to cognitive and autism-like disabilities. Molecular psychiatry *19*, 1133-1142.

Morgan-Smith, M., Wu, Y., Zhu, X., Pringle, J., and Snider, W.D. (2014). GSK-3 signaling in developing cortical neurons is essential for radial migration and dendritic orientation. eLife *3*, e02663.

Muhia, M., Thies, E., Labonte, D., Ghiretti, A.E., Gromova, K.V., Xompero, F., Lappe-Siefke, C., Hermans-Borgmeyer, I., Kuhl, D., Schweizer, M.*, et al.* (2016). The Kinesin KIF21B Regulates Microtubule Dynamics and Is Essential for Neuronal Morphology, Synapse Function, and Learning and Memory. Cell reports *15*, 968-977.

Mukai, J., Dhilla, A., Drew, L.J., Stark, K.L., Cao, L., MacDermott, A.B., Karayiorgou, M., and Gogos, J.A. (2008). Palmitoylation-dependent neurodevelopmental deficits in a mouse model of 22q11 microdeletion. Nature neuroscience *11*, 1302-1310.

Murakoshi, H., Wang, H., and Yasuda, R. (2011). Local, persistent activation of Rho GTPases during plasticity of single dendritic spines. Nature *472*, 100-104.

Niethammer, M., Smith, D.S., Ayala, R., Peng, J., Ko, J., Lee, M.S., Morabito, M., and Tsai, L.H. (2000). NUDEL is a novel Cdk5 substrate that associates with LIS1 and cytoplasmic dynein. Neuron *28*, 697-711.

Oguro-Ando, A., Rosensweig, C., Herman, E., Nishimura, Y., Werling, D., Bill, B.R., Berg, J.M., Gao, F., Coppola, G., Abrahams, B.S.*, et al.* (2015). Increased CYFIP1 dosage alters cellular and dendritic morphology and dysregulates mTOR. Molecular psychiatry *20*, 1069-1078.

Okerlund, N.D., and Cheyette, B.N. (2011). Synaptic Wnt signaling-a contributor to major psychiatric disorders? Journal of neurodevelopmental disorders *3*, 162-174.

Okerlund, N.D., Kivimae, S., Tong, C.K., Peng, I.F., Ullian, E.M., and Cheyette, B.N. (2010). Dact1 is a postsynaptic protein required for dendrite, spine, and excitatory synapse development in the mouse forebrain. The Journal of neuroscience : the official journal of the Society for Neuroscience *30*, 4362-4368.

Pathania, M., Davenport, E.C., Muir, J., Sheehan, D.F., Lopez-Domenech, G., and Kittler, J.T. (2014). The autism and schizophrenia associated gene CYFIP1 is critical for the maintenance of dendritic complexity and the stabilization of mature spines. Translational psychiatry *4*, e374.

Penzes, P., Cahill, M.E., Jones, K.A., VanLeeuwen, J.E., and Woolfrey, K.M. (2011). Dendritic spine pathology in neuropsychiatric disorders. Nature neuroscience *14*, 285-293.

Reinhard, J.R., Kriz, A., Galic, M., Angliker, N., Rajalu, M., Vogt, K.E., and Ruegg, M.A. (2016). The calcium sensor Copine-6 regulates spine structural plasticity and learning and memory. Nature communications *7*, 11613.

Riedl, J., Crevenna, A.H., Kessenbrock, K., Yu, J.H., Neukirchen, D., Bista, M., Bradke, F., Jenne, D., Holak, T.A., Werb, Z.*, et al.* (2008). Lifeact: a versatile marker to visualize F-actin. Nature methods *5*, 605-607.

Riedl, J., Flynn, K.C., Raducanu, A., Gartner, F., Beck, G., Bosl, M., Bradke, F., Massberg, S., Aszodi, A., Sixt, M.*, et al.* (2010). Lifeact mice for studying F-actin dynamics. Nature methods *7*, 168-169.

Russell, T.A., Blizinsky, K.D., Cobia, D.J., Cahill, M.E., Xie, Z., Sweet, R.A., Duan, J., Gejman, P.V., Wang, L., Csernansky, J.G.*, et al.* (2014). A sequence variant in human KALRN impairs protein function and coincides with reduced cortical thickness. Nature communications *5*, 4858.

Shiomi, K., Kanemoto, M., Keino-Masu, K., Yoshida, S., Soma, K., and Masu, M. (2005). Identification and differential expression of multiple isoforms of mouse Coiled-coil-DIX1 (Ccd1), a positive regulator of Wnt signaling. Brain research Molecular brain research *135*, 169-180.

Shiomi, K., Uchida, H., Keino-Masu, K., and Masu, M. (2003). Ccd1, a novel protein with a DIX domain, is a positive regulator in the Wnt signaling during zebrafish neural patterning. Current biology : CB *13*, 73-77.

Singh, K.K., Ge, X., Mao, Y., Drane, L., Meletis, K., Samuels, B.A., and Tsai, L.H. (2010). Dixdc1 is a critical regulator of DISC1 and embryonic cortical development. Neuron *67*, 33-48.

Soma, K., Shiomi, K., Keino-Masu, K., and Masu, M. (2006). Expression of mouse Coiled-coil-DIX1 (Ccd1), a positive regulator of Wnt signaling, during embryonic development. Gene expression patterns : GEP *6*, 325-330.

Sowers, L.P., Loo, L., Wu, Y., Campbell, E., Ulrich, J.D., Wu, S., Paemka, L., Wassink, T., Meyer, K., Bing, X.*, et al.* (2013). Disruption of the non-canonical Wnt gene PRICKLE2 leads to autism-like behaviors with evidence for hippocampal synaptic dysfunction. Molecular psychiatry *18*, 1077-1089.

Srikanth, P., Han, K., Callahan, D.G., Makovkina, E., Muratore, C.R., Lalli, M.A., Zhou, H., Boyd, J.D., Kosik, K.S., Selkoe, D.J.*, et al.* (2015). Genomic DISC1 Disruption in hiPSCs Alters Wnt Signaling and Neural Cell Fate. Cell reports *12*, 1414-1429.

Stamatakou, E., Marzo, A., Gibb, A., and Salinas, P.C. (2013). Activity-dependent spine morphogenesis: a role for the actin-capping protein Eps8. The Journal of neuroscience : the official journal of the Society for Neuroscience *33*, 2661-2670.

Sudhof, T.C. (2008). Neuroligins and neurexins link synaptic function to cognitive disease. Nature *455*, 903-911.

Tanaka, T., Serneo, F.F., Tseng, H.C., Kulkarni, A.B., Tsai, L.H., and Gleeson, J.G. (2004). Cdk5 phosphorylation of doublecortin ser297 regulates its effect on neuronal migration. Neuron *41*, 215-227.

Tanaka, Y. (1991). The evolution of social communication systems in a subdivided population. Journal of theoretical biology *149*, 145-163.

Tang, G., Gudsnuk, K., Kuo, S.H., Cotrina, M.L., Rosoklija, G., Sosunov, A., Sonders, M.S., Kanter, E., Castagna, C., Yamamoto, A.*, et al.* (2014). Loss of mTOR-dependent macroautophagy causes autistic-like synaptic pruning deficits. Neuron *83*, 1131-1143.

Topol, A., Zhu, S., Tran, N., Simone, A., Fang, G., and Brennand, K.J. (2015). Altered WNT Signaling in Human Induced Pluripotent Stem Cell Neural Progenitor Cells Derived from Four Schizophrenia Patients. Biological psychiatry *78*, e29-34.

Turner, T.N., Sharma, K., Oh, E.C., Liu, Y.P., Collins, R.L., Sosa, M.X., Auer, D.R., Brand, H., Sanders, S.J., Moreno-De-Luca, D.*, et al.* (2015). Loss of delta-catenin function in severe autism. Nature *520*, 51-56.

Um, K., Niu, S., Duman, J.G., Cheng, J.X., Tu, Y.K., Schwechter, B., Liu, F., Hiles, L., Narayanan, A.S., Ash, R.T.*, et al.* (2014). Dynamic control of excitatory synapse development by a Rac1 GEF/GAP regulatory complex. Developmental cell *29*, 701-715.

Volk, L., Chiu, S.L., Sharma, K., and Huganir, R.L. (2015). Glutamate synapses in human cognitive disorders. Annual review of neuroscience *38*, 127-149.

Wang, X., Zheng, L., Zeng, Z., Zhou, G., Chien, J., Qian, C., Vasmatzis, G., Shridhar, V., Chen, L., and Liu, W. (2006). DIXDC1 isoform, l-DIXDC1, is a novel filamentous actin-binding protein. Biochemical and biophysical research communications *347*, 22-30.

Wen, Z., Nguyen, H.N., Guo, Z., Lalli, M.A., Wang, X., Su, Y., Kim, N.S., Yoon, K.J., Shin, J., Zhang, C.*, et al.* (2014). Synaptic dysregulation in a human iPS cell model of mental disorders. Nature *515*, 414-418.

Wickersham, I.R., Lyon, D.C., Barnard, R.J., Mori, T., Finke, S., Conzelmann, K.K., Young, J.A., and Callaway, E.M. (2007). Monosynaptic restriction of transsynaptic tracing from single, genetically targeted neurons. Neuron *53*, 639-647.

Wilkinson, M.B., Dias, C., Magida, J., Mazei-Robison, M., Lobo, M., Kennedy, P., Dietz, D., Covington, H., 3rd, Russo, S., Neve, R.*, et al.* (2011). A novel role of the WNT-dishevelled-GSK3beta signaling cascade in the mouse nucleus accumbens in a social defeat model of depression. The Journal of neuroscience : the official journal of the Society for Neuroscience *31*, 9084-9092.

Woolfrey, K.M., and Srivastava, D.P. (2016). Control of Dendritic Spine Morphological and Functional Plasticity by Small GTPases. Neural plasticity *2016*, 3025948.

Wu, Q., DiBona, V.L., Bernard, L.P., and Zhang, H. (2012). The polarity protein partitioning-defective 1 (PAR-1) regulates dendritic spine morphogenesis through phosphorylating postsynaptic density protein 95 (PSD-95). The Journal of biological chemistry *287*, 30781-30788.

Wu, Y., Jing, X., Ma, X., Wu, Y., Ding, X., Fan, W., and Fan, M. (2009). DIXDC1 co-localizes and interacts with gamma-tubulin in HEK293 cells. Cell biology international *33*, 697-701.

Xie, Z., Sanada, K., Samuels, B.A., Shih, H., and Tsai, L.H. (2003). Serine 732 phosphorylation of FAK by Cdk5 is important for microtubule organization, nuclear movement, and neuronal migration. Cell *114*, 469-482.

Yi, J.J., Berrios, J., Newbern, J.M., Snider, W.D., Philpot, B.D., Hahn, K.M., and Zylka, M.J. (2015). An Autism-Linked Mutation Disables Phosphorylation Control of UBE3A. Cell *162*, 795-807.

Yoon, K.J., Nguyen, H.N., Ursini, G., Zhang, F., Kim, N.S., Wen, Z., Makri, G., Nauen, D., Shin, J.H., Park, Y.*, et al.* (2014). Modeling a genetic risk for schizophrenia in iPSCs and mice reveals neural stem cell deficits associated with adherens junctions and polarity. Cell stem cell *15*, 79-91.

Yu, X., and Malenka, R.C. (2003). Beta-catenin is critical for dendritic morphogenesis. Nature neuroscience *6*, 1169-1177.

Yuen, R.K., Thiruvahindrapuram, B., Merico, D., Walker, S., Tammimies, K., Hoang, N., Chrysler, C., Nalpathamkalam, T., Pellecchia, G., Liu, Y.*, et al.* (2015). Whole-genome sequencing of quartet families with autism spectrum disorder. Nature medicine *21*, 185-191.

CHAPTER 3: TRANSCRIPTOMIC ANALYSIS OF DIXDC1 KO MICE REVEALS ASD-ASSOCIATED SIGNALLING PATHWAYS

AUTHORS

Vickie Kwan, Nicholas T. Holzapfel, and Karun K. Singh

PREFACE

This project was designed by Vickie Kwan, Nicholas T. Holzapfel, and Dr. Karun K. Singh. The majority of the experiments were performed and data collected by Vickie Kwan. Data was analyzed by Vickie Kwan and Nicholas T. Holzapfel. All of the data was interpreted, and figures were generated by Vickie Kwan. This manuscript is being prepared for submission. The manuscript was written by Vickie Kwan and Dr. Karun K. Singh.

3.1 ABSTRACT

RNA sequencing is an unbiased global view of the transcripts expressed at a specific time-point. Many researchers have utilized this tool to identify differential gene expression and develop gene expression/signalling networks. Dixdc1 has been shown to be a regulator of neuronal development during embryonic and postnatal time-points. Despite this, the specific mechanism of action remains poorly understood. Current research has shown that Dixdc1 regulates the Wnt signaling pathway and the actin cytoskeleton pathway. To elucidate novel pathways regulated by Dixdc1 that are involved in neuronal development, we performed RNA sequencing of *Dixdc1* KO mice at two different time points, embryonic (E16) and postnatal (P21). We developed an RNA-Seq analysis workflow to visualize differentially expressed genes and specific enriched gene sets involved in developmental disorders. Interestingly, we identified that ASD-associated genes are differentially expressed in the *Dixdc1* KO mouse brain, suggesting that Dixdc1 either directly or indirectly regulates ASD signaling networks. Furthermore, we discovered through gene set enrichment analysis that collagen formation was down-regulated. This data implicates the *Dixdc1* KO model as a potential model for collagen-associated disorders. This study suggests the importance of Dixdc1 in the regulation of brain development and demonstrates the power of RNA-Seq analysis for further elucidation of signalling networks.

3.2 INTRODUCTION

RNA sequencing (RNA-Seq) is a tool used by many researchers for the identification and quantification of gene expression. With the increasing accessibility to next generation sequencing techniques and decrease in sequencing cost, RNA-Seq has been used for many new and different applications (Conesa et al., 2016). Briefly, total or fractionation RNA is collected and converted into cDNA fragments; sequencing adapters are attached to these cDNA fragments and each molecule is sequenced at one end (single-end) or both ends (paired-end), generating 30-400 bp reads (Holt and Jones, 2008; Wang et al., 2009). RNA-Seq quantification and analysis has given researchers a more detailed and comprehensive view of gene expression, alternative splicing, and allele-specific expression (Kukurba and Montgomery, 2015). RNA-Seq has been used extensively in many fields of research, specifically in the study of brain disorders; researchers have performed sequencing on the transcriptome of ASD patients (Irimia et al., 2014; Voineagu et al., 2011). These transcriptomic studies have identified new signalling networks for many genes or interest, and continue shed more light onto the pathways that are affected in different disorders.

With the increasing number of NDD- and ASD-associated risk genes, many researchers are interested in potential converging signalling pathways that contribute to these disorders (Krumm et al., 2014; O'Roak et al., 2012b; Pinto et al., 2014). Many laboratories have used RNA-Seq as a tool to study globally disrupted genes and pathways, creating a network of genes associated with ASD (Braccioli et al., 2017;

Michaelson et al., 2017; Wright et al., 2017; Zhao et al., 2017). For example, a recent paper performed RNA-Seq on *Chd8*$^{+/-}$ brain regions from adult male mice and generated a list of differentially expressed genes, differentially expressed ASD-associated genes, and enriched gene sets (Platt et al., 2017). As previously mentioned, *CHD8* is an extensively studied high confidence risk gene for ASD (SFARI), and disruptive mutations in this gene were found in children with cognitive impairment and developmental delay (Zahir et al., 2007). In this case, the RNA-Seq data supported the importance of the influence that *CHD8* has on the expression of genes related to ASD pathology and the effect on signalling pathways involved (Platt et al., 2017). Additionally, a paper that our lab has recently published in *American journal of human genetics* used RNA-Seq to characterize an NDD-associated heterozygous CNV mouse model that recapitulated the human 15q13.3 microdeletion syndrome (Uddin et al., 2018; Yin et al., 2018). RNA-seq analysis in this case was used to show the role of the 15q13.3 microdeletion in forebrain development. These applications of RNA-Seq demonstrate the usefulness of this tool to discover new pathways involved in other NDD-associated models.

Further elucidation of certain pathways that may be disrupted in ASD models is important for the potential discovery of effective drug treatments that may alleviate ASD-associated symptoms. A recent study demonstrated that treatment with the histone deacetylase (HDAC) inhibitor, romidepsin, was able to rescue certain ASD-associated social deficits in *Shank3*-deficient mice, that displayed low levels of histone acetylation in the prefrontal cortex (Qin et al., 2018). Romidepsin is also able to rescue certain actin-related deficits in these mice, another pathway that has been previously associated with

ASD.

The role of Dixdc1 during brain development has been previously described (Kwan et al., 2016; Martin et al., 2016; Singh et al., 2010). Singh et al., demonstrated the role of Dixdc1 during embryonic development, specifically how the binding of Dixdc1 to Disrupted in schizophrenia 1 (Disc1) functions to inhibit GSK3 in the canonical Wnt signalling pathway and increase neural progenitor proliferation. This group also showed that Dixdc1-Disc1 binding was also important in the regulation of neuronal migration, through a Wnt-independent pathway (Singh et al., 2010). The article that we recently published in *Cell Reports* characterized the role of *DIXDC1* in postnatal neuronal development through an actin regulation pathway (Kwan et al., 2016). A group from UCSF also showed similar neuronal morphological phenotypes as we reported, although they described the effects through the regulation of the Wnt signalling pathway (Martin et al., 2016). Both articles also showed that SNVs found within the *DIXDC1* gene were associated with ASD, and that these SNVs had an impact on the role of DIXDC1 in the brain (Kwan et al., 2016; Martin et al., 2016).

In this chapter, we attempt to discover the signalling networks regulated by Dixdc1 through RNA-Seq of the *Dixdc1* KO mouse model, and these networks change over time from embryonic to postnatal brain development. This analysis identified different pathways that may be regulated by Dixdc1 at different times during neurodevelopment. Additionally, RNA-Seq analysis identified a potential disorder, Ehlers Danlos Syndrome, which may be associated with the *Dixdc1* ASD model. RNA-Seq is an

important tool to further elucidate the signalling networks surrounding Dixdc1 and suggests an association of Dixdc1 with other developmental disorders.

3.3 MATERIALS AND METHODS

3.3.1 Animals

Dixdc1 KO mice were generated by Jackson Laboratories. Animals were bred and housed at the Central Animal Facility (CAF) at McMaster University. All procedures received the approval of the Animal Research Ethics Board (AREB).

3.3.2 RNA sequencing and pre-processing

mRNA was extracted from embryonic day 16 (E16) mouse whole brain tissue and postnatal day 21 (P21) mouse cortical brain tissue using Trizol reagent (ThermoFisher Scientific). Three WT and three *Dixdc1* KO mice were used for each time point (12 mice total). All postnatal mice used for transcriptome analysis were male, and sex was undetermined for embryonic mouse brain samples. Quality of total RNA samples was checked on an Agilent Bioanalyzer 2100 RNA Nano chip following Agilent Technologies' recommendation. The library preparation for RNA was performed following the Illumina Stranded mRNA Library Preparation protocol. In brief, 500 ng of total RNA was used as the input material and enriched for poly-A mRNA, fragmented into the 200-300-bases range for 4 minutes at 94^{o}C and converted to double stranded cDNA, end-repaired and adenylated at the 3' to create an overhang A to allow for ligation of Illumina adapters with an overhang T; library fragments were amplified under the

following conditions: initial denaturation at 98°C for 10 seconds, followed by 10 cycles of 98°C for 10 seconds, 60°C for 30 seconds and 72°C for 30 seconds, and finally an extension step for 5 minutes at 72°C; at the amplification step, each sample was amplified with different barcoded adapters to allow for multiplex sequencing. To check the size fragment, 1 µl of the final RNA libraries was loaded on a Bioanalyzer 2100 DNA High Sensitivity chip (Agilent Technologies); RNA libraries were quantified by qPCR using the Kapa Library Quantification Illumina/ABI Prism Kit protocol (KAPA Biosystems). Libraries were pooled in equimolar quantities and paired-end sequenced on an Illumina HiSeq 2500 platform using a High Throughput Run Mode flowcell and the V4 sequencing chemistry following Illumina's recommended protocol to generate paired-end reads of 126-bases in length.

The quality of the reads was analyzed using FastQC High Throughput Sequence QC Report (version 0.11.5). Illumina TruSeq adapters were trimmed from reads using CutAdapt (version 1.14). FastQC was performed on trimmed reads, and all reads had a quality score (Q score) > 30. Reads were aligned to the GRCm38 mouse transcriptome (UCSC assembly) using Salmon (version 0.8.2).

3.3.3 Differential expression analysis

To compute global differential expression (DE) analysis for each of the two time points, E16 and P21, we conducted comprehensive DE analysis using a Bioconductor package named DESeq2 in R Studio. DE was computed against control expression for each of the two time points separately, and a gene was considered significant after

Benjamini-Hotchberg false discovery rate of 0.05. Principal component analysis was performed in R Studio (version 3.4.3). Heatmaps were created using using Morpheus (open source from the Broad Institute) using normalized TPM counts of select genes. Venn diagrams were generated using BEG Venn diagram tool.

3.3.4 Gene Set Enrichment Analysis (GSEA) and network analysis

We conducted comprehensive gene set enrichment analysis on differentially expressed genes at E16 and P21 for *Dixdc1* KO mice. Using GSEA (version 3.0, Broad Institute), we ran GSEA on a pre-ranked list of DEGs, where the top of the rank list contains the highest up-regulated gene (by FDR value), and the bottom of the rank list contains the highest down-regulated gene (by FDR value). We used curated and annotated gene sets readily available from the Molecular Signatures Database (MSigDB, version 6.0). Gene sets used for analysis were: CP:REACTOME: Reactome gene sets, CP:KEGG: KEGG gene sets, BP: GO biological process, CC: GO cellular component, and MF: GO molecular function. Due to the relatively lower number of DEGs identified in E16 mouse brains, the pre-ranked gene list included genes with FDR < 0.5.

Analysis of the signalling network interactions between differentially expressed genes and enriched GO gene sets identified through GSEA was performed using STRING (version 10.5); a minimum confidence score of 0.4 was required and disconnected nodes were hidden. The network was visualized in Cytoscape (version 3.6.0). The interaction network is based on significantly differentially expressed genes (FDR<0.05) and GSEA results.

3.4 RESULTS

3.4.1 Development of RNA sequencing workflow

To elucidate the temporal transcriptomic changes in signalling networks between WT and *Dixdc1* KO mice, we utilized RNA-Seq to study these changes in an unbiased and global manner. We developed an RNA sequencing workflow in collaboration with Dr. Nicholas Holzapfel (McMaster University). We extracted RNA using Trizol (Thermo Fisher Scientific) from E16 whole brains and P21 full cortices. These samples were sent to The Centre for Applied Genomics (TCAG) facility at the Hospital for Sick Children, Toronto for next-generation sequencing. A summary of the RNA-Seq workflow we have developed is represented in the Figure 1 schematic, and will be described further in the following sections.

3.4.2 Quality control of RNA-Seq reads and sequence alignment

To assess the quality and accuracy of Sanger sequencing performed, we performed FastQC on the RNA-Seq reads. The accuracy is measured by the Phred quality score (Q score), defined as a property logarithmically related to the "base calling error" probabilities (P): $Q = -10\log_{10}P$ (Ewing and Green, 1998; Ewing et al., 1998). Phred quality scoring is the most common method for testing sequencing read quality. For example, a Q score of 30 (Q30) describes the probability of an incorrect base 1 in 1000 times, ie. Base accuracy is 99.9%. Sequencing reads with a Q score of 30, the reads are essentially perfect with virtually no errors. This Q score was achieved for our reads after

trimming the reads of Illumina adapters. Additionally, FastQC tells us more important information, such as the per sequence GC content (which should demonstrate a normal distribution), per base sequence content (which should be equally represented in all 4 bases), and overrepresented sequences. Adapter trimming involves the removal of adapter sequences identified at the end of the transcript reads. Alternatively, quality trimming involves the removal of the end of reads that show a decrease in quality score (Griffith et al., 2015). From our FastQC report, we identified the presence of adapters in some of our reads, we decided to trim these Illumina TruSeq adapters using CutAdapt which increased our Phred score to >30 for all samples. These reports give us more information about our RNA-Seq reads and can be summarized in a MultiQC report.

A fundamental analysis that is performed on RNA-Seq libraries is principal component analysis (PCA), a "dimension-reduction" tool used to reduce a large set of variables to a small set (Ringner, 2008). PCA transforms correlated variables into uncorrelated variables called "principal components", and displays the samples showing where the variation in the data is at a maximum (Figure 2A). PCA identified that the largest source of variation between samples was due to the age of the mice, where E16 (green and red) and P21 (blue and purple) contribute to 90% of the variance (Figure 2A). The second largest source of variation was identified between WT mouse brains and *Dixdc1* KO mouse brains.

3.4.3 Differential expression analysis of KO mice is prominent in P21 mice

The next step in our RNA-Seq workflow is to quantify out RNA-seq library and align our reads to the mouse transcriptome. To quantify the RNA-seq data we used the Salmon tool, an accurate and ultrafast alignment software (Patro et al., 2017), and determined that at least 80% of the reads mapped to the mouse transcriptome within each sample. When comparing the differences of sequencing reads from WT and *Dixdc1* KO, we are first interested in the differentially expressed genes (DEGs) between the two conditions. We performed differential expression analysis using DESeq2 in R Studio to generate a list of DEGs at E16 and P21 (between WT and KO). Differential expression analysis identified only 157 significantly differentially expressed genes (DEGs) in KO mice at E16, and 6618 significantly DEGs in *Dixdc1* KO at P21 (FDR < 0.05). First, we observed a significant reduction in *Dixdc1* mRNA expression in KO conditions at both E16 and P21 time points (Figure 2B). Despite being a KO mouse, these mice showed a low level of *Dixdc1* mRNA expression, however the knockout of Dixdc1 was confirmed at the protein level through immunoprecipitation (Chapter 2, Figure 3).

We have summarized the top up-regulated and down-regulated DEGs identified in *Dixdc1* KO mice at E16 and P21 (Figure 3). The DEGs identified in P21 *Dixdc1* KO mouse brains include synaptic, cytoskeletal, cell adhesion, and Wnt signalling-associated genes previously associated with ASD. Interestingly, one of the down-regulated genes discovered in the P21 KO brains was *Igf1,* which has been previously used to reverse ASD-related phenotypes in other ASD models (Castro et al., 2014; Shcheglovitov et al., 2013). Additionally, many of the DEGs identified in E16 *Dixdc1* KO brains were

takusan-like proteins, which is a mouse-specific protein previously found to be involved in synaptic function (Nakanishi et al., 2013; Tu et al., 2007).

3.4.4 GSEA reveals collagen formation as a disrupted pathway in Dixdc1 KO mice

Gene Set Enrichment Analysis is a method for further interpretation of RNA-Seq expression data (Subramanian et al., 2005). GSEA performs analysis on the entire set of RNA expression data, using in this case a pre-ranked list of significantly DEGs (FDR<0.5). The overall goal of GSEA is to determine whether the DEGs in the data set are randomly distributed throughout the list, or are localized to the top or bottom of the list (Subramanian et al., 2005). We performed GSEA using the GSEA-P software package (Broad Institute) with the REACTOME and GO (Gene Ontology) gene sets (Molecular Signature Databases, MSigDB). GSEA generates an enrichment score (ES) that reflects the enrichment of genes at either end of the pre-ranked list. A nominal p value is calculated to measure the statistical significance of the ES. Next, the ES is normalized to generate a normalized enrichment score (NES), and the false discovery rate (FDR) (Subramanian et al., 2005). GSEA will also generate a leading-edge list of genes, which is a group of genes that contribute to the ES. These genes are usually found at the top or the bottom on the pre-ranked list of DEGs.

GSEA of P21 DEGs using the REACTOME gene set database identified collagen formation and extracellular matrix organization gene sets as one of the most enriched down-regulated gene sets (Figure 4). Many of the genes within the collagen formation and extracellular matrix organization gene sets were overlapping, and suggested that these

pathways are disrupted in *Dixdc1* KO mice. More specifically, transcripts for genes like *COL5A1, COL5A2,* and *COL1A1* were significantly down-regulated, 4.3 fold, 1.7 fold, and 1.5 fold, respectively (Figure 5). Figure 5 summarizes the significantly down-regulated transcripts in the *Dixdc1* KO mouse. Additionally, GSEA using the Gene Ontology (GO) gene set list also identified down-regulated pathways associated with the extracellular matrix and collagen formation and regulation (Figure 4). We also identified negative enrichment of many neural developmental gene sets, such as neural precursor cell proliferation, cerebral cortex migration, and forebrain cell migration (Figure 4). These pathways have previously been indicated as a disrupted pathway associated with Dixdc1 regulation. As expected, the canonical Wnt signalling pathway was also disrupted within the *Dixdc1* KO mouse.

Many of the pathways that were enriched in the E16 *Dixdc1* KO mice were associated with neuronal development, which falls in line with previous reports. For example, we identified enrichment of forebrain development, neuron differentiation, nervous system development, and many others (Figure 4 and 7B). Other down-regulated pathways identified were pathways related to cytoskeletal regulation, such as actin binding, cytoskeletal protein binding, and regulation of cytoskeleton organization (Figure 4). These disrupted networks are summarized in Figure 7.

3.4.5 Dixdc1 is associated with ASD-risk genes

Previous studies have identified DEGs that have been associated with ASD (Platt et al., 2017). This led us to determine if *Dixdc1* KO mice also show a disruption in ASD-

associated genes. As previously mentioned, the SFARI Gene database (SFARI) is a collection of curated and categorized ASD-associated risk genes (Abrahams et al., 2013). As described in section 1.2.1, these genes are grouped into a syndromic category, category 1 (high confidence), category 2 (strong candidate), category 3 (suggestive evidence), category 4 (minimal evidence), category 5 (hypothesized), and category 6 (not supported). High confidence and strong candidate genes are genes that have undergone rigorous statistical analysis between control and ASD cases. These genes are the ASD-risk genes with the strongest link to ASD (Abrahams et al., 2013). We downloaded the SFARI Gene set, and generated a gene set list for analysis using GSEA software to discover if and how many ASD-risk genes are differentially expressed at E16 or P21 in *Dixdc1* KO mice (Figure 6, Table 1). We identified 2 SFARI DEGs belonging to category 1 and 3 category 2 SFARI DEGs at E16 (Table 1). Conversely, we identified 13 category 1, and 32 category 2 SFARI DEGs at P21 (Table 1); Figure 6 lists the 8 genes belonging to category 1, 2, or syndromic that were shared among E16 and P21 SFARI DEGs. Interestingly, we discovered that many of these genes were also associated with Wnt signalling and synaptic signalling genes, which have previously been associated with ASD and the *Dixdc1* KO mouse model (Figure 7A). We identified 4 ASD-associated genes that are associated with Wnt and synaptic signalling, *beta-catenin* (*CTNNB1*), *Rac family small GTPase 1* (*RAC1*), *phospholipase C, beta 1* (*PLCB1*), and *disheveled segment polarity protein 1* (*DVL1*). These data further support the *Dixdc1* KO mouse as a model for ASD, implicating the dysregulation of Wnt and synaptic signalling pathways.

3.5 DISCUSSION

3.5.1 Dixdc1 KO mouse transcriptome analysis reveals the signalling networks involved in Dixdc1 regulation of brain development

Surprisingly, we did not identify many DEGs at E16, compared to the thousands identified at P21 (Figure 3). This suggests that many of the changes in signalling networks occur between the embryonic stage and postnatal development. We discovered that P21 *Dixdc1* KO brains showed enrichment of cytoskeleton-related gene sets (Figure 4). The actin-binding domain located near the N-terminal region of Dixdc1 suggests a role for Dixdc1 in actin-associated regulations (Wang et al., 2006). In the context of neurodevelopment, a role for Dixdc1 in cytoskeletal regulation was discovered later in development (postnatal) (Kwan et al., 2016). Additionally, we identified DEGs associated with Wnt signalling, collagen formation, embryonic brain development and synaptic function (Figure 3 and 7). These pathways are crucial for the proper development of the brain, and have all been previously associated with ASD pathophysiology (Bourgeron, 2015; Caracci et al., 2016).

Excitingly, our RNA-Seq data showed a decrease in *Igf1* mRNA expression (Figure 3D). This data suggests IGF1 as a potential treatment to ameliorate ASD-related phenotypes observed in *Dixdc1* KO mice, similar to previous mouse studies (Castro et al., 2014; Shcheglovitov et al., 2013). Treatment with IGF1 has been previously used to rescue behavioural deficits in *Mecp2* mutant mice (Castro et al., 2014), and promote synapse formation in 22q13 heterozygous deletion iPS-derived neurons (Shcheglovitov et al., 2013). Preliminary results from a preclinical trial using IGF1 to treat females with

Rett syndrome (mutations in *MECP2*) indicated that IGF1 was safe to use in these patients and showed improvement in certain breathing (apnea) and ASD-related behaviours (Khwaja et al., 2014). Additionally, IGF1 is currently being tested in clinical trials for a potential treatment for ASD, specifically Rett syndrome and Phelan-McDermid syndrome (22q13 deletion) (ClinicalTrials.gov, Identifier: NCT01970345 and NCT01525901, respectively). Further research should be conducted to study whether IGF1 can rescue synaptic deficits observed in *Dixdc1* KO mice and suggests a potential role of DIXDC1 in these syndromes or the associated pathways.

3.5.2 Dixdc1 KO mouse as a model for ASD

From the list of SFARI DEGs, we identified 8 genes that were shared between embryonic and postnatal brains (Figure 6A). Among these genes, 3 genes are categorized as high confidence or strong candidate genes (category 1 and 2). *Ankyrin 2* (*ANK2*) is a high confidence gene that encodes for a protein that is important for proper attachment of integral membrane proteins to the actin cytoskeleton. NGS identified *de novo* loss-of-function mutations in the *ANK2* gene with very low frequency of mutations in the control cohorts (De Rubeis et al., 2014; Iossifov et al., 2014; Iossifov et al., 2012; Krumm et al., 2015). *Catenin delta 2* (*CTNND2*) is a strong candidate gene, where multiple missense variants were identified in patients with ASD (Turner et al., 2015). Studies have shown that loss of function of CTNND2 displayed deficits in synaptic formation in cultured neurons (Turner et al., 2015). These phenotypes observed due to CTNND2 loss of function are similar to those observed in *Dixdc1* KO mice (Kwan et al., 2016; Martin et

al., 2016). Additionally, the role of *CTNND2* in Wnt signalling also suggests that *DIXDC1* and *CTNND2* may converge on the same pathway, and play a role in ASD pathology. The final ASD-associated DEG identified was *met proto-oncogene, receptor tyrosine kinase* (*MET*), a strong candidate gene with multiple studies showing associations with ASD (Campbell et al., 2006; Sousa et al., 2009). The identification of these DEGs in the *Dixdc1* KO mouse suggests that *Dixdc1* may play an important role in regulating ASD-associated pathways through modulation of these genes.

3.5.3 Dixdc1 plays an important role in proper collagen formation, structure, and stability

The disruption in the collagen formation pathway and related genes specifically led us to investigate collagen-specific disorders that may also be associated with ASD and other neurodevelopmental disorders. Ehlers-Danlos syndromes (EDS) describe a group of heterogeneous, heritable disorders of connective tissue disorders (HDCTs) (Malfait et al., 2017). These disorders are characterized by joint hypermobility (JH), skin hyperextensibility, and generalized tissue fragility. The prevalence of EDS is at least 1 in 5,000 individuals worldwide (Bethesda et al., 2018). There are currently 13 different subtypes of EDS, and each subtype has been associated with mutations in specific genes, many of which are involved in collagen formation, structure and maintenance (Malfait et al., 2017). Classical EDS has a prevalence of 1 in 20,000 to 40,000 and is caused by mutations in the *COL5A1, COL5A2,* or *COL1A1* genes encoding collagen type V (Bethesda et al., 2018; Malfait et al., 2017). Mutations in other genes such as *COL3A1,*

encoding collagen type III, have been associated with vascular EDS that presents in patients with extensive easy bruising, and vascular ruptures (Baeza-Velasco et al., 2018).

Interestingly, many of the DEGs identified in the collagen formation gene set through GSEA were genes implicated in EDS. We found that the genes *COL5A1* and *COL5A2* were very significantly down-regulated in *Dixdc1* KO mice (FDR = 2.5×10^{-18} and 4.11×10^{-5}, respectively). *COL5A1* and *COL5A2* genes produce pro-α1(V) chains and pro-α2(V) chains, respectively, which combine together using 2 pro-α1(V) chains and one pro-α2(V) chain to form rope-like procollagen molecules. These procollagen molecules are processed to form type V collagen, which is important to strengthen and support skin, ligaments, bones, and muscles (Ricard-Blum, 2011). Researchers have identified greater than 100 mutations in the *COL5A1* gene, and 20 mutations in the *COL5A2* gene in people with classical EDS; these mutations alter the structure of the pro-α(V) chains and cause the weakening of the connective tissues in the body (Schwarze et al., 2000; Wenstrup et al., 2000). Many of the mutations discovered in the *COL5A1* gene showed a complete or nearly complete loss of one *COL5A1* allele, and that the *COL5A1* and *COL5A2* mRNA expression was very unstable (Schwarze et al., 2000; Wenstrup et al., 2000). Studies found that approximately 50% of patients diagnosed with classical EDS contained mutations in *COL5A1* or *COL5A2* (Symoens et al., 2009). The decrease of the mRNA expression of these genes in the *Dixdc1* KO mouse may suggest that this mouse model may also exhibit symptoms of EDS, such as disruption in collagen fibril assembly and a decrease in vascular strength (Cooper et al., 2010; Wenstrup et al., 2006).

Mutations in the *COL3A1* gene have been implicated in the vascular subtype of EDS, known as EDS type IV. The *COL3A1* gene encodes for pro-α1(III) chains which forms type III collagen. Similar to the classical EDS, multiple mutations have been identified in the *COL3A1* gene causing vascular type EDS (Schwarze et al., 2001). Mutations in *COL3A1* lead to the improper formation of type III collagen, and decrease the total amount of type III collagen. This decrease in type III collagen can cause EDS type IV and can lead to the tearing of blood vessels and internal organs.

Interestingly, EDS has previously been associated in psychiatric disorders and NDDs. A study published in 1985 reported the case of a 15 year old child diagnosed with ASD and EDS, this patient displayed JH, abnormally extensible skin, and moderate bleeding that is characteristic of classical EDS (Fehlow and Tennstedt, 1985). A more recent study has also reported on a 17 year old male that was diagnosed with ASD and EDS. His mother was previously diagnosed with EDS, and he displayed high flexibility of fingers, JH, and skin hyperelasticity (Takei et al., 2011). Additionally, EDS has been associated with many other neuropsychiatric disorders, such as ADHD, schizophrenia, depressive disorders, and anxiety disorders (Baeza-Velasco et al., 2015; Baeza-Velasco et al., 2018; Cederlof et al., 2016). The low mRNA expression level of these EDS-associated genes suggests that Dixdc1 may play an important role in EDS.

Further studies need to be conducted to determine whether *Dixdc1* KO mice display symptoms observed in EDS. For example, we propose to test dermis organization, collagen fibril assembly and growth which is disrupted in *Col5a1* deficient mice

(Wenstrup et al., 2006), which is also consistent with symptoms observed in patients with EDS (Vogel et al., 1979). Moreover, transcriptomic analysis of EDS patient fibroblasts identified altered expression of genes involved in cell adhesion and wnt signalling (Chiarelli et al., 2016). The disruption of these pathways further suggests a potential link between EDS and ASD.

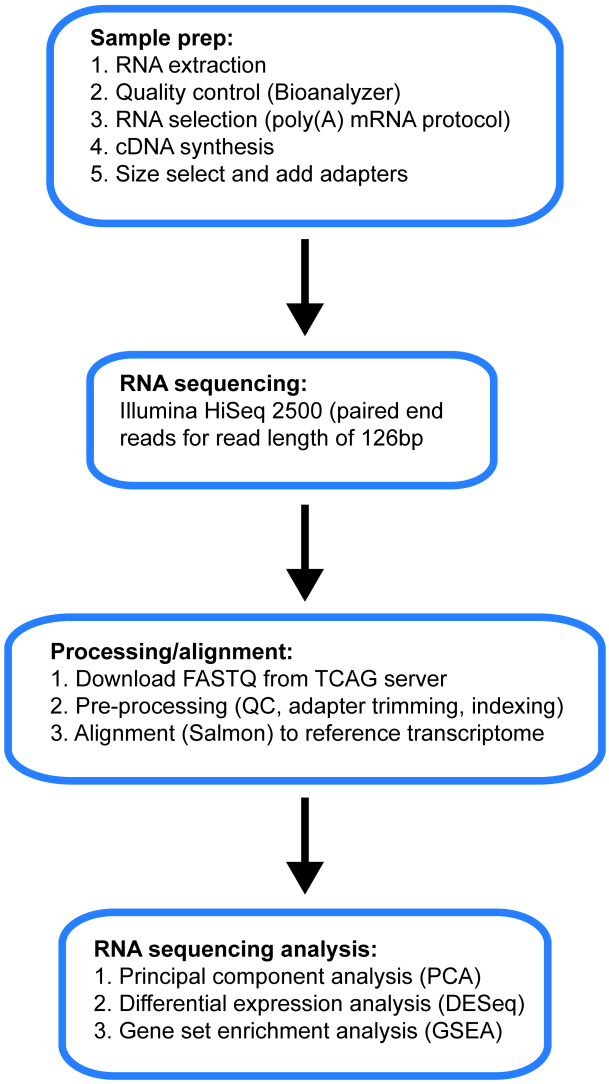

Figure 1: Schematic of RNA Sequencing workflow. Summary of the RNA-Seq workflow developed in the lab: 1) Sample preparation, 2) RNA sequencing, 3) Processing and alignment, and 4) RNA sequencing analysis.

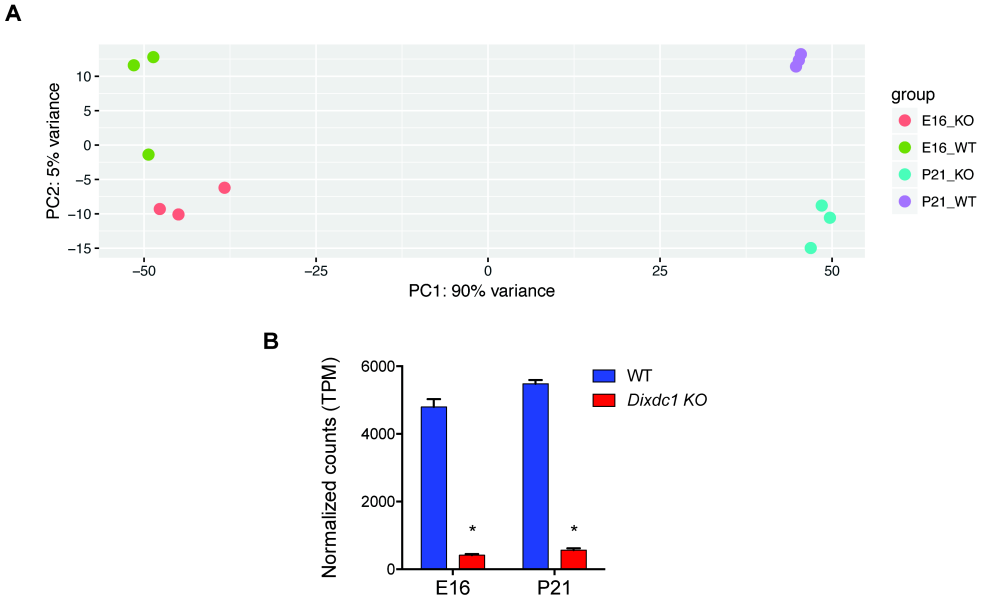

Figure 2: Principal component analysis and normalized expression of *Dixdc1* KO compared to WT. (**A**) Principal component analysis shows that 90% of variance between all 12 samples in the time-point. Additionally, 5% of variance between all samples was due to the condition (WT vs. KO). (**B**) Normalized transcript per million (TPM) counts show a decreased level of transcript in *Dixdc1* KO mice.

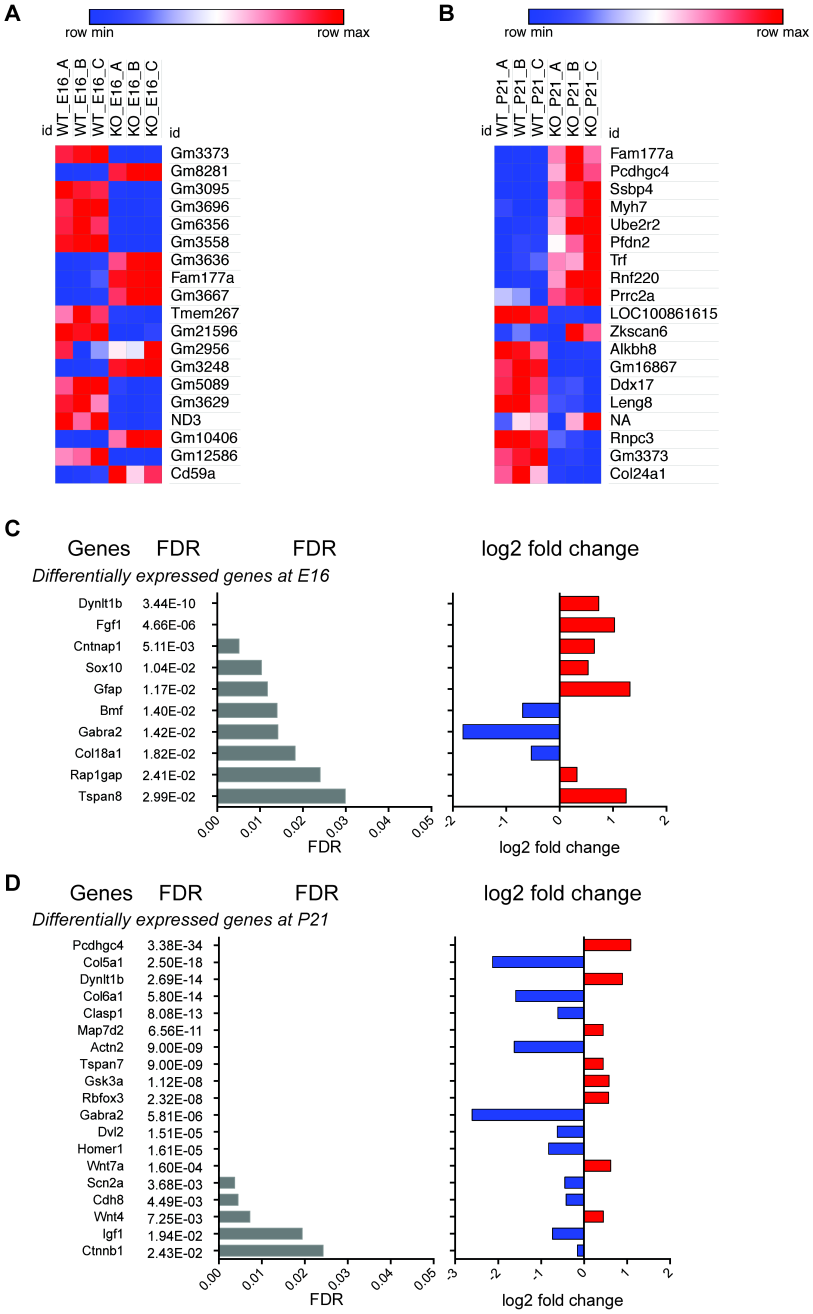
A
row min
row max
id
WT_E16_A
WT_E16_B
WT_E16_C
KO_E16_A
KO_E16_B
KO_E16_C
Gm3373
Gm8281
Gm3095
Gm3696
Gm6356
Gm3558
Gm3636
Fam177a
Gm3667
Tmem267
Gm21596
Gm2956
Gm3248
Gm5089
Gm3629
ND3
Gm10406
Gm12586
Cd59a
B
row min
row max
id
WT_P21_A
WT_P21_B
WT_P21_C
KO_P21_A
KO_P21_B
KO_P21_C
Fam177a
Pcdhgc4
Ssbp4
Myh7
Ube2r2
Pfdn2
Trf
Rnf220
Prrc2a
LOC100861615
Zkscan6
Alkbh8
Gm16867
Ddx17
Leng8
NA
Rnpc3
Gm3373
Col24a1
C
Genes
FDR
FDR
log2 fold change
Differentially expressed genes at E16
Dynlt1b 3.44E-10
Fgf1 4.66E-06
Cntnap1 5.11E-03
Sox10 1.04E-02
Gfap 1.17E-02
Bmf 1.40E-02
Gabra2 1.42E-02
Col18a1 1.82E-02
Rap1gap 2.41E-02
Tspan8 2.99E-02
0.00 0.01 0.02 0.03 0.04 0.05
FDR
-2 -1 0 1 2
log2 fold change
D
Genes
FDR
FDR
log2 fold change
Differentially expressed genes at P21
Pcdhgc4 3.38E-34
Col5a1 2.50E-18
Dynlt1b 2.69E-14
Col6a1 5.80E-14
Clasp1 8.08E-13
Map7d2 6.56E-11
Actn2 9.00E-09
Tspan7 9.00E-09
Gsk3a 1.12E-08
Rbfox3 2.32E-08
Gabra2 5.81E-06
Dvl2 1.51E-05
Homer1 1.61E-05
Wnt7a 1.60E-04
Scn2a 3.68E-03
Cdh8 4.49E-03
Wnt4 7.25E-03
Igf1 1.94E-02
Ctnnb1 2.43E-02
0.00 0.01 0.02 0.03 0.04 0.05
FDR
-3 -2 -1 0 1 2
log2 fold change

Figure 3: Differentially expressed genes in *Dixdc1* KO mouse brains at E16 and P21 time points. (**A**) Normalized expression of top DEGs in E16 *Dixdc1* KO mice (FDR < 0.05). Heat map shows normalized TPM. (**B**) Normalized expression of top DEGs in P21 *Dixdc1* KO mice (FDR < 0.05). Heat map shows normalized TPM. (**C**) Differentially expressed genes in E16 *Dixdc1* KO mouse brains compared to WT mouse brains (FDR < 0.05). Differential expression analysis was performed using DEseq2 on TPM expression. (**D**) Differentially expressed genes in P21 *Dixdc1* KO mouse cortex compared to P21 WT mouse cortex (FDR < 0.05).

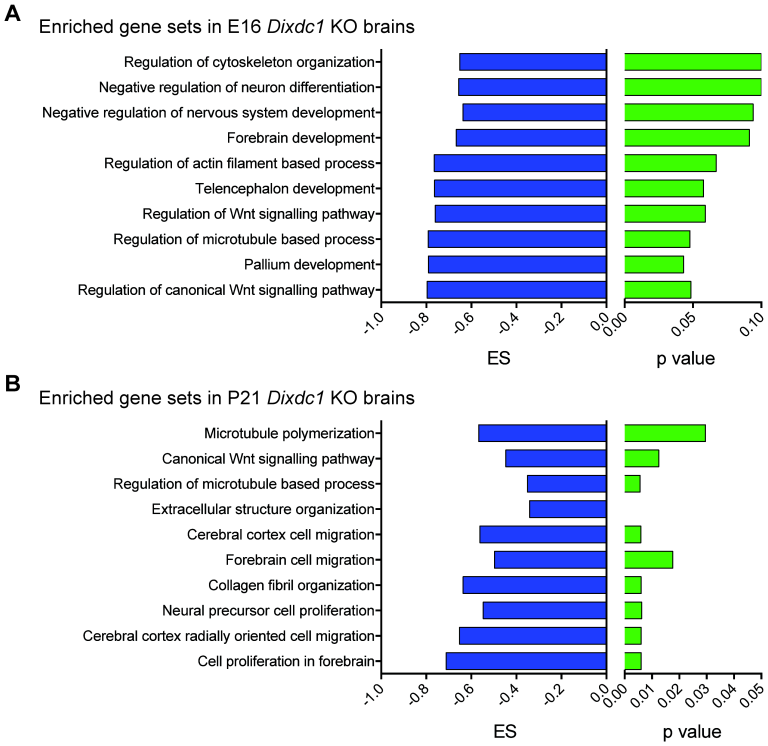

Figure 4: Gene set enrichment analysis of differentially expressed genes identified disrupted pathways in *Dixdc1* KO mice. (**A**) Enriched gene sets in E16 *Dixdc1* KO mice was performed using GSEA on a pre-ranked list of DEGs with p value < 0.05. GSEA was performed using Gene Ontology (GO) gene sets (MSigDB, v6.1). (**B**) Enriched gene sets in P21 *Dixdc1* KO mice was performed using GSEA on a pre-ranked list of DEGs with FDR < 0.05. GSEA was performed using GO gene sets.

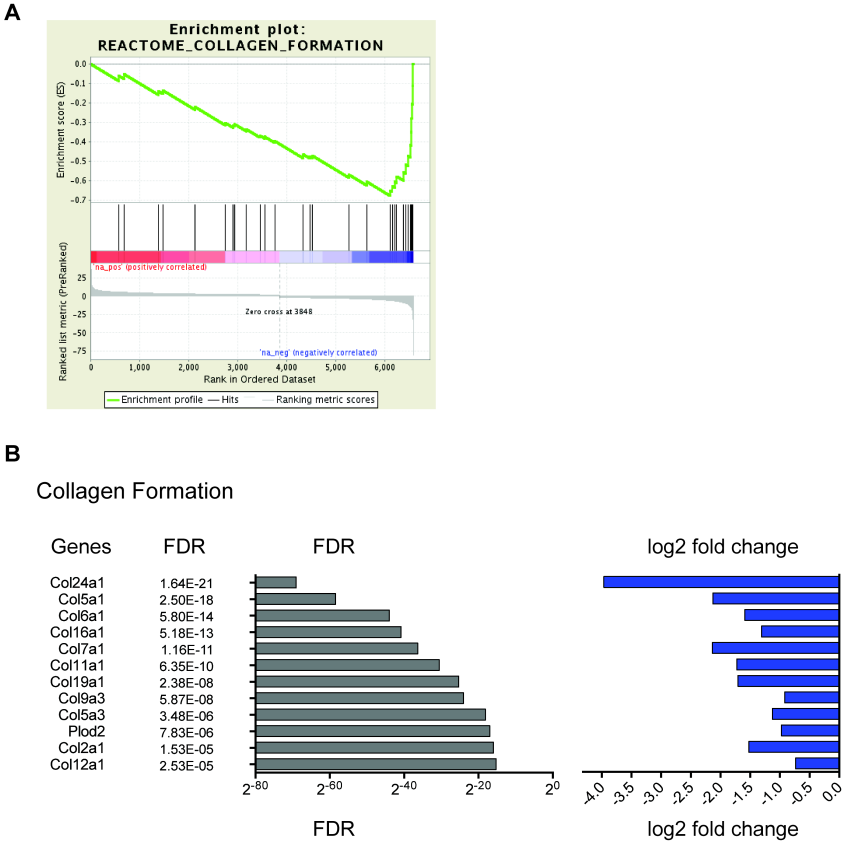

Figure 5: The collagen formation pathway is disrupted in *Dixdc1* KO mice. (**A**) GSEA identified collagen formation as an enriched gene set from using the REACTOME gene set list (MSigDB). The enrichment plot shows the enrichment profile and enrichment score (ES). (**B**) A list of differentially expressed down-regulated genes that play a role in collagen formation (FDR < 0.05).

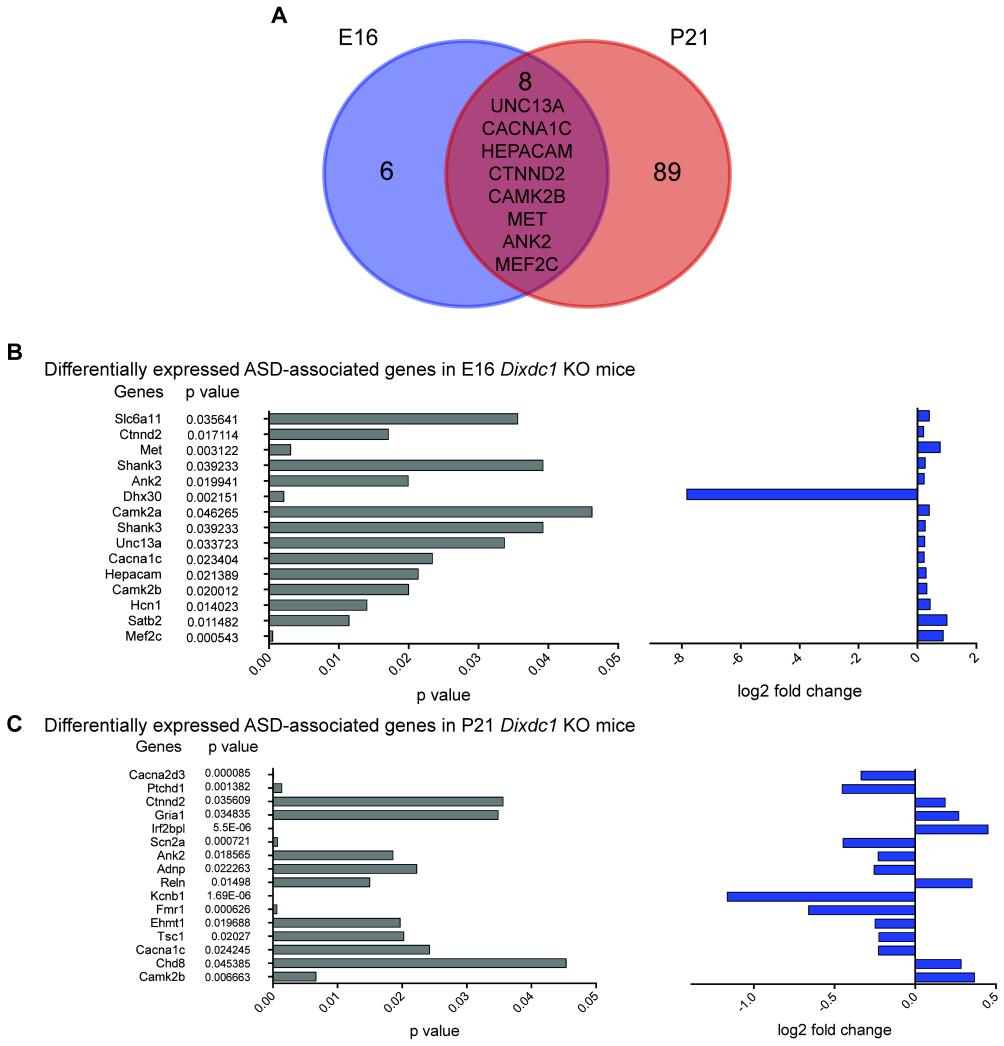

Figure 6: Differentially expressed and ASD-associated genes in *Dixdc1* KO mice. (**A**) Venn diagram DEGs from E16 and P21 *Dixdc1* KO mice; DEGs are SFARI ASD-associated genes from category 1, 2, and syndromic. 8 DEGs are shared between E16 and P21 *Dixdc1* KO mice. (**B**, **C**) ASD-associated DEGs found at E16 (**B**) and P21 (**C**) in *Dixdc1* KO mice showing log2 fold change (p value < 0.05).

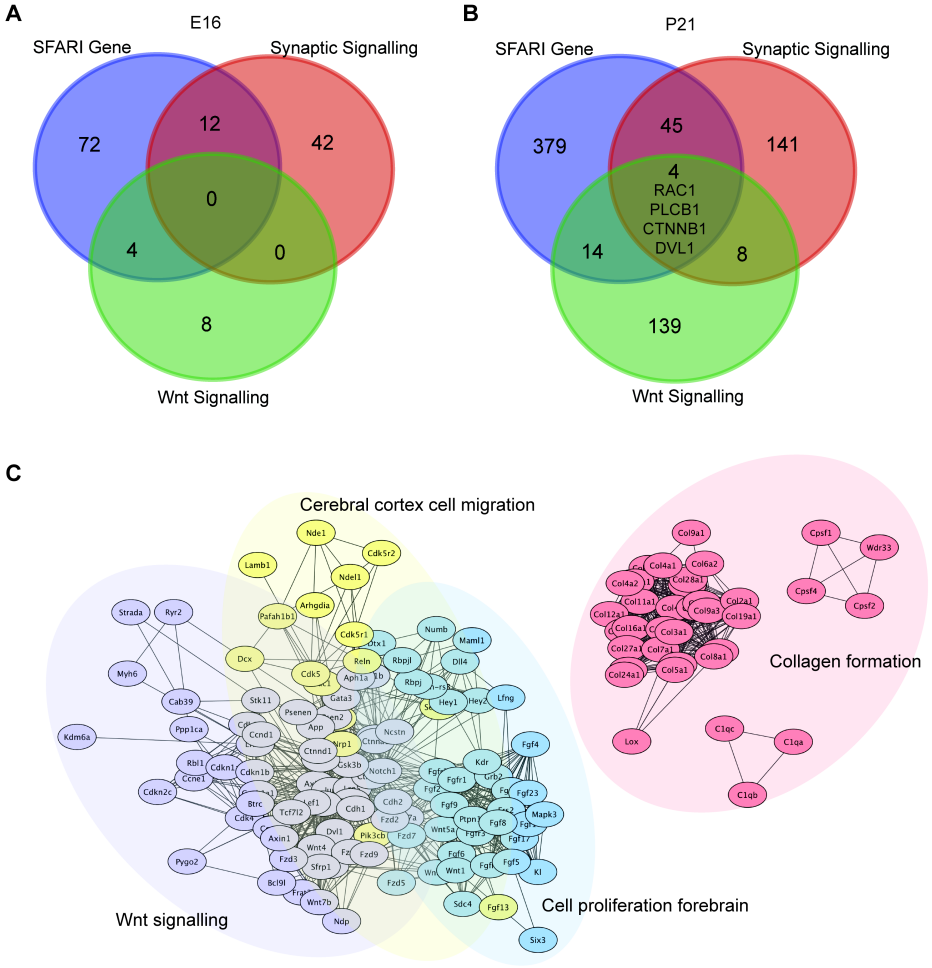

Figure 7: RNA-Seq of P21 *Dixdc1* KO brain show disrupted signalling networks. (**A**, **B**) Venn diagram of SFARI Gene, synaptic signalling, and Wnt signalling gene sets in E16 (**A**) and P21 (**B**) *Dixdc1* KO mice. (**C**) Network analysis was generated by STRING database (v10.5), visualized using Cytoscape (v3.6.0). Genes are grouped into gene sets identified through GSEA using GO gene set; the colour of nodes indicates the gene set. Disconnected genes are not shown.

	E16	P21	Total SFARI Genes
Syndromic	10	66	128
Category 1	2	13	24
Category 2	3	32	59
Category 3	15	87	169
Category 4	30	137	339
Category 5	13	62	142
Category 6	2	8	19
No category	23	103	238
			990

Table 1: ASD-associated differentially expressed genes in E16 and P21 *Dixdc1* KO mice.

SFARI Gene – Synaptic signalling (45)		SFARI Gene – Wnt signalling (14)	Synaptic signalling – Wnt signalling (8)	SFARI Gene – Synaptic signalling – Wnt signalling (4)
Rit2	*Dlg4*	*Gpc4*	*Arrb2*	*Rac1*
Dlg1	*Synj1*	*Chd8*	*Lrp6*	*Plcb1*
Slc6a4	*Gabra5*	*Ctnnd2*	*Ppp3ca*	*Ctnnb1*
Syn3	*Grin2b*	*Tbl1x*	*Wnt7a*	*Dvl1*
Lrfn5	*Stxbp1*	*Kdm6a*	*Lrrk2*	
Pafah1b1	*Kcnq3*	*Psmd10*	*Gnb1*	
Syt3	*Gria1*	*Med12*	*Gsk3a*	
Grik5	*Myo5a*	*Ccdc88c*	*Psen1*	
Cacna1a	*Dlgap2*	*Dixdc1*		
Homer1	*Htr2a*	*Psmd12*		
Clstn3	*Park2*	*Apc*		
Kcnq2	*Mapk8ip2*	*Wwox*		
Akap9	*Gad1*	*Tnrc6b*		
Syn1	*Cask*	*Lzts2*		
Unc13a	*Gabra1*			
Pcdh8	*Cacna1g*			
Cacna1b	*Slc6a3*			
Cdh8	*Nrxn2*			
Grik4	*Chrna7*			
Slc12a5	*Mef2c*			
Gabra4	*Syn2*			
Grm7	*Drd1*			
Th				

Table 2: DEGs in P21 *Dixdc1* KO mice found in the ASD-associated gene list and associated with synaptic and Wnt signalling. There are 45 DEGs overlapping between the SFARI Gene list, synaptic, and Wnt signalling gene set. There are 14 overlapping DEGs between SFARI Gene list and Wnt signalling gene set. There are 8 overlapping DEGs between the synaptic and Wnt signalling gene set. The 4 genes overlapping the SFARI Gene set list, synaptic signalling gene set, and Wnt signalling gene set are *Rac1*, *Plcb1*, *Ctnnb1*, and *Dvl1*.

SFARI Gene – Synaptic signalling (12)	SFARI Gene –Wnt signalling (8)
Slc1a1 *Grin1* *Kcnq2* *Snap25* *Park2* *Dlgap1* *Stx1a* *Unc13a* *Ache* *Slc6a1* *Slc12a5* *Mef2c*	*Camk2a* *Ctnnd2* *Dixdc1* *Wnt2*

Table 3: DEGs in E16 *Dixdc1* KO mice found in the ASD-associated gene list and associated with synaptic and Wnt signalling. There are 12 DEGs overlapping the SFARI Gene list and the synaptic signalling gene set. There are 4 DEGs overlapping the SFARI Gene list and Wnt signalling gene set.

CHAPTER 4: DEVELOPMENT OF A HIGH-CONTENT IMAGING PLATFORM TO CHARACTERIZE HUMAN IPS-DERIVED NEURONS

AUTHORS

Vickie Kwan, Elyse Rosa, Eric Deneault, Sean H. White, Stephen W. Scherer, and Karun K. Singh

PREFACE

This project was designed by Vickie Kwan and Dr. Karun K. Singh. The majority of the experiments were performed and data collected by Vickie Kwan, with assistance from Dr. Elyse Rosa. Dr. Eric Deneault generated ASD-associated iPS cell lines. Dr. Sean White performed electrophysiology experiments. All of the data in the manuscript was analyzed, interpreted, and figures were generated by Vickie Kwan. This manuscript is in preparation to submit to *Molecular Neuropsychiatry*. The manuscript was written by Vickie Kwan.

4.1 ABSTRACT

With the development of next-generation sequencing technology, the number of ASD-risk genes has increased into the hundreds. This increase in the number of risk genes has left researchers with the dilemma of which genes they should investigate. Due to the nature of experiments to characterize the effects of these mutations in mouse models or human iPS-derived neurons, laboratories are only able to study a handful of risk-genes at once. We have attempted to develop a high-content imaging and phentoyping platform to characterize neuronal morphology and synaptic connectivity of human iPS-derived neurons. This has never been performed due to the difficult nature of culturing these cells, and the ability to uncover a robust phenotype. We show that our platform is able to detect a disruption in synaptic formation in *KCNQ2* KO iPS-derived neurons, however the platform was not sensitive enough to detect robust changes in other ASD-associated cell lines. Further research and development into this platform may be a crucial tool for any future genetic rescue screen or drug treatment screen.

4.2 INTRODUCTION

High-throughput screening (HTS) is a tool used to discover and identify drugs and small molecules that have the potential to rescue deficits observed in the assay. Current studies have attempted to develop screens with mouse and human neurons, however these attempts have had minimal success. As previously mentioned in Chapter 1, previous studies have used primary mouse cultures for automated microscopy and survival assays (Sharma et al., 2012). Some of the advantages of culturing primary mouse neurons are the

ease of culturing and viability of cells in a high-throughput format, compared to human iPS-derived neurons. Additionally, primary mouse neurons allow researchers to assay fully mature neurons in a shorter timespan, and compared to certain cell lines, provides more biologically relevant phenotypes (Sharma et al., 2012). Using this system, researchers were also able to quantify synaptic phenotypes, however still found difficulty with generating quantitatively consistent results (Hempel et al., 2011; Sharma et al., 2013). Current research has attempted to develop these platforms to discover potential drug treatments for human disorders; the use of human iPS-derived neurons is essential for studying human neurodevelopmental disorders, and provides a more biologically relevant model for drug treatment of human disorders. Recent studies have used human iPSC-derived neurons, iCell Neurons, which are commercially available human neurons from Cellular Dynamics (Berry et al., 2015). Multiple studies have used these commercially available neurons, due to the ease of culturing and species relevant phenotypes (Sherman et al., 2016; Sirenko et al., 2014). The assays performed using these cells remain simple and required further research and development for detecting subtle and robust phenotypes.

Directed differentiation of human iPS cells into neurons and other cells of the brain have become a powerful tool for researchers in the field of neurodevelopment disorders. Additionally, the emergence of many new and important ASD-susceptibility genes discovered through next generation sequencing technology has emphasized the importance of developing human-associated assays to more quickly assess disruptions in neuronal function and potential drug treatments to reverse these effects (Jiang et al., 2013;

Yuen et al., 2015). In fact, many studies have begun to model ASD in human iPS-derived neurons (Brennand et al., 2015; Habela et al., 2016; Pasca et al., 2011; Shcheglovitov et al., 2013; Wang et al., 2015; Yi et al., 2016). Many studies have shown synaptic defects in ASD models (Berkel et al., 2012; Durand et al., 2012; Penzes et al., 2011b), and to date, there is no platform to screen neurons for their synaptic phenotypes in a higher-throughput manner. One of the most important factors for a high-throughput screen is the ability to culture a homogenous population of cells. Although there are many different methods to generate neurons from embryonic stem cells (ESCs) and iPSCs, the ability to generate one single population of neurons remains elusive. Many studies have demonstrated that iPS cell differentiation into neurons generates a mixed population of neuronal cells, and varied subtypes of neurons (Espuny-Camacho et al., 2013; Hu et al., 2010). The lack of a homogenous population of neurons suggest that these differentiation methods are not suitable for a high-throughput screen, in addition to the time to generate functional synapses (4-8+ weeks). Moreover, human neuronal high-throughput screens use very simple assays, such as cell toxicity, and protein secretion screens (Kondo et al., 2017). There are currently no high-throughput studies using human iPS-derived neurons that are able to look at synaptic connectivity, and only screening platforms using primary mouse cultures have been able to observe synaptic phenotypes in a robust platform (Sharma et al., 2013; Spicer et al., 2017).

Zhang et al. recently showed an approach to convert iPS cells into induced neurons using a single transcription factor, *NEUROGENIN-2* (*NGN2*) (Zhang et al., 2013). This method allows for the rapid conversion of iPS cells into induced neurons that

readily form synapses and have been shown to form functional connections (Ho et al., 2016; Zhang et al., 2013). These neurons have also been shown to produce proper cortical neuron markers, such was VGLUT1, and CUX1 (Boccitto et al., 2016), and have demonstrated synapse formation as early as 2 weeks in culture (Zhang et al., 2013).

Our goal is to develop a platform to perform high-content imaging and analysis of human iPS-derived neurons in order to phenotype morphological and synaptic defects. The use of *NGN2*-induced neurons addresses the need for a homogenous population of human neurons in a short timeframe that have also demonstrated synaptic phenotypes. Preliminary data has shown that we are able to grow iPS-derived neurons in a higher-throughput format (in 96-well plates), with successful immunostaining of mature neurons. However, we are unable to observe a robust phenotype in this format that is observable in the traditional lower-throughput, in this case 24-well plates. We must continue to develop this platform, to increase neuronal health and adjust the automated imaging platform to be able to detect these subtle changes in phenotype in a more robust manner.

4.3 MATERIALS AND METHODS

4.3.1 iPSCs thawing and maintenance

Induced pluripotent stem cells (iPSCs) were thawed in a 37°C water bath. Cells were transferred into a 15 mL falcon tube and resuspended in DMEM/F12 (Corning) media added dropwise. Cells were centrifuged at 1,100 rpm for 3 minutes. The cell pellet was resuspended in mTeSR media (STEMCELL Technologies Inc.), supplemented with

10 μM Rho-associated kinase (ROCK) inhibitor (Y-27632; STEMCELL Technologies Inc.), and 1X Pen/Strep (Thermo Fisher Scientific). Cells were plated into 1 well of a 6-well plate coated with Matrigel (Corning). All iPS cell lines were maintained on Matrigel coated-plates, with complete media change every day (<24 hours) in mTeSR. Cells were passaged using ReLeSR (STEMCELL Technologies Inc.). Accutase™ (STEMCELL Technologies Inc.) and ROCK inhibitor were used for single-cell dissociation for experiments.

4.3.2 Lentivirus production

$9.0x10^6$ HEK293FT cells were seeded in a T-150 flask (Corning), grown in 10% fetal bovine serum (FBS) in DMEM (Gibco). The next day (24 hours later), cells were transfected using Lipofectamine 2000 with plasmids psPAX2 (13 μg) and pMD2.G (7 μg), and the target constructs FUW-TetO-Ngn2-P2A-EGFP-T2A-puromycin or FUW-rtTA (23 μg; gift from T.C. Südhof laboratory). The media was changed 12 hours post-transfection, and the supernatant was collected 48 hours post-transfection. The supernatant was ultracentrifuged at 25,000 rpm at 4°C for 2 hours. The supernatant was discarded and 75 μl PBS was added to the pellet, triturated, aliquoted and frozen at -80°C (15 aliquots for 1 T-150 flask).

4.3.3 Differentiation of iPS into glutamatergic neurons

iPS cells were seeded into matrigel-coated 6-well plates at $5.0x10^6$ cells/well in 2mL of mTeSR supplemented with 10 μM Y-27632. Next day, media in each well was

replaced with 2 mL fresh media plus 10 μM Y-27632, 0.8 μg/mL polybrene (Sigma), and the minimal amount of Ngn2 and rtTA lentivirus necessary to generate >90% GFP+ cells upon doxycycline induction. The day after, virus-containing media were replaced with fresh mTeSR, and cells were expanded until near confluency. These infection cells are referred to as iPS-NGN2 cells.

iPS-NGN2 cells were detached using Accutase, and seeded in a new matrigel-coated 6-well plate at a density of $5x10^5$ cells per well in 2 ml of mTeSR supplemented with 10 μM Y-27632 (Day -1). Next day (day 0), media in each well was changed for 2 ml of neural induction media 1 (iN1) (DMEM-F12 [Gibco], 1x N2 [Gibco], 1x NEAA [Gibco], 1x pen/strep [Gibco]) supplemented with fresh doxycycline hyclate (2 μg/ml: Sigma). The next two days (day 1 and 2), media was replaced with 2 ml of iN1 supplemented with fresh doxycycline hyclate (2 μg/ml) and puromycin (1 μg/ml; Sigma). Day 3, media was replaced with neural induction media 2 (iN2) (Neurobasal media [Gibco], 1x B27 supplement [Gibco], 1x glutamax [Gibco], 1x pen/strep [Gibco], laminin (Sigma Aldrich, 10 μg/mL), BDNF (Peprotech, 10 ng/μL) and GDNF (Peprotech, 10 ng/μL)]. Day 4, induced neurons were re-plated onto poly-ornithine (50 μg/mL) and laminin (15 μg/mL)-coated 24- and 96-well plates (previously seeded with glia co-culture). Media was replaced with iN2 every 2 days; FBS (2%) was added to the iN2 at day 10, and cells were fixed at day 21. Primary mouse glial cells were seeded onto poly-ornithine and laminin-coated 12mm coverslips (in 24-well plates) and 96-well plates on day -1, at a density of 40,000 – 70,000 cells/well in a 24-well plate and ~15,000 cells/well in a 96-well plate.

4.3.4 Immunostaining and antibodies

Cells were washed in PBS and fixed with 4% paraformaldehyde (PFA) for 15 minutes at room temperature. Cells (coverslips and 96-wells) were washed with PBS 3 x 10 minutes. Cells were incubated with blocking/permeabilization solution (B/P solution; 10% normal donkey serum, 0.3% Triton X-100, in PBS) for 45 minutes at room temperature. Primary antibodies were incubated in B/P solution overnight at 4°C. Cells were washed with PBS 3 x 10 minutes. Secondary antibodies were incubated in 50% B/P solution (in PBS) for 1.5 hours at room temperature. Cells were washed once with PBS, incubated in 300nM DAPI (in PBS) for 10 minutes, and again with PBS. 96-well paltes were stored at 4°C and coverslips at -20°C prior to imaging.

Primary antibodies: MAP2 (anti-chicken; Cedarlane CLN182, 1:2000), synapsin1 (anti-rabbit, Invitrogen A-6442, 1:1000), synapsin-1 (anti-mouse; Synaptic Systems 106 011, 1:1000), NeuN (anti-rabbit; Cell signalling, 1:500). *Secondary antibodies*: Alexa Fluor® 488 AffiniPure Donkey Anti-Chicken IgY (IgG) (H+L) (1:500, Jackson ImmunoResearch Laborartories Inc.), Cy™3 AffiniPure Donkey Anti-Rabbit IgG (H+L) (1:500, Jackson ImmunoResearch Laborartories Inc.), Alexa Fluor® 647 AffiniPure Donkey Anti-Mouse IgG (H+L) (1:500, Jackson ImmunoResearch Laborartories Inc,).

4.3.5 Imaging and analysis

96-well plates were imaged using the Operetta HCS imaging system (Perkin Elmer) using the 20x objective lens. We acquired images from every well, and selected

the same 4x4 fields within the well. Custom Acapella scripts were written (by Dr. Tony Collins, SCC-RI, McMaster University) to identify the nuclei through DAPI signal. The neuron was identified through DAPI+ and MAP2+ nuclei, and from those MAP2+/DAPI+ nuclei, the cytoplasm was identified using the MAP2 signal. Next, neurites were identified in the MAP2 image using the nuclei as a starting point. The "spots" of synapsin1 puncta were found using synapsin1 channel, and the spots were associated with a neurite using a synapsin threshold.

Cells grown in a 24-well plate were imaged using the Zeiss LSM700 laser confocal microscope. Synaptic puncta images were acquired using the 63x objective lens, with a speed of 4, average of 2, and zoom of 0.5. Synaptic puncta was quantified using ImageJ software. Briefly, the synaptic channel was thresholded to 1-2%, and the synaptic puncta within a 5um diameter selection brush was measured and analyzed.

4.3.6 Data analysis

Data are expressed as mean ± s.e.m. We performed one-way ANOVA with *post hoc* Tukey tests for statistical analyses (as indicated). The *P* values in the Results are from *t* tests unless specified otherwise. $P < 0.05$ was considered statistically significant.

4.4 RESULTS & DISCUSSION

4.4.1 Generation of neurons from human iPS-derived neurons using the NGN2 induction method

As previously described, several labs have been able to successfully generate

cortical neurons through NGN2 induction of human iPS cells (Ho et al., 2016; Yi et al., 2016; Zhang et al., 2013). In collaboration with Dr. Eric Deneault from Dr. Stephen Scherer's laboratory at Sick Kids Hospital (Toronto), we have generated *SCN2A* KO and *KCNQ2* KO human iPS cell lines. Dr. Deneault generated these isogenic KO iPS cell lines through generated using CRISPR technology. Briefly, guide RNA sequences (gRNA), the pCas9D10A-GFP plasmid, and single-stranded oligodeoxynucleotides (ssODN) were nucleofected into iPSCs. KO iPSCs were selected for and enriched using droplet digital PCR (ddPCR) and limiting-dilution steps. The KO iPSCs were characterized using PCR performed on genomic DNA from cells (Deneault el al., *in submission*).

Sodium voltage-gated channel alpha subunit 2 (SCN2A) is a transmembrane glycoprotein that functions in the generation of propagation of action potentials in neurons and muscles (Catterall, 2012). *SCN2A* is a high confidence risk gene that has been associated with ASD, intellectual disability (ID), attention deficit hyperactivity disorder (ADHD), and other neurodevelopmental disorders (Epi et al., 2013). Studies have found that *de novo* mutations in the *SCN2A* gene are strongly associated with ASD (Sanders et al., 2012; Touma et al., 2013). *KCNQ2* encodes for Potassium voltage-gated channel, KWT-like subfamily, member 2, which is important for synaptic transmission through proper transport of potassium ions. Mutations in *KCNQ2* have been previously implicated in epilepsy in newborns, and variations in *KCNQ2* have been identified in patients with ASD (Jiang et al., 2013; Singh et al., 1998). These two genes, *SCN2A* and *KCNQ2*, were specifically chosen to develop KO human iPS cell lines because they were

identified in a recent study published by the Scherer lab as candidate genes for ASD through whole genome sequencing through the Autism Speaks MSSSNG project ASD (Yuen et al., 2016; Yuen et al., 2015; Yuen et al., 2017). *SCN2A* and *KCNQ2* are known to play an imporant role in both synaptic function and cell adhesion, which are pathways theorized to be disrupted in certain cases of ASD (Bourgeron, 2015).

We performed NGN2 induction on human iPS cell lines using a modified protocol from Zhang et al., 2013 (Figure 1). This process involves the transduction of iPS cells with two lentiviral vectors: the first is a virus expressing rtTA (reverse tetracycline-control transactivator), and the second is a virus expressing Ngn2/EGFP/puromycin linked by P2A and T2A sequences (Zhang et al., 2013). Briefly, iPSCs are infected with the two viral vectors; these cells are then induced with doxycycline (Day 0) to turn on the expression of NGN2. The following days (Day 1 and 2), the cells are treated with puromycin to select for cells properly expressing the NGN2 transcription factor. Next, the media is changed into neural differentiating media, with the addition of fetal bovine serum (FBS) at day 10. After 14 days, these cells are mature MAP2 expressing neurons and ready to be analyzed, either through electrophysiology or immunostaining. Figure 1B shows 21-day-old induced neurons, generated in the lab, that have been immunostained for MAP2 (marker of mature neurons), DAPI (nuclear marker), and synapsin 1 (pre-synaptic protein marker).

4.4.2 Development and optimization of a high-throughput culturing system of human iPS-derived neurons

The protocol modified from Zhang et al., 2013 as described in Figure 1 was modified for culturing in the 96-well format. In this system, we were interested in semi-automated imaging and high-content analysis of dendrites and synapses. As described in the Materials and Methods section of this chapter, NGN2-infected iPS cells are seeded into a 6-well plate (day -1), followed by Dox induction (day 0), and puromycin selection (day 1 and 2). At day 4, cells were re-plated into a 96-well plate. The media is half-changed every other day and FBS is added to the media on day 10 to maintain the health of the glia co-culture. For the purposes of this platform, we fixed cells with paraformaldehyde at day 21, when neurons are mature and have formed synapses. Concurrently, previously frozen primary mouse glia cells are thawed at day -7 in T75 flasks. The glia cells are re-plated into 96-well plates (pre-coated with poly-ornithine and laminin) at day -1; at day 4, the induced cells are re-plated onto glia-coated plates. This timeline is summarized in the schematic diagram in Figure 1A.

Although primary cortical neurons, and human iPS-derived neurons (form iCell) have been previously cultured in a high-throughput format, NGN-induced iPS-derived neurons have never been cultured in this format. We proceeded to optimize many steps to obtain healthy, mature, and functional neurons. First, we tested types and concentrations of cell matrix to use. Previous studies that have cultured human iPS-derived neurons have used a combination of poly-L-ornithine and laminin. Poly-L-ornithine is a synthetic amino acid chain that is positively charged and is used to enhance cell adhesion onto plastic or glass surfaces (Ge et al., 2015). Laminin is a glycoprotein that is a component of the basal lamina that supports adhesion (Kleinman et al., 1987). These two components

are very commonly used together for neuronal and neural stem cell cultures. We observed that 40 μg/mL poly-L-ornithine and 15 μg/mL laminin provided a cell matrix for healthy neurons to grow. Additionally, we tested a number of different cell densities for growth in these wells. We tested from 10,000 cells/well, 5,000 cells/well, 3,000 cells/well, 2,000 cells/well, and 1,000 cells/well; these densities were counted at day 4 on the day of re-plating. After acquiring images using the Operetta HCS, we determined that 3,000 cells/well density showed optimal cells growth with the ability to discriminate between different neurons (Figure 2). The ability to decipher separate neurons is important for future automated analysis of the synaptic puncta on single neurons.

As mentioned, induced neurons are co-cultured with primary mouse glial cells, which is an important component to grow the NGN2-induced neurons to maturity (Zhang et al., 2013). Glia is necessary for the proper formation of synaptic connections, and previous attempts at culturing these cells without glia support cells showed an absence of synaptic marker proteins (Lam et al., 2017; Zhang et al., 2013). Another component to consider is the length of culturing these induced neurons. As demonstrated by Zhang et al., these neurons are mature at day 14. We were able to recapitulate this same finding with our own cultures, however we observed that the complexity of neurite growth (via MAP2 staining) was minimal and we saw limited synaptic marker staining (Figure 1B and 2). Neurons fixed at day 21 showed more complex neurite outgrowth (branching) and showed extensive synaptic maker staining, as demonstrated in Figure 2A. In addition to observing the differences in neurite growth at day 14 and day 21, we were optimizing the immunostaining protocol to determine if we should stain neurons with beta-III tubulin.

Although, beta-III tubulin is not specifically for only neurons (whereas MAP2 is), beta-III tubulin may be able to detect the smaller processes that are missed by MAP2 staining. A potential caveat of staining with beta-III tubulin is the possibility of staining the glia cells as well; there is evidence of beta-III tubulin expression in fetal astrocytes (Draberova et al., 2008). Immunostaining with beta-III tubulin proved to be too complex, and neurites belonging to a single cell body were indecipherable (Figure 2B). These optimization steps and final conditions are summarized in Table 1.

Finally, we acquired images using a 40x and a 20x objective lens; the advantage of the 20x objective lens is that images can be acquired much faster and there is less stitching of images required, whereas the 40x object lens may be the only way to properly detect synaptic puncta for analysis. We found that synapsin 1 staining showed characteristic puncta (single points of high intensity) using the 40x objective (Figure 3A and 3B); fortunately, this puncta staining was also visible using the 20x objective lens (Figure 3C). Ultimately in the interest of high-content imaging, we decided to use the 20x objective lens for automated imaging to reduce the total elapsed time for imaging multiple wells and multiple fields per well.

4.4.3 High-content imaging and analysis of NGN2-induced neurons

After we determined that induced neurons are mature and healthy in a 96-well format, through MAP2 and synaptic marker staining, we collaborated with Dr. Tony Collins (SCC-RI, McMaster University) to write a custom script to perform automated analysis to characterize these neurons using the Operetta High-Content Imaging System

(Perkin Elmer) in the SCC-RI. First, we were interested to determine the proportion of MAP2+ cells that were positive for NeuN (mature neuronal nuclear marker) staining. We determined that 80-90% of MAP+ cells were also NeuN+ (Figure 4A). Ideally, this number should be 100%, which is to say that every MAP+ cell should also be NeuN+ if they are mature neurons. This discrepancy could be due to the difference in growth speed between the cells in a single well, where not all neurons are fully mature. Within this platform, we decided to use only the MAP2 signal to detect neurons because the MAP2 signal will also be used for neurite detection and analysis.

The parameters we were interested in for our automated analysis included total cell count, neurite length, neurite branching, soma size, and synaptic marker densities and size (of presynaptic marker synapsin 1). The script was written in a couple of different steps (Figure 4B). First, to identify nuclei through DAPI signal; this includes neuronal nuclei and glial nuclei. The neurons were identified through DAPI+ and MAP2+ co-localization, and from those MAP2+/DAPI+ nuclei, the cytoplasm was identified using the MAP2 signal. Next, neurites were identified in the MAP2 image using the nuclei as a starting point to form branches (neurites). Finally, the "spots" of synapsin 1 puncta were found using the synapsin1 channel, and these spots (synapsin 1) were associated with a neurite (MAP2) using a synapsin threshold. Thus far, we have demonstrated that we are able to detect MAP2+ neurons with punctate synapsin 1 staining in this 96-well platform (Figure 3). In order to determine if the script is able to analyze these images to detect a strong or subtle phenotype, we decided to culture the same cell lines in a "lower-throughput" format, and perform traditional methods for analysis using a confocal

microscope with the potential of validating the phenotypes.

4.4.4 Validation of high-content screen of neurons in a low-throughput format

One of the main concerns with developing a high-throughput imaging platform is the translation of phenotypes observed in the traditional "low-throughput" format, specifically in a 24-well plate format. To ensure that the phenotypes we may observe using the screening platform are translatable to the ASD model, we must first perform analysis on ASD-associated iPS-derived neurons in a commonly used format for culturing and analysis of these neurons, and eventually validate in a mouse model, if available. The analysis performed on these neurons mimics the analysis performed by the Sudhof group (Yi et al., 2016), specifically looking at dendrite length, primary branches, synaptic puncta density and size.

In order to test our imaging and analysis platform, we used ASD-associated iPS cell lines generated by Dr. Eric Deneault from the Scherer lab. We started with two cell lines as previously described, the *SCN2A* KO and *KCNQ2* KO human iPS cell lines. Both SCN2A and KCNQ2 are important channels in neurons for the proper generation of action potentials and synaptic transmission. Additionally, ASD-associated variants have been discovered in both genes through next generation sequencing (Yuen et al., 2016; Yuen et al., 2015; Yuen et al., 2017). The Scherer lab specifically chose these ASD-associated risk genes to study due to their identification through whole genome sequencing and the follow-up study showing disruptions in synaptic function (Data not shown, Deneault et al., *paper in submission*).

We cultured 21-day-old control, *SCN2A* KO, and *KCNQ2* KO induced neurons onto glass coverslips in 24-well plates and in 96-well plates, simultaneously. These cultures were stained with MAP2 and synapsin 1, as performed in the Yi et al., study (Figure 5A and 5C). Manual analysis *SCN2A* KO and *KCNQ2* KO induced neurons cultured on 24-well coverslips demonstrated a decrease in number of primary neurites (Figure 5B). Additionally, we observed a significant decrease in synapsin 1 puncta density in both *SCN2A* KO and *KCNQ2* KO induced neurons (Figure 5D) and no changes in puncta size (Figure 5E). This data validates the electrophysiology phenotypes, observed by the Scherer lab, where *SCN2A* KO and *KCNQ2* KO induced neurons showed a decrease in in synaptic activity (data not shown).

We performed high-content imaging and analysis on induced neurons in the 96-well format. Unfortunately, we were unable to observe all of the same synaptic phenotype demonstrated in the 24-well plate (Figure 6). There are many possible reasons for the discrepancies in our results. First, we were able to show that total cell count and MAP2+ cell count were not significantly different between conditions (Figure 6A and 6B). This observation is important because we want to ensure that any phenotypes we may observe are not due to cell viability. We did not observe any changes in total MAP2 neurite length in *SCN2A* KO and *KCNQ2* KO induced neurons compared to control neurons (Figure 6C). The measure of neurite length per cell describes an aspect of neurite growth, and in 24-well cultures we counted the number of primary neurites per cell. The trends of decreased number of primary neurites we observed in 24-well plates were not mimicked in the measurement of neurite length per cell (Figure 5B and 6C). Next, the automated

analysis measured synapse density per μm of neurite length. We observed a decrease in synaptic puncta density in *KCNQ2* KO neurons (Figure 6D), consistent with the phenotype observed in our low-throughput platform (Figure 5D). Unfortunately, we did not observe any changes in synaptic density in the *SCN2A* KO induced neurons (Figure 6D).

There are a number of potential causes for the inconsistencies observed between the 24-well (low-throughput) format compared to what the program analyzed in the 96-well platform. First, the consistency of cell culture may remain an issue. For example, in Figure 3A we observe several islands of cells. We hypothesize that these cells may be undifferentiated iPS cells or neural progenitor cells (NPCs). These clusters of cells may affect the analysis of neurites and synaptic puncta, and may dilute the phenotype that exists within these cell lines. Additionally, these clusters are not analyzed in the low-throughput format and highlight the disadvantages of automated image acquisition. Another potential source for this discrepancy may be the script designed to detect nuclei, neurites, and synaptic puncta. As previously mentioned, we used DAPI+ and MAP2+ co-localization to identify neuronal nuclei. This presents a potential problem, if a glia nuclei overlaps with a MAP2 signal resulting in a false positive detection of neuronal nuclei. One potential method to detect more robust phenotypes in our 96-well platform is to specifically immunostain for neuronal nuclei, rather than have the script try to decipher neuronal nuclei from glial nuclei. We have previously successfully immunostained induced neurons with NeuN, a marker for mature neuronal nuclei. We proposed that in the future, we might use NeuN only (or NeuN and DAPI, or NeuN and MAP2 together)

to specifically detect neuronal nuclei. Additionally, the custom script currently calculates total neurite length and total synaptic puncta within each field and does not differentiate between single neurons. This global view of neurite length and synaptic puncta may result in the dilution of a subtle effect and may result in the inability to detect a phenotype. This may be solved with further changes and improvements to the script.

Despite the inconsistencies between the 24-well format phenotype and the 96-well format, we believe that high content imaging and analysis of induced neurons in a 96-well format will be able to produce robust phenotypes in the future. We hypothesize that specific cell lines that demonstrate specific phenotypes are conducive to using this platform, which still requires further optimization. As observed in our preliminary experiments, we were able to detect a synaptic phenotype in the *KCNQ2* KO induced neuron and not in the *SCN2A* KO neurons. This leads us to believe that the platform is not sensitive enough to discern subtle changes in morphological and synaptic phenotypes. Further optimizations in cell culture and the custom script for analysis is required to be able to use this platform across all different ASD-associated neurons and for the potential in any potential drug screen.

The inability to detect a robust synaptic phenotype through immunostaining of synaptic puncta leads to the development and interest in other methods to observe a synaptic function phenotype in a human model. For example, expression of c-fos is an indirect method to detect neuronal connections (Dragunow and Faull, 1989). Additionally, an ASD-associated *Ctnnb1* conditional KO mouse model used c-Fos

staining as a method to assess neuronal activity (Dong et al., 2016). The immunostaining of c-Fos in our 96-well format is a potential assay that may generate robust phenotypes in human iPS-derived induced neurons. Another method to assess synaptic function is to perform electrophysiological recordings in a high-throughput format using multi-well microelectrode arrays (MEA). MEA plates contain many electrodes per well with the capability to record from cultured cells, and re-analyze the same wells at a later time. This new technology has allowed for the efficient and unbiased measurement and analysis of basic electrophysiological properties. Multiple studies have demonstrated the efficient use of MEA technology, and also show results that are consistent with traditional patch-clamp electrophysiological recordings (Liu et al., 2018; Marchetto et al., 2017). For example, MEA recordings displayed altered excitatory and inhibitory synaptic function in *Shank3* KO mice (Lu et al., 2016), which is consistent with previous studies investigating *Shank3* mouse models (Durand et al., 2012).

Ultimately, there is a need for the development of a high-throughput screen that is able to detect robust synaptic phenotypes in ASD-associated human iPS-derived neurons. The success of this platform will allow for the potential discovery of new drugs or treatments to rescue disrupted phenotypes.

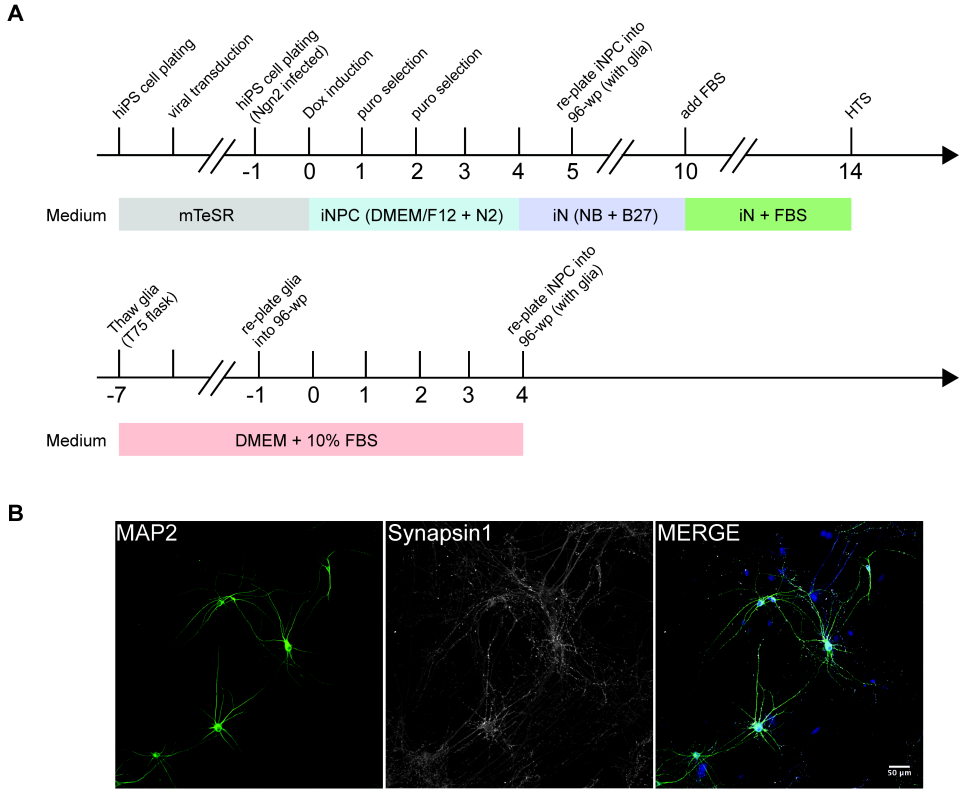

Figure 1: Overview of *NEUROGENIN2* induction of human iPS cells to generate cortical excitatory neurons. (**A**) Flow diagram of induced neuron generation and plating into 96-well format. iPSCs are transduced with the NGN2 and rt-TA lentiviruses prior to the timeline start. NGN2-infected iPSCs are seeded into a 6-well plate (Day -1) and Dox induction beings at day 0. Cells are selected using puromycin for 2 days (day 1 and 2). Neurons are re-plated into 96-well plate at day 4. The media is half-changed every other day and at Day 10, FBS is added to the media. Fixing and analysis can be performed at day 14 or any later date. Concurrently, previously frozen primary glia cells are thawed at day -7 in T75 flasks. The glia cells are seeded into plates (pre-coated with poly-ornithine and laminin) at day -1. (**B**) 4-week-old NGN2-induced neurons, immunostained with MAP2 (marker of mature neurons) and synapsin 1 (pre-synaptic marker).

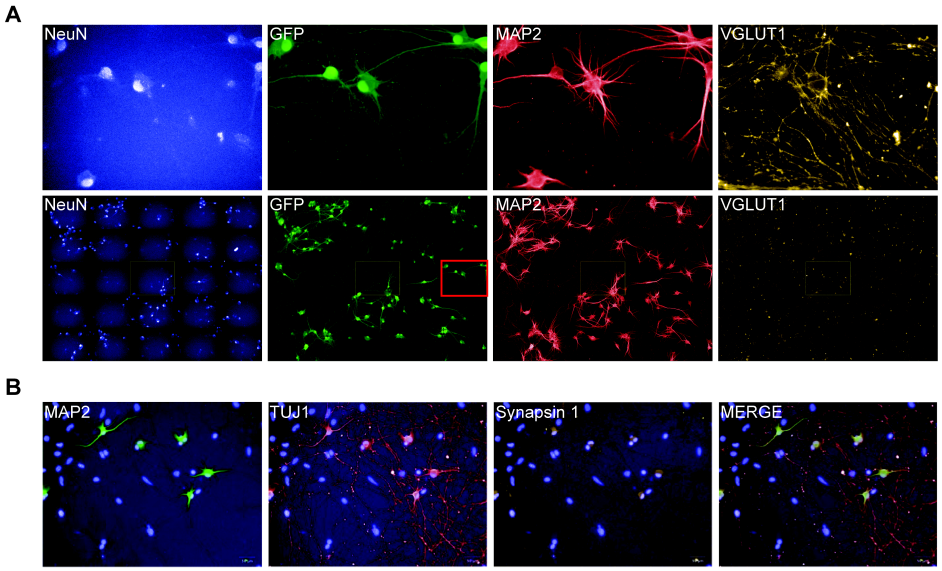

Figure 2: Culturing of human iPS-derived neurons and optimization of staining protocol. (**A**) Images were acquired using a 40x objective lens, and neurons were stained with GFP, MAP2 and VGLUT1. Images were stiched to show a full portion of the well that was imaged (bottom). (**B**) 14-day-old neurons showing MAP2, TUJ1, and synapsin 1 immunostaining.

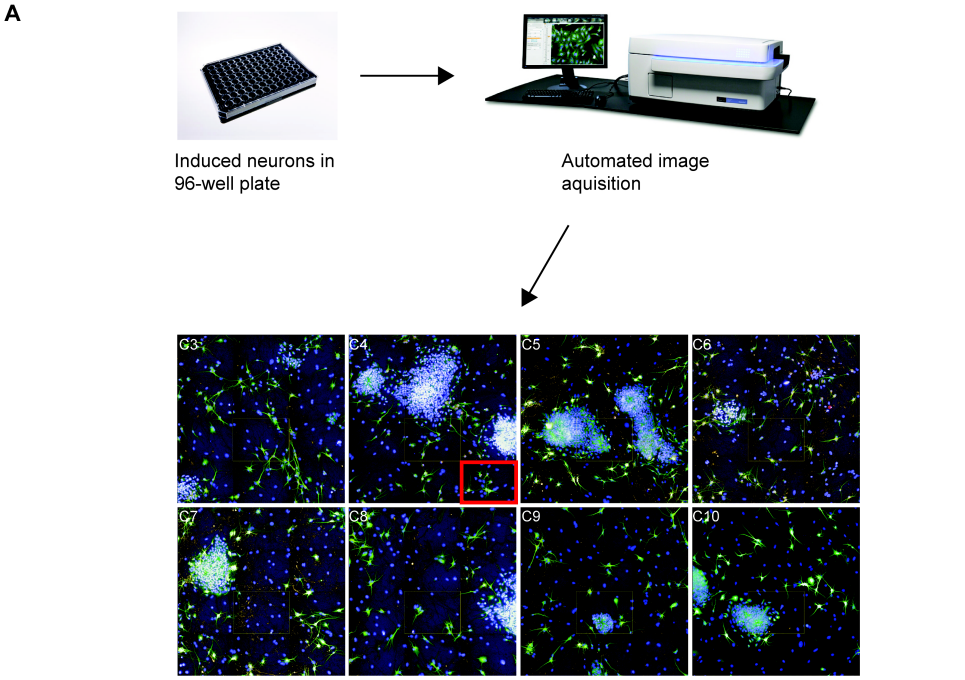
A
Induced neurons in 96-well plate
Automated image aquisition
C3
C4
C5
C6
C7
C8
C9
C10
B
DAPI
MAP2
synapsin1
MERGE
C
DAPI
MAP2
synapsin1
NeuN
MERGE

Figure 3: Development of high-content imaging platform of human induced neurons. (**A**) Schematic diagram of culturing iPS-derived induced neurons in a 96-well plate, followed by automated image acquisition and analysis. Representative images demonstrate 3x4 fields in a multiple wells immunostained with MAP2, synapsin 1 and DAPI, using 40x objective lens. (**B**) 40x images immunostained with DAPI, MAP2, and synapsin 1. (**C**) Representative images acquired using the 20x objective lens, showing MAP2, synapsin 1, and NeuN staining.

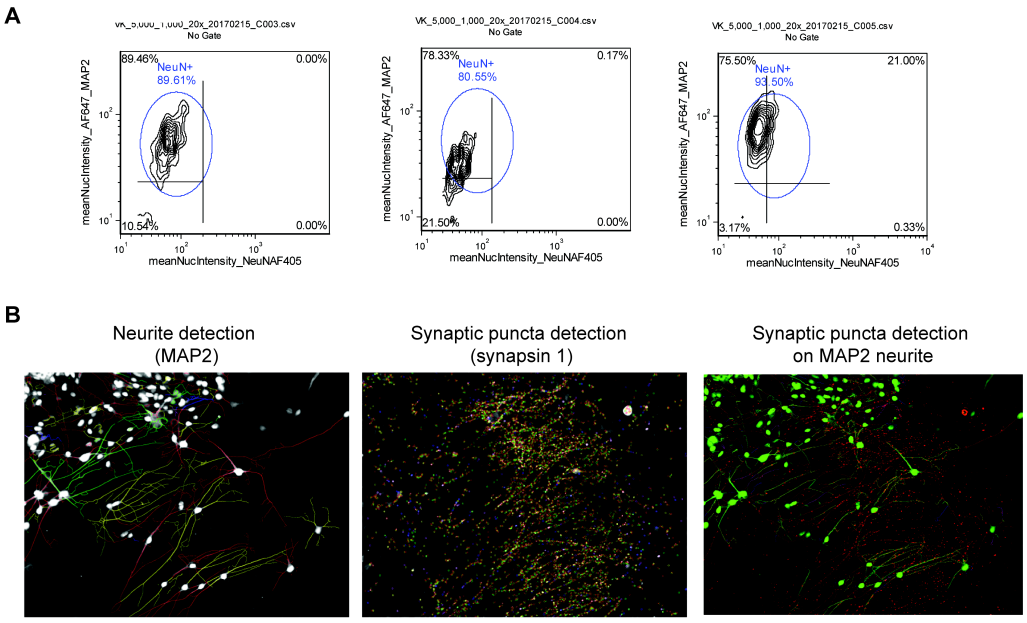

Figure 4: Automated analysis of mature neurons, neurite and synaptic puncta detection. (**A**) Analysis of images showed that 80-90% MAP+ cells were NeuN+ (top), and 75-80% of cells were double positive for GFP and MAP2. (**B**) Representative images showing neurite detection, synapsin 1 (spot) detection, and synaptic puncta detection on neurite through custom script.

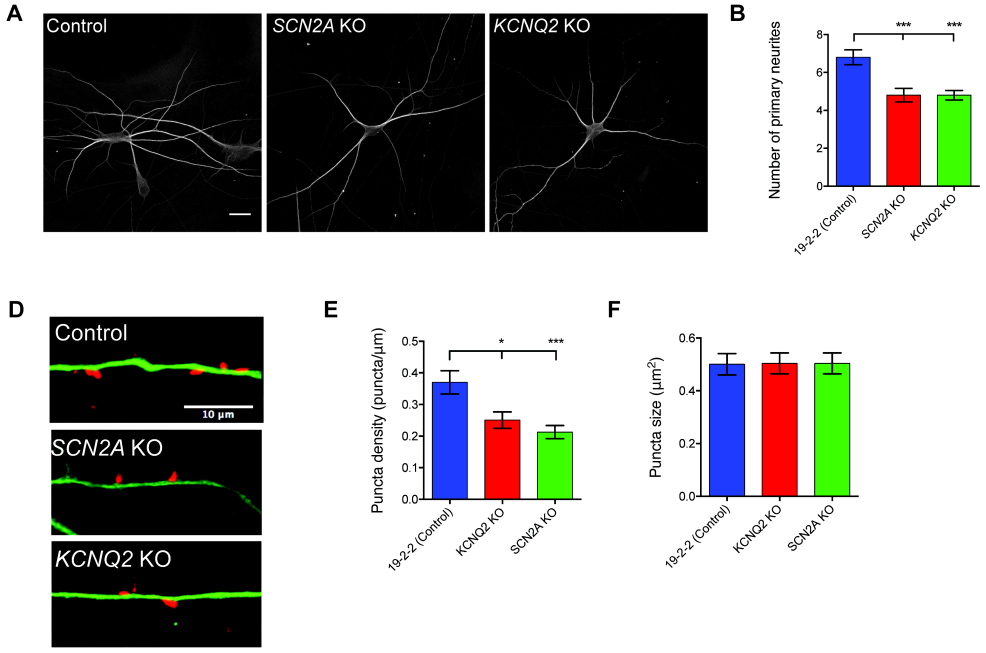

Figure 5: **ASD-associated knockout human induced neurons show a disruption in synapse formation.** (**A**) Representative images of 21-day-old induced neurons derived from human iPS cells, immunostained with MAP2, cultured in low-throughput. (**B**) *KCNQ2* KO and *SCN2A* KO lines show a decrease in synapsin1 puncta density (n = 2 cultures, 10 neurons; one-way ANOVA; post hoc Sidak test: *p < 0.05, ***p < 0.001). (**C**) Representative images of dendrites from 21-day-old induced neurons, immunostained with MAP2, and synapsin1. (**D**) *KCNQ2* KO and *SCN2A* KO lines show a decrease in synapsin1 puncta density (n = 2 cultures, 10 neurons, 20 dendrites; one-way ANOVA; post hoc Sidak test: *p < 0.05, ***p < 0.001). (**E**) *KCNQ2* KO and *SCN2A* KO lines demonstrate no changes in synaptic puncta size (n = 2 cultures, 10 neurons, 20 dendrites; one-way ANOVA; post hoc Sidak test). All numerical data are given as mean ± SEM. The scale bars represent 10 µm for (**C**), and 20 µm for (**A**).

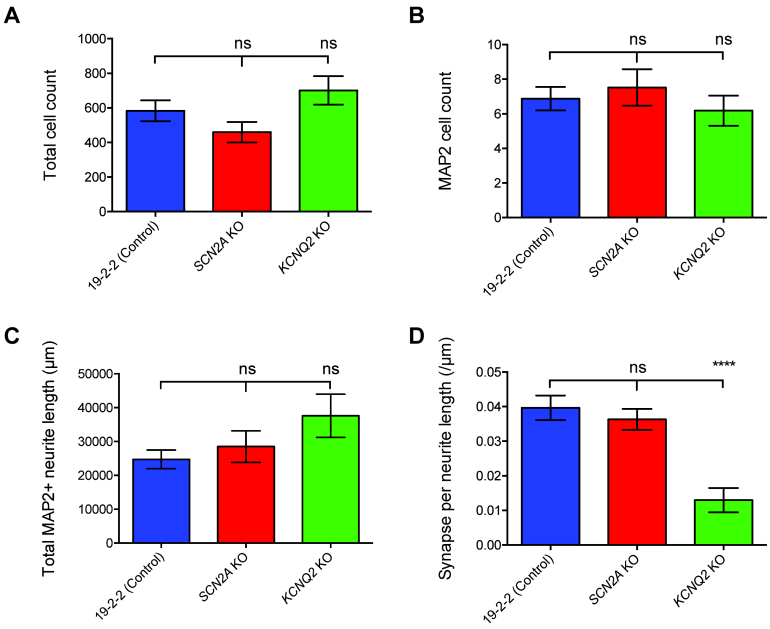

Figure 6: Automated analysis of *SCN2A* KO and *KCNQ2* KO induced neurons in our preliminary high-content platform. (**A, B**) Total cell count and MAP2 cell count showed no changes with *SCN2A* KO and *KCNQ2* KO neurons compared to control neurons (n = 2 cultures, 40 wells per condition; one-way ANOVA; post hoc Sidak test). (**C**) No changes in total neurite length were observed in *SCN2A* KO and *KCNQ2* KO neurons (n = 2 cultures, 40 wells; one-way ANOVA; post hoc Sidak test). (**D**) No changes in *SCN2A* KO neurons showed no changes in synapse puncta/length, and a decrease in puncta density in *KCNQ2* KO neurons (n = 2 cultures, 40 wells; one-way ANOVA; post hoc Sidak test: ****$p < 0.0001$). All numerical data are given as mean ± SEM.

	96-well plate	24-well plate
Cell matrix	Poly-ornithine and laminin	
Plating density	3,000 cells/well (at day 4)	25,000 cells/well (at day 4)
Co-culture	With primary mouse glia (to support synapse formation)	
Maturity	21 days	
Immunostaining	MAP2, synapsin1, NeuN	
Analysis	Cell counting, neurite length/branching, synaptic density and size	

Table 1: Summary of optimal conditions for culturing human iPS-derived neurons in a 96- and 24-well format.

CHAPTER 5: CONCLUSIONS & FUTURE DIRECTIONS

5.1 Elucidation of a DIXDC1 signalling network

ASD describes a group of highly heterogeneous neurodevelopmental disorders where there remains a lack of understanding of the etiology and pathophysiology underlying these disorders. The work presented here has revealed a novel ASD-associated gene, *DIXDC1*, which plays an important role in neurodevelopment in early embryonic and postnatal time periods. We identified rare-inherited missense variants in this gene through whole genome sequencing, and discovered that these specific single nucleotide variants may cause a disruption in neuronal morphology and synaptic activity.

Additionally, we were able to further elucidate the signalling networks surrounding Dixdc1, using RNA sequencing of *Dixdc1* KO mouse brains. RNA sequencing analysis identified disrupted signalling networks associated with ASD, such as synaptic function, cell adhesion, and wnt signalling. Additionally, many of the genes with disrupted expression levels are ASD-susceptibility genes that have been recognized by SFARI Gene and the Autism Speaks MSSNG Project. These results suggest that the *Dixdc1* KO mouse may be a model for ASD, demonstrating many ASD-associated deficits, and highlights the need to further study the role of Dixdc1 in normal brain development. Furthermore, we identified differentially expressed genes that may implicate Dixdc1 in other genetic disorders, such as Ehlers-Danlos syndrome (EDS). Further experiments need to be performed to determine if *Dixdc1* KO mice display EDS phenotypes.

5.2 Development of an automated high-content imaging platform to characterize ASD-associated neurons

An emerging problem in the field of neurodevelopmental disorders is the large increase in disease-associated susceptibility genes. This is due to the advancement of next generation sequencing technology. There is a need within the field to develop a platform for the high-throughput and high-content analysis of many of these genes within a translatable model. We developed a platform to culture human iPS-derived NGN2-induced neurons. Since many of the current high confidence and strong candidate genes associated with ASD are genes that are implicated in synaptic function, we were interested in analyzing a synaptic phenotype within these neurons. We were able to successfully culture, immunostain, image, and analyze these induced neurons and synaptic markers. Though, the results we generated showed us the need for further development into this platform. There are different methods to assess synaptic function: through immunostaining for indirect markers of synaptic transmission (e.g. c-fos) or using the multi-well microelectrode array (MEA) to measure synaptic function. We are interested in using these techniques in combination with the 96-well high-content imaging format we developed using human iPS-derived neurons.

5.3 Significance and future directions

This work has uncovered a novel actin polymerization-associated pathway where DIXDC1 phosphorylation by MARK1 regulates dendrite and dendritic spine growth and cytoskeleton dynamics. This study also emphasized the importance of studying ASD-

associated genes that may not contain *de novo* mutations, and alternatively carry rare-inherited or common variants within the gene, discovered through whole exome and whole genome sequencing. Additionally, transcriptomic analysis of *Dixdc1* KO mouse brains highlights the importance of Dixdc1 in ASD pathophysiology and also other genetic disorders (e.g. EDS) that may also be associated with ASD.

Future studies should continue to elucidate the mechanism of DIXDC1 regulation of dendrite and spine growth, and the isoform-specific roles within this mechanism. BioID is a method to detect for protein interactions through a proximity-dependent manner (Roux et al., 2013). The BirA* ligase may be fused to the DIXDC1 to promiscuously biotinylate proteins in close proximity. Fusion of BirA* to the N-terminal end of DIXDC1 allows us to select for the different isoforms of DIXDC1 which can be used to identify interactors of DIXDC1 isoform 1 and isoform 2. We hypothesize that we may identify protein interactions related to cytoskeletal dynamics when performed with DIXDC1 isoform 1.

Finally, the development of a high-throughput and high-content imaging platform to detect for morphological and synaptic phenotypes is crucial for the future of ASD research. With the increasing number of ASD-susceptibility genes, the need for a platform to phenotype the effects of these genes, quickly and robustly, are important. Additionally, this platform may be used in the future for the screening of drugs and small molecules to potentially reverse the morphological and synaptic phenotypes observed.

REFERENCES

Abrahams, B.S., Arking, D.E., Campbell, D.B., Mefford, H.C., Morrow, E.M., Weiss, L.A., Menashe, I., Wadkins, T., Banerjee-Basu, S., and Packer, A. (2013). SFARI Gene 2.0: a community-driven knowledgebase for the autism spectrum disorders (ASDs). Mol Autism *4*, 36.

Akhmanova, A., and Hoogenraad, C.C. (2005). Microtubule plus-end-tracking proteins: mechanisms and functions. Current opinion in cell biology *17*, 47-54.

Amir, R.E., Van den Veyver, I.B., Wan, M., Tran, C.Q., Francke, U., and Zoghbi, H.Y. (1999). Rett syndrome is caused by mutations in X-linked MECP2, encoding methyl-CpG-binding protein 2. Nature genetics *23*, 185-188.

Baeza-Velasco, C., Pailhez, G., Bulbena, A., and Baghdadli, A. (2015). Joint hypermobility and the heritable disorders of connective tissue: clinical and empirical evidence of links with psychiatry. General hospital psychiatry *37*, 24-30.

Baeza-Velasco, C., Sinibaldi, L., and Castori, M. (2018). Attention-deficit/hyperactivity disorder, joint hypermobility-related disorders and pain: expanding body-mind connections to the developmental age. Attention deficit and hyperactivity disorders.

Barnard, R.A., Pomaville, M.B., and O'Roak, B.J. (2015). Mutations and Modeling of the Chromatin Remodeler CHD8 Define an Emerging Autism Etiology. Frontiers in neuroscience *9*, 477.

Belinson, H., Nakatani, J., Babineau, B.A., Birnbaum, R.Y., Ellegood, J., Bershteyn, M., McEvilly, R.J., Long, J.M., Willert, K., Klein, O.D.*, et al.* (2016). Prenatal beta-catenin/Brn2/Tbr2 transcriptional cascade regulates adult social and stereotypic behaviors. Molecular psychiatry.

Ben-David, E., and Shifman, S. (2012). Networks of neuronal genes affected by common and rare variants in autism spectrum disorders. PLoS genetics *8*, e1002556.

Berkel, S., Marshall, C.R., Weiss, B., Howe, J., Roeth, R., Moog, U., Endris, V., Roberts, W., Szatmari, P., Pinto, D.*, et al.* (2010). Mutations in the SHANK2 synaptic scaffolding gene in autism spectrum disorder and mental retardation. Nature genetics *42*, 489-491.

Berkel, S., Tang, W., Trevino, M., Vogt, M., Obenhaus, H.A., Gass, P., Scherer, S.W., Sprengel, R., Schratt, G., and Rappold, G.A. (2012). Inherited and de novo SHANK2 variants associated with autism spectrum disorder impair neuronal morphogenesis and physiology. Human molecular genetics *21*, 344-357.

Bernard, L.P., and Zhang, H. (2015). MARK/Par1 Kinase Is Activated Downstream of NMDA Receptors through a PKA-Dependent Mechanism. PloS one *10*, e0124816.

Bernier, R., Golzio, C., Xiong, B., Stessman, H.A., Coe, B.P., Penn, O., Witherspoon, K., Gerdts, J., Baker, C., Vulto-van Silfhout, A.T.*, et al.* (2014). Disruptive CHD8 mutations define a subtype of autism early in development. Cell *158*, 263-276.

Berry, B.J., Akanda, N., Smith, A.S., Long, C.J., Schnepper, M.T., Guo, X., and Hickman, J.J. (2015). Morphological and functional characterization of human induced

pluripotent stem cell-derived neurons (iCell Neurons) in defined culture systems. Biotechnology progress *31*, 1613-1622.

Bethesda, N.L.o.M.U.G.H.R.I., The, M., and Library (2018). Ehlers-Danlos syndrome.

Bhakar, A.L., Dolen, G., and Bear, M.F. (2012). The pathophysiology of fragile X (and what it teaches us about synapses). Annual review of neuroscience *35*, 417-443.

Bianchi, V.E., Locatelli, V., and Rizzi, L. (2017). Neurotrophic and Neuroregenerative Effects of GH/IGF1. International journal of molecular sciences *18*.

Boccitto, M., Doshi, S., Newton, I.P., Nathke, I., Neve, R., Dong, F., Mao, Y., Zhai, J., Zhang, L., and Kalb, R. (2016). Opposing actions of the synapse-associated protein of 97-kDa molecular weight (SAP97) and Disrupted in Schizophrenia 1 (DISC1) on Wnt/beta-catenin signaling. Neuroscience *326*, 22-30.

Boisvert, E.M., Engle, S.J., Hallowell, S.E., Liu, P., Wang, Z.W., and Li, X.J. (2015). The Specification and Maturation of Nociceptive Neurons from Human Embryonic Stem Cells. Scientific reports *5*, 16821.

Bourgeron, T. (2015). From the genetic architecture to synaptic plasticity in autism spectrum disorder. Nature reviews Neuroscience *16*, 551-563.

Bozdagi, O., Sakurai, T., Dorr, N., Pilorge, M., Takahashi, N., and Buxbaum, J.D. (2012). Haploinsufficiency of Cyfip1 produces fragile X-like phenotypes in mice. PloS one *7*, e42422.

Braccioli, L., Vervoort, S.J., Adolfs, Y., Heijnen, C.J., Basak, O., Pasterkamp, R.J., Nijboer, C.H., and Coffer, P.J. (2017). FOXP1 Promotes Embryonic Neural Stem Cell Differentiation by Repressing Jagged1 Expression. Stem cell reports *9*, 1530-1545.

Brennand, K.J., Marchetto, M.C., Benvenisty, N., Brustle, O., Ebert, A., Izpisua Belmonte, J.C., Kaykas, A., Lancaster, M.A., Livesey, F.J., McConnell, M.J.*, et al.* (2015). Creating Patient-Specific Neural Cells for the In Vitro Study of Brain Disorders. Stem cell reports *5*, 933-945.

Brennand, K.J., Simone, A., Jou, J., Gelboin-Burkhart, C., Tran, N., Sangar, S., Li, Y., Mu, Y., Chen, G., Yu, D.*, et al.* (2011). Modelling schizophrenia using human induced pluripotent stem cells. Nature *473*, 221-225.

Brentani, H., Paula, C.S., Bordini, D., Rolim, D., Sato, F., Portolese, J., Pacifico, M.C., and McCracken, J.T. (2013). Autism spectrum disorders: an overview on diagnosis and treatment. Revista brasileira de psiquiatria *35 Suppl 1*, S62-72.

Broek, J.A., Guest, P.C., Rahmoune, H., and Bahn, S. (2014). Proteomic analysis of post mortem brain tissue from autism patients: evidence for opposite changes in prefrontal cortex and cerebellum in synaptic connectivity-related proteins. Mol Autism *5*, 41.

Budnik, V., and Salinas, P.C. (2011). Wnt signaling during synaptic development and plasticity. Current opinion in neurobiology *21*, 151-159.

Bush, W.S., and Moore, J.H. (2012). Chapter 11: Genome-wide association studies. PLoS computational biology *8*, e1002822.

Busskamp, V., Lewis, N.E., Guye, P., Ng, A.H., Shipman, S.L., Byrne, S.M., Sanjana, N.E., Murn, J., Li, Y., Li, S.*, et al.* (2014). Rapid neurogenesis through transcriptional activation in human stem cells. Molecular systems biology *10*, 760.

Calabrese, B., and Halpain, S. (2014). Lithium prevents aberrant NMDA-induced F-actin reorganization in neurons. Neuroreport *25*, 1331-1337.

Campbell, D.B., Sutcliffe, J.S., Ebert, P.J., Militerni, R., Bravaccio, C., Trillo, S., Elia, M., Schneider, C., Melmed, R., Sacco, R.*, et al.* (2006). A genetic variant that disrupts MET transcription is associated with autism. Proceedings of the National Academy of Sciences of the United States of America *103*, 16834-16839.

Cao, F., Yin, A., Wen, G., Sheikh, A.M., Tauqeer, Z., Malik, M., Nagori, A., Schirripa, M., Schirripa, F., Merz, G.*, et al.* (2012). Alteration of astrocytes and Wnt/beta-catenin signaling in the frontal cortex of autistic subjects. Journal of neuroinflammation *9*, 223.

Capelluto, D.G., Kutateladze, T.G., Habas, R., Finkielstein, C.V., He, X., and Overduin, M. (2002). The DIX domain targets dishevelled to actin stress fibres and vesicular membranes. Nature *419*, 726-729.

Caracci, M.O., Avila, M.E., and De Ferrari, G.V. (2016). Synaptic Wnt/GSK3beta Signaling Hub in Autism. Neural plasticity *2016*, 9603751.

Castro, J., Garcia, R.I., Kwok, S., Banerjee, A., Petravicz, J., Woodson, J., Mellios, N., Tropea, D., and Sur, M. (2014). Functional recovery with recombinant human IGF1

treatment in a mouse model of Rett Syndrome. Proceedings of the National Academy of Sciences of the United States of America *111*, 9941-9946.

Catterall, W.A. (2012). Voltage-gated sodium channels at 60: structure, function and pathophysiology. The Journal of physiology *590*, 2577-2589.

Cederlof, M., Larsson, H., Lichtenstein, P., Almqvist, C., Serlachius, E., and Ludvigsson, J.F. (2016). Nationwide population-based cohort study of psychiatric disorders in individuals with Ehlers-Danlos syndrome or hypermobility syndrome and their siblings. BMC psychiatry *16*, 207.

Chailangkarn, T., Trujillo, C.A., Freitas, B.C., Hrvoj-Mihic, B., Herai, R.H., Yu, D.X., Brown, T.T., Marchetto, M.C., Bardy, C., McHenry, L.*, et al.* (2016). A human neurodevelopmental model for Williams syndrome. Nature *536*, 338-343.

Chambers, S.M., Fasano, C.A., Papapetrou, E.P., Tomishima, M., Sadelain, M., and Studer, L. (2009). Highly efficient neural conversion of human ES and iPS cells by dual inhibition of SMAD signaling. Nature biotechnology *27*, 275-280.

Chen, J.A., Penagarikano, O., Belgard, T.G., Swarup, V., and Geschwind, D.H. (2015a). The emerging picture of autism spectrum disorder: genetics and pathology. Annual review of pathology *10*, 111-144.

Chen, Y., Huang, W.C., Sejourne, J., Clipperton-Allen, A.E., and Page, D.T. (2015b). Pten Mutations Alter Brain Growth Trajectory and Allocation of Cell Types through

Elevated beta-Catenin Signaling. The Journal of neuroscience : the official journal of the Society for Neuroscience *35*, 10252-10267.

Chiarelli, N., Carini, G., Zoppi, N., Dordoni, C., Ritelli, M., Venturini, M., Castori, M., and Colombi, M. (2016). Transcriptome-Wide Expression Profiling in Skin Fibroblasts of Patients with Joint Hypermobility Syndrome/Ehlers-Danlos Syndrome Hypermobility Type. PloS one *11*, e0161347.

Chikano, Y., Domoto, T., Furuta, T., Sabit, H., Kitano-Tamura, A., Pyko, I.V., Takino, T., Sai, Y., Hayashi, Y., Sato, H.*, et al.* (2015). Glycogen synthase kinase 3beta sustains invasion of glioblastoma via the focal adhesion kinase, Rac1, and c-Jun N-terminal kinase-mediated pathway. Molecular cancer therapeutics *14*, 564-574.

Ching, M.S., Shen, Y., Tan, W.H., Jeste, S.S., Morrow, E.M., Chen, X., Mukaddes, N.M., Yoo, S.Y., Hanson, E., Hundley, R.*, et al.* (2010). Deletions of NRXN1 (neurexin-1) predispose to a wide spectrum of developmental disorders. American journal of medical genetics Part B, Neuropsychiatric genetics : the official publication of the International Society of Psychiatric Genetics *153B*, 937-947.

Christensen, D.L., Baio, J., Van Naarden Braun, K., Bilder, D., Charles, J., Constantino, J.N., Daniels, J., Durkin, M.S., Fitzgerald, R.T., Kurzius-Spencer, M.*, et al.* (2012). Prevalence and Characteristics of Autism Spectrum Disorder Among Children Aged 8 Years — Autism and Developmental Disabilities Monitoring Network. In MMWR Surveillance Summaries, pp. 1-23.

Ciani, L., Marzo, A., Boyle, K., Stamatakou, E., Lopes, D.M., Anane, D., McLeod, F., Rosso, S.B., Gibb, A., and Salinas, P.C. (2015). Wnt signalling tunes neurotransmitter release by directly targeting Synaptotagmin-1. Nature communications *6*, 8302.

Clipperton-Allen, A.E., and Page, D.T. (2014). Pten haploinsufficient mice show broad brain overgrowth but selective impairments in autism-relevant behavioral tests. Human molecular genetics *23*, 3490-3505.

Comery, T.A., Harris, J.B., Willems, P.J., Oostra, B.A., Irwin, S.A., Weiler, I.J., and Greenough, W.T. (1997). Abnormal dendritic spines in fragile X knockout mice: maturation and pruning deficits. Proceedings of the National Academy of Sciences of the United States of America *94*, 5401-5404.

Conesa, A., Madrigal, P., Tarazona, S., Gomez-Cabrero, D., Cervera, A., McPherson, A., Szczesniak, M.W., Gaffney, D.J., Elo, L.L., Zhang, X.*, et al.* (2016). A survey of best practices for RNA-seq data analysis. Genome biology *17*, 13.

Cooper, T.K., Zhong, Q., Krawczyk, M., Tae, H.J., Muller, G.A., Schubert, R., Myers, L.A., Dietz, H.C., Talan, M.I., and Briest, W. (2010). The haploinsufficient Col3a1 mouse as a model for vascular Ehlers-Danlos syndrome. Veterinary pathology *47*, 1028-1039.

Courchesne, E., Mouton, P.R., Calhoun, M.E., Semendeferi, K., Ahrens-Barbeau, C., Hallet, M.J., Barnes, C.C., and Pierce, K. (2011). Neuron number and size in prefrontal cortex of children with autism. Jama *306*, 2001-2010.

Cross-Disorder Group of the Psychiatric Genomics, C., Lee, S.H., Ripke, S., Neale, B.M., Faraone, S.V., Purcell, S.M., Perlis, R.H., Mowry, B.J., Thapar, A., Goddard, M.E*., et al.* (2013). Genetic relationship between five psychiatric disorders estimated from genome-wide SNPs. Nature genetics *45*, 984-994.

de Anda, F.C., Rosario, A.L., Durak, O., Tran, T., Graff, J., Meletis, K., Rei, D., Soda, T., Madabhushi, R., Ginty, D.D*., et al.* (2012). Autism spectrum disorder susceptibility gene TAOK2 affects basal dendrite formation in the neocortex. Nature neuroscience *15*, 1022-1031.

De Rubeis, S., He, X., Goldberg, A.P., Poultney, C.S., Samocha, K., Cicek, A.E., Kou, Y., Liu, L., Fromer, M., Walker, S*., et al.* (2014). Synaptic, transcriptional and chromatin genes disrupted in autism. Nature *515*, 209-215.

De Rubeis, S., Pasciuto, E., Li, K.W., Fernandez, E., Di Marino, D., Buzzi, A., Ostroff, L.E., Klann, E., Zwartkruis, F.J., Komiyama, N.H*., et al.* (2013). CYFIP1 coordinates mRNA translation and cytoskeleton remodeling to ensure proper dendritic spine formation. Neuron *79*, 1169-1182.

Dean, C., Scholl, F.G., Choih, J., DeMaria, S., Berger, J., Isacoff, E., and Scheiffele, P. (2003). Neurexin mediates the assembly of presynaptic terminals. Nature neuroscience *6*, 708-716.

Delorme, R., Ey, E., Toro, R., Leboyer, M., Gillberg, C., and Bourgeron, T. (2013). Progress toward treatments for synaptic defects in autism. Nature medicine *19*, 685-694.

Deriziotis, P., O'Roak, B.J., Graham, S.A., Estruch, S.B., Dimitropoulou, D., Bernier, R.A., Gerdts, J., Shendure, J., Eichler, E.E., and Fisher, S.E. (2014). De novo TBR1 mutations in sporadic autism disrupt protein functions. Nature communications *5*, 4954.

Developmental Disabilities Monitoring Network Surveillance Year Principal, I., Centers for Disease, C., and Prevention (2014). Prevalence of autism spectrum disorder among children aged 8 years - autism and developmental disabilities monitoring network, 11 sites, United States, 2010. Morbidity and mortality weekly report Surveillance summaries *63*, 1-21.

Dolan, B.M., Duron, S.G., Campbell, D.A., Vollrath, B., Shankaranarayana Rao, B.S., Ko, H.Y., Lin, G.G., Govindarajan, A., Choi, S.Y., and Tonegawa, S. (2013). Rescue of fragile X syndrome phenotypes in Fmr1 KO mice by the small-molecule PAK inhibitor FRAX486. Proceedings of the National Academy of Sciences of the United States of America *110*, 5671-5676.

Dong, F., Jiang, J., McSweeney, C., Zou, D., Liu, L., and Mao, Y. (2016). Deletion of CTNNB1 in inhibitory circuitry contributes to autism-associated behavioral defects. Human molecular genetics.

Doyle, C.A., and McDougle, C.J. (2012). Pharmacotherapy to control behavioral symptoms in children with autism. Expert opinion on pharmacotherapy *13*, 1615-1629.

Draberova, E., Del Valle, L., Gordon, J., Markova, V., Smejkalova, B., Bertrand, L., de Chadarevian, J.P., Agamanolis, D.P., Legido, A., Khalili, K.*, et al.* (2008). Class III beta-

tubulin is constitutively coexpressed with glial fibrillary acidic protein and nestin in midgestational human fetal astrocytes: implications for phenotypic identity. Journal of neuropathology and experimental neurology *67*, 341-354.

Dragunow, M., and Faull, R. (1989). The use of c-fos as a metabolic marker in neuronal pathway tracing. J Neurosci Methods *29*, 261-265.

Duffney, L.J., Wei, J., Cheng, J., Liu, W., Smith, K.R., Kittler, J.T., and Yan, Z. (2013). Shank3 deficiency induces NMDA receptor hypofunction via an actin-dependent mechanism. The Journal of neuroscience : the official journal of the Society for Neuroscience *33*, 15767-15778.

Duffney, L.J., Zhong, P., Wei, J., Matas, E., Cheng, J., Qin, L., Ma, K., Dietz, D.M., Kajiwara, Y., Buxbaum, J.D.*, et al.* (2015). Autism-like Deficits in Shank3-Deficient Mice Are Rescued by Targeting Actin Regulators. Cell reports *11*, 1400-1413.

Durak, O., de Anda, F.C., Singh, K.K., Leussis, M.P., Petryshen, T.L., Sklar, P., and Tsai, L.H. (2015). Ankyrin-G regulates neurogenesis and Wnt signaling by altering the subcellular localization of beta-catenin. Molecular psychiatry *20*, 388-397.

Durak, O., Gao, F., Kaeser-Woo, Y.J., Rueda, R., Martorell, A.J., Nott, A., Liu, C.Y., Watson, L.A., and Tsai, L.H. (2016). Chd8 mediates cortical neurogenesis via transcriptional regulation of cell cycle and Wnt signaling. Nature neuroscience.

Durand, C.M., Perroy, J., Loll, F., Perrais, D., Fagni, L., Bourgeron, T., Montcouquiol, M., and Sans, N. (2012). SHANK3 mutations identified in autism lead to modification of

dendritic spine morphology via an actin-dependent mechanism. Molecular psychiatry *17*, 71-84.

Ebert, D.H., and Greenberg, M.E. (2013). Activity-dependent neuronal signalling and autism spectrum disorder. Nature *493*, 327-337.

Ebrahimi-Fakhari, D., and Sahin, M. (2015). Autism and the synapse: emerging mechanisms and mechanism-based therapies. Current opinion in neurology *28*, 91-102.

Epi, K.C., Epilepsy Phenome/Genome, P., Allen, A.S., Berkovic, S.F., Cossette, P., Delanty, N., Dlugos, D., Eichler, E.E., Epstein, M.P., Glauser, T.*, et al.* (2013). De novo mutations in epileptic encephalopathies. Nature *501*, 217-221.

Espuny-Camacho, I., Michelsen, K.A., Gall, D., Linaro, D., Hasche, A., Bonnefont, J., Bali, C., Orduz, D., Bilheu, A., Herpoel, A.*, et al.* (2013). Pyramidal neurons derived from human pluripotent stem cells integrate efficiently into mouse brain circuits in vivo. Neuron *77*, 440-456.

Ewing, B., and Green, P. (1998). Base-calling of automated sequencer traces using phred. II. Error probabilities. Genome research *8*, 186-194.

Ewing, B., Hillier, L., Wendl, M.C., and Green, P. (1998). Base-calling of automated sequencer traces using phred. I. Accuracy assessment. Genome research *8*, 175-185.

Fang, W.Q., Chen, W.W., Jiang, L., Liu, K., Yung, W.H., Fu, A.K., and Ip, N.Y. (2014). Overproduction of upper-layer neurons in the neocortex leads to autism-like features in mice. Cell reports *9*, 1635-1643.

Farley, M., Cottle, K.J., Bilder, D., Viskochil, J., Coon, H., and McMahon, W. (2018). Mid-life social outcomes for a population-based sample of adults with ASD. Autism research : official journal of the International Society for Autism Research *11*, 142-152.

Farley, M.A., McMahon, W.M., Fombonne, E., Jenson, W.R., Miller, J., Gardner, M., Block, H., Pingree, C.B., Ritvo, E.R., Ritvo, R.A.*, et al.* (2009). Twenty-year outcome for individuals with autism and average or near-average cognitive abilities. Autism research : official journal of the International Society for Autism Research *2*, 109-118.

Farra, N., Zhang, W.B., Pasceri, P., Eubanks, J.H., Salter, M.W., and Ellis, J. (2012). Rett syndrome induced pluripotent stem cell-derived neurons reveal novel neurophysiological alterations. Molecular psychiatry *17*, 1261-1271.

Fatehullah, A., Tan, S.H., and Barker, N. (2016). Organoids as an in vitro model of human development and disease. Nature cell biology *18*, 246-254.

Fehlow, P., and Tennstedt, A. (1985). [Concomitant neuropsychiatric symptoms in a case of Ehlers-Danlos syndrome]. Psychiatrie, Neurologie, und medizinische Psychologie *37*, 215-220.

Folstein, S., and Rutter, M. (1977). Infantile autism: a genetic study of 21 twin pairs. Journal of child psychology and psychiatry, and allied disciplines *18*, 297-321.

Forsingdal, A., Fejgin, K., Nielsen, V., Werge, T., and Nielsen, J. (2016). 15q13.3 homozygous knockout mouse model display epilepsy-, autism- and schizophrenia-related phenotypes. Translational psychiatry *6*, e860.

Gandal, M.J., Haney, J.R., Parikshak, N.N., Leppa, V., Ramaswami, G., Hartl, C., Schork, A.J., Appadurai, V., Buil, A., Werge, T.M.*, et al.* (2018). Shared molecular neuropathology across major psychiatric disorders parallels polygenic overlap. Science *359*, 693-697.

Garcia, I., Huang, L., Ung, K., and Arenkiel, B.R. (2012). Tracing synaptic connectivity onto embryonic stem cell-derived neurons. Stem cells *30*, 2140-2151.

Gaugler, T., Klei, L., Sanders, S.J., Bodea, C.A., Goldberg, A.P., Lee, A.B., Mahajan, M., Manaa, D., Pawitan, Y., Reichert, J.*, et al.* (2014). Most genetic risk for autism resides with common variation. Nature genetics *46*, 881-885.

Gdalyahu, A., Lazaro, M., Penagarikano, O., Golshani, P., Trachtenberg, J.T., and Geschwind, D.H. (2015). The Autism Related Protein Contactin-Associated Protein-Like 2 (CNTNAP2) Stabilizes New Spines: An In Vivo Mouse Study. PloS one *10*, e0125633.

Ge, H., Tan, L., Wu, P., Yin, Y., Liu, X., Meng, H., Cui, G., Wu, N., Lin, J., Hu, R.*, et al.* (2015). Poly-L-ornithine promotes preferred differentiation of neural stem/progenitor cells via ERK signalling pathway. Scientific reports *5*, 15535.

Geschwind, D.H., and Levitt, P. (2007). Autism spectrum disorders: developmental disconnection syndromes. Current opinion in neurobiology *17*, 103-111.

Geschwind, D.H., and State, M.W. (2015). Gene hunting in autism spectrum disorder: on the path to precision medicine. The Lancet Neurology *14*, 1109-1120.

Ghosh, A., Michalon, A., Lindemann, L., Fontoura, P., and Santarelli, L. (2013). Drug discovery for autism spectrum disorder: challenges and opportunities. Nature reviews Drug discovery *12*, 777-790.

Goodwin, J.M., Svensson, R.U., Lou, H.J., Winslow, M.M., Turk, B.E., and Shaw, R.J. (2014). An AMPK-independent signaling pathway downstream of the LKB1 tumor suppressor controls Snail1 and metastatic potential. Molecular cell *55*, 436-450.

Greer, P.L., Hanayama, R., Bloodgood, B.L., Mardinly, A.R., Lipton, D.M., Flavell, S.W., Kim, T.K., Griffith, E.C., Waldon, Z., Maehr, R.*, et al.* (2010). The Angelman Syndrome protein Ube3A regulates synapse development by ubiquitinating arc. Cell *140*, 704-716.

Griffith, M., Walker, J.R., Spies, N.C., Ainscough, B.J., and Griffith, O.L. (2015). Informatics for RNA Sequencing: A Web Resource for Analysis on the Cloud. PLoS computational biology *11*, e1004393.

Gu, J., Lee, C.W., Fan, Y., Komlos, D., Tang, X., Sun, C., Yu, K., Hartzell, H.C., Chen, G., Bamburg, J.R.*, et al.* (2010). ADF/cofilin-mediated actin dynamics regulate AMPA receptor trafficking during synaptic plasticity. Nature neuroscience *13*, 1208-1215.

Guilmatre, A., Huguet, G., Delorme, R., and Bourgeron, T. (2014). The emerging role of SHANK genes in neuropsychiatric disorders. Developmental neurobiology *74*, 113-122.

Habela, C.W., Song, H., and Ming, G.L. (2016). Modeling synaptogenesis in schizophrenia and autism using human iPSC derived neurons. Molecular and cellular neurosciences *73*, 52-62.

Hallmayer, J., Cleveland, S., Torres, A., Phillips, J., Cohen, B., Torigoe, T., Miller, J., Fedele, A., Collins, J., Smith, K.*, et al.* (2011). Genetic heritability and shared environmental factors among twin pairs with autism. Archives of general psychiatry *68*, 1095-1102.

Han, K., Holder, J.L., Jr., Schaaf, C.P., Lu, H., Chen, H., Kang, H., Tang, J., Wu, Z., Hao, S., Cheung, S.W.*, et al.* (2013). SHANK3 overexpression causes manic-like behaviour with unique pharmacogenetic properties. Nature *503*, 72-77.

Handrigan, G.R., Chitayat, D., Lionel, A.C., Pinsk, M., Vaags, A.K., Marshall, C.R., Dyack, S., Escobar, L.F., Fernandez, B.A., Stegman, J.C.*, et al.* (2013). Deletions in 16q24.2 are associated with autism spectrum disorder, intellectual disability and congenital renal malformation. Journal of medical genetics *50*, 163-173.

Hayashi-Takagi, A., Araki, Y., Nakamura, M., Vollrath, B., Duron, S.G., Yan, Z., Kasai, H., Huganir, R.L., Campbell, D.A., and Sawa, A. (2014). PAKs inhibitors ameliorate schizophrenia-associated dendritic spine deterioration in vitro and in vivo during late adolescence. Proceedings of the National Academy of Sciences of the United States of America *111*, 6461-6466.

Hayashi-Takagi, A., Takaki, M., Graziane, N., Seshadri, S., Murdoch, H., Dunlop, A.J., Makino, Y., Seshadri, A.J., Ishizuka, K., Srivastava, D.P.*, et al.* (2010). Disrupted-in-Schizophrenia 1 (DISC1) regulates spines of the glutamate synapse via Rac1. Nature neuroscience *13*, 327-332.

Hazelbaker, D.Z., Beccard, A., Bara, A.M., Dabkowski, N., Messana, A., Mazzucato, P., Lam, D., Manning, D., Eggan, K., and Barrett, L.E. (2017). A Scaled Framework for CRISPR Editing of Human Pluripotent Stem Cells to Study Psychiatric Disease. Stem cell reports *9*, 1315-1327.

Hempel, C.M., Sivula, M., Levenson, J.M., Rose, D.M., Li, B., Sirianni, A.C., Xia, E., Ryan, T.A., Gerber, D.J., and Cottrell, J.R. (2011). A system for performing high throughput assays of synaptic function. PloS one *6*, e25999.

Ho, S.M., Hartley, B.J., Tcw, J., Beaumont, M., Stafford, K., Slesinger, P.A., and Brennand, K.J. (2016). Rapid Ngn2-induction of excitatory neurons from hiPSC-derived neural progenitor cells. Methods *101*, 113-124.

Holt, R.A., and Jones, S.J. (2008). The new paradigm of flow cell sequencing. Genome research *18*, 839-846.

Hori, K., Nagai, T., Shan, W., Sakamoto, A., Taya, S., Hashimoto, R., Hayashi, T., Abe, M., Yamazaki, M., Nakao, K.*, et al.* (2014). Cytoskeletal regulation by AUTS2 in neuronal migration and neuritogenesis. Cell reports *9*, 2166-2179.

Hotulainen, P., and Hoogenraad, C.C. (2010). Actin in dendritic spines: connecting dynamics to function. The Journal of cell biology *189*, 619-629.

Hu, B.Y., Weick, J.P., Yu, J., Ma, L.X., Zhang, X.Q., Thomson, J.A., and Zhang, S.C. (2010). Neural differentiation of human induced pluripotent stem cells follows developmental principles but with variable potency. Proceedings of the National Academy of Sciences of the United States of America *107*, 4335-4340.

Huang, W., Zhu, P.J., Zhang, S., Zhou, H., Stoica, L., Galiano, M., Krnjevic, K., Roman, G., and Costa-Mattioli, M. (2013). mTORC2 controls actin polymerization required for consolidation of long-term memory. Nature neuroscience *16*, 441-448.

Huber, K.M., Klann, E., Costa-Mattioli, M., and Zukin, R.S. (2015). Dysregulation of Mammalian Target of Rapamycin Signaling in Mouse Models of Autism. The Journal of neuroscience : the official journal of the Society for Neuroscience *35*, 13836-13842.

Hutsler, J.J., and Zhang, H. (2010). Increased dendritic spine densities on cortical projection neurons in autism spectrum disorders. Brain research *1309*, 83-94.

Ikeuchi, Y., Stegmuller, J., Netherton, S., Huynh, M.A., Masu, M., Frank, D., Bonni, S., and Bonni, A. (2009). A SnoN-Ccd1 pathway promotes axonal morphogenesis in the mammalian brain. The Journal of neuroscience : the official journal of the Society for Neuroscience *29*, 4312-4321.

Iossifov, I., O'Roak, B.J., Sanders, S.J., Ronemus, M., Krumm, N., Levy, D., Stessman, H.A., Witherspoon, K.T., Vives, L., Patterson, K.E.*, et al.* (2014). The contribution of de novo coding mutations to autism spectrum disorder. Nature *515*, 216-221.

Iossifov, I., Ronemus, M., Levy, D., Wang, Z., Hakker, I., Rosenbaum, J., Yamrom, B., Lee, Y.H., Narzisi, G., Leotta, A.*, et al.* (2012). De novo gene disruptions in children on the autistic spectrum. Neuron *74*, 285-299.

Irimia, M., Weatheritt, R.J., Ellis, J.D., Parikshak, N.N., Gonatopoulos-Pournatzis, T., Babor, M., Quesnel-Vallieres, M., Tapial, J., Raj, B., O'Hanlon, D.*, et al.* (2014). A highly conserved program of neuronal microexons is misregulated in autistic brains. Cell *159*, 1511-1523.

Ishizuka, K., Kamiya, A., Oh, E.C., Kanki, H., Seshadri, S., Robinson, J.F., Murdoch, H., Dunlop, A.J., Kubo, K., Furukori, K.*, et al.* (2011). DISC1-dependent switch from progenitor proliferation to migration in the developing cortex. Nature *473*, 92-96.

Jeste, S.S., and Geschwind, D.H. (2014). Disentangling the heterogeneity of autism spectrum disorder through genetic findings. Nature reviews Neurology *10*, 74-81.

Jiang, Y.H., Yuen, R.K., Jin, X., Wang, M., Chen, N., Wu, X., Ju, J., Mei, J., Shi, Y., He, M.*, et al.* (2013). Detection of clinically relevant genetic variants in autism spectrum disorder by whole-genome sequencing. American journal of human genetics *93*, 249-263.

Johe, K.K., Hazel, T.G., Muller, T., Dugich-Djordjevic, M.M., and McKay, R.D. (1996). Single factors direct the differentiation of stem cells from the fetal and adult central nervous system. Genes & development *10*, 3129-3140.

Kalkman, H.O. (2012). A review of the evidence for the canonical Wnt pathway in autism spectrum disorders. Molecular autism *3*, 10.

Katayama, Y., Nishiyama, M., Shoji, H., Ohkawa, Y., Kawamura, A., Sato, T., Suyama, M., Takumi, T., Miyakawa, T., and Nakayama, K.I. (2016). CHD8 haploinsufficiency results in autistic-like phenotypes in mice. Nature *537*, 675-679.

Khwaja, O.S., Ho, E., Barnes, K.V., O'Leary, H.M., Pereira, L.M., Finkelstein, Y., Nelson, C.A., 3rd, Vogel-Farley, V., DeGregorio, G., Holm, I.A.*, et al.* (2014). Safety, pharmacokinetics, and preliminary assessment of efficacy of mecasermin (recombinant human IGF-1) for the treatment of Rett syndrome. Proceedings of the National Academy of Sciences of the United States of America *111*, 4596-4601.

Kim, H.G., Kishikawa, S., Higgins, A.W., Seong, I.S., Donovan, D.J., Shen, Y., Lally, E., Weiss, L.A., Najm, J., Kutsche, K.*, et al.* (2008). Disruption of neurexin 1 associated with autism spectrum disorder. American journal of human genetics *82*, 199-207.

Kivimae, S., Martin, P.M., Kapfhamer, D., Ruan, Y., Heberlein, U., Rubenstein, J.L., and Cheyette, B.N. (2011). Abnormal behavior in mice mutant for the Disc1 binding partner, Dixdc1. Translational psychiatry *1*, e43.

Kleinman, H.K., Luckenbill-Edds, L., Cannon, F.W., and Sephel, G.C. (1987). Use of extracellular matrix components for cell culture. Analytical biochemistry *166*, 1-13.

Knuesel, I., Chicha, L., Britschgi, M., Schobel, S.A., Bodmer, M., Hellings, J.A., Toovey, S., and Prinssen, E.P. (2014). Maternal immune activation and abnormal brain development across CNS disorders. Nature reviews Neurology *10*, 643-660.

Kogan, J.H., Gross, A.K., Featherstone, R.E., Shin, R., Chen, Q., Heusner, C.L., Adachi, M., Lin, A., Walton, N.M., Miyoshi, S.*, et al.* (2015). Mouse Model of Chromosome 15q13.3 Microdeletion Syndrome Demonstrates Features Related to Autism Spectrum Disorder. The Journal of neuroscience : the official journal of the Society for Neuroscience *35*, 16282-16294.

Kondo, T., Imamura, K., Funayama, M., Tsukita, K., Miyake, M., Ohta, A., Woltjen, K., Nakagawa, M., Asada, T., Arai, T.*, et al.* (2017). iPSC-Based Compound Screening and In Vitro Trials Identify a Synergistic Anti-amyloid beta Combination for Alzheimer's Disease. Cell reports *21*, 2304-2312.

Korobova, F., and Svitkina, T. (2010). Molecular architecture of synaptic actin cytoskeleton in hippocampal neurons reveals a mechanism of dendritic spine morphogenesis. Molecular biology of the cell *21*, 165-176.

Krey, J.F., Pasca, S.P., Shcheglovitov, A., Yazawa, M., Schwemberger, R., Rasmusson, R., and Dolmetsch, R.E. (2013). Timothy syndrome is associated with activity-dependent dendritic retraction in rodent and human neurons. Nature neuroscience *16*, 201-209.

Krishnan, A., Zhang, R., Yao, V., Theesfeld, C.L., Wong, A.K., Tadych, A., Volfovsky, N., Packer, A., Lash, A., and Troyanskaya, O.G. (2016). Genome-wide prediction and functional characterization of the genetic basis of autism spectrum disorder. Nature neuroscience *19*, 1454-1462.

Krumm, N., O'Roak, B.J., Shendure, J., and Eichler, E.E. (2014). A de novo convergence of autism genetics and molecular neuroscience. Trends in neurosciences *37*, 95-105.

Krumm, N., Turner, T.N., Baker, C., Vives, L., Mohajeri, K., Witherspoon, K., Raja, A., Coe, B.P., Stessman, H.A., He, Z.X.*, et al.* (2015). Excess of rare, inherited truncating mutations in autism. Nature genetics *47*, 582-588.

Kukurba, K.R., and Montgomery, S.B. (2015). RNA Sequencing and Analysis. Cold Spring Harbor protocols *2015*, 951-969.

Kwan, V., Meka, D.P., White, S.H., Hung, C.L., Holzapfel, N.T., Walker, S., Murtaza, N., Unda, B.K., Schwanke, B., Yuen, R.K.*, et al.* (2016). DIXDC1 Phosphorylation and Control of Dendritic Morphology Are Impaired by Rare Genetic Variants. Cell reports *17*, 1892-1904.

Kwon, C.H., Luikart, B.W., Powell, C.M., Zhou, J., Matheny, S.A., Zhang, W., Li, Y., Baker, S.J., and Parada, L.F. (2006). Pten regulates neuronal arborization and social interaction in mice. Neuron *50*, 377-388.

Kwon, S.E., and Chapman, E.R. (2011). Synaptophysin regulates the kinetics of synaptic vesicle endocytosis in central neurons. Neuron *70*, 847-854.

Lam, R.S., Topfer, F.M., Wood, P.G., Busskamp, V., and Bamberg, E. (2017). Functional Maturation of Human Stem Cell-Derived Neurons in Long-Term Cultures. PloS one *12*, e0169506.

LeBlanc, J.J., and Fagiolini, M. (2011). Autism: a "critical period" disorder? Neural plasticity *2011*, 921680.

Lei, W., Omotade, O.F., Myers, K.R., and Zheng, J.Q. (2016). Actin cytoskeleton in dendritic spine development and plasticity. Current opinion in neurobiology *39*, 86-92.

Levine, S.Z., Kodesh, A., Goldberg, Y., Reichenberg, A., Furukawa, T.A., Kolevzon, A., and Leucht, S. (2016). Initial severity and efficacy of risperidone in autism: Results from the RUPP trial. European psychiatry : the journal of the Association of European Psychiatrists *32*, 16-20.

Lichtenstein, P. (2010). The Genetics of Autism Spectrum Disorders and Related Neuropsychiatric Disorders in Childhood. The American Journal of Psychiatry

.

Lichtenstein, P., Carlstrom, E., Rastam, M., Gillberg, C., and Anckarsater, H. (2010). The genetics of autism spectrum disorders and related neuropsychiatric disorders in childhood. Am J Psychiatry *167*, 1357-1363.

Lijam, N., Paylor, R., McDonald, M.P., Crawley, J.N., Deng, C.X., Herrup, K., Stevens, K.E., Maccaferri, G., McBain, C.J., Sussman, D.J.*, et al.* (1997). Social interaction and sensorimotor gating abnormalities in mice lacking Dvl1. Cell *90*, 895-905.

Lim, E.T., Uddin, M., De Rubeis, S., Chan, Y., Kamumbu, A.S., Zhang, X., D'Gama, A.M., Kim, S.N., Hill, R.S., Goldberg, A.P.*, et al.* (2017). Rates, distribution and implications of postzygotic mosaic mutations in autism spectrum disorder. Nature neuroscience.

Lin, G.N., Corominas, R., Lemmens, I., Yang, X., Tavernier, J., Hill, D.E., Vidal, M., Sebat, J., and Iakoucheva, L.M. (2015). Spatiotemporal 16p11.2 protein network implicates cortical late mid-fetal brain development and KCTD13-Cul3-RhoA pathway in psychiatric diseases. Neuron *85*, 742-754.

Liu, X.S., Wu, H., Krzisch, M., Wu, X., Graef, J., Muffat, J., Hnisz, D., Li, C.H., Yuan, B., Xu, C.*, et al.* (2018). Rescue of Fragile X Syndrome Neurons by DNA Methylation Editing of the FMR1 Gene. Cell *172*, 979-992 e976.

Liu, Y., Liu, H., Sauvey, C., Yao, L., Zarnowska, E.D., and Zhang, S.C. (2013). Directed differentiation of forebrain GABA interneurons from human pluripotent stem cells. Nature protocols *8*, 1670-1679.

Long, J.M., LaPorte, P., Paylor, R., and Wynshaw-Boris, A. (2004). Expanded characterization of the social interaction abnormalities in mice lacking Dvl1. Genes, Brain and Behavior *3*, 51-62.

Lord, C., Risi, S., Lambrecht, L., Cook, E.H., Jr., Leventhal, B.L., DiLavore, P.C., Pickles, A., and Rutter, M. (2000). The autism diagnostic observation schedule-generic: a

standard measure of social and communication deficits associated with the spectrum of autism. Journal of autism and developmental disorders *30*, 205-223.

Lord, C., Rutter, M., and Le Couteur, A. (1994). Autism Diagnostic Interview-Revised: a revised version of a diagnostic interview for caregivers of individuals with possible pervasive developmental disorders. Journal of autism and developmental disorders *24*, 659-685.

Lu, C., Chen, Q., Zhou, T., Bozic, D., Fu, Z., Pan, J.Q., and Feng, G. (2016). Micro-electrode array recordings reveal reductions in both excitation and inhibition in cultured cortical neuron networks lacking Shank3. Molecular psychiatry *21*, 159-168.

Lugo, J.N., Smith, G.D., Arbuckle, E.P., White, J., Holley, A.J., Floruta, C.M., Ahmed, N., Gomez, M.C., and Okonkwo, O. (2014). Deletion of PTEN produces autism-like behavioral deficits and alterations in synaptic proteins. Frontiers in molecular neuroscience *7*, 27.

Malfait, F., Francomano, C., Byers, P., Belmont, J., Berglund, B., Black, J., Bloom, L., Bowen, J.M., Brady, A.F., Burrows, N.P.*, et al.* (2017). The 2017 international classification of the Ehlers-Danlos syndromes. American journal of medical genetics Part C, Seminars in medical genetics *175*, 8-26.

Mao, Y., Ge, X., Frank, C.L., Madison, J.M., Koehler, A.N., Doud, M.K., Tassa, C., Berry, E.M., Soda, T., Singh, K.K.*, et al.* (2009). Disrupted in schizophrenia 1 regulates

neuronal progenitor proliferation via modulation of GSK3beta/beta-catenin signaling. Cell *136*, 1017-1031.

Marchetto, M.C., Belinson, H., Tian, Y., Freitas, B.C., Fu, C., Vadodaria, K., Beltrao-Braga, P., Trujillo, C.A., Mendes, A.P.D., Padmanabhan, K.*, et al.* (2017). Altered proliferation and networks in neural cells derived from idiopathic autistic individuals. Molecular psychiatry *22*, 820-835.

Martin, P.M., Stanley, R.E., Ross, A.P., Freitas, A.E., Moyer, C.E., Brumback, A.C., Iafrati, J., Stapornwongkul, K.S., Dominguez, S., Kivimae, S.*, et al.* (2016). DIXDC1 contributes to psychiatric susceptibility by regulating dendritic spine and glutamatergic synapse density via GSK3 and Wnt/beta-catenin signaling. Molecular psychiatry.

Martin, P.M., Yang, X., Robin, N., Lam, E., Rabinowitz, J.S., Erdman, C.A., Quinn, J., Weiss, L.A., Hamilton, S.P., Kwok, P.Y.*, et al.* (2013). A rare WNT1 missense variant overrepresented in ASD leads to increased Wnt signal pathway activation. Translational psychiatry *3*, e301.

Maussion, G., Carayol, J., Lepagnol-Bestel, A.M., Tores, F., Loe-Mie, Y., Milbreta, U., Rousseau, F., Fontaine, K., Renaud, J., Moalic, J.M.*, et al.* (2008). Convergent evidence identifying MAP/microtubule affinity-regulating kinase 1 (MARK1) as a susceptibility gene for autism. Human molecular genetics *17*, 2541-2551.

McCarthy, S.E., Gillis, J., Kramer, M., Lihm, J., Yoon, S., Berstein, Y., Mistry, M., Pavlidis, P., Solomon, R., Ghiban, E.*, et al.* (2014). De novo mutations in schizophrenia

implicate chromatin remodeling and support a genetic overlap with autism and intellectual disability. Molecular psychiatry *19*, 652-658.

Merico, D., Zarrei, M., Costain, G., Ogura, L., Alipanahi, B., Gazzellone, M.J., Butcher, N.J., Thiruvahindrapuram, B., Nalpathamkalam, T., Chow, E.W.*, et al.* (2015). Whole-Genome Sequencing Suggests Schizophrenia Risk Mechanisms in Humans with 22q11.2 Deletion Syndrome. G3 *5*, 2453-2461.

Merner, N., Forgeot d'Arc, B., Bell, S.C., Maussion, G., Peng, H., Gauthier, J., Crapper, L., Hamdan, F.F., Michaud, J.L., Mottron, L.*, et al.* (2016). A de novo frameshift mutation in chromodomain helicase DNA-binding domain 8 (CHD8): A case report and literature review. American journal of medical genetics Part A *170*, 1225-1235.

Michaelsen-Preusse, K., Zessin, S., Grigoryan, G., Scharkowski, F., Feuge, J., Remus, A., and Korte, M. (2016). Neuronal profilins in health and disease: Relevance for spine plasticity and Fragile X syndrome. Proceedings of the National Academy of Sciences of the United States of America *113*, 3365-3370.

Michaelson, J.J., Shin, M.K., Koh, J.Y., Brueggeman, L., Zhang, A., Katzman, A., McDaniel, L., Fang, M., Pufall, M., and Pieper, A.A. (2017). Neuronal PAS Domain Proteins 1 and 3 Are Master Regulators of Neuropsychiatric Risk Genes. Biological psychiatry *82*, 213-223.

Miles, J.H. (2011). Autism spectrum disorders--a genetics review. Genetics in medicine : official journal of the American College of Medical Genetics *13*, 278-294.

Modabbernia, A., Velthorst, E., and Reichenberg, A. (2017). Environmental risk factors for autism: an evidence-based review of systematic reviews and meta-analyses. Mol Autism *8*, 13.

Mohn, J.L., Alexander, J., Pirone, A., Palka, C.D., Lee, S.Y., Mebane, L., Haydon, P.G., and Jacob, M.H. (2014). Adenomatous polyposis coli protein deletion leads to cognitive and autism-like disabilities. Molecular psychiatry *19*, 1133-1142.

Molyneaux, B.J., Arlotta, P., Menezes, J.R., and Macklis, J.D. (2007). Neuronal subtype specification in the cerebral cortex. Nature reviews Neuroscience *8*, 427-437.

Morgan-Smith, M., Wu, Y., Zhu, X., Pringle, J., and Snider, W.D. (2014). GSK-3 signaling in developing cortical neurons is essential for radial migration and dendritic orientation. eLife *3*, e02663.

Muhia, M., Thies, E., Labonte, D., Ghiretti, A.E., Gromova, K.V., Xompero, F., Lappe-Siefke, C., Hermans-Borgmeyer, I., Kuhl, D., Schweizer, M.*, et al.* (2016). The Kinesin KIF21B Regulates Microtubule Dynamics and Is Essential for Neuronal Morphology, Synapse Function, and Learning and Memory. Cell reports *15*, 968-977.

Mukai, J., Dhilla, A., Drew, L.J., Stark, K.L., Cao, L., MacDermott, A.B., Karayiorgou, M., and Gogos, J.A. (2008). Palmitoylation-dependent neurodevelopmental deficits in a mouse model of 22q11 microdeletion. Nature neuroscience *11*, 1302-1310.

Mullins, C., Fishell, G., and Tsien, R.W. (2016). Unifying Views of Autism Spectrum Disorders: A Consideration of Autoregulatory Feedback Loops. Neuron *89*, 1131-1156.

Munji, R.N., Choe, Y., Li, G., Siegenthaler, J.A., and Pleasure, S.J. (2011). Wnt signaling regulates neuronal differentiation of cortical intermediate progenitors. The Journal of neuroscience : the official journal of the Society for Neuroscience *31*, 1676-1687.

Murakoshi, H., Wang, H., and Yasuda, R. (2011). Local, persistent activation of Rho GTPases during plasticity of single dendritic spines. Nature *472*, 100-104.

Nagaoka, T., Tabuchi, K., and Kishi, M. (2015). PDZ interaction of Vangl2 links PSD-95 and Prickle2 but plays only a limited role in the synaptic localisation of Vangl2. Scientific reports *5*, 12916.

Nakanishi, N., Ryan, S.D., Zhang, X., Khan, A., Holland, T., Cho, E.G., Huang, X., Liao, F.F., Xu, H., Lipton, S.A.*, et al.* (2013). Synaptic protein alpha1-takusan mitigates amyloid-beta-induced synaptic loss via interaction with tau and postsynaptic density-95 at postsynaptic sites. The Journal of neuroscience : the official journal of the Society for Neuroscience *33*, 14170-14183.

Namba, T., and Kaibuchi, K. (2010). Switching DISC1 function in neurogenesis: Dixdc1 selects DISC1 binding partners. Developmental cell *19*, 7-8.

Neale, B.M., Kou, Y., Liu, L., Ma'ayan, A., Samocha, K.E., Sabo, A., Lin, C.F., Stevens, C., Wang, L.S., Makarov, V.*, et al.* (2012). Patterns and rates of exonic de novo mutations in autism spectrum disorders. Nature *485*, 242-245.

Nguyen, H.N., Byers, B., Cord, B., Shcheglovitov, A., Byrne, J., Gujar, P., Kee, K., Schule, B., Dolmetsch, R.E., Langston, W.*, et al.* (2011). LRRK2 mutant iPSC-derived

DA neurons demonstrate increased susceptibility to oxidative stress. Cell stem cell *8*, 267-280.

Niethammer, M., Smith, D.S., Ayala, R., Peng, J., Ko, J., Lee, M.S., Morabito, M., and Tsai, L.H. (2000). NUDEL is a novel Cdk5 substrate that associates with LIS1 and cytoplasmic dynein. Neuron *28*, 697-711.

Nimchinsky, E.A., Sabatini, B.L., and Svoboda, K. (2002). Structure and function of dendritic spines. Annual review of physiology *64*, 313-353.

O'Roak, B.J., Vives, L., Fu, W., Egertson, J.D., Stanaway, I.B., Phelps, I.G., Carvill, G., Kumar, A., Lee, C., Ankenman, K.*, et al.* (2012a). Multiplex targeted sequencing identifies recurrently mutated genes in autism spectrum disorders. Science *338*, 1619-1622.

O'Roak, B.J., Vives, L., Girirajan, S., Karakoc, E., Krumm, N., Coe, B.P., Levy, R., Ko, A., Lee, C., Smith, J.D.*, et al.* (2012b). Sporadic autism exomes reveal a highly interconnected protein network of de novo mutations. Nature *485*, 246-250.

Oguro-Ando, A., Rosensweig, C., Herman, E., Nishimura, Y., Werling, D., Bill, B.R., Berg, J.M., Gao, F., Coppola, G., Abrahams, B.S.*, et al.* (2015). Increased CYFIP1 dosage alters cellular and dendritic morphology and dysregulates mTOR. Molecular psychiatry *20*, 1069-1078.

Okerlund, N.D., and Cheyette, B.N. (2011). Synaptic Wnt signaling-a contributor to major psychiatric disorders? Journal of neurodevelopmental disorders *3*, 162-174.

Okerlund, N.D., Kivimae, S., Tong, C.K., Peng, I.F., Ullian, E.M., and Cheyette, B.N. (2010). Dact1 is a postsynaptic protein required for dendrite, spine, and excitatory synapse development in the mouse forebrain. The Journal of neuroscience : the official journal of the Society for Neuroscience *30*, 4362-4368.

Oliva, C.A., Vargas, J.Y., and Inestrosa, N.C. (2013). Wnts in adult brain: from synaptic plasticity to cognitive deficiencies. Frontiers in cellular neuroscience *7*, 224.

Oskvig, D.B., Elkahloun, A.G., Johnson, K.R., Phillips, T.M., and Herkenham, M. (2012). Maternal immune activation by LPS selectively alters specific gene expression profiles of interneuron migration and oxidative stress in the fetus without triggering a fetal immune response. Brain, behavior, and immunity *26*, 623-634.

Page, D.T., Kuti, O.J., Prestia, C., and Sur, M. (2009). Haploinsufficiency for Pten and Serotonin transporter cooperatively influences brain size and social behavior. Proceedings of the National Academy of Sciences of the United States of America *106*, 1989-1994.

Pagnamenta, A.T., Wing, K., Sadighi Akha, E., Knight, S.J., Bolte, S., Schmotzer, G., Duketis, E., Poustka, F., Klauck, S.M., Poustka, A.*, et al.* (2009). A 15q13.3 microdeletion segregating with autism. European journal of human genetics : EJHG *17*, 687-692.

Pasca, S.P., Portmann, T., Voineagu, I., Yazawa, M., Shcheglovitov, A., Pasca, A.M., Cord, B., Palmer, T.D., Chikahisa, S., Nishino, S.*, et al.* (2011). Using iPSC-derived

neurons to uncover cellular phenotypes associated with Timothy syndrome. Nature medicine *17*, 1657-1662.

Pathania, M., Davenport, E.C., Muir, J., Sheehan, D.F., Lopez-Domenech, G., and Kittler, J.T. (2014). The autism and schizophrenia associated gene CYFIP1 is critical for the maintenance of dendritic complexity and the stabilization of mature spines. Translational psychiatry *4*, e374.

Patro, R., Duggal, G., Love, M.I., Irizarry, R.A., and Kingsford, C. (2017). Salmon provides fast and bias-aware quantification of transcript expression. Nature methods *14*, 417-419.

Peca, J., Feliciano, C., Ting, J.T., Wang, W., Wells, M.F., Venkatraman, T.N., Lascola, C.D., Fu, Z., and Feng, G. (2011). Shank3 mutant mice display autistic-like behaviours and striatal dysfunction. Nature *472*, 437-442.

Penagarikano, O., Abrahams, B.S., Herman, E.I., Winden, K.D., Gdalyahu, A., Dong, H., Sonnenblick, L.I., Gruver, R., Almajano, J., Bragin, A.*, et al.* (2011). Absence of CNTNAP2 leads to epilepsy, neuronal migration abnormalities, and core autism-related deficits. Cell *147*, 235-246.

Penzes, P., Cahill, M.E., Jones, K.A., VanLeeuwen, J.E., and Woolfrey, K.M. (2011a). Dendritic spine pathology in neuropsychiatric disorders. Nature neuroscience *14*, 285-293.

Penzes, P., Woolfrey, K.M., and Srivastava, D.P. (2011b). Epac2-mediated dendritic spine remodeling: implications for disease. Molecular and cellular neurosciences *46*, 368-380.

pfeliciano@simonsfoundation.org, S.C.E.a., and Consortium, S. (2018). SPARK: A US Cohort of 50,000 Families to Accelerate Autism Research. Neuron *97*, 488-493.

Pinto, D., Delaby, E., Merico, D., Barbosa, M., Merikangas, A., Klei, L., Thiruvahindrapuram, B., Xu, X., Ziman, R., Wang, Z.*, et al.* (2014). Convergence of genes and cellular pathways dysregulated in autism spectrum disorders. American journal of human genetics *94*, 677-694.

Platt, R.J., Zhou, Y., Slaymaker, I.M., Shetty, A.S., Weisbach, N.R., Kim, J.A., Sharma, J., Desai, M., Sood, S., Kempton, H.R.*, et al.* (2017). Chd8 Mutation Leads to Autistic-like Behaviors and Impaired Striatal Circuits. Cell reports *19*, 335-350.

Purro, S.A., Galli, S., and Salinas, P.C. (2014). Dysfunction of Wnt signaling and synaptic disassembly in neurodegenerative diseases. Journal of molecular cell biology *6*, 75-80.

Qi, L.S., Larson, M.H., Gilbert, L.A., Doudna, J.A., Weissman, J.S., Arkin, A.P., and Lim, W.A. (2013). Repurposing CRISPR as an RNA-guided platform for sequence-specific control of gene expression. Cell *152*, 1173-1183.

Qin, L., Ma, K., Wang, Z.J., Hu, Z., Matas, E., Wei, J., and Yan, Z. (2018). Social deficits in Shank3-deficient mouse models of autism are rescued by histone deacetylase (HDAC) inhibition. Nature neuroscience.

Quadrato, G., Brown, J., and Arlotta, P. (2016). The promises and challenges of human brain organoids as models of neuropsychiatric disease. Nature medicine *22*, 1220-1228.

Ran, F.A., Hsu, P.D., Lin, C.Y., Gootenberg, J.S., Konermann, S., Trevino, A.E., Scott, D.A., Inoue, A., Matoba, S., Zhang, Y.*, et al.* (2013a). Double nicking by RNA-guided CRISPR Cas9 for enhanced genome editing specificity. Cell *154*, 1380-1389.

Ran, F.A., Hsu, P.D., Wright, J., Agarwala, V., Scott, D.A., and Zhang, F. (2013b). Genome engineering using the CRISPR-Cas9 system. Nature protocols *8*, 2281-2308.

Reinhard, J.R., Kriz, A., Galic, M., Angliker, N., Rajalu, M., Vogt, K.E., and Ruegg, M.A. (2016). The calcium sensor Copine-6 regulates spine structural plasticity and learning and memory. Nature communications *7*, 11613.

Ricard-Blum, S. (2011). The collagen family. Cold Spring Harbor perspectives in biology *3*, a004978.

Riedl, J., Crevenna, A.H., Kessenbrock, K., Yu, J.H., Neukirchen, D., Bista, M., Bradke, F., Jenne, D., Holak, T.A., Werb, Z.*, et al.* (2008). Lifeact: a versatile marker to visualize F-actin. Nature methods *5*, 605-607.

Riedl, J., Flynn, K.C., Raducanu, A., Gartner, F., Beck, G., Bosl, M., Bradke, F., Massberg, S., Aszodi, A., Sixt, M.*, et al.* (2010). Lifeact mice for studying F-actin dynamics. Nature methods *7*, 168-169.

Riikonen, R. (2016). Treatment of autistic spectrum disorder with insulin-like growth factors. European journal of paediatric neurology : EJPN : official journal of the European Paediatric Neurology Society *20*, 816-823.

Ringner, M. (2008). What is principal component analysis? Nature biotechnology *26*, 303-304.

Robinson, E.B., St Pourcain, B., Anttila, V., Kosmicki, J.A., Bulik-Sullivan, B., Grove, J., Maller, J., Samocha, K.E., Sanders, S.J., Ripke, S.*, et al.* (2016). Genetic risk for autism spectrum disorders and neuropsychiatric variation in the general population. Nature genetics *48*, 552-555.

Roux, K.J., Kim, D.I., and Burke, B. (2013). BioID: a screen for protein-protein interactions. Current protocols in protein science *74*, Unit 19 23.

Russell, T.A., Blizinsky, K.D., Cobia, D.J., Cahill, M.E., Xie, Z., Sweet, R.A., Duan, J., Gejman, P.V., Wang, L., Csernansky, J.G.*, et al.* (2014). A sequence variant in human KALRN impairs protein function and coincides with reduced cortical thickness. Nature communications *5*, 4858.

Sajan, S.A., Jhangiani, S.N., Muzny, D.M., Gibbs, R.A., Lupski, J.R., Glaze, D.G., Kaufmann, W.E., Skinner, S.A., Annese, F., Friez, M.J.*, et al.* (2016). Enrichment of

mutations in chromatin regulators in people with Rett syndrome lacking mutations in MECP2. Genetics in medicine : official journal of the American College of Medical Genetics.

Salinas, P.C., and Zou, Y. (2008). Wnt signaling in neural circuit assembly. Annual review of neuroscience *31*, 339-358.

Sances, S., Bruijn, L.I., Chandran, S., Eggan, K., Ho, R., Klim, J.R., Livesey, M.R., Lowry, E., Macklis, J.D., Rushton, D.*, et al.* (2016). Modeling ALS with motor neurons derived from human induced pluripotent stem cells. Nature neuroscience *19*, 542-553.

Sanders, S.J., Murtha, M.T., Gupta, A.R., Murdoch, J.D., Raubeson, M.J., Willsey, A.J., Ercan-Sencicek, A.G., DiLullo, N.M., Parikshak, N.N., Stein, J.L.*, et al.* (2012). De novo mutations revealed by whole-exome sequencing are strongly associated with autism. Nature *485*, 237-241.

Sandin, S., Lichtenstein, P., Kuja-Halkola, R., Larsson, H., Hultman, C.M., and Reichenberg, A. (2014). The familial risk of autism. Jama *311*, 1770-1777.

Schmeisser, M.J., Ey, E., Wegener, S., Bockmann, J., Stempel, A.V., Kuebler, A., Janssen, A.L., Udvardi, P.T., Shiban, E., Spilker, C.*, et al.* (2012). Autistic-like behaviours and hyperactivity in mice lacking ProSAP1/Shank2. Nature *486*, 256-260.

Schwarze, U., Atkinson, M., Hoffman, G.G., Greenspan, D.S., and Byers, P.H. (2000). Null alleles of the COL5A1 gene of type V collagen are a cause of the classical forms of

Ehlers-Danlos syndrome (types I and II). American journal of human genetics *66*, 1757-1765.

Schwarze, U., Schievink, W.I., Petty, E., Jaff, M.R., Babovic-Vuksanovic, D., Cherry, K.J., Pepin, M., and Byers, P.H. (2001). Haploinsufficiency for one COL3A1 allele of type III procollagen results in a phenotype similar to the vascular form of Ehlers-Danlos syndrome, Ehlers-Danlos syndrome type IV. American journal of human genetics *69*, 989-1001.

Sharma, K., Choi, S.Y., Zhang, Y., Nieland, T.J., Long, S., Li, M., and Huganir, R.L. (2013). High-throughput genetic screen for synaptogenic factors: identification of LRP6 as critical for excitatory synapse development. Cell reports *5*, 1330-1341.

Sharma, P., Ando, D.M., Daub, A., Kaye, J.A., and Finkbeiner, S. (2012). High-throughput screening in primary neurons. Methods in enzymology *506*, 331-360.

Shcheglovitov, A., Shcheglovitova, O., Yazawa, M., Portmann, T., Shu, R., Sebastiano, V., Krawisz, A., Froehlich, W., Bernstein, J.A., Hallmayer, J.F.*, et al.* (2013). SHANK3 and IGF1 restore synaptic deficits in neurons from 22q13 deletion syndrome patients. Nature *503*, 267-271.

Shepherd, G.M., and Katz, D.M. (2011). Synaptic microcircuit dysfunction in genetic models of neurodevelopmental disorders: focus on Mecp2 and Met. Current opinion in neurobiology *21*, 827-833.

Sherman, S.A., Phillips, J.K., Costa, J.T., Cho, F.S., Oungoulian, S.R., and Finan, J.D. (2016). Stretch Injury of Human Induced Pluripotent Stem Cell Derived Neurons in a 96 Well Format. Scientific reports *6*, 34097.

Shi, Y., Kirwan, P., and Livesey, F.J. (2012a). Directed differentiation of human pluripotent stem cells to cerebral cortex neurons and neural networks. Nature protocols *7*, 1836-1846.

Shi, Y., Kirwan, P., Smith, J., Robinson, H.P., and Livesey, F.J. (2012b). Human cerebral cortex development from pluripotent stem cells to functional excitatory synapses. Nature neuroscience *15*, 477-486, S471.

Shiomi, K., Kanemoto, M., Keino-Masu, K., Yoshida, S., Soma, K., and Masu, M. (2005). Identification and differential expression of multiple isoforms of mouse Coiled-coil-DIX1 (Ccd1), a positive regulator of Wnt signaling. Brain research Molecular brain research *135*, 169-180.

Shiomi, K., Uchida, H., Keino-Masu, K., and Masu, M. (2003). Ccd1, a novel protein with a DIX domain, is a positive regulator in the Wnt signaling during zebrafish neural patterning. Current biology : CB *13*, 73-77.

Shishido, E., Aleksic, B., and Ozaki, N. (2014). Copy-number variation in the pathogenesis of autism spectrum disorder. Psychiatry and clinical neurosciences *68*, 85-95.

Singh, K.K., Ge, X., Mao, Y., Drane, L., Meletis, K., Samuels, B.A., and Tsai, L.H. (2010). Dixdc1 is a critical regulator of DISC1 and embryonic cortical development. Neuron *67*, 33-48.

Singh, N.A., Charlier, C., Stauffer, D., DuPont, B.R., Leach, R.J., Melis, R., Ronen, G.M., Bjerre, I., Quattlebaum, T., Murphy, J.V.*, et al.* (1998). A novel potassium channel gene, KCNQ2, is mutated in an inherited epilepsy of newborns. Nature genetics *18*, 25-29.

Sirenko, O., Hesley, J., Rusyn, I., and Cromwell, E.F. (2014). High-content high-throughput assays for characterizing the viability and morphology of human iPSC-derived neuronal cultures. Assay and drug development technologies *12*, 536-547.

Soma, K., Shiomi, K., Keino-Masu, K., and Masu, M. (2006). Expression of mouse Coiled-coil-DIX1 (Ccd1), a positive regulator of Wnt signaling, during embryonic development. Gene expression patterns : GEP *6*, 325-330.

Sousa, I., Clark, T.G., Toma, C., Kobayashi, K., Choma, M., Holt, R., Sykes, N.H., Lamb, J.A., Bailey, A.J., Battaglia, A.*, et al.* (2009). MET and autism susceptibility: family and case-control studies. European journal of human genetics : EJHG *17*, 749-758.

Sowers, L.P., Loo, L., Wu, Y., Campbell, E., Ulrich, J.D., Wu, S., Paemka, L., Wassink, T., Meyer, K., Bing, X.*, et al.* (2013a). Disruption of the non-canonical Wnt gene PRICKLE2 leads to autism-like behaviors with evidence for hippocampal synaptic dysfunction. Molecular psychiatry *18*, 1077-1089.

Sowers, L.P., Mouw, T.J., Ferguson, P.J., Wemmie, J.A., Mohapatra, D.P., and Bassuk, A.G. (2013b). The non-canonical Wnt ligand Wnt5a rescues morphological deficits in Prickle2-deficient hippocampal neurons. Molecular psychiatry *18*, 1049.

Spicer, T.P., Hubbs, C., Vaissiere, T., Collia, D., Rojas, C., Kilinc, M., Vick, K., Madoux, F., Baillargeon, P., Shumate, J.*, et al.* (2017). Improved Scalability of Neuron-Based Phenotypic Screening Assays for Therapeutic Discovery in Neuropsychiatric Disorders. Molecular Neuropsychiatry *3*, 141-150.

Splawski, I., Timothy, K.W., Sharpe, L.M., Decher, N., Kumar, P., Bloise, R., Napolitano, C., Schwartz, P.J., Joseph, R.M., Condouris, K.*, et al.* (2004). Ca(V)1.2 calcium channel dysfunction causes a multisystem disorder including arrhythmia and autism. Cell *119*, 19-31.

Srikanth, P., Han, K., Callahan, D.G., Makovkina, E., Muratore, C.R., Lalli, M.A., Zhou, H., Boyd, J.D., Kosik, K.S., Selkoe, D.J.*, et al.* (2015). Genomic DISC1 Disruption in hiPSCs Alters Wnt Signaling and Neural Cell Fate. Cell reports *12*, 1414-1429.

Staal, F.J., Luis, T.C., and Tiemessen, M.M. (2008). WNT signalling in the immune system: WNT is spreading its wings. Nature reviews Immunology *8*, 581-593.

Stamatakou, E., Marzo, A., Gibb, A., and Salinas, P.C. (2013). Activity-dependent spine morphogenesis: a role for the actin-capping protein Eps8. The Journal of neuroscience : the official journal of the Society for Neuroscience *33*, 2661-2670.

Stamatakou, E., and Salinas, P.C. (2014). Postsynaptic assembly: a role for Wnt signaling. Developmental neurobiology *74*, 818-827.

Stefansson, H., Rujescu, D., Cichon, S., Pietilainen, O.P., Ingason, A., Steinberg, S., Fossdal, R., Sigurdsson, E., Sigmundsson, T., Buizer-Voskamp, J.E.*, et al.* (2008). Large recurrent microdeletions associated with schizophrenia. Nature *455*, 232-236.

Subramanian, A., Tamayo, P., Mootha, V.K., Mukherjee, S., Ebert, B.L., Gillette, M.A., Paulovich, A., Pomeroy, S.L., Golub, T.R., Lander, E.S.*, et al.* (2005). Gene set enrichment analysis: a knowledge-based approach for interpreting genome-wide expression profiles. Proceedings of the National Academy of Sciences of the United States of America *102*, 15545-15550.

Subtil-Rodriguez, A., Vazquez-Chavez, E., Ceballos-Chavez, M., Rodriguez-Paredes, M., Martin-Subero, J.I., Esteller, M., and Reyes, J.C. (2014). The chromatin remodeller CHD8 is required for E2F-dependent transcription activation of S-phase genes. Nucleic acids research *42*, 2185-2196.

Sudhof, T.C. (2008). Neuroligins and neurexins link synaptic function to cognitive disease. Nature *455*, 903-911.

Sugathan, A., Biagioli, M., Golzio, C., Erdin, S., Blumenthal, I., Manavalan, P., Ragavendran, A., Brand, H., Lucente, D., Miles, J.*, et al.* (2014). CHD8 regulates neurodevelopmental pathways associated with autism spectrum disorder in neural

progenitors. Proceedings of the National Academy of Sciences of the United States of America *111*, E4468-4477.

Symoens, S., Malfait, F., Renard, M., Andre, J., Hausser, I., Loeys, B., Coucke, P., and De Paepe, A. (2009). COL5A1 signal peptide mutations interfere with protein secretion and cause classic Ehlers-Danlos syndrome. Human mutation *30*, E395-403.

Takahashi, K., Tanabe, K., Ohnuki, M., Narita, M., Ichisaka, T., Tomoda, K., and Yamanaka, S. (2007). Induction of pluripotent stem cells from adult human fibroblasts by defined factors. Cell *131*, 861-872.

Takei, A., Mera, K., Sato, Y., and Haraoka, Y. (2011). High-functioning autistic disorder with Ehlers-Danlos syndrome. Psychiatry and clinical neurosciences *65*, 605-606.

Talkowski, M.E., Rosenfeld, J.A., Blumenthal, I., Pillalamarri, V., Chiang, C., Heilbut, A., Ernst, C., Hanscom, C., Rossin, E., Lindgren, A.M.*, et al.* (2012). Sequencing chromosomal abnormalities reveals neurodevelopmental loci that confer risk across diagnostic boundaries. Cell *149*, 525-537.

Tan, C., Qiao, F., Wei, P., Chi, Y., Wang, W., Ni, S., Wang, Q., Chen, T., Sheng, W., Du, X.*, et al.* (2016). DIXDC1 activates the Wnt signaling pathway and promotes gastric cancer cell invasion and metastasis. Molecular carcinogenesis *55*, 397-408.

Tanaka, T., Serneo, F.F., Tseng, H.C., Kulkarni, A.B., Tsai, L.H., and Gleeson, J.G. (2004). Cdk5 phosphorylation of doublecortin ser297 regulates its effect on neuronal migration. Neuron *41*, 215-227.

Tanaka, Y. (1991). The evolution of social communication systems in a subdivided population. Journal of theoretical biology *149*, 145-163.

Tang, G., Gudsnuk, K., Kuo, S.H., Cotrina, M.L., Rosoklija, G., Sosunov, A., Sonders, M.S., Kanter, E., Castagna, C., Yamamoto, A.*, et al.* (2014). Loss of mTOR-dependent macroautophagy causes autistic-like synaptic pruning deficits. Neuron *83*, 1131-1143.

Thomson, J.A., Itskovitz-Eldor, J., Shapiro, S.S., Waknitz, M.A., Swiergiel, J.J., Marshall, V.S., and Jones, J.M. (1998). Embryonic stem cell lines derived from human blastocysts. Science *282*, 1145-1147.

Topol, A., Zhu, S., Tran, N., Simone, A., Fang, G., and Brennand, K.J. (2015). Altered WNT Signaling in Human Induced Pluripotent Stem Cell Neural Progenitor Cells Derived from Four Schizophrenia Patients. Biological psychiatry *78*, e29-34.

Touma, M., Joshi, M., Connolly, M.C., Grant, P.E., Hansen, A.R., Khwaja, O., Berry, G.T., Kinney, H.C., Poduri, A., and Agrawal, P.B. (2013). Whole genome sequencing identifies SCN2A mutation in monozygotic twins with Ohtahara syndrome and unique neuropathologic findings. Epilepsia *54*, e81-85.

Tu, S., Shin, Y., Zago, W.M., States, B.A., Eroshkin, A., Lipton, S.A., Tong, G.G., and Nakanishi, N. (2007). Takusan: a large gene family that regulates synaptic activity. Neuron *55*, 69-85.

Turner, T.N., Sharma, K., Oh, E.C., Liu, Y.P., Collins, R.L., Sosa, M.X., Auer, D.R., Brand, H., Sanders, S.J., Moreno-De-Luca, D.*, et al.* (2015). Loss of delta-catenin function in severe autism. Nature *520*, 51-56.

Uddin, M., Unda, B.K., Kwan, V., Holzapfel, N.T., White, S.H., Chalil, L., Woodbury-Smith, M., Ho, K.S., Harward, E., Murtaza, N.*, et al.* (2018). OTUD7A Regulates Neurodevelopmental Phenotypes in the 15q13.3 Microdeletion Syndrome. The American Journal of Human Genetics *102*, 278-295.

Um, K., Niu, S., Duman, J.G., Cheng, J.X., Tu, Y.K., Schwechter, B., Liu, F., Hiles, L., Narayanan, A.S., Ash, R.T.*, et al.* (2014). Dynamic control of excitatory synapse development by a Rac1 GEF/GAP regulatory complex. Developmental cell *29*, 701-715.

Vogel, A., Holbrook, K.A., Steinmann, B., Gitzelmann, R., and Byers, P.H. (1979). Abnormal collagen fibril structure in the gravis form (type I) of Ehlers-Danlos syndrome. Laboratory investigation; a journal of technical methods and pathology *40*, 201-206.

Voineagu, I., Wang, X., Johnston, P., Lowe, J.K., Tian, Y., Horvath, S., Mill, J., Cantor, R.M., Blencowe, B.J., and Geschwind, D.H. (2011). Transcriptomic analysis of autistic brain reveals convergent molecular pathology. Nature *474*, 380-384.

Volk, L., Chiu, S.L., Sharma, K., and Huganir, R.L. (2015). Glutamate synapses in human cognitive disorders. Annual review of neuroscience *38*, 127-149.

Wang, L., Li, H., Chen, Q., Zhu, T., Zhu, H., and Zheng, L. (2010). Wnt signaling stabilizes the DIXDC1 protein through decreased ubiquitin-dependent degradation. Cancer science *101*, 700-706.

Wang, P., Lin, M., Pedrosa, E., Hrabovsky, A., Zhang, Z., Guo, W., Lachman, H.M., and Zheng, D. (2015). CRISPR/Cas9-mediated heterozygous knockout of the autism gene CHD8 and characterization of its transcriptional networks in neurodevelopment. Mol Autism *6*, 55.

Wang, P., Mokhtari, R., Pedrosa, E., Kirschenbaum, M., Bayrak, C., Zheng, D., and Lachman, H.M. (2017). CRISPR/Cas9-mediated heterozygous knockout of the autism gene CHD8 and characterization of its transcriptional networks in cerebral organoids derived from iPS cells. Mol Autism *8*, 11.

Wang, X., Zheng, L., Zeng, Z., Zhou, G., Chien, J., Qian, C., Vasmatzis, G., Shridhar, V., Chen, L., and Liu, W. (2006). DIXDC1 isoform, l-DIXDC1, is a novel filamentous actin-binding protein. Biochemical and biophysical research communications *347*, 22-30.

Wang, Z., Gerstein, M., and Snyder, M. (2009). RNA-Seq: a revolutionary tool for transcriptomics. Nature reviews Genetics *10*, 57-63.

Weiner, D.J., Wigdor, E.M., Ripke, S., Walters, R.K., Kosmicki, J.A., Grove, J., Samocha, K.E., Goldstein, J.I., Okbay, A., Bybjerg-Grauholm, J.*, et al.* (2017). Polygenic transmission disequilibrium confirms that common and rare variation act additively to create risk for autism spectrum disorders. Nature genetics.

Wen, Z., Nguyen, H.N., Guo, Z., Lalli, M.A., Wang, X., Su, Y., Kim, N.S., Yoon, K.J., Shin, J., Zhang, C.*, et al.* (2014). Synaptic dysregulation in a human iPS cell model of mental disorders. Nature *515*, 414-418.

Wenstrup, R.J., Florer, J.B., Davidson, J.M., Phillips, C.L., Pfeiffer, B.J., Menezes, D.W., Chervoneva, I., and Birk, D.E. (2006). Murine model of the Ehlers-Danlos syndrome. col5a1 haploinsufficiency disrupts collagen fibril assembly at multiple stages. The Journal of biological chemistry *281*, 12888-12895.

Wenstrup, R.J., Florer, J.B., Willing, M.C., Giunta, C., Steinmann, B., Young, F., Susic, M., and Cole, W.G. (2000). COL5A1 haploinsufficiency is a common molecular mechanism underlying the classical form of EDS. American journal of human genetics *66*, 1766-1776.

Wickersham, I.R., Lyon, D.C., Barnard, R.J., Mori, T., Finke, S., Conzelmann, K.K., Young, J.A., and Callaway, E.M. (2007). Monosynaptic restriction of transsynaptic tracing from single, genetically targeted neurons. Neuron *53*, 639-647.

Wilkinson, M.B., Dias, C., Magida, J., Mazei-Robison, M., Lobo, M., Kennedy, P., Dietz, D., Covington, H., 3rd, Russo, S., Neve, R.*, et al.* (2011). A novel role of the WNT-dishevelled-GSK3beta signaling cascade in the mouse nucleus accumbens in a social defeat model of depression. The Journal of neuroscience : the official journal of the Society for Neuroscience *31*, 9084-9092.

Williams, S.K., Scahill, L., Vitiello, B., Aman, M.G., Arnold, L.E., McDougle, C.J., McCracken, J.T., Tierney, E., Ritz, L., Posey, D.J., *et al.* (2006). Risperidone and adaptive behavior in children with autism. Journal of the American Academy of Child and Adolescent Psychiatry *45*, 431-439.

Woolfrey, K.M., and Srivastava, D.P. (2016). Control of Dendritic Spine Morphological and Functional Plasticity by Small GTPases. Neural plasticity *2016*, 3025948.

Woolfrey, K.M., Srivastava, D.P., Photowala, H., Yamashita, M., Barbolina, M.V., Cahill, M.E., Xie, Z., Jones, K.A., Quilliam, L.A., Prakriya, M., *et al.* (2009). Epac2 induces synapse remodeling and depression and its disease-associated forms alter spines. Nature neuroscience *12*, 1275-1284.

Wright, C., Shin, J.H., Rajpurohit, A., Deep-Soboslay, A., Collado-Torres, L., Brandon, N.J., Hyde, T.M., Kleinman, J.E., Jaffe, A.E., Cross, A.J., *et al.* (2017). Altered expression of histamine signaling genes in autism spectrum disorder. Translational psychiatry *7*, e1126.

Wu, H., Xu, J., Pang, Z.P., Ge, W., Kim, K.J., Blanchi, B., Chen, C., Sudhof, T.C., and Sun, Y.E. (2007). Integrative genomic and functional analyses reveal neuronal subtype differentiation bias in human embryonic stem cell lines. Proceedings of the National Academy of Sciences of the United States of America *104*, 13821-13826.

Wu, Q., DiBona, V.L., Bernard, L.P., and Zhang, H. (2012). The polarity protein partitioning-defective 1 (PAR-1) regulates dendritic spine morphogenesis through

phosphorylating postsynaptic density protein 95 (PSD-95). The Journal of biological chemistry *287*, 30781-30788.

Wu, Y., Jing, X., Ma, X., Wu, Y., Ding, X., Fan, W., and Fan, M. (2009). DIXDC1 co-localizes and interacts with gamma-tubulin in HEK293 cells. Cell biology international *33*, 697-701.

Xie, Z., Sanada, K., Samuels, B.A., Shih, H., and Tsai, L.H. (2003). Serine 732 phosphorylation of FAK by Cdk5 is important for microtubule organization, nuclear movement, and neuronal migration. Cell *114*, 469-482.

Xu, X., Miller, E.C., and Pozzo-Miller, L. (2014a). Dendritic spine dysgenesis in Rett syndrome. Frontiers in neuroanatomy *8*, 97.

Xu, Z., Liu, D., Fan, C., Luan, L., Zhang, X., and Wang, E. (2014b). DIXDC1 increases the invasion and migration ability of non-small-cell lung cancer cells via the PI3K-AKT/AP-1 pathway. Molecular carcinogenesis *53*, 917-925.

Yi, F., Danko, T., Botelho, S.C., Patzke, C., Pak, C., Wernig, M., and Sudhof, T.C. (2016). Autism-associated SHANK3 haploinsufficiency causes Ih channelopathy in human neurons. Science *352*, aaf2669.

Yi, J.J., Berrios, J., Newbern, J.M., Snider, W.D., Philpot, B.D., Hahn, K.M., and Zylka, M.J. (2015). An Autism-Linked Mutation Disables Phosphorylation Control of UBE3A. Cell *162*, 795-807.

Yin, J., Chen, W., Chao, E.S., Soriano, S., Wang, L., Wang, W., Cummock, S.E., Tao, H., Pang, K., Liu, Z.*, et al.* (2018). Otud7a Knockout Mice Recapitulate Many Neurological Features of 15q13.3 Microdeletion Syndrome. The American Journal of Human Genetics *102*, 296-308.

Yoon, K.J., Nguyen, H.N., Ursini, G., Zhang, F., Kim, N.S., Wen, Z., Makri, G., Nauen, D., Shin, J.H., Park, Y.*, et al.* (2014). Modeling a genetic risk for schizophrenia in iPSCs and mice reveals neural stem cell deficits associated with adherens junctions and polarity. Cell stem cell *15*, 79-91.

Yu, H.E., Hawash, K., Picker, J., Stoler, J., Urion, D., Wu, B.L., and Shen, Y. (2012). A recurrent 1.71 Mb genomic imbalance at 2q13 increases the risk of developmental delay and dysmorphism. Clinical genetics *81*, 257-264.

Yu, X., and Malenka, R.C. (2003). Beta-catenin is critical for dendritic morphogenesis. Nature neuroscience *6*, 1169-1177.

Yuen, R.K., Merico, D., Cao, H., Pellecchia, G., Alipanahi, B., Thiruvahindrapuram, B., Tong, X., Sun, Y., Cao, D., Zhang, T.*, et al.* (2016). Genome-wide characteristics of de novo mutations in autism. NPJ genomic medicine *1*, 160271-1602710.

Yuen, R.K., Thiruvahindrapuram, B., Merico, D., Walker, S., Tammimies, K., Hoang, N., Chrysler, C., Nalpathamkalam, T., Pellecchia, G., Liu, Y.*, et al.* (2015). Whole-genome sequencing of quartet families with autism spectrum disorder. Nature medicine *21*, 185-191.

Yuen, R.K.C., Merico, D., Bookman, M., J, L.H., Thiruvahindrapuram, B., Patel, R.V., Whitney, J., Deflaux, N., Bingham, J., Wang, Z.*, et al.* (2017). Whole genome sequencing resource identifies 18 new candidate genes for autism spectrum disorder. Nature neuroscience *20*, 602-611.

Zahir, F., Firth, H.V., Baross, A., Delaney, A.D., Eydoux, P., Gibson, W.T., Langlois, S., Martin, H., Willatt, L., Marra, M.A.*, et al.* (2007). Novel deletions of 14q11.2 associated with developmental delay, cognitive impairment and similar minor anomalies in three children. Journal of medical genetics *44*, 556-561.

Zhang, Y., Pak, C., Han, Y., Ahlenius, H., Zhang, Z., Chanda, S., Marro, S., Patzke, C., Acuna, C., Covy, J.*, et al.* (2013). Rapid single-step induction of functional neurons from human pluripotent stem cells. Neuron *78*, 785-798.

Zhao, D., Mokhtari, R., Pedrosa, E., Birnbaum, R., Zheng, D., and Lachman, H.M. (2017). Transcriptome analysis of microglia in a mouse model of Rett syndrome: differential expression of genes associated with microglia/macrophage activation and cellular stress. Mol Autism *8*, 17.

Zhou, J., and Parada, L.F. (2012). PTEN signaling in autism spectrum disorders. Current opinion in neurobiology *22*, 873-879.

Zhou, Y., Kaiser, T., Monteiro, P., Zhang, X., Van der Goes, M.S., Wang, D., Barak, B., Zeng, M., Li, C., Lu, C.*, et al.* (2016). Mice with Shank3 Mutations Associated with ASD and Schizophrenia Display Both Shared and Distinct Defects. Neuron *89*, 147-162.